



Universiteit
Leiden
The Netherlands

Crossing barriers, delivery of llama antibody fragments into the brain

Rotman, M.

Citation

Rotman, M. (2017, April 19). *Crossing barriers, delivery of llama antibody fragments into the brain*. Retrieved from <https://hdl.handle.net/1887/48860>

Version: Not Applicable (or Unknown)

License: [Licence agreement concerning inclusion of doctoral thesis in the Institutional Repository of the University of Leiden](#)

Downloaded from: <https://hdl.handle.net/1887/48860>

Note: To cite this publication please use the final published version (if applicable).

Cover Page



Universiteit Leiden



The handle <http://hdl.handle.net/1887/48860> holds various files of this Leiden University dissertation

Author: Rotman, M.

Title: Crossing barriers, delivery of llama antibody fragments into the brain

Issue Date: 2017-04-19

CROSSING BARRIERS

DELIVERY OF LLAMA ANTIBODY FRAGMENTS INTO THE BRAIN

M. ROTMAN

Colophon

CROSSING BARRIERS, delivery of llama antibody fragments into the brain
Thesis Leiden University Medical Center

Typesetting: Brill by BRILL, Leiden
Cover design: M. Rotman
Layout: M. Rotman
Printed by: Proefschriftmaken.nl || Uitgeverij BOXPress, Vianen
ISBN: 978-94-6295-618-6

Copyright 2010-2017 by Maarten Rotman, Leiden, The Netherlands. All rights reserved.

No part of this book may be reproduced, stored in a retrieval system, or transmitted in any form or by any means, without prior written permission of the author.

CROSSING BARRIERS

DELIVERY OF LLAMA ANTIBODY FRAGMENTS INTO THE BRAIN

Proefschrift

ter verkrijging van
de graad van Doctor aan de Universiteit Leiden,
op gezag van Rector Magnificus prof.mr. C.J.J.M. Stolker,
volgens besluit van het College voor Promoties
te verdedigen op woensdag 19 april 2017
klokke 10:00 uur

door

Maarten Rotman
geboren te De Wijk
in 1984

Promotores:

Prof. Dr. Ir. S.M. van der Maarel

Prof. Dr. M.A. van Buchem

Co-promotor:

Dr. Ir. L. van der Weerd

Leden promotiecommissie:

Prof. Dr. H.J. Tanke

Prof. Dr. J.M. Rozemuller, VUmc, Amsterdam

Prof. Dr. A.D. Windhorst, VUmc, Amsterdam

The studies presented in this thesis were performed at the department of Human Genetics, the department of Radiology and the department of Pathology at Leiden University Medical Center, Leiden, the Netherlands, the department of Molecular Cell Biology at Utrecht University, Utrecht, the Netherlands, and at the department of Neurology at Mayo Clinic, Jacksonville, Florida, the United States of America.

This work was financially supported by grants from the IOP Genomics Centre [IGE05005]; the Centre for Medical Systems Biology (CMSB₂) [grants S-MRI-110010 and S-MRI-110030] within the framework of the Netherlands Genomics Initiative (NGI)/Netherlands Organization for Scientific Research (NWO); project LeARN [grant 02N-101] within the framework of the Center for Translational Molecular Medicine (CTMM); the Dutch CAA foundation/mr Jan Fens via a donation to the LUMC *Bontius Stichting* and by a personal fellowship to Maarten Rotman from *Alzheimer Nederland* (Amersfoort) [WE.15-2013-09].

Financial support for the publication of this thesis by *Alzheimer Nederland* (Amersfoort) is gratefully acknowledged.

TABLE OF CONTENTS

CHAPTER 1	PAGE 7
GENERAL INTRODUCTION	
CHAPTER 2	PAGE 35
VHH AGAINST BACE1 INHIBITS BETA-SECRETASE ACTIVITY <i>IN VITRO</i> AND <i>IN VIVO</i>	
CHAPTER 3	PAGE 61
ENHANCED GSH-PEG LIPOSOMAL BRAIN DELIVERY OF VHH-PA2H IN A MOUSE MODEL FOR AD	
<i>Supplementary Data</i>	<i>page 85</i>
CHAPTER 4	PAGE 89
FUSION OF HUMAN FC TO VHH-PA2H INCREASES BLOOD RESIDENTIAL TIME, BUT NOT BRAIN UPTAKE	
CHAPTER 5	PAGE 109
FUNCTIONALLY SECRETED VHH-EMGFP BINDS AMYLOID PLAQUES AND CAN BE VISUALIZED <i>IN VIVO</i>	
<i>Supplementary Data</i>	<i>page 136</i>
CHAPTER 6	PAGE 149
GENERAL DISCUSSION	
CHAPTER 7	PAGE 175
APPENDICES	
<i>Summary</i>	<i>page 177</i>
<i>Nederlandstalige samenvatting</i>	<i>page 181</i>
<i>List of publications</i>	<i>page 185</i>
<i>Curriculum vitae</i>	<i>page 189</i>
<i>Acknowledgements / dankwoord</i>	<i>page 191</i>

1

CHAPTER

GENERAL INTRODUCTION

ABSTRACT

Llama antibody fragments (VHH) have the intrinsic potential to be developed as diagnostic, therapeutic and even theragnostic tools in a wide variety of diseases and afflictions. Their potential application includes the diagnosis and treatment of neurodegenerative disorders, among which Alzheimer's disease (AD). However, currently this application is hampered by, amongst other factors, the blood-brain barrier (BBB). The BBB strictly regulates what goes into and out of the brain. Drugs that can theoretically be used to detect or fight neurodegenerative disorders often do not cross this barrier. Yet delivery of compounds into the brain is of vital importance for both detection and treatment of cerebral diseases such as AD. This thesis focusses on the delivery of VHH into the brain. It discusses a variety of delivery methods and provides a platform for both diagnostic and therapeutic applications of VHH in neurodegenerative disorders in general and in particular in dementia and AD.

1. INTRODUCTION

1.1 *Dementia & Alzheimer's disease*

Dementia is a syndrome caused by a number of progressive illnesses that affect memory, thinking, behavior and the ability to perform everyday activities. With age being the major risk factor, prevalence of dementia above the age of 65 doubles with every five year age increments. Currently, an estimated 44 million patients worldwide are affected by dementia, a number expected to double by 2030 and more than triple by 2050 [1].

AD is the most prevalent (50-75%) form of dementia. It is clinically characterized by a gradual decline in memory and cognitive function. Early clinical symptoms of AD, e.g. short-term memory loss, steadily progress to more extensive cognitive and emotional dysfunction. Eventually, the patient becomes completely bedridden and dependent on fulltime professional care for activities of daily living. Death, as a direct result of the disease, occurs on average nine years after the moment the first clinical symptoms can be noticed in the patient. Due to the devastating and relentless nature of the affliction, dementia in general and AD in particular are one of the main causes of dependence and disability at older ages, one for which no cure has yet been developed [2].

AD has two main pathological hallmarks, i.e. intercellular neurofibrillary tangles (NFT) of hyperphosphorylated tau protein and extracellular aggregates of the peptide amyloid beta ($A\beta$). Aggregates of $A\beta$ can occur in senile or diffuse plaques in the neuropil, or in the vasculature of the cerebral cortex. Cerebrovascular deposition of $A\beta$ in the vessel walls (*tunica media*) of the parenchymal and leptomeningeal arteries and arterioles is referred to as cerebral amyloid angiopathy (CAA), with a subset of CAA involving deposition around capillaries (capCAA). CAA occurs in approximately 70% up to 100% of AD patients [3–6]. Other neuropathological changes associated with AD include pronounced atrophy of certain brain regions, substantial enlargement of the cerebral ventricles, widening of the cortical sulci and narrowing of the gyri [7], see also Figure 1.1. The yet irreversible, and damaging, neuropathological changes start as early as two to three decades before cognitive decline is clinically noticeable [8–10], and accumulation and aggregation of $A\beta$ is currently thought to be the first of all these pathological changes to occur [11].

1.2 *$A\beta$ and AD*

Formation of the peptide $A\beta$ is the result of one of the two posttranslational pathways of sequential cleavage of its precursor protein, the type-1 transmembrane glycoprotein APP (human amyloid beta A4 precursor protein) [12,13]. Cleavage of APP follows either the amyloidogenic or the non-amyloidogenic pathway. In the amyloidogenic pathway APP is sequentially cleaved

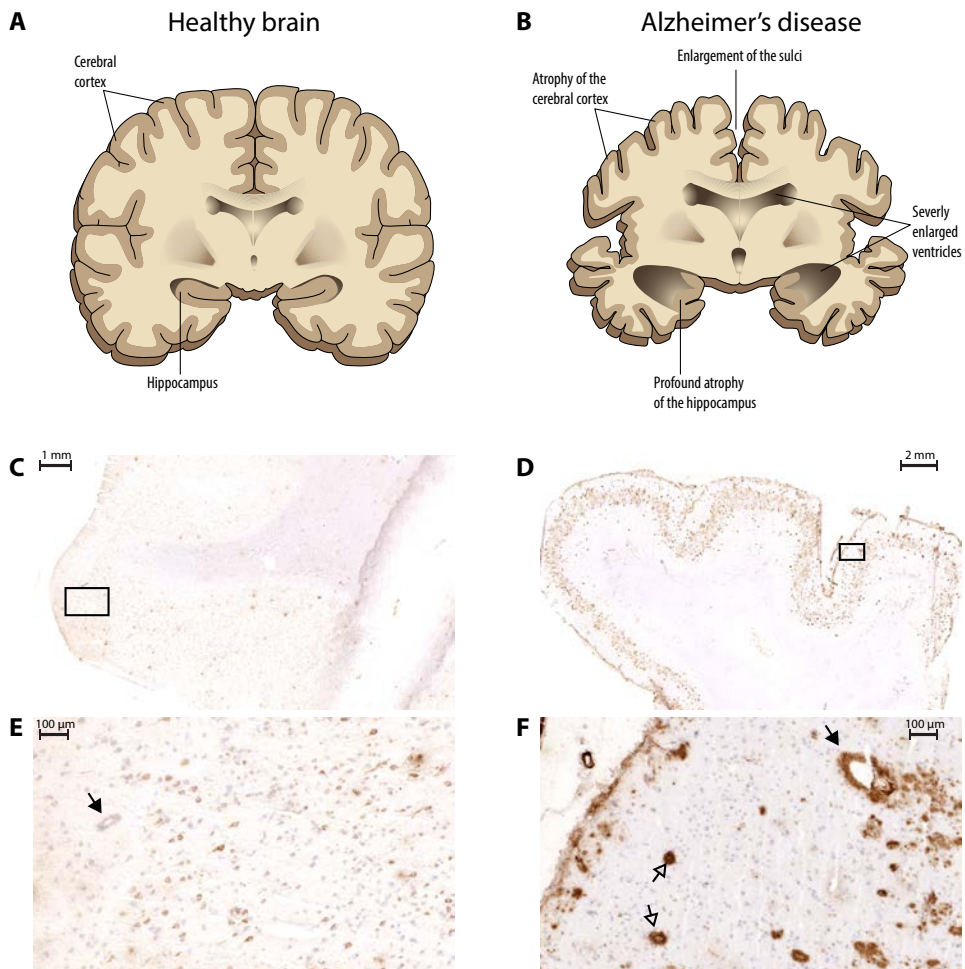


Figure 1.1. One of the most evident neuropathological changes associated with Alzheimer's disease is extreme atrophy of the brain. The sulci, or grooves, pressed together by the gyri of the healthy brain (A), are enlarged in the brain of patients as the gyri atrophy (B). Also the cerebral ventricles become bigger and significant shrinkage of the hippocampus, the short-term memory control center of the brain, is observed. On a microscopic scale, depositions of the aggregated peptide amyloid beta ($A\beta$) is visible in the parenchyma (open arrows) and the around the cerebral vasculature (closed arrows) in the diseased brain (D and F) but not in the healthy age matched brain (C and E). Figures A and B are modelled after scientific images from the National Institute on Aging/National Institutes of Health, Bethesda, MD, USA. Parts C-F are 5 μ m thick cryosections stained with murine monoclonal anti- $A\beta$ antibody 4G8 (C and E) and the anti- $A\beta$ VHH pazH (D and F) following methods described in chapters 2-5 in this thesis.

by first the β -secretase followed by the γ -secretase and results in the formation of the peptide $A\beta$. On the other hand, in the non-amyloidogenic pathway APP is cleaved by the α -secretase before cleavage by the γ -secretase and is consequently cut into putatively harmless fragments [14–16], Figure 1.2. See also Box 1.1. The Processing of APP for more details.

Following the amyloidogenic pathway, the $A\beta$ fragment can range in size from 38 to 43 amino acids. Most of the $A\beta$ that gets produced is 40 amino acids long, $A\beta_{40}$, followed by $A\beta_{42}$. The exact physiological function of $A\beta$, of any length, in both healthy and diseased states of the

Box 1.1. The Processing of APP

The type-1 transmembrane glycoprotein APP is processed by sequential cleavages in either the non-amyloidogenic or the amyloidogenic pathway, and only the latter leads to A β .

In the non-amyloidogenic pathway APP is first cleaved by α -secretase. The activity of α -secretase is mediated by one or more of the 26 enzymes from the family of disintegrin and metalloproteinase domain proteins (ADAM), with most evidence pointing towards either exclusively or mainly ADAM10 [17,18]. The α -secretase cleaves APP between its Lys683 and Leu684 residues, or the 16th and 17th amino acid inside what could have become the A β fragment [15,19]. This divides APP into a large soluble extracellular domain (sAPP- α) and a membrane-associated C-terminal fragment of 83 amino acids (C83, or CTF- α). The CTF- α fragment is then cleaved by the γ -secretase, a large proteinase complex made up by presenilin (PS1 or PS2), nicastrin, presenilin enhancer 2 (PEN2), and anterior pharynx-defective 1 (APH1) [20–23]. The γ -secretase complex cleaves the CTF- α fragment into the P3 peptide and the C-terminal APP intracellular domain (AICD). The two smaller fragments may likely have functions in downstream signaling pathways, including a role for the AICD in a negative-feedback loop for the γ -secretase complex, but their exact functions are still poorly understood [24,25].

In the amyloidogenic pathway, which eventually leads to A β , APP is first cleaved by β -secretase, a single enzyme also known as BACE1 [26–29]. BACE1 can cleave APP at two different sites, i.e. either between Met596 and Asp597 of APP (the Asp-1 cleavage site) or between Tyr606 and Glu607 (the Glu-11 cleavage site), where the Glu-11 site is the preferred site *in vivo* and *in vitro* [30]. The BACE1 cleavage produces a secreted, extracellular sAPP- β and either a 99 or 89 residue membrane associated CTF- β (C99 or C89, respectively). The CTF- β fragments are subsequently cleaved by the γ -secretase complex creating the intracellular AICD and, in the case of C99, the amyloidogenic A β peptide.

While α -secretase and β -secretase both have only one or two very precise cleavage sites, the γ -secretase complex can cleave the membrane-associated CTF- β at a variety of locations within its transmembrane domain. Therefore, the resulting A β peptide can vary in length between 38 and 43 amino acids *in vivo*. Longer variants of A β are known, e.g. A β 46 and A β 49 [31]. However, they may be the product of pathways involving other secretases, aptly named ϵ - and ζ -secretase. The functions of the longer peptides are as of yet unknown and they are likely intermediate peptides before being further cleaved to A β peptides of 40 and 42 amino acids in length (A β 40 and A β 42, respectively) [32,33]. Peptides of these two lengths, A β 40 and A β 42, are the two most common forms of the A β fragment found *in vivo*; especially A β 40, which accounts for approximately 90% of the produced A β variants [34,35].

Finally, which of the processing pathways APP follows depends on its subcellular localization as it can encounter the different secretases at different locations throughout the cell and the cell surface. Only a small proportion of APP is found on the cell surface, and over 50% is internalized within 10 minutes and sorted into early endosomes (reviewed by Zhang et al. [36]). BACE1 and APP interact predominantly in the early endosomes, while the α -secretase predominantly acts on the cell surface. Trafficking of APP is subjected to a number of different sorting and transporting proteins, among which members of the Vps10p-domain receptor family, Sortilins [37]. Removal of existing, aggregated A β has become a controversial therapeutic target, as promising antibody-based candidates show both negative (e.g. bapineuzumab in two phase 3 randomized trials; NCT00574132 and NCT00575055 [38]) as well positive results (e.g. aducanumab in the phase 1b randomized trial PRIME; NCT01677572 [39]) in clinical trials. As a result, general research interest should be and has been including modulation of A β production and aggregation via any of the targets within the APP processing pathways, be it the secretases themselves, the cleavage sites on the protein or sorting of the protein into more favorable compartments [40].

brain is still debated. Fragments of A β have been correlated to a variety of functions, including neurogenesis, pro-inflammatory response, long-term potentiation, and anti-microbial and anti-viral functions [41–46]. Indeed, soluble monomeric A β is not considered a threat for

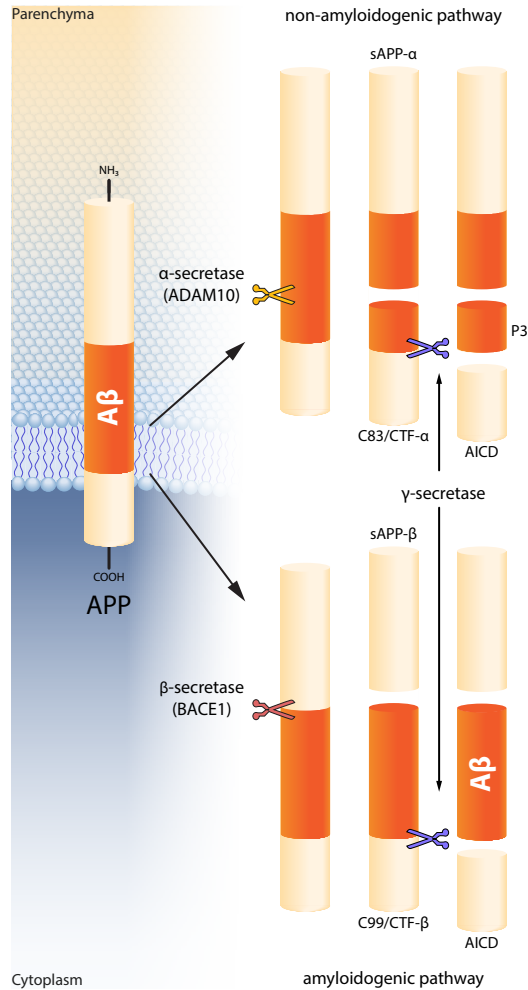


Figure 1.2. Amyloid precursor protein (APP) is a type 1 transmembrane protein with the majority of the protein exposed to the extracellular space, i.e. brain parenchyma in the case of neuronal expression. APP follows sequential cleavage in either the non-amyloidogenic pathway (top) or the amyloidogenic pathway (bottom). APP gets cleaved by either α -secretase (yellow scissors) or β -secretase (red scissors), releasing a soluble fragment called sAPP- α and sAPP- β respectively. The membrane-bound fraction then gets cleaved by the γ -secretase complex in either pathway. In the non-amyloidogenic pathway this second cleavage creates a P3 fragment and an APP Intracellular Domain (AICD). In the amyloidogenic pathway, the second cleavage releases the amyloid beta ($A\beta$) peptide, which eventually will aggregate into deposits in the brain parenchyma, in the *tunica media* of the vessel walls and around capillaries.

neuroviability; the problem arises when the peptide starts to self-aggregate. The longer $A\beta_{42}$ is much more prone to aggregation and is more abundant in the characteristic amyloid plaques found in AD, despite being produced significantly less than $A\beta_{40}$ [34,47]. The propensity of $A\beta_{42}$ to aggregate is influenced by the additional two amino acids on the C-terminus of the $A\beta_{42}$ peptide (i.e. I41 and A42) which make $A\beta_{42}$ both more hydrophobic and significantly more rigid than $A\beta_{40}$. The increased hydrophobicity favors aggregation to reduce exposure of the hydrophobic tail and the increased rigidity makes aggregation entropically affordable [48].

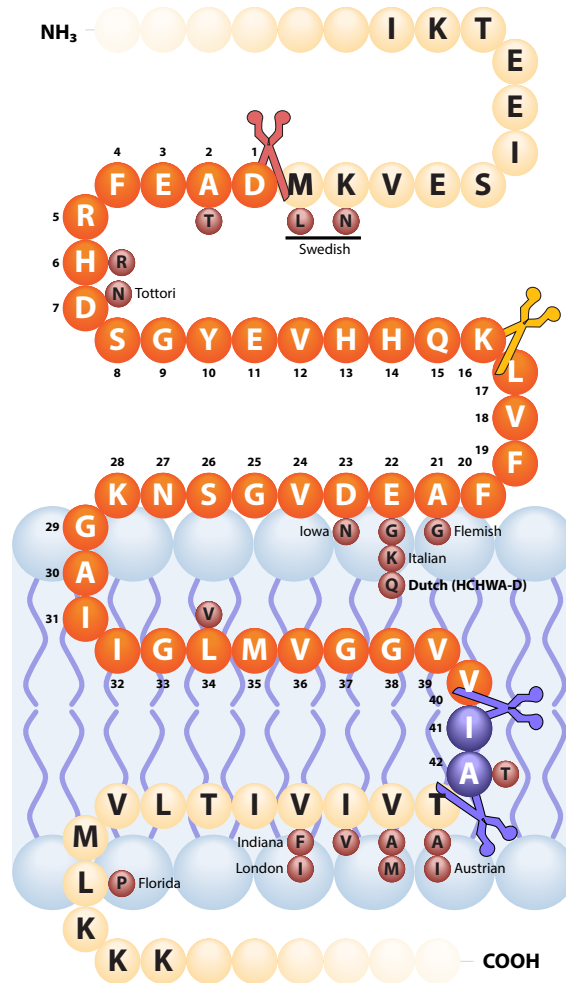


Figure 1.3. Mutations on the amyloid precursor protein (APP) in and around the 40-42 amino acid long A β fragment (indicated in orange) lead to altered processing of the transmembrane protein and can change the rate at which A β is formed, the ratio between A β ₄₀ and β ₄₂, and the propensity of the A β fragments to aggregate inside the brain. A few known point mutations are indicated by the smaller, red bubbles underneath the corresponding consensus sequence. The names next to a number of these mutations correspond to the location where the mutation was first described, or originates from, or to which location it is generally restricted. For example: E22Q corresponds to the mutation leading to HCHWA-D and both originates in, and is predominantly restricted to, a municipality in the Netherlands (i.e. Dutch). Numbering is based on the start of the A β fragment, immediately following the cleavage site for BACE1 (indicated by the red scissors), i.e. A β fragments start at D1. Calculated from the start of the most common form of APP, the A β fragment would start at D672. Yellow scissors indicate the cleavage site of α -secretase and blue scissors indicate two possible cleavage sites for the γ -secretase complex, leading to the production of A β ₄₀ and A β ₄₂. APP breaches the cellular membrane at the indicated locations, e.g. between K28 and G29. Not all known single nucleotide polymorphisms are indicated, and not all known nomenclature is supplied. Suggested secondary structure is not based on factual data and is solely designed to ensure proper fitment within the figure.

For almost three decades, aggregation and deposition of A β has been postulated as the initial causative event in the formation of Alzheimer's disease, a theory called the amyloid cascade hypothesis [49]. The many genetic variations found on the APP gene that cause altered APP

Box 1.2. APP genetics and HCHWA-D

The importance of A β in the development of AD is underlined by the presence of autosomal dominant genetic risk factors found on the genes for both APP and members of the γ -secretase complex [50]. A plethora of point mutations have been described for the APP gene, each having a slightly different effect on A β production and aggregation [51]: some increase total A β production by promoting cleavage by BACE1 over the α -secretase (e.g. Swedish mutation KM670/671NL [52]), some favor production of A β ₄₂ over A β ₄₀ (e.g. Leuven mutation E682K [53]), or the other way around (e.g. Italian mutation E693K [54]), some increase the propensity to form harmful aggregates and even one mutation has been found to be protective against aggregation of A β (i.e. A673T [55,56]), Figure 1.3. Also the other proteins involved in the formation of A β have been found to carry genetic risk factors. For example, over 180 point mutations have been described for the gene encoding for PS1, one of the members of the γ -secretase complex [51]. Most of these mutations, such as one leading to the deletion of exon 9 of PS1 [57], have clear pathogenic effects on AD formation. Many of these mutations have been introduced in mice in order to model for AD [58–60]. An example is the mouse model APP^{swe}/PS1^{dE9} (APP/PS1) [61]. The APP/PS1 mouse develops A β aggregates as early as 6 months of age, and shows signs of spatial and memory deficits at 12 months [62–64]. The APP/PS1 mouse model has been used as a model for the disease throughout the studies described in this thesis.

One mutation in APP, E693Q, leads to a variant of severe CAA with secondary haemorrhages and infarcts at a relatively early age of onset (40–50 years) [65–68]. This variant is called Hereditary Cerebral Haemorrhage With Amyloidosis – Dutch-type (HCHWA-D). HCHWA-D is found in a demographic mostly restricted to the coastal village Katwijk in the Netherlands. The A β peptide derived from this mutated APP (counting from the Asp1 cleavage site of BACE1, the mutation becomes E22Q in the A β peptide) is more prone to aggregation and more resistant to degradation by proteolytic enzymes compared to the wildtype variant [69–72]. Importantly, clearance from the brain into the blood stream at the cerebral vasculature is significantly less efficient for the E22Q-bearing A β peptide than for the wildtype variant [73]. This reduced clearance creates a permeation barrier in the BBB endothelium, which can explain why A β aggregation in HCHWA-D is predominantly found in the cerebral vasculature, rather than in the parenchyma [73,74]. Over the years, the Leiden University Medical Center and others have done much research into the etiology, the diagnosis and the possible treatments of particularly this variant of CAA [75] and in recent years The Dutch CAA Foundation has been initiated to increase public exposure and raise research funding for research into CAA in general and HCHWA-D in particular.

processing and lead directly to onset of familial hereditary AD variants, strongly corroborate the amyloid cascade hypothesis (see also Box 1.2. APP genetics and HCHWA-D).

Scientific focus on the amyloid cascade hypothesis has driven initial research into AD therapeutics mainly towards anti-A β applications [76]. Large-scale anti-A β antibody-based clinical trials have been started in the first decade of the 21st century and at least one of them, the solanezumab trial, showed that the use of antibodies may indeed mobilize A β (especially A β ₄₂) from amyloid plaques [77]. More recently, the PRIME study, a phase 1b clinical trial involving the antibody aducanumab directed specifically against aggregated A β , showed very promising dose- and time-dependent reduction of soluble and insoluble A β in the brains of patients with prodromal or mild AD [39]. However, other anti-A β antibody trails further down the clinical trial procedures, such as phase 3 bapineuzumab trials, did not improve clinical outcomes in patients with mild to moderate AD (NCT00574132; NCT00575055) [38,78]. The varying results

of the trials led to question the hypothesis and many agree that the original amyloid cascade hypothesis as linear causality is an oversimplification [40,79,80]. Nonetheless, A β remains the main target of high interest for pharmacological intervention [81]. As such, solanezumab continues to be tested as a promising therapeutic approach, specifically for patients with mild AD (ExpeditionPRO, NCT02760602)[82]. Also the PRIME study continued and started recruiting participants for the phase 3 clinical trial of aducanumab in 2016 (ENGAGE, NCT02477800 and EMERGE, NCT02484547). Furthermore, anti-A β therapeutics may be of pivotal importance in the fight against the familial hereditary AD variants, in which aberrant processing of APP as a result of mutations invariably leads to increased aggregation of A β accompanied by early onset dementia (i.e. onset < 65 years of age). For such applications phase 2 and phase 3 clinical trials have already started, using amongst others the anti-A β antibody solanezumab (DIAN-TU, NCT01760005) [83].

1.3. APP/PS1: a murine model for AD

Familial hereditary early onset AD (EOAD) is the result of mutations found on one or more of the main players in AD; such as APP and the various members of the γ -secretase complex, especially Presenilin 1 (PS1). The mutations that were found to lead to EOAD were not only pivotal in the basic research towards the etiology of AD, they also opened the path towards an impressive number of murine models for the disease. In this thesis one of the models, APP^{swe}/PS1^{Eg} (APP/PS1), has been used as mouse model for Alzheimer's disease. The APP/PS1 model has been well characterized over the years and has proven to be a robust model for rapid amyloid aggregation, although no hyperphosphorylated tau will be observed along the amyloid pathology. Amyloid depositions in the APP/PS1 mice begin to develop around six months of age, with abundant plaques in the hippocampus and cortex by nine months, and continue to increase up to around 12 months of age [63,84]. The mice develop not only parenchymal plaques, but also a CAA-like phenotype, with amyloid depositions in cerebral and meningeal blood vessel walls [85,86]. Furthermore, the mice present severe astrogliosis in the vicinity of the plaques around six months of age and the number of GFAP-positive cells, a marker for activated astrocytes, increases progressively with age [87]. Abnormal behavior of the mice has been reported extensively, but the severity and timing of the behavioral deficits strongly depend on which specific test has been used [88]. Contextual memory, spatial learning, and spontaneous behavior, such as nest-building, have all been reported to be impaired, starting anywhere from six to 12 months of age [88–91]. Interestingly, the APP/PS1 mouse model has a relatively high incidence of spontaneous epileptic seizures, starting at a relatively young age, and presenting in approximately 55% of the mice at an age of 4.5 months [92]. Studies regarding the blood-brain barrier (BBB) integrity in the APP/PS1 model are contradicting, suggesting

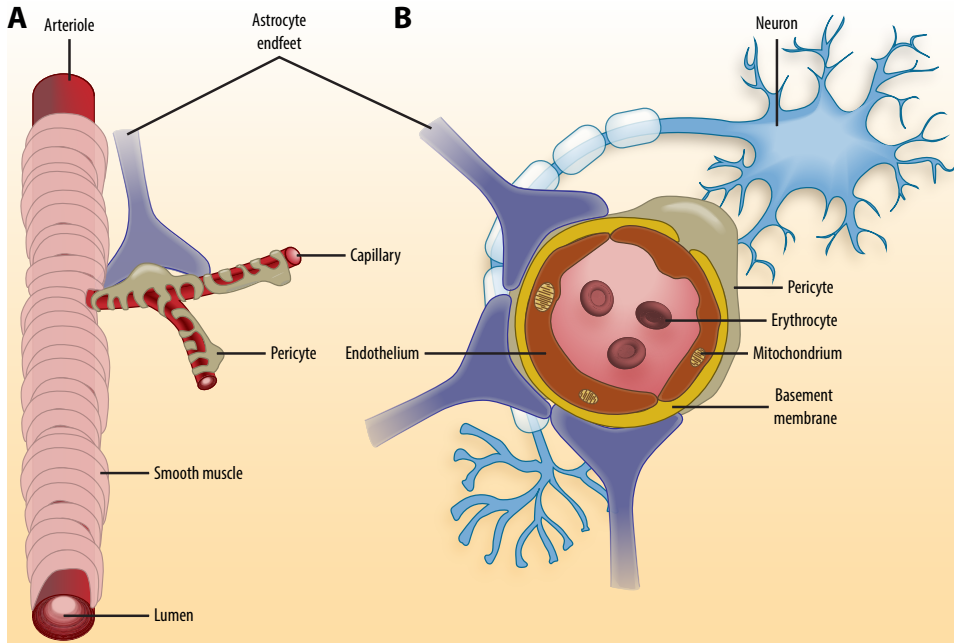


Figure 1.4. The blood brain barrier (BBB) is formed at the level of the capillary endothelium to separate the central nervous system from the bloodstream (A). Pericytes and endothelial cells are separated for the most part by the basement membrane, save from a few points of contact through which the pericytes can communicate directly with the endothelium. Astrocyte endfeet cover the pericyte, basement membrane and endothelium, contributing to the tight regulation of the BBB. Together they form the neurovascular unit, supplemented by microglia (not depicted) and service one or more nearby neurons in the brain (B). Figure modeled after data and figures from Zlokovic et al. [97] with permission by Cell Press and Hamilton et al. [98] under CC BY 4.0.

fundamental structural alterations at the interface between the brain and the blood, but often only minor permeability changes compared to wildtype [93–95].

1.4. The Blood-Brain Barrier

The BBB is the vascular barrier that separates the central nervous system (CNS) from the bloodstream and actively contributes to the maintenance of the crucial microenvironment of the brain parenchyma [96]. The BBB is formed by a tight network of highly polarized capillary endothelium, combined with pericytes, astrocyte endfeet, and the capillary basement membrane, Figure 1.4.

Tight and adherens junctions between adjacent endothelial cells close what normally would be the fenestræ; openings in the blood vessels that allow fast and efficient exchange of nutrients, macromolecules and circulating immune cells between the capillary bed and the organ [97]. Since there are no fenestræ at the blood-brain interface, permeability of the BBB is restricted to small lipid-soluble compounds with a molecular weight below 400 Da [99]. Larger compounds have to be actively transported; either via specialized influx and efflux transporters, or

via receptor- and adsorptive-mediated transcytosis [100]. The presence of the BBB is vital for the correct functioning of the brain; in virtually all human neurodegenerative disorders BBB disruption is evident to some degree, with corresponding changes in for example transporters and tight and adherens junctions [101], although it is hard to say whether BBB disruption or neurodegeneration starts first [97,102,103].

However, even an impaired BBB in an AD brain is still able to remove exogenous compounds, such as potential therapeutic drugs, out of the brain. This complicates the development of diagnostic, therapeutic and theragnostic compounds for neurodegenerative disorders significantly [104]. Any candidate, however promising during the developmental phase, will fail *in vivo* if brain delivery is needed but BBB passage not addressed. The development of *in vitro* blood-brain barrier models (for examples see references [105–108]) allowed for relatively high-throughput screening of possible compounds. One such a system, a static trans-well model with co-cultured astrocytes and bovine cerebral endothelial cells, was used to investigate the BBB passage propensity of a number of different llama derived heavy chain antibody fragments (VHH) directed against A β [109]. In these studies, the VHH showed promising *in vitro* BBB passage, depending strongly on the primary conformation of the N-terminus of the VHH. Unfortunately, this *in vitro* BBB passage observed for certain VHH could not be efficiently replicated *in vivo* in the APP/PS1 mouse model [85].

1.5. VHH: llama heavy chain only antibody fragments

A VHH is the variable domain of a heavy chain only antibody present in the blood of members of the camelid genus. In a serendipitous finding in 1989, a Belgian research group led by Dr. Hamers discovered seemingly incomplete circulating antibodies in the blood of camels. Next to the commonly known four-chain IgG antibodies, they found smaller antibodies composed only of one pair of heavy chain domains, lacking all light chain fragments [110]. In conventional heterodimeric IgG a heavy and a light chain variable domain (VH and VL, respectively) work together to form the antigen binding domain. The random association of the two domain repertoires allows for a great diversity of antigen recognition. However, in the llama heavy chain only antibodies (HCABs), as there is no light chain present, the N-terminal domain of the single heavy chain forms this antigen recognition domain independently [111]. Even when this domain is completely isolated from the rest of the molecule, the isolated fragment is capable of binding antigens with affinities similar or exceeding those of conventional antibodies [112,113]. This isolated llama antibody fragment is called VHH and is, with a molecular size of 12–15 kDa, the smallest naturally occurring antigen-binding unit currently known, Figure 1.5 A and B [114].

Isolation of the approximately 600 base pair (bp) single gene fragment encoding the VHH revealed that the VHH is made up by four conserved framework (FR) regions surrounding three

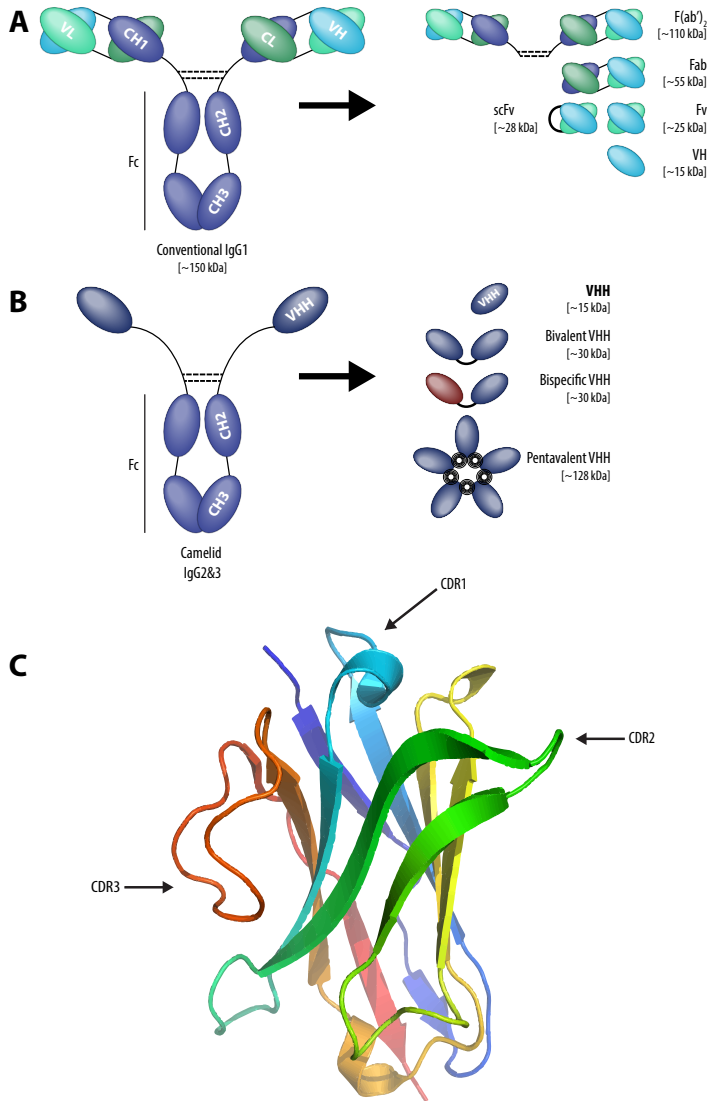


Figure 1.5. A variety of different antigen binding fragments can be derived from conventional (A) or heavy chain only (B) antibodies. The variable heavy chain, or antigen binding domain (VHH) of the camelid heavy chain only antibody is the smallest naturally occurring antigen-binding unit currently known. The VHH consists of four conserved frameworks separated by three complementary determining regions (CDR) (C). The third CDR loop is elongated in VHH, compared to conventional heavy chain fragments, and attribute to the special characteristics of VHH. Part C is modeled after publicly available work by S. Jähnichen on commons.wikimedia.org, based on crystal structure data from PDB (1I3V).

hypervariable (HV) regions. When the protein is folded, these HV regions form three loops that stick out of the antibody fragment and form the complementary-determining regions (CDR) of the VHH. The sequence within the loops is highly variable; while the length of loops 1 and 2 is quite restricted, loop 3 is significantly extended, especially in the dromedary derived VHH [115–117], Figure 1.5 C. This extended loop, stabilized by interloop disulfide bonds [118], allows

the VHH to enter hard-to-reach epitopes, such as the active sites of enzymes, which are often hidden for conventional antibodies [119–123]. As a result, VHH have become a very successful class of therapeutics, with applications ranging from interference with enzymatic active sites leading to neutralization of toxins [124–126], viruses [127,128], and fungi [129], blocking of apoptotic pathways in autoimmune diseases [130] and preventing aberrant protein aggregation [131], to binding spatially different A β depositions [75]. Other reported applications for VHH include early clinical diagnostics of rheumatoid arthritis, and affinity purification of conventional IgG [132,133].

Selection of the desired VHH is generally done through phage-display techniques [134,135]. In phage-display a fragment of interest, the VHH in this case, is expressed on the outside of a phage particle and is usually selected through various panning rounds of binding to exposed antigen epitopes [136,137]. Because the VHH is encoded by a single gene fragment of only 600 bp, genetic handling and modifications are relatively easily performed. As such, cloning of isolated VHH cDNA into phagemid vectors is rather straightforward and ensures easy construction of VHH-phage libraries. It has been done for naive [138,139], immunized [140,141] and (semi-)synthetic libraries [142,143]. The llama-derived VHH described in this thesis have been derived from both naive libraries (e.g. VHH-ni3A) and immunized libraries (e.g. VHH-pa2H). For the immunized libraries, llama immunization was performed using either vascular brain tissue from an HCHWA-D patient, supplemented with recombinant A β ₄₂ or alternatively, grey matter brain parenchyma from a Down syndrome patient with extensive plaque formation; strategies chosen to enrich the repertoire of amyloid-specific antibodies in the libraries [75,135,144]. As mentioned earlier, the obtained VHH showed remarkable A β recognition and some showed promising results in an *in vitro* BBB model, however, single tail-vein injections of the VHH in APP/PS1 mice failed to show sufficient delivery of the VHH into the brain [85,109].

1.6. Brain delivery of VHH

To develop VHH as useful tools to detect and fight neurodegeneration, efficient delivery into the brain is required. While VHH, at 12–15 kDa, are too big to passively diffuse over the BBB, various VHH have found to transmigrate over the BBB nonetheless. Specific and stringent selection yielded VHH that cross the BBB *in vivo* via receptor-mediated transcytosis, e.g. VHH FC5 [145,146], but also other VHH have been found to cross the BBB either *in vitro* or *in vivo* [109,147]. However, not every VHH is able to cross the BBB, and slight changes in the amino acid composition of the antibody fragments may drastically change their crossing propensity [109]. In general, it seems that a high isoelectric point (pI) is favorable for BBB passage [148].

The small size of VHH results in very rapid clearance by the renal system [85]. When VHH pa-2H, selected against A β , is injected the APP/PS1 mouse model for AD, the VHH will show a

blood half-life of approximately 15-20 minutes [85] (and this thesis). The short blood half-life is also found for other peripherally injected VHH [149–152], and suggests that BBB passage can be hampered by the relatively short time that the VHH have to interact with the BBB *in vivo*. To increase the passage, and make VHH suitable for neurological applications, certain adaptations must be considered.

Examples of such adaptations can be found in research pertaining to brain delivery of other small molecules and proteins. They include direct cranial delivery via invasive injection methods, increasing blood half-life by prevention of renal clearance, and targeting the molecule to bind BBB transporters, and in the case of smaller proteins, gene therapy may be used as a delivery method. Direct cranial delivery has been performed via intracisternal injection [153], lumbar spinal injection [154,155], and direct topical application to exposed parenchyma [85], however, the procedure is often excessively invasive. Prevention of renal clearance can be obtained by increasing the size of the protein above the renal cut-off of (i.e. ≥ 65 kDa), e.g. via polymerization, PEGylation, or pentamerization [156,157], however, the method used to increase the protein in size may alter the characteristics of the protein itself, including physically impairing BBB passage due to its increased circumference. Continuous vascular infusion may help to keep blood levels of the protein at acceptable heights without altering the structure, but require significantly more amounts of the protein, production of which may not necessarily be practical or economically feasible [158,159]. To circumvent both alterations of the protein and unfavorable production requirements, the protein can be encapsulated in liposomes, which even can be targeted to the BBB directly. However, encapsulation has generally been limited to small, non-biological molecules and drug compounds [160–163].

In this thesis, four different methods of brain delivery of VHH have been explored: direct intracisternal injection, encapsulation in BBB targeted liposomes, fusion to a human IgG1-Fc-tail, and a gene therapy approach using Adeno Associated Virus (AAV).

1.7. Intracisternal injection of VHH to enter the brain

The method of direct intracisternal injection has been chosen to circumvent all delivery uncertainties, in order to proof the concept of functional VHH having a physiological effect in the murine brain. The method involves delivering a small amount (i.e. $\leq 10 \mu\text{l}$ at 7.5 mg/ml) of VHH into the cisterna magna, or fourth ventricle, via a percutaneous bolus injection. To follow its biodistribution in the living animals, the VHH was labeled with an infrared dye and the injected mice were imaged for up to two days in an *in vivo* optical small animal imaging system.

1.8. Liposomal encapsulation of VHH to target the BBB

The second method explored in this thesis is that of encapsulation of VHH in glutathione targeted liposomes, denoted G-technology [164,165]. The use of glutathione on the outside of liposomes targets the particle to the BBB, where the VHH carried inside the particle, will be delivered to the parenchyma. To follow the biodistribution of liposomal deliveries, conventionally the liposomes are radiolabeled, with for example the radioactive tracer Indium-111 (¹¹¹In) [166]. In the approach in this thesis, however, we opted to radiolabel the VHH itself, in order to truly determine the delivery of the internally carried payload into the brain. In order to increase shelf-life of the liposomal encapsulated VHH formulations, a novel radiolabeling protocol was developed to radiolabel the VHH after encapsulation.

1.9. IgG1-Fc fusion of VHH to prolong blood half life

To explore the effect of prolonged blood retention on the BBB passage of the VHH, the third delivery method involved the fusion of an Fc fragment to the VHH. In this method the VHH is complemented with the heavy chain crystallizable fragments 1 and 2 (CH1 and CH2) plus the hinge area, of a conventional human IgG1 [167]. By doing so, the reported rapid renal clearance could be prevented via two separate pathways. First of all, due to the Fc's inherent dimeric nature, the addition of an Fc-tail to the VHH causes the fusion protein to dimerize, increasing the size beyond the renal cut-off of 65 kDa (the dimeric VHH-Fc will become approximately 80 kDa in size). Secondly, presence of the Fc-tail allows interaction with the neonatal Fc receptor (FcRn), promoting recycling of the construct in the periphery [168–171]. The effect of Fc-fusion on BBB passage is a method that has not often been investigated for llama antibody fragments. Once again, biodistribution of the VHH-Fc construct was followed via In¹¹¹ labeling.

1.10. Gene therapy to express VHH directly inside the brain

Finally, as VHH are transcribed from a single, 600 bp stretch of DNA, it is possible to employ genetic strategies to deliver the VHH at the site of interest. A DNA fragment of 600 bp easily fits in any viral vector, including the Adeno-Associated Virus (AAV) [172], which is known to efficiently transduce neurons after intracerebral injection, without eliciting an immunological response from either mouse models or human patients [173–175]. Depending on the packaging of the viral particle, antibody fragments can be expressed from virtually any desired location, both peripherally [176], and within the CNS [177,178]. By delivering the VHH as a gene-fragment directly to the neuronal cells in the APP/PS1 mice, a unique situation was created in which it was possible to follow the effect of the VHH on for example amyloid burden over a very long period of time, without the need for repeated injections or other interventions. To make optimal use of this situation, Emerald GFP (EmGFP: an exceedingly bright Green Fluorescent Protein)

was fused to the C-terminus of the VHH, allowing, in combination with intravital multi-photon microscopy through a cranial window, for the real-time longitudinal monitoring of expression, distribution and therapeutic efficacy of the VHH in living mice.

AIM AND OUTLINE OF THIS THESIS

This thesis is aimed at the development of VHH as therapeutic tools for neurodegenerative diseases with intracranial A β aggregation, such as AD, CAA and HCHWA-D, with a specific focus on the delivery of VHH to the brain.

Chapter 2 describes how the use of VHH can influence the production of A β in effort to reduce the amyloid burden in the brain. The chapter serves as a proof of principle that when the right VHH is applied at the correct location, the course of the disease might be modified. However, as safe, non-invasive and sustained delivery of compounds, including VHH, across the BBB is a hurdle not to be underestimated, the remainder of the thesis is focused on various methods of cranial delivery of VHH, in particular of VHH-pa2H. **Chapter 3** describes how encapsulation of VHH-pa2H in glutathione targeted liposomes significantly increases BBB penetration. **Chapter 4** shows that addition of a human IgG1-Fc tail to the VHH increases the time that the compound stays in the blood, but does not help to transfer the VHH across the BBB. Finally, in **chapter 5** the VHH is expressed directly in the brain. Here, AAV is used as a basis for viral gene therapy delivery. With the presented work in this thesis, a foundation is laid down for delivery of VHH to the brain.

REFERENCES

1. Prince, M., Prina, M. & Guerchet, M. World Alzheimer Report 2013. Alzheimer's Disease International (2013).
2. Prince, M., Albanese, E., Guerchet, M. & Prina, M. World Alzheimer Report 2014. Alzheimer's Disease International (2014).
3. Ellis, R. J., Olichney, J. M., Thal, L. J., Mirra, S. S., Morris, J. C., Beekly, D. & Heyman, A. Cerebral amyloid angiopathy in the brains of patients with Alzheimer's disease: the CERAD experience, Part XV. *Neurology* 46(6):1592–1596 (1996).
4. Richard, E., Carrano, A., Hoozemans, J. J., van Horsen, J., van Haastert, E. S., Eurelings, L. S., de Vries, H. E., Thal, D. R., Eikelenboom, P., van Gool, W. a, et al. Characteristics of dyschoric capillary cerebral amyloid angiopathy. *J. Neuropathol. Exp. Neurol.* 69(11):1158–67 (2010).
5. Carrano, A., Hoozemans, J. J. M., van der Vies, S. M., Rozemuller, A. J. M., van Horsen, J. & de Vries, H. E. Amyloid Beta induces oxidative stress-mediated blood-brain barrier changes in capillary amyloid angiopathy. *Antioxid. Redox Signal.* 15(5):1167–1178 (2011).
6. Thal, D. R., Von Arnim, C., Griffin, W. S. T., Yamaguchi, H., Mrak, R. E., Attems, J. & Uphadaya, A. R. Pathology of clinical and preclinical alzheimer's disease. *Eur. Arch. Psychiatry Clin. Neurosci.* 263(SUPPL.2):S137-45 (2013).
7. Ballard, C., Gauthier, S., Corbett, A., Brayne, C., Aarsland, D. & Jones, E. Alzheimer's disease. *Lancet* 377(9770):1019–1031 (2011).
8. Jack, C. R., Knopman, D. S., Jagust, W. J., Shaw, L. M., Aisen, P. S., Weiner, M. W., Petersen, R. C. & Trojanowski, J. Q. Hypothetical model of dynamic biomarkers of the Alzheimer's pathological cascade. *Lancet Neurol.* 9(1):119–128 (2010).
9. Frisoni, G. B., Fox, N. C., Jack, C. R., Scheltens, P. & Thompson, P. M. The clinical use of structural MRI in Alzheimer disease. *Nat. Rev. Neurol.* 6(2):67–77 (2010).
10. Jack, C. R., Knopman, D. S., Jagust, W. J., Petersen, R. C., Weiner, M. W., Aisen, P. S., Shaw, L. M., Vemuri, P., Wiste, H. J., Weigand, S. D., et al. Tracking pathophysiological processes in Alzheimer's disease: An updated hypothetical model of dynamic biomarkers. *Lancet Neurol.* 12(2):207–216 (2013).
11. Villemagne, V. L., Burnham, S., Bourgeat, P., Brown, B., Ellis, K. a, Salvado, O., Szoek, C., Macaulay, S. L., Martins, R., Maruff, P., et al. Amyloid β deposition, neurodegeneration, and cognitive decline in sporadic Alzheimer's disease: a prospective cohort study. *Lancet Neurol.* 12(4):357–67 (2013).
12. Zhang, H., Ma, Q., Zhang, Y. & Xu, H. Proteolytic processing of Alzheimer's β -amyloid precursor protein. *J. Neurochem.* 120 Suppl:9–21 (2012).
13. Tanzi, R. E., Gusella, J. F., Watkins, P. C., Bruns, G. A., St George-Hyslop, P., Van Keuren, M. L., Patterson, D., Pagan, S., Kurnit, D. M. & Neve, R. L. Amyloid beta protein gene: cDNA, mRNA distribution, and genetic linkage near the Alzheimer locus. *Science* 235(4791):880–4 (1987).
14. Kojro, E. & Fahrenholz, F. The non-amyloidogenic pathway: structure and function of alpha-secretases. *Subcell. Biochem.* 38:105–27 (2005).
15. Lammich, S., Kojro, E., Postina, R., Gilbert, S., Pfeiffer, R., Jasionowski, M., Haass, C. & Fahrenholz, F. Constitutive and regulated alpha-secretase cleavage of Alzheimer's amyloid precursor protein by a disintegrin metalloprotease. *Proc. Natl. Acad. Sci. U. S. A.* 96(7):3922–7 (1999).
16. Agostinho, P., Pliássova, A., Oliveira, C. R. & Cunha, R. A. Localization and Trafficking of Amyloid- β Protein Precursor and Secretases: Impact on Alzheimer's Disease. *J. Alzheimers. Dis.* 45(2):329–47 (2015).
17. Chow, V. W., Mattson, M. P., Wong, P. C. & Gleichmann, M. An overview of APP processing enzymes and products. *Neuromolecular Med.* 12(1):1–12 (2010).
18. Vincent, B. Regulation of the α -secretase ADAM10 at transcriptional, translational and post-translational levels. *Brain Res. Bull.* (2016). doi:10.1016/j.brainresbull.2016.03.020

19. Lannfelt, L., Basun, H., Wahlund, L. O., Rowe, B. A. & Wagner, S. L. Decreased alpha-secretase-cleaved amyloid precursor protein as a diagnostic marker for Alzheimer's disease. *Nat. Med.* 1(8):829–32 (1995).
20. Sherrington, R., Rogaev, E. I., Liang, Y., Rogaeva, E. A., Levesque, G., Ikeda, M., Chi, H., Lin, C., Li, G., Holman, K., et al. Cloning of a gene bearing missense mutations in early-onset familial Alzheimer's disease. *Nature* 375(6534):754–60 (1995).
21. Levy-Lahad, E., Wasco, W., Poorkaj, P., Romano, D. M., Oshima, J., Pettingell, W. H., Yu, C. E., Jondro, P. D., Schmidt, S. D. & Wang, K. Candidate gene for the chromosome 1 familial Alzheimer's disease locus. *Science* 269(5226):973–7 (1995).
22. Rogaev, E. I., Sherrington, R., Rogaeva, E. A., Levesque, G., Ikeda, M., Liang, Y., Chi, H., Lin, C., Holman, K. & Tsuda, T. Familial Alzheimer's disease in kindreds with missense mutations in a gene on chromosome 1 related to the Alzheimer's disease type 3 gene. *Nature* 376(6543):775–8 (1995).
23. De Strooper, B., Aph-1, Pen-2, and Nicastrin with Presenilin generate an active gamma-Secretase complex. *Neuron* 38(1):9–12 (2003).
24. Postina, R. Activation of α -secretase cleavage. *J. Neurochem.* 120 Suppl:46–54 (2012).
25. Roncarati, R., Sestan, N., Scheinfeld, M. H., Berechid, B. E., Lopez, P. A., Meucci, O., McGlade, J. C., Rakic, P. & D'Adamio, L. The gamma-secretase-generated intracellular domain of beta-amyloid precursor protein binds Numb and inhibits Notch signaling. *Proc. Natl. Acad. Sci. U. S. A.* 99(10):7102–7 (2002).
26. Sinha, S., Anderson, J. P., Barbour, R., Basl, G. S., Caccavello, R., Davis, D., Doan, M., Dovey, H. F., Frigon, N., Hong, J., et al. Purification and cloning of amyloid precursor protein beta-secretase from human brain. *Nature* 402(6761):537–540 (1999).
27. Vassar, R., Bennett, B. D., Babu-Khan, S., Kahn, S., Mendiaz, E. a, Denis, P., Teplow, D. B., Ross, S., Amarante, P., Loeloff, R., et al. Beta-secretase cleavage of Alzheimer's amyloid precursor protein by the transmembrane aspartic protease BACE. *Science* 286(5440):735–741 (1999).
28. Yan, R., Bienkowski, M. J., Shuck, M. E., Miao, H., Tory, M. C., Pauley, a M., Brashier, J. R., Stratman, N. C., Mathews, W. R., Buhl, a E., et al. Membrane-anchored aspartyl protease with Alzheimer's disease beta-secretase activity. *Nature* 402(6761):533–537 (1999).
29. Lin, X., Koelsch, G., Wu, S., Downs, D., Dashti, a & Tang, J. Human aspartic protease memapsin 2 cleaves the beta-secretase site of beta-amyloid precursor protein. *Proc. Natl. Acad. Sci. U. S. A.* 97(4):1456–1460 (2000).
30. Deng, Y., Wang, Z., Wang, R., Zhang, X., Zhang, S., Wu, Y., Staufienbiel, M., Cai, F. & Song, W. Amyloid- β protein (A β) Glu1 is the major β -secretase site of β -site amyloid- β precursor protein-cleaving enzyme 1(BACE1), and shifting the cleavage site to A β Asp1 contributes to Alzheimer pathogenesis. *Eur. J. Neurosci.* 37(12):1962–9 (2013).
31. Qi-Takahara, Y., Morishima-Kawashima, M., Tanimura, Y., Dolios, G., Hirofumi, N., Horikoshi, Y., Kametani, F., Maeda, M., Saido, T. C., Wang, R., et al. Longer forms of amyloid beta protein: implications for the mechanism of intramembrane cleavage by gamma-secretase. *J. Neurosci.* 25(2):436–45 (2005).
32. Zhao, G., Cui, M.-Z., Mao, G., Dong, Y., Tan, J., Sun, L. & Xu, X. gamma-Cleavage is dependent on zeta-cleavage during the proteolytic processing of amyloid precursor protein within its transmembrane domain. *J. Biol. Chem.* 280(45):37689–97 (2005).
33. Takami, M., Nagashima, Y., Sano, Y., Ishihara, S., Morishima-Kawashima, M., Funamoto, S. & Ihara, Y. gamma-Secretase: successive tripeptide and tetrapeptide release from the transmembrane domain of beta-carboxyl terminal fragment. *J. Neurosci.* 29(41):13042–52 (2009).
34. Gravina, S. A., Ho, L., Eckman, C. B., Long, K. E., Otvos, L., Younkin, L. H., Suzuki, N. & Younkin, S. G. Amyloid beta protein (A beta) in Alzheimer's disease brain. Biochemical and immunocytochemical analysis with antibodies specific for forms ending at A beta 40 or A beta 42(43). *J. Biol. Chem.* 270(13):7013–6 (1995).
35. Suzuki, N., Cheung, T. T., Cai, X. D., Odaka, A., Otvos, L., Eckman, C., Golde, T. E. & Younkin, S. G. An increased percentage of long amyloid beta protein secreted by familial amyloid beta protein precursor (beta APP717) mutants. *Science* 264(5163):1336–40 (1994).

36. Zhang, X. & Song, W. The role of APP and BACE_i trafficking in APP processing and amyloid- β generation. *Alzheimers. Res. Ther.* 5(5):46 (2013).
37. Gustafsen, C., Glerup, S., Palleisen, L. T., Olsen, D., Andersen, O. M., Nykjær, A., Madsen, P. & Petersen, C. M. Sortilin and SorLA display distinct roles in processing and trafficking of amyloid precursor protein. *J. Neurosci.* 33(1):64–71 (2013).
38. Salloway, S., Sperling, R., Fox, N. C., Blennow, K., Klunk, W., Raskind, M., Sabbagh, M., Honig, L. S., Porsteinsson, A. P., Ferris, S., et al. Two phase 3 trials of bapineuzumab in mild-to-moderate Alzheimer's disease. *N. Engl. J. Med.* 370(4):322–33 (2014).
39. Sevigny, J., Chiao, P., Bussière, T., Weinreb, paul H., Williams, L., Maier, M., Dunstan, R., Salloway, S., Chen, T., Ling, Y., et al. The antibody aducanumab reduces A β plaques in Alzheimer's disease. *Nature* 537(7618):50–6 (2016).
40. Scheltens, P., Blennow, K., Breteler, M. M. B., de Strooper, B., Frisoni, G. B., Salloway, S. & Van der Flier, W. M. Alzheimer's disease. *Lancet (London, England)* 388(10043):505–17 (2016).
41. Struble, R. G., Ala, T., Patrylo, P. R., Brewer, G. J. & Yan, X.-X. Is brain amyloid production a cause or a result of dementia of the Alzheimer's type? *J. Alzheimers. Dis.* 22(2):393–9 (2010).
42. Chen, Y. & Dong, C. Abeta₄₀ promotes neuronal cell fate in neural progenitor cells. *Cell Death Differ.* 16(3):386–94 (2009).
43. Kumar, D. K. V., Choi, S. H., Washicosky, K. J., Eimer, W. A., Tucker, S., Ghofrani, J., Lefkowitz, A., McColl, G., Goldstein, L. E., Tanzi, R. E., et al. Amyloid- peptide protects against microbial infection in mouse and worm models of Alzheimer's disease. *Sci. Transl. Med.* 8(340):340ra72–340ra72 (2016).
44. Bourgade, K., Le Page, A., Bocti, C., Witkowski, J. M., Dupuis, G., Frost, E. H. & Fülöp, T. Protective Effect of Amyloid- β Peptides Against Herpes Simplex Virus-1 Infection in a Neuronal Cell Culture Model. *J. Alzheimers. Dis.* 50(4):1227–41 (2016).
45. Plant, L. D., Boyle, J. P., Smith, I. F., Peers, C. & Pearson, H. a. The production of amyloid beta peptide is a critical requirement for the viability of central neurons. *J. Neurosci.* 23(13):5531–5535 (2003).
46. Puzzo, D., Privitera, L., Leznik, E., Fà, M., Staniszewski, A., Palmeri, A. & Arancio, O. Picomolar amyloid-beta positively modulates synaptic plasticity and memory in hippocampus. *J. Neurosci.* 28(53):14537–45 (2008).
47. Roher, A. E., Lowenson, J. D., Clarke, S., Woods, A. S., Cotter, R. J., Gowing, E. & Ball, M. J. beta-Amyloid-(1-42) is a major component of cerebrovascular amyloid deposits: implications for the pathology of Alzheimer disease. *Proc. Natl. Acad. Sci. U. S. A.* 90(22):10836–40 (1993).
48. Yan, Y. & Wang, C. Abeta₄₂ is more rigid than Abeta₄₀ at the C terminus: implications for Abeta aggregation and toxicity. *J. Mol. Biol.* 364(5):853–62 (2006).
49. Hardy, J. A. & Higgins, G. A. Alzheimer's disease: the amyloid cascade hypothesis. *Science* 256(5054):184–5 (1992).
50. Bertram, L., Lill, C. M. & Tanzi, R. E. The genetics of Alzheimer disease: back to the future. *Neuron* 68(2):270–81 (2010).
51. Bertram, L., McQueen, M. B., Mullin, K., Blacker, D. & Tanzi, R. E. Systematic meta-analyses of Alzheimer disease genetic association studies: the AlzGene database. *Nat. Genet.* 39(1):17–23 (2007).
52. Mullan, M., Crawford, F., Axelman, K., Houlden, H., Lilius, L., Winblad, B. & Lannfelt, L. A pathogenic mutation for probable Alzheimer's disease in the APP gene at the N-terminus of beta-amyloid. *Nat. Genet.* 1(5):345–7 (1992).
53. Zhou, L., Brouwers, N., Benilova, I., Vandersteen, A., Mercken, M., Van Laere, K., Van Damme, P., Demedts, D., Van Leuven, F., Sleegers, K., et al. Amyloid precursor protein mutation E682K at the alternative β -secretase cleavage β -site increases A β generation. *EMBO Mol. Med.* 3(5):291–302 (2011).
54. Bugiani, O., Giaccone, G., Rossi, G., Mangieri, M., Capobianco, R., Morbin, M., Mazzoleni, G., Cupidi, C., Marcon, G., Giovagnoli, A., et al. Hereditary cerebral hemorrhage with amyloidosis associated with the E693K mutation of APP. *Arch. Neurol.* 67(8):987–95 (2010).
55. Peacock, M. L., Warren, J. T., Roses, A. D. & Fink, J. K. Novel polymorphism in the A4 region of the amyloid precursor protein gene in a patient without Alzheimer's disease. *Neurology* 43(6):1254–6 (1993).

56. Jonsson, T., Atwal, J. K., Steinberg, S., Snaedal, J., Jonsson, P. V., Bjornsson, S., Stefansson, H., Sulem, P., Gudbjartsson, D., Maloney, J., et al. A mutation in APP protects against Alzheimer's disease and age-related cognitive decline. *Nature* 488(7409):96–9 (2012).
57. Crook, R., Verkkoniemi, A., Perez-Tur, J., Mehta, N., Baker, M., Houlden, H., Farrer, M., Hutton, M., Lincoln, S., Hardy, J., et al. A variant of Alzheimer's disease with spastic paraparesis and unusual plaques due to deletion of exon 9 of presenilin 1. *Nat. Med.* 4(4):452–5 (1998).
58. Chin, J. Selecting a mouse model of Alzheimer's disease. *Methods Mol. Biol.* 670:169–89 (2011).
59. Puzzo, D., Gulisano, W., Palmeri, A. & Arancio, O. Rodent models for Alzheimer's disease drug discovery. *Expert Opin. Drug Discov.* 10(7):703–11 (2015).
60. Onos, K. D., Sukoff Rizzo, S. J., Howell, G. R. & Sasner, M. Toward more predictive genetic mouse models of Alzheimer's disease. *Brain Res. Bull.* 122:1–11 (2016).
61. Reiserer, R. S., Harrison, F. E., Syverud, D. C. & McDonald, M. P. Impaired spatial learning in the APPSwe + PSEN1DeltaEg bigenic mouse model of Alzheimer's disease. *Genes. Brain. Behav.* 6(1):54–65 (2007).
62. Jankowsky, J. L., Slunt, H. H., Ratovitski, T., Jenkins, N. a, Copeland, N. G. & Borchelt, D. R. Co-expression of multiple transgenes in mouse CNS: a comparison of strategies. *Biomol. Eng.* 17(6):157–65 (2001).
63. Garcia-Alloza, M., Robbins, E. M., Zhang-Nunes, S. X., Purcell, S. M., Betensky, R. A., Raju, S., Prada, C., Greenberg, S. M., Bacskai, B. J. & Frosch, M. P. Characterization of amyloid deposition in the APPSwe/PS1dEg mouse model of Alzheimer disease. *Neurobiol. Dis.* 24(3):516–524 (2006).
64. Yan, P., Bero, A. W., Cirrito, J. R., Xiao, Q., Hu, X., Wang, Y., Gonzales, E., Holtzman, D. M. & Lee, J.-M. Characterizing the appearance and growth of amyloid plaques in APP/PS1 mice. *J. Neurosci.* 29(34):10706–14 (2009).
65. van Duinen, S. G., Castaño, E. M., Prelli, F., Bots, G. T., Luyendijk, W. & Frangione, B. Hereditary cerebral hemorrhage with amyloidosis in patients of Dutch origin is related to Alzheimer disease. *Proc. Natl. Acad. Sci. U. S. A.* 84(16):5991–5994 (1987).
66. Levy, E., Carman, M. D., Fernandez-Madrid, I. J., Power, M. D., Lieberburg, I., van Duinen, S. G., Bots, G. T., Luyendijk, W. & Frangione, B. Mutation of the Alzheimer's disease amyloid gene in hereditary cerebral hemorrhage, Dutch type. *Science* 248(4959):1124–6 (1990).
67. Van Broeckhoven, C., Haan, J., Bakker, E., Hardy, J. A., Van Hul, W., Wehnert, A., Vegter-Van der Vlis, M. & Roos, R. A. Amyloid beta protein precursor gene and hereditary cerebral hemorrhage with amyloidosis (Dutch). *Science* 248(4959):1120–2 (1990).
68. Fernandez-Madrid, I., Levy, E., Marder, K. & Frangione, B. Codon 618 variant of Alzheimer amyloid gene associated with inherited cerebral hemorrhage. *Ann. Neurol.* 30(5):730–3 (1991).
69. Wisniewski, T., Ghiso, J. & Frangione, B. Peptides homologous to the amyloid protein of Alzheimer's disease containing a glutamine for glutamic acid substitution have accelerated amyloid fibril formation. *Biochem. Biophys. Res. Commun.* 179(3):1247–54 (1991).
70. Clements, A., Walsh, D. M., Williams, C. H. & Allsop, D. Effects of the mutations Glu22 to Gln and Ala21 to Gly on the aggregation of a synthetic fragment of the Alzheimer's amyloid beta/A4 peptide. *Neurosci. Lett.* 161(1):17–20 (1993).
71. Fabian, H., Szendrei, G. I., Mantsch, H. H. & Otvos, L. Comparative analysis of human and Dutch-type Alzheimer beta-amyloid peptides by infrared spectroscopy and circular dichroism. *Biochem. Biophys. Res. Commun.* 191(1):232–9 (1993).
72. Tsubuki, S., Takaki, Y. & Saido, T. C. Dutch, Flemish, Italian, and Arctic mutations of APP and resistance of Aβeta to physiologically relevant proteolytic degradation. *Lancet* 361(9373):1957–8 (2003).
73. Monro, O. R., Mackic, J. B., Yamada, S., Segal, M. B., Ghiso, J., Maurer, C., Calero, M., Frangione, B. & Zlokovic, B. V. Substitution at codon 22 reduces clearance of Alzheimer's amyloid-beta peptide from the cerebrospinal fluid and prevents its transport from the central nervous system into blood. *Neurobiol. Aging* 23(3):405–412 (2002).

74. Agyare, E. K., Leonard, S. R., Curran, G. L., Yu, C. C., Lowe, V. J., Paravastu, A. K., Poduslo, J. F. & Kandimalla, K. K. Traffic jam at the blood-brain barrier promotes greater accumulation of Alzheimer's disease amyloid- β proteins in the cerebral vasculature. *Mol. Pharm.* 10(5):1557–65 (2013).
75. Rutgers, K. S., van Remoortere, A., van Buchem, M. A., Verrips, C. T., Greenberg, S. M., Bacsikai, B. J., Frosch, M. P., van Duinen, S. G., Maat-Schieman, M. L. & Van der Maarel, S. M. Differential recognition of vascular and parenchymal beta amyloid deposition. *Neurobiol. Aging* 32(10):1774–1783 (2009).
76. Karran, E., Mercken, M. & Strooper, B. De. The amyloid cascade hypothesis for Alzheimer's disease: an appraisal for the development of therapeutics. *Nat. Rev. Drug Discov.* 10(September) (2011).
77. Farlow, M., Arnold, S. E., van Dyck, C. H., Aisen, P. S., Snider, B. J., Porsteinsson, A. P., Friedrich, S., Dean, R. A., Gonzales, C., Sethuraman, G., et al. Safety and biomarker effects of solanezumab in patients with Alzheimer's disease. *Alzheimers. Dement.* 8(4):261–71 (2012).
78. Vandenberghe, R., Rinne, J. O., Boada, M., Katayama, S., Scheltens, P., Vellas, B., Tuchman, M., Gass, A., Fiebich, J. B., Hill, D., et al. Bapineuzumab for mild to moderate Alzheimer's disease in two global, randomized, phase 3 trials. *Alzheimers. Res. Ther.* 8(1):18 (2016).
79. Reitz, C. Alzheimer's disease and the amyloid cascade hypothesis: a critical review. *Int. J. Alzheimers. Dis.* 2012:369808 (2012).
80. Tayeb, H. O., Murray, E. D., Price, B. H. & Tarazi, F. I. Bapineuzumab and solanezumab for Alzheimer's disease: is the 'amyloid cascade hypothesis' still alive? *Expert Opin. Biol. Ther.* 13(7):1075–84 (2013).
81. Mohamed, T., Shakeri, A. & Rao, P. P. N. Amyloid cascade in Alzheimer's disease: Recent advances in medicinal chemistry. *Eur. J. Med. Chem.* 113:258–272 (2016).
82. Siemers, E. R., Sundell, K. L., Carlson, C., Case, M., Sethuraman, G., Liu-Seifert, H., Dowsett, S. A., Pontecorvo, M. J., Dean, R. A. & Demattos, R. Phase 3 solanezumab trials: Secondary outcomes in mild Alzheimer's disease patients. *Alzheimers. Dement.* 12(2):110–20 (2015).
83. Bateman, R. J., Xiong, C., Benzinger, T. L. S., Fagan, A. M., Goate, A., Fox, N. C., Marcus, D. S., Cairns, N. J., Xie, X., Blazey, T. M., et al. Clinical and biomarker changes in dominantly inherited Alzheimer's disease. *N. Engl. J. Med.* 367(9):795–804 (2012).
84. Jankowsky, J. L., Fadale, D. J., Anderson, J., Xu, G. M., Gonzales, V., Jenkins, N. A., Copeland, N. G., Lee, M. K., Younkin, L. H., Wagner, S. L., et al. Mutant presenilins specifically elevate the levels of the 42 residue beta-amyloid peptide in vivo: evidence for augmentation of a 42-specific gamma secretase. *Hum. Mol. Genet.* 13(2):159–70 (2004).
85. Nabuurs, R. J. A., Rutgers, K. S., Welling, M. M., Metaxas, A., de Backer, M. E., Rotman, M., Bacsikai, B. J., van Buchem, M. A., van der Maarel, S. M. & van der Weerd, L. In vivo detection of amyloid- β deposits using heavy chain antibody fragments in a transgenic mouse model for Alzheimer's disease. *PLoS One* 7(6):e38284 (2012).
86. Kanekiyo, T., Liu, C.-C., Shinohara, M., Li, J. & Bu, G. LRP1 in brain vascular smooth muscle cells mediates local clearance of Alzheimer's amyloid- β . *J. Neurosci.* 32(46):16458–65 (2012).
87. Kamphuis, W., Mamber, C., Moeton, M., Kooijman, L., Sluijs, J. A., Jansen, A. H. P., Vermeer, M., de Groot, L. R., Smith, V. D., Rangarajan, S., et al. GFAP isoforms in adult mouse brain with a focus on neurogenic astrocytes and reactive astrogliosis in mouse models of Alzheimer disease. *PLoS One* 7(8):e42823 (2012).
88. Janus, C., Flores, A. Y., Xu, G. & Borchelt, D. R. Behavioral abnormalities in APPSwe/PS1dE9 mouse model of AD-like pathology: comparative analysis across multiple behavioral domains. *Neurobiol. Aging* 36(9):2519–32 (2015).
89. Kilgore, M., Miller, C. A., Fass, D. M., Hennig, K. M., Haggarty, S. J., Sweatt, J. D. & Rumbaugh, G. Inhibitors of class 1 histone deacetylases reverse contextual memory deficits in a mouse model of Alzheimer's disease. *Neuropsychopharmacology* 35(4):870–80 (2010).
90. Lalonde, R., Kim, H. D., Maxwell, J. A. & Fukuchi, K. Exploratory activity and spatial learning in 12-month-old APP(695)SWE/co+PS1/DeltaE9 mice with amyloid plaques. *Neurosci. Lett.* 390(2):87–92 (2005).

91. Volianskis, A., Køstner, R., Mølgaard, M., Hass, S. & Jensen, M. S. Episodic memory deficits are not related to altered glutamatergic synaptic transmission and plasticity in the CA1 hippocampus of the APP^{swe}/PS1^{ΔE9}-deleted transgenic mice model of β -amyloidosis. *Neurobiol. Aging* 31(7):1173–87 (2010).
92. Minkevičienė, R., Rheims, S., Dobszay, M. B., Zilberter, M., Hartikainen, J., Fülöp, L., Penke, B., Zilberter, Y., Harkany, T., Pitkänen, A., et al. Amyloid beta-induced neuronal hyperexcitability triggers progressive epilepsy. *J. Neurosci.* 29(11):3453–62 (2009).
93. Poduslo, J. F., Curran, G. L., Wengenack, T. M., Malester, B. & Duff, K. Permeability of proteins at the blood-brain barrier in the normal adult mouse and double transgenic mouse model of Alzheimer's disease. *Neurobiol. Dis.* 8(4):555–67 (2001).
94. Wang, Y., Liu, J., Zhang, Z., Wang, X. & Zhang, C. Structure and permeability changes of the blood-brain barrier in APP/PS1 mice: an Alzheimer's disease animal model. *Neurochem. J.* 5(3):220–222 (2011).
95. Minogue, A. M., Jones, R. S., Kelly, R. J., McDonald, C. L., Connor, T. J. & Lynch, M. A. Age-associated dysregulation of microglial activation is coupled with enhanced blood-brain barrier permeability and pathology in APP/PS1 mice. *Neurobiol. Aging* 35(6):1442–52 (2014).
96. Abbott, N. J. Blood-brain barrier structure and function and the challenges for CNS drug delivery. *J. Inher. Metab. Dis.* 36(3):437–49 (2013).
97. Zlokovic, B. V. The blood-brain barrier in health and chronic neurodegenerative disorders. *Neuron* 57(2):178–201 (2008).
98. Hamilton, N. B., Attwell, D. & Hall, C. N. Pericyte-mediated regulation of capillary diameter: a component of neurovascular coupling in health and disease. *Front. Neuroenergetics* 2 (2010).
99. Hawkins, R. A., O'Kane, R. L., Simpson, I. A. & Viña, J. R. Structure of the blood-brain barrier and its role in the transport of amino acids. *J. Nutr.* 136(1 Suppl):218S–26S (2006).
100. Abbott, N. J., Patabendige, A. a K., Dolman, D. E. M., Yusof, S. R. & Begley, D. J. Structure and function of the blood-brain barrier. *Neurobiol. Dis.* 37(1):13–25 (2010).
101. Carrano, A., Snkhchyan, H., Kooij, G., van der Pol, S., van Horsen, J., Veerhuis, R., Hoozemans, J., Rozemuller, A. & de Vries, H. E. ATP-binding cassette transporters P-glycoprotein and breast cancer related protein are reduced in capillary cerebral amyloid angiopathy. *Neurobiol. Aging* 35(3):565–75 (2014).
102. Zlokovic, B. V. Neurovascular pathways to neurodegeneration in Alzheimer's disease and other disorders. *Nat. Rev. Neurosci.* 12(12):723–738 (2011).
103. Obermeier, B., Daneman, R. & Ransohoff, R. M. Development, maintenance and disruption of the blood-brain barrier. *Nat. Med.* 19(12):1584–96 (2013).
104. Carvey, P. M., Hendey, B. & Monahan, A. J. The blood-brain barrier in neurodegenerative disease: a rhetorical perspective. *J. Neurochem.* 111(2):291–314 (2009).
105. Naik, P. & Cucullo, L. In vitro blood-brain barrier models: current and perspective technologies. *J. Pharm. Sci.* 101(4):1337–54 (2012).
106. Wilhelm, I. & Krizbai, I. A. In vitro models of the blood-brain barrier for the study of drug delivery to the brain. *Mol. Pharm.* 11(7):1949–63 (2014).
107. Czupalla, C. J., Liebner, S. & Devraj, K. In vitro models of the blood-brain barrier. *Methods Mol. Biol.* 1135:415–37 (2014).
108. Vernon, H., Clark, K. & Bressler, J. P. In vitro models to study the blood brain barrier. *Methods Mol. Biol.* 758:153–68 (2011).
109. Rutgers, K. S., Nabuurs, R. J. A., van den Berg, S. A. A., Schenk, G. J., Rotman, M., Verrips, C. T., van Duinen, S. G., Maat-Schieman, M. L., van Buchem, M. A., de Boer, A. G., et al. Transmigration of beta amyloid specific heavy chain antibody fragments across the in vitro blood-brain barrier. *Neuroscience* 190:37–42 (2011).
110. Hamers-Casterman, C., Atarhouch, T., Muyldermans, S., Robinson, G., Hamers, C., Songa, E. B., Bendahman, N. & Hamers, R. Naturally occurring antibodies devoid of light chains. *Nature* 363(6428):446–448 (1993).

111. Muyldermans, S., Atarhouch, T., Saldanha, J., Barbosa, J. A. & Hamers, R. Sequence and structure of VH domain from naturally occurring camel heavy chain immunoglobulins lacking light chains. *Protein Eng.* 7(9):1129–35 (1994).
112. Zhang, J., Liu, X., Bell, A., To, R., Baral, T. N., Azizi, A., Li, J., Cass, B. & Durocher, Y. Transient expression and purification of chimeric heavy chain antibodies. *Protein Expr. Purif.* 65(1):77–82 (2009).
113. Saerens, D., Kinne, J., Bosmans, E., Wernery, U., Muyldermans, S. & Conrath, K. Single domain antibodies derived from dromedary lymph node and peripheral blood lymphocytes sensing conformational variants of prostate-specific antigen. *J. Biol. Chem.* 279(50):51965–72 (2004).
114. Muyldermans, S., Baral, T. N., Retamozzo, V. C., De Baetselier, P., De Genst, E., Kinne, J., Leonhardt, H., Magez, S., Nguyen, V. K., Revets, H., et al. Camelid immunoglobulins and nanobody technology. *Vet. Immunol. Immunopathol.* 128(1–3):178–83 (2009).
115. Vu, K. B., Ghahroudi, M. A., Wyns, L. & Muyldermans, S. Comparison of llama V(H) sequences from conventional and heavy chain antibodies. *Mol. Immunol.* 34(16–17):1121–1131 (1997).
116. Harmsen, M. M., Ruuls, R. C., Nijman, I. J., Niewold, T. A., Frenken, L. G. & de Geus, B. Llama heavy-chain V regions consist of at least four distinct subfamilies revealing novel sequence features. *Mol. Immunol.* 37(10):579–90 (2000).
117. Maass, D. R., Sepulveda, J., Pernthaler, A. & Shoemaker, C. B. Alpaca (*Lama pacos*) as a convenient source of recombinant camelid heavy chain antibodies (VHHs). *J. Immunol. Methods* 324(1–2):13–25 (2007).
118. Govaert, J., Pellis, M., Deschacht, N., Vincke, C., Conrath, K., Muyldermans, S. & Saerens, D. Dual beneficial effect of interloop disulfide bond for single domain antibody fragments. *J. Biol. Chem.* 287(3):1970–9 (2012).
119. De Genst, E., Silence, K., Decanniere, K., Conrath, K., Loris, R., Kinne, J., Muyldermans, S. & Wyns, L. Molecular basis for the preferential cleft recognition by dromedary heavy-chain antibodies. *Proc. Natl. Acad. Sci. U. S. A.* 103(12):4586–91 (2006).
120. De Meyer, T., Muyldermans, S. & Depicker, A. Nanobody-based products as research and diagnostic tools. *Trends in Biotechnology* 32(5):263–70 (2014).
121. Muyldermans, S. Nanobodies: natural single-domain antibodies. *Annu. Rev. Biochem.* 82(1):775–797 (2013).
122. Wesolowski, J., Alzogaray, V., Reyelt, J., Unger, M., Juarez, K., Urrutia, M., Cauerhff, A., Danquah, W., Rissiek, B., Scheuplein, F., et al. Single domain antibodies: promising experimental and therapeutic tools in infection and immunity. *Med. Microbiol. Immunol.* 198(3):157–74 (2009).
123. Desmyter, A., Transue, T. R., Ghahroudi, M. A., Thi, M. H., Poortmans, F., Hamers, R., Muyldermans, S. & Wyns, L. Crystal structure of a camel single-domain VH antibody fragment in complex with lysozyme. *Nat. Struct. Biol.* 3(9):803–811 (1996).
124. Yardehnavi, N., Behdani, M., Pooshang Bagheri, K., Mahmoodzadeh, A., Khanahmad, H., Shahbazzadeh, D., Habibi-Anbouhi, M., Ghassabeh, G. H. & Muyldermans, S. A camelid antibody candidate for development of a therapeutic agent against *Hemiscorpius lepturus* envenomation. *FASEB J.* 28(9):4004–14 (2014).
125. Hmila, I., Abdallah R, B. A. Ben, Saerens, D., Benlasfar, Z., Conrath, K., Ayeb, M. El, Muyldermans, S. & Bouhaouala-Zahar, B. VHH, bivalent domains and chimeric Heavy chain-only antibodies with high neutralizing efficacy for scorpion toxin AaH1. *Mol. Immunol.* 45(14):3847–3856 (2008).
126. Gad, W., Ben-Abderrazek, R., Wahni, K., Vertommen, D., Muyldermans, S., Bouhaouala-Zahar, B. & Messens, J. Wheat germ in vitro translation to produce one of the most toxic sodium channel specific toxins. *Biosci. Rep.* 34(4) (2014).
127. Cardoso, F. M., Ibañez, L. I., Van den Hoecke, S., De Baets, S., Smet, A., Roose, K., Schepens, B., Descamps, F. J., Fiers, W., Muyldermans, S., et al. Single-domain antibodies targeting neuraminidase protect against an H5N1 influenza virus challenge. *J. Virol.* 88(15):8278–96 (2014).

128. Garaicoechea, L., Aguilar, A., Parra, G. I., Bok, M., Sosnovtsev, S. V., Canziani, G., Green, K. Y., Bok, K. & Parreño, V. Llama nanoantibodies with therapeutic potential against human norovirus diarrhea. *PLoS One* 10(8):e0133665 (2015).
129. Dolk, E., van der Vaart, M., Lutje Hulsik, D., Vriend, G., de Haard, H., Spinelli, S., Cambillau, C., Frenken, L. & Verrips, T. Isolation of llama antibody fragments for prevention of dandruff by phage display in shampoo. *Appl. Environ. Microbiol.* 71(1):442–50 (2005).
130. Scheuplein, F., Rissiek, B., Driver, J. P., Chen, Y.-G., Koch-Nolte, F. & Serreze, D. V. A recombinant heavy chain antibody approach blocks ART2 mediated deletion of an iNKT cell population that upon activation inhibits autoimmune diabetes. *J. Autoimmun.* 34(2):145–54 (2010).
131. Impagliazzo, A., Tepper, A. W., Verrips, T. C., Ubbink, M. & van der Maarel, S. M. Structural basis for a PABPN1 aggregation-preventing antibody fragment in OPMD. *FEBS Lett.* 584(8):1558–64 (2010).
132. Tu, Z., Xu, Y., Fu, J., Huang, Z., Wang, Y., Liu, B. & Tao, Y. Preparation and characterization of novel IgG affinity resin coupling anti-Fc camelid single-domain antibodies. *J. Chromatogr. B. Analyt. Technol. Biomed. Life Sci.* 983–984:26–31 (2015).
133. Zheng, F., Put, S., Bouwens, L., Lahoutte, T., Matthys, P., Muyldermans, S., De Baetselier, P., Devoogdt, N., Raes, G. & Schoonooghe, S. Molecular imaging with macrophage CR1g-targeting nanobodies for early and preclinical diagnosis in a mouse model of rheumatoid arthritis. *J. Nucl. Med.* 55(5):824–9 (2014).
134. Dolk, E., Verrips, T. & de Haard, H. Selection of VHHs under application conditions. *Methods Mol. Biol.* 911:199–209 (2012).
135. Klooster, R., Rutgers, K. S. & van der Maarel, S. M. Selection of VHH antibody fragments that recognize different A β depositions using complex immune libraries. *Methods Mol. Biol.* 911:241–53 (2012).
136. Hammers, C. M. & Stanley, J. R. Antibody phage display: technique and applications. *J. Invest. Dermatol.* 134(2):e17 (2014).
137. Scott, J. K. & Smith, G. P. Searching for peptide ligands with an epitope library. *Science* 249(4967):386–90 (1990).
138. Sabir, J. S. M., Atef, A., El-Domyati, F. M., Edris, S., Hajrah, N., Alzohairy, A. M. & Bahieldin, A. Construction of naïve camelids VHH repertoire in phage display-based library. *C. R. Biol.* 337(4):244–9 (2014).
139. Verheesen, P., Roussis, A., de Haard, H. J., Groot, A. J., Stam, J. C., den Dunnen, J. T., Frants, R. R., Verkleij, A. J., Theo Verrips, C. & van der Maarel, S. M. Reliable and controllable antibody fragment selections from Camelid non-immune libraries for target validation. *Biochim. Biophys. Acta* 1764(8):1307–19 (2006).
140. Forsman, A., Beirmaert, E., Aasa-Chapman, M. M. I., Hoorelbeke, B., Hijazi, K., Koh, W., Tack, V., Szynol, A., Kelly, C., McKnight, A., et al. Llama antibody fragments with cross-subtype human immunodeficiency virus type 1 (HIV-1)-neutralizing properties and high affinity for HIV-1 gp120. *J. Virol.* 82(24):12069–81 (2008).
141. Garaicoechea, L., Olichon, A., Marcoppido, G., Wigdorovitz, A., Mozgovoij, M., Saif, L., Surrey, T. & Parreño, V. Llama-derived single-chain antibody fragments directed to rotavirus VP6 protein possess broad neutralizing activity in vitro and confer protection against diarrhea in mice. *J. Virol.* 82(19):9753–64 (2008).
142. Goldman, E. R., Anderson, G. P., Liu, J. L., Delehanty, J. B., Sherwood, L. J., Osborn, L. E., Cummins, L. B. & Hayhurst, A. Facile generation of heat-stable antiviral and antitoxin single domain antibodies from a semisynthetic llama library. *Anal. Chem.* 78(24):8245–55 (2006).
143. Yan, J., Li, G., Hu, Y., Ou, W. & Wan, Y. Construction of a synthetic phage-displayed Nanobody library with CDR3 regions randomized by trinucleotide cassettes for diagnostic applications. *J. Transl. Med.* 12(1):343 (2014).
144. Dorresteyn, B., Rotman, M., Faber, D., Schraevesande, R., Suidgeest, E., van der Weerd, L., van der Maarel, S. M., Verrips, C. T. & El Khattabi, M. Camelid heavy chain only antibody fragment domain against β -site of amyloid precursor protein cleaving enzyme 1 inhibits β -secretase activity in vitro and in vivo. *FEBS J.* 282(18):3618–3631 (2015).
145. Muruganandam, A., Tanha, J., Narang, S. & Stanimirovic, D. Selection of phage-displayed llama single-domain antibodies that transmigrate across human blood-brain barrier endothelium. *FASEB J.* 16(2):240–2 (2002).

146. Abulrob, A., Sprong, H., Van Bergen en Henegouwen, P. & Stanimirovic, D. The blood-brain barrier transmigration single domain antibody: mechanisms of transport and antigenic epitopes in human brain endothelial cells. *J. Neurochem.* 95(4):1201–14 (2005).
147. Tayebi, M., Taylor, W. A., Jones, D. R., Bate, C. & David, M. PrP-specific camel antibodies with the ability to immunodetect intracellular prion protein. *J. Gen. Virol.* 91(Pt 8):2121–31 (2010).
148. Li, T., Bourgeois, J.-P., Celli, S., Glacial, F., Le Sourd, A.-M., Mecheri, S., Weksler, B., Romero, I., Couraud, P.-O., Rougeon, F., et al. Cell-penetrating anti-GFAP VHH and corresponding fluorescent fusion protein VHH-GFP spontaneously cross the blood-brain barrier and specifically recognize astrocytes: application to brain imaging. *FASEB J.* 26(10):3969–79 (2012).
149. Morais, M., Cantante, C., Gano, L., Santos, I., Lourenço, S., Santos, C., Fontes, C., Aires da Silva, F., Gonçalves, J. & Correia, J. D. G. Biodistribution of a (67)Ga-labeled anti-TNF VHH single-domain antibody containing a bacterial albumin-binding domain (Zag). *Nucl. Med. Biol.* 41 Suppl:e44–8 (2014).
150. De Groeve, K., Deschacht, N., De Koninck, C., Caveliers, V., Lahoutte, T., Devoogdt, N., Muyldermans, S., De Baetselier, P. & Raes, G. Nanobodies as tools for in vivo imaging of specific immune cell types. *J. Nucl. Med.* 51(5):782–9 (2010).
151. Olafsen, T. & Wu, A. M. Antibody vectors for imaging. *Semin. Nucl. Med.* 40(3):167–81 (2010).
152. Rosik, D., Orlova, A., Malmberg, J., Altai, M., Varasteh, Z., Sandström, M., Karlström, A. E. & Tolmachev, V. Direct comparison of 111In-labelled two-helix and three-helix Affibody molecules for in vivo molecular imaging. *Eur. J. Nucl. Med. Mol. Imaging* 39(4):693–702 (2012).
153. DeVos, S. L. & Miller, T. M. Direct intraventricular delivery of drugs to the rodent central nervous system. *J. Vis. Exp.* 75:e50326 (2013).
154. Calias, P., Papisov, M., Pan, J., Savioli, N., Belov, V., Huang, Y., Lotterhand, J., Alessandrini, M., Liu, N., Fischman, A. J., et al. CNS penetration of intrathecal-lumbar idursulfase in the monkey, dog and mouse: implications for neurological outcomes of lysosomal storage disorder. *PLoS One* 7(1):e30341 (2012).
155. Papisov, M. I., Belov, V., Fischman, A. J., Belova, E., Titus, J., Gagne, M. & Gillooly, C. Delivery of proteins to CNS as seen and measured by positron emission tomography. *Drug Deliv. Transl. Res.* 2(3):201–9 (2012).
156. Kubetzko, S., Balic, E., Waibel, R., Zangemeister-Wittke, U. & Plückthun, A. PEGylation and multimerization of the anti-p185HER-2 single chain Fv fragment 4D5: effects on tumor targeting. *J. Biol. Chem.* 281(46):35186–201 (2006).
157. Willuda, J., Kubetzko, S., Waibel, R., Schubiger, P. a, Zangemeister-Wittke, U. & Plückthun, a. Tumor targeting of mono-, di-, and tetravalent anti-p185(HER-2) miniantibodies multimerized by self-associating peptides. *J. Biol. Chem.* 276(17):14385–92 (2001).
158. Kontermann, R. E. Strategies to extend plasma half-lives of recombinant antibodies. *BioDrugs* 23(2):93–109 (2009).
159. Kontermann, R. E. Strategies for extended serum half-life of protein therapeutics. *Curr. Opin. Biotechnol.* 22(6):868–76 (2011).
160. Schnyder, A. & Huwyler, J. Drug transport to brain with targeted liposomes. *NeuroRx* 2(1):99–107 (2005).
161. Spuch, C. & Navarro, C. Liposomes for Targeted Delivery of Active Agents against Neurodegenerative Diseases (Alzheimer's Disease and Parkinson's Disease). *J. Drug Deliv.* 2011:469679 (2011).
162. Gao, J.-Q., Lv, Q., Li, L.-M., Tang, X.-J., Li, F.-Z., Hu, Y.-L. & Han, M. Glioma targeting and blood-brain barrier penetration by dual-targeting doxorubicin liposomes. *Biomaterials* 34(22):5628–39 (2013).
163. Salvati, E., Re, F., Sesana, S., Cambianica, I., Sancini, G., Masserini, M. & Gregori, M. Liposomes functionalized to overcome the blood-brain barrier and to target amyloid- β peptide: the chemical design affects the permeability across an in vitro model. *Int. J. Nanomedicine* 8:1749–58 (2013).
164. Lindqvist, A., Rip, J., Gaillard, P. J., Björkman, S. & Hammarlund-Udenaes, M. Enhanced brain delivery of the opioid peptide damgo in glutathione pegylated liposomes: A microdialysis study. *Mol. Pharm.* 10(5):1533–1541 (2013).

165. Rip, J., Chen, L., Hartman, R., van den Heuvel, A., Reijerkerk, A., van Kregten, J., van der Boom, B., Appeldoorn, C., de Boer, M., Maussang, D., et al. Glutathione PEGylated liposomes: pharmacokinetics and delivery of cargo across the blood-brain barrier in rats. *J. Drug Target.* 22(5):460–7 (2014).
166. Ogawa, M., Umeda, I. O., Kosugi, M., Kawai, A., Hamaya, Y., Takashima, M., Yin, H., Kudoh, T., Seno, M. & Magata, Y. Development of ¹¹¹In-labeled liposomes for vulnerable atherosclerotic plaque imaging. *J. Nucl. Med.* 55(1):115–20 (2014).
167. Farrington, G. K., Caram-Salas, N., Haqqani, A. S., Brunette, E., Eldredge, J., Pepinsky, B., Antognetti, G., Baumann, E., Ding, W., Garber, E., et al. A novel platform for engineering blood-brain barrier-crossing bispecific biologics. *FASEB J.* 28(11):4764–4778 (2014).
168. Martin, W. L., West, A. P., Gan, L. & Bjorkman, P. J. Crystal structure at 2.8 Å of an FcRn/heterodimeric Fc complex: mechanism of pH-dependent binding. *Mol. Cell* 7(4):867–77 (2001).
169. Olafsen, T., Kenanova, V. E. & Wu, A. M. Tunable pharmacokinetics: modifying the in vivo half-life of antibodies by directed mutagenesis of the Fc fragment. *Nat. Protoc.* 1(4):2048–60 (2006).
170. Ying, T., Ju, T. W., Wang, Y., Prabakaran, P. & Dimitrov, D. S. Interactions of IgG1 CH2 and CH3 Domains with FcRn. *Front. Immunol.* 5:146 (2014).
171. Caram-Salas, N., Boileau, E., Farrington, G. K., Garber, E., Brunette, E., Abulrob, A. & Stanimirovic, D. In vitro and in vivo methods for assessing FcRn-mediated reverse transcytosis across the blood-brain barrier. *Methods Mol. Biol.* 763:383–401 (2011).
172. Rajabibazl, M., Rasaei, M. J., Forouzandeh, M. & Rahimpour, A. Retroviral transduction of fluonanobody and the variable domain of camelid heavy-chain antibodies to chicken embryonic cells. *Iran. J. Immunol.* 10(4):247–58 (2013).
173. Kotterman, M. A. & Schaffer, D. V. Engineering adeno-associated viruses for clinical gene therapy. *Nat. Rev. Genet.* 15(7):445–51 (2014).
174. Mingozzi, F. & High, K. A. Therapeutic in vivo gene transfer for genetic disease using AAV: progress and challenges. *Nat. Rev. Genet.* 12(5):341–55 (2011).
175. Gonçalves, M. A. F. V. Adeno-associated virus: from defective virus to effective vector. *Virol. J.* 2:43 (2005).
176. Wang, Y.-J., Gao, C.-Y., Yang, M., Liu, X.-H., Sun, Y., Pollard, A., Dong, X.-Y., Wu, X.-B., Zhong, J.-H., Zhou, H.-D., et al. Intramuscular delivery of a single chain antibody gene prevents brain Aβ deposition and cognitive impairment in a mouse model of Alzheimer's disease. *Brain. Behav. Immun.* 24(8):1281–93 (2010).
177. Fukuchi, K., Tahara, K., Kim, H.-D., Maxwell, J. A., Lewis, T. L., Accavitti-Loper, M. A., Kim, H., Ponnazhagan, S. & Lalonde, R. Anti-Abeta single-chain antibody delivery via adeno-associated virus for treatment of Alzheimer's disease. *Neurobiol. Dis.* 23(3):502–11 (2006).
178. de Backer, M. W. A., Fitzsimons, C. P., Brans, M. A. D., Luijendijk, M. C. M., Garner, K. M., Vreugdenhil, E. & Adan, R. A. H. An adeno-associated viral vector transduces the rat hypothalamus and amygdala more efficient than a lentiviral vector. *BMC Neurosci.* 11:81 (2010).

1. Department of Biology, Utrecht University, The Netherlands
2. Department of Human Genetics, Leiden University Medical Center, The Netherlands
3. Department of Radiology, Leiden University Medical Center, The Netherlands

2

CHAPTER

VHH AGAINST BACE1 INHIBITS BETA-SECRETASE ACTIVITY *IN VITRO* AND *IN VIVO*

Adapted from

Camelid heavy chain only antibody fragment domain against β -site of amyloid precursor protein cleaving enzyme 1 inhibits β -secretase activity in vitro and in vivo.

Bram Dorresteyn¹, Maarten Rotman^{2,3}, Dorien Faber¹, Ruud Schravensande¹, Ernst Suidgeest³,
Louise van der Weerd^{2,3}, Silvère M. van der Maarel², Theo C. Verrips¹ and Mohamed el Khattabi¹.
FEBS Journal 282 (2015) 3618-3631

ABSTRACT

Introduction: Accumulation and aggregation of the amyloid-beta ($A\beta$) peptide is associated with Alzheimer's disease (AD). $A\beta$ is generated from the amyloid precursor protein by the successive action of two membrane-associated processing enzymes: β -secretase or β -site of amyloid precursor protein cleaving enzyme 1 (BACE1) and γ -secretase. Inhibition of one or both of these enzymes prevents $A\beta$ generation and the accompanying $A\beta$ accumulation. Antigen binding fragments from camelid heavy chain only antibodies (VHHs) were found to exert excellent enzyme inhibition activity.

Methods: In the present study, we generated VHHs against BACE1 by active immunization of *Lama glama* with the recombinant BACE1 protein. Two classes of VHHs were selected from a VHH-phage display library by competitive elution with a peptide encoding the Swedish mutation variant of the BACE1 processing site.

Results: One VHH was found to inhibit the enzyme activity of BACE1 *in vitro* and in cell culture, whereas two other VHHs were found to stimulate BACE1 activity under the same conditions *in vitro*. Furthermore, an *in vivo* study with a transgenic AD mouse model, using intracisternal injection of the inhibitory VHH, led to acute reduction of the $A\beta$ load in the blood and brain.

Conclusion: This inhibitory VHH may be considered as a candidate molecule for a therapy directed towards reduction of $A\beta$ load and prevention of AD progression. Both the inhibitory and stimulatory VHH may be useful for improving our understanding of the structure-function relationship of BACE1, as well as its role in AD progression.

1. INTRODUCTION

Alzheimer's disease (AD) is a devastating neurodegenerative disease and the most common form of dementia [1]. AD is characterized pathologically by the presence of extracellular senile plaques and intracellular degeneration, including neurofibrillary tangles, dystrophic neuritis and neuropil threads [2]. The major constituent of senile plaques is amyloid-beta ($A\beta$), a small 4-kDa peptide. $A\beta$ is the result of the proteolytic processing of a larger membrane bound precursor protein named amyloid precursor protein (APP). Processing of APP starts with the cleavage of APP by β -secretase, also named β -site of APP cleaving enzyme (BACE1), which generates an extracellular soluble APP β fragments and a membrane bound C-terminal fragment (CTF β or C99) [3]. Subsequently, C99 is cleaved by γ -secretase into $A\beta$ peptides of predominantly 40 and 42 amino acids long ($A\beta_{40}$ and $A\beta_{42}$) on one side and a small membrane bound peptide (AICD) on the other [4]. This proteolytic processing is known as the pathologic processing pathway or amyloidogenic pathway. An alternative processing pathway initiated by α -secretase prevents the generation of CTF β , as the α -secretase cleaves APP within the $A\beta$ region and generates a soluble extracellular APP α and a C-terminal fragment (CTF α or C83). After subsequent cleavage of CTF α with γ -secretase, a small peptide (P3) is generated. This P3 peptide does not have any known pathological effects and its function is unknown [5]. This alternative processing pathway is known as the non-pathological pathway or non-amyloidogenic pathway.

BACE1, also known as Asp2 [6] and Memapsin2 [7], is a 501 amino acid long transmembrane aspartic protease. A total of four different splice variants can be transcribed from the BACE1 locus, of which the most active isoform is predominantly found in the brain [8]. β -secretase activity is solely dependent of BACE1 protein [6,7,9–11], whereas γ -secretase is a complex of many proteins, including presenilin, nicastrin, anterior pharynx-defective 1 and presenilin enhancer 2 [12].

In AD patients, both expression levels and activity of BACE1 are found to be increased [13,14]. Furthermore, the highest levels of BACE1 are found at sites close to amyloid plaque deposits [14–16]. Involvement of BACE1 in AD pathology was confirmed in transgenic mice *in vivo*. Cross-breeding transgenic mice overexpressing human APP with BACE1-null mice abolishes $A\beta$ production and $A\beta$ plaque formation [17,18], even in the brains of old mice [19]. Because embryonic knockdown of BACE1 is well tolerated [20], and an absence of BACE1 activity abolished the $A\beta$ load, it is expected that inhibition of BACE1 may stop AD progression without any major side effects. Therefore, several BACE1 inhibitor candidates, *e.g.* TAK-070, TC-1, AZ-4217, have been developed, of which 10 candidates are currently investigated in clinical trials [21–26]. Moreover, and relevant for a highly selective therapy, BACE1 activity was found to be susceptible to antibody-mediated inhibition [27,28]. Active immunization of transgenic

AD mice (Tg2576) with BACE1 [29], as well as treatment with BACE1 inhibitory antibodies [27], reduce A β load and block APP processing.

Despite all efforts, no BACE1 inhibitor has been approved for therapy so far. Therefore, new approaches to develop BACE1 inhibitors are needed. Both small molecule inhibitors and conventional antibodies have benefits, as well as disadvantages. With antibodies, great specificity can be achieved by careful selection, resulting in less possible side effects upon administration. Next to that, a more homogenous maintained level of therapeutic molecules is generally achieved among patients, as well as the possibility of a more patient-friendly administration regime (lesser dosing), compared to small molecule inhibitors [26,30]. A special class of antibodies, found in *Camelidae*, could be utilized to develop an alternative candidate belonging to the antibody approach. The antibody repertoire of *Camelidae* (*Lama glama*, *Vicunga pacos*, *Camelus bactrianus* and *Camelus dromedaries*) consists of two classes of the IgG family. Next to conventional IgG made by the combination of heavy and light chain dimers, another IgG class devoid of light chains was discovered in the early 1990's [31]. The isolated variable domain of this heavy chain only IgG (camelid heavy chain only antibody fragment; VHH) was found to be fully functional and therefore the smallest known naturally derived antigen-binding fragment. VHHs show a number of advantages over conventional IgGs and IgG derivatives such as Fabs or scFv. Among those advantages are easy production [30], inhibition of enzymatic activity by proteolytic cleft entry [32], and possible passage through the blood-brain barrier (BBB) [33,34].

The present study aimed to develop BACE1-targeting VHHs for passive immune therapy of AD. We describe the generation of BACE1 VHH-immune libraries, *in vitro* selection of VHHs that bind BACE1 and the characterization of VHHs that inhibit or stimulate the enzymatic activity of BACE1. VHHs exerted their inhibition or stimulation of BACE1 *in vitro* using purified BACE1 protein. The *in vitro* inhibition was validated in a cellular assay, using mouse neuroblastoma cells (N2a), which express BACE1 and which were transfected with the human APP gene harboring the Swedish mutation (N2a-APP_{swe}) [35]. The inhibitory VHH (VHH-B3a) showed a significant effect on the activity of BACE1 in the cell assay when measured using a fluorogenic peptide as a BACE1-specific substrate. Furthermore, the effect of the inhibitory VHH was validated in an *in vivo* experiment. A bolus dose of VHH-B3a injected into the cisterna magna of double transgenic mice, overexpressing both human APP with the Swedish mutation and human presenilin 1 with exon 9 deletion (APP_{swe}/PS1dE9) reduced A β concentration in both plasma and brain.

2. MATERIALS AND METHODS

2.1. Immunization and library construction

The immunizations were approved by the Utrecht University institutional Animal Experiments Committee (DEC permit: 2007.III.01.013). Two llamas were immunized with 50 µg of purified BACE1 (product number 931-AS; R&D systems, USA) in 1 ml of PBS mixed with the adjuvant Stimune (Prionics, NL) and injected intramuscularly. The immunization scheme consisted of a priming immunization (at day 0), followed by three boosts (at days 14, 28 and 35).

The immune response was measured in the immune sera taken at days 28 and 43 and were compared with the pre-immune serum taken at day 0. BACE1 (100 ng) in PBS was coated into wells of a 96-wells Maxisorb plate (Nunc, USA) overnight at 4°C. After blocking with 4% skimmed milk (Marvel; Premier Foods, UK) in PBS (mPBS), serial dilutions of the immune and pre-immune sera were added to the wells. A heavy chain only IgG response was detected with a rabbit polyclonal serum directed against VHH (RaVHH; in-house made) and a secondary donkey anti-rabbit antibody coupled to horseradish peroxidase (DaRPO; Invitrogen, USA). Peroxidase activity was measured using orthophenylenediamine (OPD) + H₂O₂, and A₄₉₀ via a spectrophotometer (Bio-Rad, USA).

At day 43, peripheral blood lymphocytes were purified from 150 ml of blood on a Ficoll gradient (GE Healthcare, UK). RNA was isolated from these peripheral blood lymphocytes and converted into cDNA using SuperscriptIII kit (Invitrogen). IgG binding domains were amplified via PCR using primers annealing at the signal sequence of the IgGs and the hinge region [36]. The approximately 700-bp fragments corresponding to the antigen binding domain of the heavy chain only antibodies (VHH) were excised from gel, and the *Sfi*I restriction site was introduced at the 5' end by a nested PCR step to facilitate cloning into the display vector. The purified 700-bp fragment was digested with *Bst*EII (a restriction site found in the hinge region of heavy chain only antibodies) and *Sfi*I (Fermentas, USA). The resulting approximately 400-bp antigen binding fragment of the heavy chain only antibodies was cloned in a phage-display plasmid. The plasmids were transferred to *Escherichia coli* strain TG1 [*supE hsd₅ thi (lac-proAB) F₁(traD36 proAB lacIq lacZ M15)*] by electroporation. *E. coli* TG1 was used for the production of phages, the infection by selected phages, and for expression of selected VHH.

2.2. Selection and screening of anti-BACE1 VHH

Phage display [37] was used to select phages that specifically bind recombinant BACE1 (931-AS; R&D systems). Maxisorp 96-wells plates (Nunc) were coated overnight at 4°C with 2, 10 or 50 µg/ml BACE1 in PBS. The next day, wells were blocked with 4% mPBS. Subsequently, phages

produced from the BACE1 immune VHH-phage library were pre-incubated in 2% mPBS and added to the wells containing BACE1. As a control, phages were added to non-coated, blocked wells. Phages were incubated for 2 h at room temperature (RT). After extensive washing with PBS containing 0.05% Tween-20 (PBST; Sigma-Aldrich, USA) and with PBS, bound phages were eluted with 100 mM triethylamine (TEA; Sigma-Aldrich) by 15 min. incubation at RT. Eluted phages were directly neutralized by the addition of 1 M Tris-HCl (pH 7.5). These output phages were used to infect exponentially growing *E. coli* TG1 cells. Infected cells were plated on LB agar plates containing 2% glucose and 100 µg/ml ampicillin. For the production of phages, *E. coli* containing phagemids were infected with helper phage VCSM13, and phage particles were produced overnight at 37°C in medium supplemented with 100 µg/ml ampicillin and 25 µg/ml kanamycin. After purification, phages were used for a second round of panning selection against recombinant BACE1 as described above. However, bound phages were now selectively eluted by incubation with either peptide APP_{swe} (EEISEVNLDAE) or APPwt (EEISEVKMDAE) for various time periods. The peptides represented the BACE1 processing site in APP with and without the Swedish mutation, respectively (mutation sites underlined) [38]. Peptides were synthesized at the department of Membrane Enzymology (Utrecht University, NL).

For screening, single clones were grown into 96-wells plates and phage production was induced by infection with helper phage and selection for kanamycin and ampicillin resistance. Phages were separated from bacteria by centrifugation. BACE1 (2 µg/ml) was coated overnight onto Maxisorp 96-wells plates (Nunc) and the purified phages were incubated on the coated plates at RT for 2 h. After extensive washing with PBST and PBS, bound phages were detected using an anti-M13 antibody conjugated to horseradish peroxidase (GE Healthcare) and OPD. Twelve independent clones that showed high ELISA signals were selected for sequencing (ServiceXS, NL) and further characterization.

For production of VHH proteins, selected VHHs were subcloned into an expression plasmid. The 400-bp *Sfi*I-*Bst*EII fragments were excised from the selected plasmids and cloned into the expression plasmid pMEK222 (present study), using the same restriction sites. VHHs expressed from pMEK222 are fused to carboxyterminal FLAG and hexa-histidine tags.

2.3. Production and purification of anti-BACE1 VHH

VHHs were expressed from the plasmid pMEK222 by inducing a 400 ml log-phase *E. coli* culture with 1 mM IPTG (Fermentas) and incubation for 5 h at 37°C. The bacteria were harvested by centrifugation (15 min. at 4566 × g) and frozen overnight at -20°C. After thawing the bacteria and resuspending them in 20 ml of sonication buffer (50 mM sodium phosphate, 300 mM NaCl, pH 7.0), periplasmic fractions were prepared by incubating the resuspended bacteria head-over-head for 1 h at RT, and separating periplasmic soluble fractions, containing the

VHHs, from cellular debris by 15 min. of centrifugation at $4566 \times g$. VHHs were purified from the soluble periplasmic fractions via the hexa-histidine tag using Talon beads (product number 635504; Clontech, USA). Talon beads were incubated with the periplasmic fraction for 1 h at RT. After several washings with PBS (or sonication buffer), bound VHHs were eluted with 300 mM imidazole in sonication buffer. Fractions containing purified VHH were subsequently pooled and dialyzed overnight at 4°C against PBS.

2.4. Characterization of anti-BACE1 VHH

Purified VHHs were evaluated for binding of immobilized BACE1. Maxisorp 96-wells plates (Nunc) were incubated with 1 µg/ml BACE1 overnight at 4°C. Subsequently, serial dilutions of VHHs in 2% mPBS were added and incubated while shaking for 2 h at RT. The wells were washed three times with PBST and once with PBS before the addition of 100 µl of RaVHH (1:2000; in-house made) in 1% mPBS to detect VHHs. After washing the wells as before, DaRPO (1:10000; Invitrogen) in 1% mPBS was used as secondary antibody. OPD and H₂O₂ were used as before to visualize VHH binding. K_d values for VHH were calculated using GraphPad Prism version 5.01 for Windows (GraphPad Software, USA) using a one site-specific binding curve.

2.5. Cell culture

Mouse N2a neuroblastoma cells stably transfected with APP_{swe} (N2a-APP_{swe}) were kindly provided by Dr. B. Kleizen (Department of Chemistry, Faculty of Science, Utrecht University). N2a-APP_{swe} were cultured at 37 °C and 5% CO₂ in medium made up by 47.5% DMEM (Gibco, USA), 47.5% OptiMEM reduced serum medium (Gibco), 5% Fetal Bovine Serum (FBS; Gibco), 300 µg/ml L-Glutamine, 100 µg/ml penicillin, 100 µg/ml streptomycin, and 200 µg/ml geneticin (Invitrogen)

2.6. BACE1 activity assay

BACE1 activity was measured using the fluorogenic peptide MCA-[SEVNLDAEFRK](Dnp)RR (R&D Systems). A highly fluorescent 7-methoxycoumarin group (MCA) was combined with a peptide containing the BACE1 processing sequence of APP_{swe}. This fluorophore-peptide combination was connected to a 2,4-dinitrophenyl group (Dnp), which functions as a quencher of MCA. After digestion of the peptide by BACE1, the fluorescent group and the quencher will be separated and fluorescence can be measured. In this assay, the amount of fluorescence is proportional to BACE1 activity.

Purified BACE1 (~35 nM) was incubated with 10 nM MCA-[SEVNLDAEFRK](Dnp)RR in sodium acetate buffer, pH 5.5 at 37°C for 2 h. MCA fluorescence was measured every 2 min. using FluoSTAR Optima (320 nm excitation, 405 nm emission; BMG Labtech, DE) for the entire 2 h.

The effect of VHH on the activity of the BACE₁ enzyme was assayed by the addition of various concentrations VHH (between 10 nM to 20 μM) to the mixture at the beginning of the 2 h incubation and measurement time. The effect was compared to the effect of 5 nM of BACE₁-Inhibitor-IV (Calbiochem, USA), which inhibits the activity of the enzyme completely. GraphPad Prism v5.01 was used to determine slopes of activity as described for the recombinant BACE₁ activity assay, as well as for the statistical analysis.

The effect of VHH-B3a on BACE₁ activity was also measured by determining the concentration of produced Aβ₄₀. Fresh medium or medium containing 10 μM VHH-B3a was added to cultured N2a-APP_{swe} cells. After 1, 5 and 24 h, Aβ₄₀ concentration was determined in undiluted cell culture medium using a commercial ELISA kit (product number KHB3482; Invitrogen) in accordance with the manufacturer's instructions. The determined Aβ₄₀ concentration of untreated cell medium was set at 100% for each time point and was related to the Aβ₄₀ concentration of the treated cell medium.

2.7. Animal studies

The *in vivo* study to determine the therapeutic value of the BACE₁-inhibiting VHH-B3a was performed in 4-5 months old female transgenic mice or female wildtype littermates from a colony set up using the APP_{swe}/PS1dE9 strain (APP/PS1; JAX[®] Mice and Services, The Jackson Laboratory, USA). The animal study was carried out in compliance with the Dutch laws related to the conduct of animal experiments and approved by the institutional Animal Experiments Committee (DEC permit 1133) of the Leiden University Medical Center.

2.8. VHH biodistribution

VHH were labelled with an infrared dye (IRD800CW; LiCor, USA) to image VHH distribution throughout the brain. VHH-B3a was incubated for 2 h. at RT while tumbling with NHS-IRD800CW (LiCor). Subsequently, uncoupled IRD800CW was removed with a Zeba Desalting spin column (Invitrogen) in accordance with the manufacturer's instructions. Coupling of NHS-IRD800CW was validated by gel electrophoresis and the concentration was determined using a spectrophotometer (NanoDrop, USA). Activity of VHH-B3a-IRD800CW (B3a-IRD800) was measured as described with recombinant BACE₁ and compared with non-conjugated VHH-B3a.

The mouse heads were shaved before 75 μg of B3a-IRD800 was administered via a percutaneous intracisternal bolus injection in wildtype mice (n = 4) to evaluate the efficacy of the injection procedure and the distribution of VHH over the brain [39]. *In vivo* fluorescence was determined at six time points (0, 1, 3, 6, 24, and 48 h) in the same mice. Mice were anaesthetized using continuous 1-2% isoflurane inhalation gas and dorsal images were taken using a LiCor

Pearl Impulse Imager (LiCor). Acquired *in vivo* images were quantified with LiCor software, by assigning a region of interest and determining fluorescence intensity. At 6, 24, and 48 h, directly after imaging, one mouse was sacrificed by perfusion-fixation (PBS and 4% PFA) under deep anaesthesia from pentobarbital (Euthasol; NL). Post-mortem fluorescence imaging was performed on the intact brain to confirm the VHH distribution. Brains were sectioned in 1 mm thick slices and imaged using LiCor Odyssey imager to visualize the B3a-IRD800 distribution throughout the brain. Intracisternal injection failed in one mouse. This mouse was excluded from the VHH biodistribution determination.

2.9. *In vivo* therapy

A bolus of 75 µg B3a-IRD800 was administered intracisternally in transgenic mice (n = 5) as described above. A control group (n = 5) was injected with PBS. Wildtype mice received the same treatment (n = 5 for both groups). Blood samples were collected just before injection and at 6, 24, and 48 h after injection. Blood samples were immediately centrifuged for 10 min. at 3000 × g. Plasma was separated from the cellular component and aliquots were stored at -80°C until use. Mice were sacrificed after 48 h by perfusion-fixation as described above. After fixation, brains were separated into left and right hemispheres. The right hemisphere was frozen in isobutanol on dry ice and stored at -80°C. The left hemisphere was further fixed in either 4% PFA or 2% PFA with 0.2% glutaraldehyde for 3 h at RT followed by 24 h of incubation at 4°C. Subsequently, fixative solutions were replaced for all brains by 2% PFA and brains were stored at 4°C. The right hemisphere was weighed, homogenized with an ultrathorax in extraction buffer (25 mM Tris-HCl, pH 7.6, 150 mM sodium chloride, and Complete Protease Inhibitor Cocktail; Roche Diagnostics, CH), and then sonicated with an M-150 sonicator. For analysis of the soluble Aβ fraction, brain homogenates were centrifuged at 100 000 × g for 1 h at 4°C. Supernatants were used to determine soluble Aβ. The concentrations of Aβ₄₀ in both plasma and brain samples were determined with a commercial ELISA kit (product number KHB3482; Invitrogen). The concentrations of Aβ₄₂ were determined only in the plasma samples (ELISA, product number KHB3544, Invitrogen). Because of technical difficulties, the reported value of Aβ₄₂ concentration in plasma at 6 h consists of samples from two mice, all other reported Aβ₄₀ and Aβ₄₂ values are derived from samples from all five mice. Despite careful treatment, minor differences in, for example, transport and storage influences the measured absolute Aβ concentration [40,41]. To exclude any difference in absolute Aβ as a result of treatment per time point, Aβ concentrations are plotted against the control at that time point.

The wet weight of the brain was used to calculate the density of soluble Aβ₄₀ in the brain (pmol/g). Both Aβ₄₀ and Aβ₄₂ concentrations in plasma were calculated and expressed as the

A β concentration (pM). GraphPad Prism v5.01 was used to perform statistics on differences between treated and untreated groups.

2.10. Statistical analysis

GraphPad Prism v5.01 was used to determine the slope of the BACE1 activity curves of each VHH concentration by linear regression. IC₅₀ and EC₅₀ of BACE1 inhibition or activity was calculated by nonlinear fitting log(inhibitor/agonist) versus response and variable response. A Student's *t*-test to evaluate differences between two groups and an analysis of variance (ANOVA) with Tukey's post-hoc test to evaluate differences between more than two groups were performed with $p < 0.05$ considered statistically significant.

3. RESULTS

3.1. Selection of BACE1 VHH

VHHs binding specifically to BACE1 were selected using phage display from an immune library obtained from llama immunized with BACE1. Two rounds of panning selection were applied. In the first round, phages binding to BACE1 were eluted by pH shock. These phages were used as input for a second round of selection, in which bound phages were eluted selectively by competition with a peptide containing the recognition sequence of BACE1 on the APP_{swE} mutation (KM670/671NL). Monoclonal phages were further characterized using binding to immobilized BACE1 and immune detection. This resulted in the selection of 28 different clones.

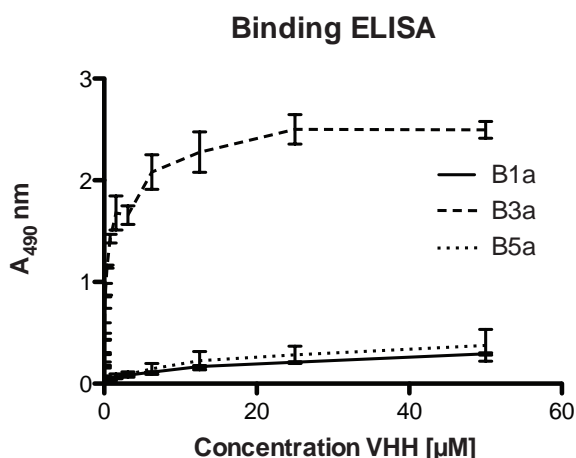


Figure 2.1. VHH binding to BACE1. BACE1 (100 ng) was immobilized onto a Nunc 96-well Maxisorb plate and incubated with serial dilutions of the indicated VHH. Bound VHHs were detected with rabbit anti-VHH and donkey anti-rabbit coupled to horseradish peroxidase.

Table 2.1. Binding affinities of anti-BACE1 VHH. VHHs were titrated and allowed to bind immobilized BACE1 in an ELISA. Affinity calculations were performed with a 'one site specific binding curve' algorithm (GrapPad Prism v5.01).

VHH	K_d (μM)
B1a	10.8 ± 1.33
B3a	0.3 ± 0.03
B5a	9.3 ± 1.67

The VHHs from these clones were produced and purified, and then tested for binding to immobilized BACE1 and immune detection. This second round of characterization resulted in 12 VHHs, which displayed a 175% higher signal by ELISA compared to non-coated control wells. Sequencing of these 12 independent clones revealed three different sequences, represented by VHH-B1a, -B3a, and -B5a. Figure 2.1 shows a typical dose-response curve for the VHHs binding to immobilized BACE1. The values were used for the calculation of the K_d values (Table 2.1). VHH-B1a and VHH-B5a have low affinity to immobilized BACE1 ($K_d = \sim 10 \mu\text{M}$), whereas VHH-B3a has an affinity that is ~ 33 -fold higher ($K_d = \sim 0.3 \mu\text{M}$).

3.2. Inhibition of recombinant BACE1 by VHH

The effect of VHH on recombinant BACE1 activity, either inhibitory or stimulatory, was evaluated using a reporter substrate that consists of a fluorescent group connected to a quencher. Figure 2.2 shows representative fluorescent signals recorded during a triplicate experiment of a single concentration of VHH-B1a ($20 \mu\text{M}$) with BACE1 (35 nM) and a BACE1 (35 nM) without VHH as control. The slope reflects the relative BACE1 activity, with lower values indicating more efficient inhibition. The addition of $20 \mu\text{M}$ VHH-B1a increased BACE1 activity by 400% and $20 \mu\text{M}$ VHH-B5a increased the activity by 200% (Figure 2.3 A and C). However, the addi-

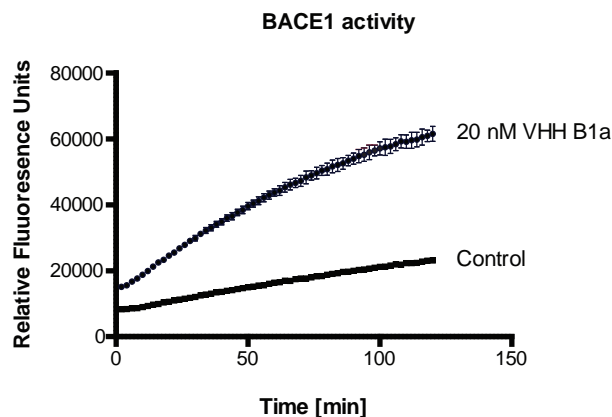


Figure 2.2. Stimulation of BACE1 activity by VHH-B1a. Recombinant BACE1 ($\sim 35 \text{ nM}$) was incubated alone or with $20 \mu\text{M}$ VHH-B1a, and enzymatic activity was assayed using MCA-[SEVNLDAEFRK](Dnp)RR. Fluorescent MCA, separated from the Dnp quencher after cleavage of the substrate by BACE1, was measured of 2 h with Fluostar. BACE1 without any additions (Control) was used as positive control. Best fit linear was calculated to determine slope (RFU/ Δt).

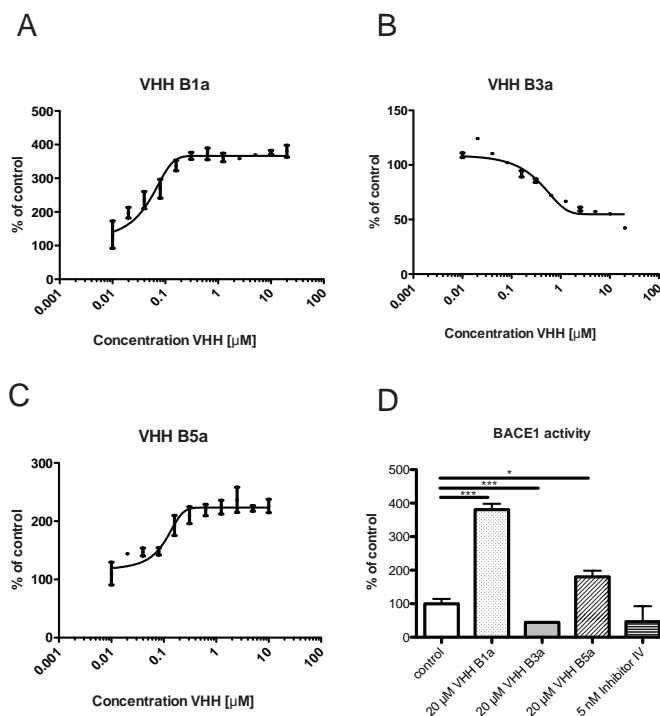


Figure 2.3. Effect of the selected VHH on BACE1 enzyme activity. Recombinant BACE1 (~35 nM) was incubated with serial dilutions of VHH-B1a (A), VHH-B3a (B) and VHH-B5a (C). Enzymatic activity was assayed using MCA-[SEVN-LDAEFRK](Dnp)RR. Fluorescent MCA, separated from the Dnp quencher after cleavage of the substrate by BACE1, was measured with Fluostar. As a control for the inhibition of BACE1 activity, 5 nM Inhibitor IV was used (D). Data represent the relative BACE1 activity compared to control with the SEM indicated. VHH-B1a and -B5a show BACE1 activity increase (relative $\log EC_{50} \sim 0.3 \mu\text{M}$ and $\log EC_{50} \sim 0.1 \mu\text{M}$, respectively) while VHH-B3a shows inhibition of activity (relative $\log IC_{50} \sim 0.9 \mu\text{M}$). One-way ANOVA was performed. * = $p < 0.05$, *** = $p < 0.0005$.

tion of 20 μM VHH-B3a to BACE1 was found to decrease BACE1 activity by 50% compared to control (Figure 2.3 B). The inhibition of BACE1 activity by VHH-B3a is equal to the effect of 5 nM Inhibitor IV (Figure 2.3 D).

VHH-B1a and -B3a were subsequently tested in an N2a-APP_{swe} cellular assay. The two VHHs and the reporter peptide were incubated with the cells for 2 h. Figure 2.4 shows the relative increase of fluorescence signal recorded during 2 h. VHH-B3a was found to decrease BACE1 activity (Figure 2.4 B). An inhibition of BACE1 activity of 50% was reached with 6.5 μM VHH, which is comparable to the inhibition of purified BACE1 *in vitro* at an equal concentration. By contrast to the *in vitro* results, VHH-B1a had only minor effect on the cellular BACE1 activity (Figure 2.4 A). Similar to the *in vitro* results, VHH-B3a inhibits BACE1 activity in the cellular assay equally compared to 5 nM Inhibitor IV (Figure 2.4 C).

The observed decrease in activity was validated by the detection of Aβ₄₀ concentration in the

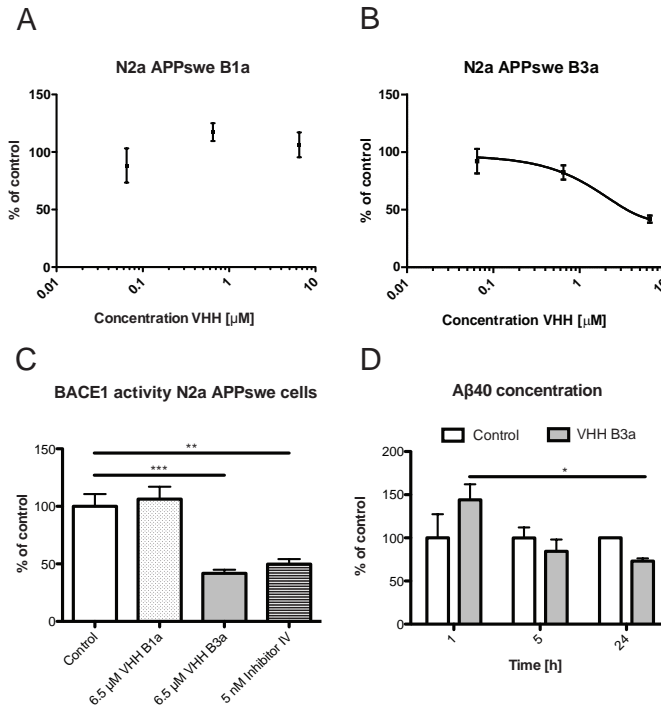


Figure 2.4. Inhibition of cellular BACE1 by VHH-B3a. N2a-APP_{swc} cells incubated with serial dilutions of VHH-B1a (A) and VHH-B3a (B) and enzymatic activity was assayed using MCA-[SEVNLDAEFRK](Dnp)RR. Fluorescent MCA, separated from the Dnp quencher after cleavage of the substrate by BACE1, was measured with FluoSTAR. VHH-B3a shows BACE1 activity inhibition activity (relative logIC₅₀ ~ 0.9 μ M), whereas for VHH-B1a no relative logEC₅₀ could be calculated. As a control for the inhibition of BACE1 activity, 5 nM Inhibitor IV was used (C). Data represent the relative BACE1 activity compared to control with the SEM indicated. One-way ANOVA was performed. * = $p < 0.05$, ** = $p < 0.005$, *** = $p < 0.0005$. A β 40 produced by N2a-APP_{swc} cells treated with VHH-B3a was quantified using an ELISA and compared with untreated cells (D). Data represent duplicate experiments, except $t = 24$ h in the control situation, which is a single experiment. One-way ANOVA showed a significant difference between 1 and 24 h treatment ($p < 0.05$)

supernatant of N2a-APP_{swc} cells. Fresh medium containing a 10 μ M concentration of VHH-B3a was added to the cells and aliquots of the medium were sampled over time. After treatment of the cells for 5 h with VHH-B3a, a reduction in A β 40 amount was measured. At 24 h this reduction was significant compared to the concentration obtained from the medium of control cells (Figure 2.4 D).

3.3. *In vivo* imaging of VHH-B3a

For *in vivo* analysis of the BACE1-specific VHH-B3a, we delivered the VHH directly into the *cisterna magna* using an intracisternal injection. To be able to image the distribution of the VHH from the *cisterna* over the brain, VHH-B3a was randomly labelled with the near infrared dye IRD800, as confirmed by SDS gel electrophoresis (Figure 2.5 A). Inhibition of BACE1 activity by VHH-B3a-IRD800 was measured to assess whether the labelled VHH was still functional. The

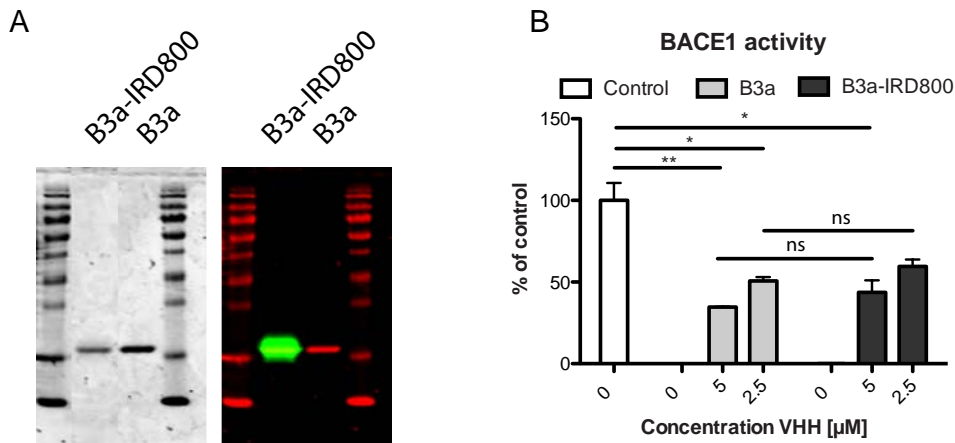


Figure 2.5. Labeling of VHH-B3a with NHS-IRD800CW. VHH-B3a was coupled to NHS-IRD800CW, analyzed by SDS-PAGE and imaged with a LiCor Odyssey Imager (A). Inhibition of BACE1 activity by IRD800 labeled VHH-B3a was compared to non-labeled VHH-B3a. No significant (ns) difference between equal concentrations of IRD800 labeled and non-labeled VHH-B3a was observed (B). One-way ANOVA was performed. * = $p < 0.05$, ** = $p < 0.005$.

inhibitory effect was still present, and only slightly reduced by 10% compared to non-labelled VHH-B3a (Figure 2.5 B).

Intracisternal injections of VHH-B3a-IRD800 resulted in a clear distribution of the labelled VHH over the entire mouse brain (Figure 2.6). With complete distribution throughout the brain, a theoretical concentration of 1 μM VHH in brain tissue could be expected. Two mice showed a similar accumulation and distribution of VHH-B3a-IRD800 throughout the brain (Figure 2.6 A, mouse 1 and mouse 2), whereas the control mice, injected with PBS, did not show any signal (Figure 2.6 A, mouse 3). With increasing time after injection, the amount of VHH-B3a-IRD800 gradually decreased, likely as a result of brain clearance (Table 2.2). Subsequently, 1 mm thick slices of the brains of all three mice were imaged to visualize the distribution of VHH-B3a-IRD800 throughout the brain (Figure 2.6 B). These brain slices demonstrate a homogeneous distribution of the VHH through the entire brain, indicating that intracisternal

Table 2.2. *In vivo* quantification of injected VHH-B3a-IRD800. A bolus injection of VHH-B3a-IRD800 was administered intracisternally into wildtype mice. At six time points after injection *in vivo* images were acquired and quantified. Values are expressed as the mean IRD800 signal in the Region of Interest (mean ± SEM).

Time after injection (h)	Mouse 1	Mouse 2	Mouse 3
0	$3.40 \pm 1.12 \times 10^4$	$4.14 \pm 0.31 \times 10^3$	$3.78 \pm 4.60 \times 10^{-3}$
1	$2.76 \pm 1.15 \times 10^4$	$6.48 \pm 0.48 \times 10^3$	$4.49 \pm 4.87 \times 10^{-3}$
3	$1.56 \pm 0.62 \times 10^4$	$6.31 \pm 0.47 \times 10^3$	$7.84 \pm 5.33 \times 10^{-3}$
6	$1.90 \pm 0.57 \times 10^4$	$5.80 \pm 0.43 \times 10^3$	$8.26 \pm 8.26 \times 10^{-4}$
24		$1.87 \pm 0.43 \times 10^3$	$3.87 \pm 3.87 \times 10^{-4}$
48			$2.47 \pm 2.47 \times 10^{-4}$

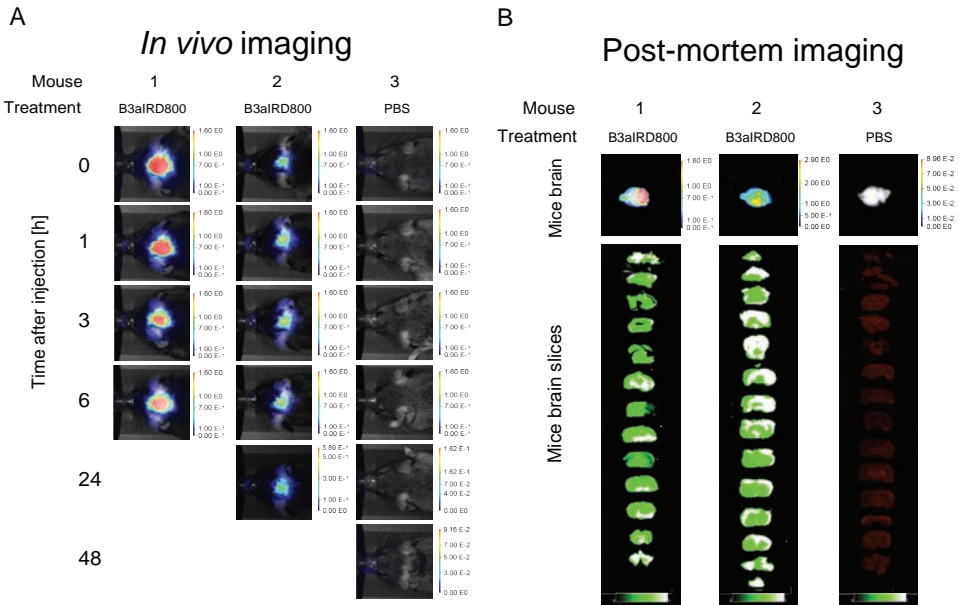


Figure 2.6. Cranial distribution of IRD800 labeled VHH-B3a injected in *cisterna magna*. Three wildtype mice were successfully injected intracisternally with a bolus of 75 μg of VHH-B3a-IRD800 (1-2) or PBS (3) and dorsally imaged *in vivo* at the indicated time points (A). Mice were sacrificed at different time points after injection (6, 24 and 48 h, respectively) by perfusion-fixation with PBS and 4% PFA. Fixed brains were imaged from the dorsal side (B). Entire fixed brains were cut in 1 mm thick slices and imaged to visualize the distribution of VHH-B3a-IRD800 (same mouse indication).

injection can be used to deliver VHH-B3a-IRD800 into the brains of mice for an *in vivo* BACE1 inhibition assay.

3.4. *In vivo* BACE1 inhibition

To assess *in vivo* BACE1 inhibition, we injected a bolus of 75 μg of VHH-IRD800 intracisternally into APP_{swe}/PS1dE9 double transgenic mice and wildtype littermates. A bolus of PBS was injected in equally sized groups as untreated controls. Concentration of both A β ₄₀ and A β ₄₂ in plasma, as well as the concentration of A β ₄₀ in whole brain homogenates were measured (Figure 2.7).

Prior to injection, blood samples were taken to determine the plasma levels of A β ₄₀ and A β ₄₂ in the transgenic mice for both the VHH treated group and the control group, to exclude group specific differences in A β concentration. To evaluate plasma concentrations over time, the concentration of the control group is set 100% for each time point and compared with VHH-B3a-IRD800. Concentrations of A β ₄₀ in plasma were equal prior to treatment (Figure 2.7 A) but A β ₄₂ plasma concentrations differed slightly, though not significantly, between the treated and untreated groups (Figure 2.7 B). At different time points after injection, we observed an almost significant decline in A β ₄₀ concentration (Figure 2.7 A). The largest

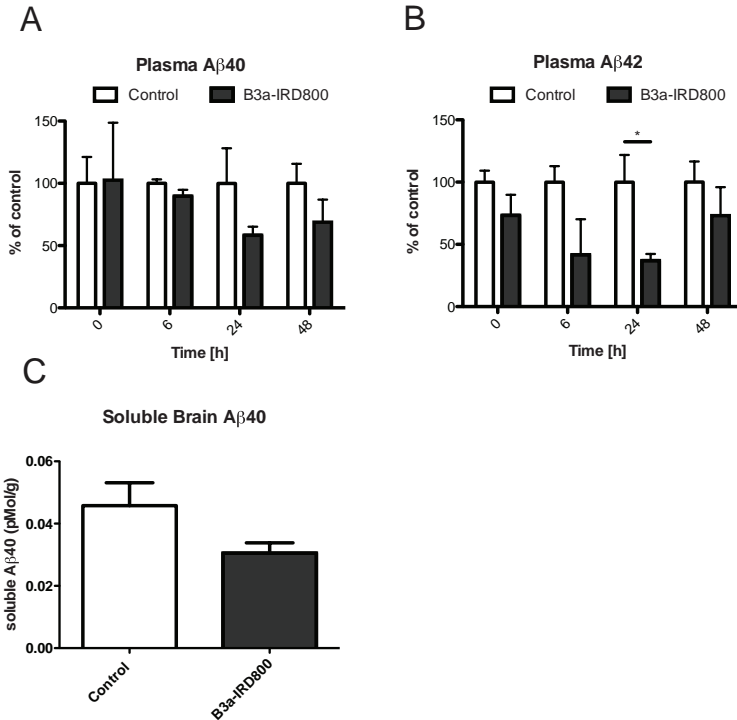


Figure 2.7. *In vivo* BACE1 inhibition by VHH-B3a-IRD800. Aβ concentrations in plasma of double transgenic APP^{swE}/PS1dE9 mice were measured before and after injection of VHH-B3a-IRD800 (n = 5) or PBS (n = 5) at the indicated time points. Plasma concentrations of the PBS control group are set at 100% for each time point. An equal plasma concentration of both Aβ40 and Aβ42 was measured before injection between the VHH treated and the control group. An almost significant difference in plasma Aβ40 concentration was observed after 24 h (A). For the Aβ42 plasma concentration the difference after 24 h was clearly significant (* = p < 0.05; B). The reduction of soluble Aβ40 in homogenized brain extracts showed a decreased density of Aβ40 in the treated group compared to the control (C). Bars represent the average concentration per treatment. The SEM is indicated. Student's *t*-test analysis was performed.

decline in Aβ40 plasma concentrations is reached at 24 h after injection. At 48 h after injection, the decline in plasma concentration appears to be less apparent compared to 24 h after injection. A similar pattern is observed for the concentration of Aβ42 in plasma (Figure 2.7 B). A significant decrease of Aβ42 plasma concentration was observed at 24 h after injection (p < 0.05).

At 48 h after injection, PFA perfused brains were extracted and the density of soluble Aβ40 in the brain was determined. An almost significant decrease of Aβ40 was observed in the treated group. As expected, the control wildtype mice did not show any detectable Aβ40 or Aβ42 in the plasma, nor detectable concentrations of Aβ40 in the brain (data not shown).

4. DISCUSSION

A β aggregation is considered to be directly involved in AD pathogenesis [42] and therefore inhibiting A β generation is of therapeutic interest.

In the present study, an immune VHH library for BACE1 affinity binders was successfully constructed. From this library, 28 phages were selected via phage display. A VHH ELISA identified 12 putative VHH candidates that bind to BACE1. Sequence analysis showed that these 12 VHHs represented three unique VHH sequences. This pool of three unique sequences is rather small for phage display selection, although, with selective elution, a lower number of unique sequences is generally found compared to panning selection and general elution using pH-shock. Selective elution was performed to enhance the discovery of inhibitory VHHs. Unexpectedly, the analysis of BACE1 activity modulation provided not only one inhibitory VHH (VHH-B3a), but also two stimulatory VHHs (VHH-B1a and -B5a).

The selected VHH-B3a consistently inhibited BACE1 activity in the biochemical and cellular assays, with only slight quantitative differences between the assays. Because the local available concentration of BACE1 in the cellular assay is unknown, the quantitative slope can vary from the biochemical slope. Although the most robust data are from biochemical assays, the cellular assay supports the biochemical data. By contrast, VHH-B1a functions inconsistently between the two assays, where the stimulation of BACE1 activity by VHH-B1a is clearly not as potent in the cellular assay compared to the stimulation of activity of purified BACE1 *in vitro*. This may be a result of the epitope that is targeted by VHH-B1a and the availability of this epitope for plasma membrane bound BACE1 [38]. By contrast, VHH-B3a shows a dose-dependent inhibition of BACE1 *in vitro* with a lower affinity compared to Inhibitor-IV, a known inhibitor of BACE1. A reduced activity of BACE1, rather than a complete inhibition, might be the preferred strategy for therapy, because a reduced A β ₄₀ and A β ₄₂ concentration already results in positive effects on AD symptoms [16,43–45]. Cross-breeding specific mice (BACE +/-) shows that a 50% reduction of BACE1 already has significant effects on AD pathology [43,44]. Full inhibition of BACE1 is most likely undesirable because a minimal concentration of A β might be crucial for cell survival [46]. However, the positive effects of a partially reduced BACE1 concentration do diminish with age and AD progression as a result of progressed pathology [22,47,48]. Nonetheless, for treatment of early AD patients and long-term treatment, it is significant not to diminish potential A β positive effects.

The *in vitro* finding of BACE1 inhibition was further evaluated *in vivo* by injecting IRD800 labelled VHH directly into the *cisterna magna* of APP_{swe}/PS1E9 double transgenic mice. Random conjugation of a fluorophore to lysines may reduce the affinity of the VHH [49]. However, despite the presence of a lysine residue in the CDR3 of VHH-B3a, its activity is only slightly

reduced with random conjugation compared to non-conjugated VHH. Consequently, we could utilize the random conjugated VHH for *in vivo* application and evaluate its potential therapeutic effect.

First, distribution of the injected VHH in the brain was determined in wildtype mice. Next, transgenic mice at an age before the onset of A β plaque formation were injected with VHH-B3a-IRD800. Brain distribution showed that, with intracisternal injection, the VHH was distributed over the brain and resident for at least 24 h. The 24 h retention provided a sufficient time frame to evaluate A β concentration in plasma samples. Blood sampling of the mice treated with VHH-B3a-IRD800 showed a lowered concentration of A β ₄₀ and A β ₄₂ in plasma. Furthermore, a lowered density of soluble A β ₄₀ in the brain was measured.

The inhibition of BACE1 activity can be achieved by modulation of the active site of BACE1 or by allosteric inhibition [50]. By using a peptide containing the cleaving target of BACE1 for selective elution, we aimed to find VHH binding near or at the active site of BACE1. VHH could possibly bind to or near the flap region that covers the active site and modulate activity [51]. However, the stimulation of BACE1 activity is more unexpected because changing the active site of a protease normally results in decreased activity. A stimulatory effect of antibodies on BACE1 activity has been reported by Zhou *et al.* [52]. The authors describe how the tested antibodies (full length murine IgGs) bind unique structural loops on BACE1. The structural loops are identified as regulatory elements for BACE1 activity, yet are outside the active site of the enzyme [52]. It is possible that by capturing the peptide in our phage display set-up, the conformation of these structural loops is altered and VHHs that bind outside the BACE1 active site are eluted. Because co-crystallization of BACE1 with an inhibitor is possible [53], co-crystallization of BACE1 with VHH-B1a and -B3a might provide insight in the manner by which these VHHs modulate BACE1 activity.

Furthermore, the exact mechanism and relevance by which VHH-B3a lowers plasma A β concentrations remains to be fully determined. A chronic treatment of young transgenic mice before plaque formation may provide more information about the possibility for inhibiting plaque formation and neurodegeneration. Subsequently, chronic treatment of these mice after onset of AD pathology will determine the potential for inhibiting the progression of pathogenesis. In addition to mono treatment, combination treatment to target BACE1 as well as A β , can be considered using anti-A β antibodies or anti-A β VHH to improve overall efficacy in treatment [54].

Several strategies for BACE1 activity inhibition have already been explored and found to be useful. Next to small molecule inhibitors, antibodies have been raised and characterized to inhibit BACE1 activity. Inhibition of secretases with antibodies is successful in a number of diseases

[55–57] and antibodies are available to inhibit BACE1 activity [27,28]. Despite the availability of functional antibodies, we consider that VHH offer multiple benefits over conventional full length antibodies, provided that the selected VHHs bind specifically and with high affinity [58]. Several intrinsic characteristics make VHHs extremely qualified for inhibiting secretase activity compared to conventional antibodies. First of all, VHHs are equipped with a long protruding CDR3 loop that is suitable for inserting into cavities on the surface of the antigen [30,59]. Inhibition of lysozyme is an example in which this protruding loop is inserted into the active site of the enzyme [59]. Furthermore, VHHs have a very low immunogenic potential as a result of great homology with human VH domains, as well as the lack of an Fc-domain [30], and can be further humanized with relative ease [60]. These characteristics make VHHs very interesting for targeting and inhibiting secretase activity.

In the present study we deliberately circumvented the problem of brain delivery of VHHs by direct intracisternal injection. Circulation of VHHs upon systemic injection gives rise to additional problems such as rapid renal clearance and limited BBB passage. Solutions to minimize size-dependent renal clearance, while the molecule remains relatively small, are known for VHHs. An example is the noncovalent binding of serum albumin to temporarily increase size and serum retention [61,62]. Besides clearance, the protective function of the BBB obstructs the brain delivery of VHHs. However, BBB passage has been shown for specific VHHs. VHHs can cross the BBB both specifically for a certain VHH [34,63] and non-specifically for VHHs with a high isoelectric point (*i.e.* $pI > 9.4$) [64]. Because VHH-B3a does not comply with either criterion, other solutions need to be examined. VHH transport over the BBB via receptor-mediated transcytosis [65] or liposomes [66] are methods that have demonstrated the delivery of VHH into the brain.

5. CONCLUSION

Despite the remaining challenges, the present study shows that VHHs inhibiting BACE1 activity leading to lowered A β production can be selected from a llama immunized with recombinant BACE1. This finding provides optimism with respect to the generation of VHH-based therapeutics for the treatment of AD in the future.

DISCLOSURE

CTV and MEK are employees and shareholders of QVQ Holding BV, a biotechnology company developing single domain antibodies from camelids. BD, MR, ES, LW, SM, CTV, and MEK planned the experiments. BD, MR, DF, RS, ES, and MEK performed the experiments. BD, MR,

DF, RS, and MEK analysed data. LW, SM, and CTV contributed essential material. BD, MR, LW, SM, CTV, and MEK wrote and revised the published manuscript.

ACKNOWLEDGMENTS

The authors would like to thank Ivo Que of the Department of Endocrinology, LUMC, for acquiring the *in vivo* images of transgenic mice. The present study was supported financially by Agentschap NL (IOP IGE5005) and the Center for Medical Systems Biology (grants S-MRI-110010 and S-MRI-110030).

REFERENCES

1. Fargo, K. & Bleiler, L. Alzheimer's Association Report. 2014 Alzheimer's disease facts and figures. *Alzheimers Dement* 10(2):e47–92 (2014).
2. Glenner, G. G. & Wong, C. W. Alzheimer's disease: initial report of the purification and characterization of a novel cerebrovascular amyloid protein. *Biochem. Biophys. Res. Commun.* 120(3):885–890 (1984).
3. Tanzi, R. E. & Bertram, L. Twenty years of the Alzheimer's disease amyloid hypothesis: A genetic perspective. *Cell* 120(4):545–555 (2005).
4. Selkoe, D. J. Cell biology of the amyloid beta-protein precursor and the mechanism of Alzheimer's disease. *Annu. Rev. Cell Biol.* 10:373–403 (1994).
5. Han, W., Ji, T., Mei, B. & Su, J. Peptide p3 may play a neuroprotective role in the brain. *Med. Hypotheses* 76(4):543–546 (2011).
6. Hussain, I., Powell, D., Howlett, D. R., Tew, D. G., Meek, T. D., Chapman, C., Gloger, I. S., Murphy, K. E., Southan, C. D., Ryan, D. M., *et al.* Identification of a novel aspartic protease (Asp 2) as beta-secretase. *Mol. Cell. Neurosci.* 14(6):419–427 (1999).
7. Lin, X., Koelsch, G., Wu, S., Downs, D., Dashti, a & Tang, J. Human aspartic protease memapsin 2 cleaves the beta-secretase site of beta-amyloid precursor protein. *Proc. Natl. Acad. Sci. U. S. A.* 97(4):1456–1460 (2000).
8. Bodendorf, U., Fischer, F., Bodian, D., Multhaup, G. & Paganetti, P. A Splice Variant of Beta-Secretase Deficient in the Amyloidogenic Processing of the Amyloid Precursor Protein. *J. Biol. Chem.* 276(15):12019–12023 (2001).
9. Vassar, R., Bennett, B. D., Babu-Khan, S., Kahn, S., Mendiaz, E. a, Denis, P., Teplow, D. B., Ross, S., Amarante, P., Loeloff, R., *et al.* Beta-secretase cleavage of Alzheimer's amyloid precursor protein by the transmembrane aspartic protease BACE. *Science* 286(5440):735–741 (1999).
10. Sinha, S., Anderson, J. P., Barbour, R., Basl, G. S., Caccavello, R., Davis, D., Doan, M., Dovey, H. F., Frigon, N., Hong, J., *et al.* Purification and cloning of amyloid precursor protein beta-secretase from human brain. *Nature* 402(6761):537–540 (1999).
11. Yan, R., Bienkowski, M. J., Shuck, M. E., Miao, H., Tory, M. C., Pauley, a M., Brashier, J. R., Stratman, N. C., Mathews, W. R., Buhl, a E., *et al.* Membrane-anchored aspartyl protease with Alzheimer's disease beta-secretase activity. *Nature* 402(6761):533–537 (1999).
12. De Strooper, B. Aph-1, Pen-2, and Nicastrin with Presenilin generate an active gamma-Secretase complex. *Neuron* 38(1):9–12 (2003).
13. Fukumoto, H., Cheung, B. S., Hyman, B. T. & Irizarry, M. C. Beta-secretase protein and activity are increased in the neocortex in Alzheimer disease. *Arch. Neurol.* 59(9):1381–1389 (2002).
14. Ahmed, R. R., Holler, C. J., Webb, R. L., Li, F., Beckett, T. L. & Murphy, M. P. BACE1 and BACE2 enzymatic activities in Alzheimer's disease. *J. Neurochem.* 112(4):1045–1053 (2010).
15. Harada, H., Tamaoka, A., Ishii, K., Shoji, S., Kametaka, S., Kametani, F., Saito, Y. & Murayama, S. Beta-site APP cleaving enzyme 1 (BACE1) is increased in remaining neurons in Alzheimer's disease brains. *Neurosci. Res.* 54(1):24–29 (2006).
16. Laird, F. M., Cai, H., Savonenko, A. V, Farah, M. H., He, K., Melnikova, T., Wen, H., Chiang, H.-C., Xu, G., Koliatsos, V. E., *et al.* BACE1, a major determinant of selective vulnerability of the brain to amyloid-beta amyloidogenesis, is essential for cognitive, emotional, and synaptic functions. *J. Neurosci.* 25(50):11693–11709 (2005).
17. Cai, H., Wang, Y., McCarthy, D., Wen, H., Borchelt, D. R., Price, D. L. & Wong, P. C. BACE1 is the major beta-secretase for generation of Abeta peptides by neurons. *Nat. Neurosci.* 4(3):233–234 (2001).
18. Luo, Y., Bolon, B., Kahn, S., Bennett, B. D., Babu-Khan, S., Denis, P., Fan, W., Kha, H., Zhang, J., Gong, Y., *et al.* Mice deficient in BACE1, the Alzheimer's β -secretase, have normal phenotype and abolished β -amyloid generation. *Nat. Neurosci.* 4(3):231–232 (2001).

19. Roberds, S. L., Anderson, J., Basi, G., Bienkowski, M. J., Branstetter, D. G., Chen, K. S., Freedman, S. B., Frigon, N. L., Games, D., Hu, K., *et al.* BACE knockout mice are healthy despite lacking the primary beta-secretase activity in brain: implications for Alzheimer's disease therapeutics. *Hum. Mol. Genet.* 10(12):1317–1324 (2001).
20. Ohno, M., Sametsky, E. a., Younkin, L. H., Oakley, H., Younkin, S. G., Citron, M., Vassar, R. & Disterhoft, J. F. BACE1 Deficiency Rescues Memory Deficits and Cholinergic Dysfunction in a Mouse Model of Alzheimer's Disease. *Neuron* 41(1):27–33 (2004).
21. Sankaranarayanan, S., Holahan, M. a., Colussi, D., Crouthamel, M.-C., Devanarayan, V., Ellis, J., Espeseth, A., Gates, A. T., Graham, S. L., Grego, A. R., *et al.* First demonstration of cerebrospinal fluid and plasma A β lowering with oral administration of a β -site amyloid precursor protein-cleaving enzyme 1 inhibitor in nonhuman primated. *J. Pharmacol. Exp. Ther.* 328(1):131–140 (2009).
22. Fukumoto, H., Takahashi, H., Tarui, N., Matsui, J., Tomita, T., Hirode, M., Sagayama, M., Maeda, R., Kawamoto, M., Hirai, K., *et al.* A noncompetitive BACE1 inhibitor TAK-070 ameliorates Abeta pathology and behavioral deficits in a mouse model of Alzheimer's disease. *J. Neurosci.* 30(33):11157–11166 (2010).
23. Mancini, F., De Simone, A. & Andrisano, V. Beta-secretase as a target for Alzheimer's disease drug discovery: An overview of *in vitro* methods for characterization of inhibitors. *Anal. Bioanal. Chem.* 400(7):1979–1996 (2011).
24. Cully, M. Deal watch: Lilly buys back into the BACE race for Alzheimer's disease. *Nat. Rev. Drug Discov.* 13(11):804–804 (2014).
25. Eketjall, S., Janson, J., Jeppsson, F., Svanhagen, a., Kolmodin, K., Gustavsson, S., Radesater, a.-C., Eliason, K., Briem, S., Appellkvist, P., *et al.* AZ-4217: A High Potency BACE Inhibitor Displaying Acute Central Efficacy in Different *In Vivo* Models and Reduced Amyloid Deposition in Tg2576 Mice. *J. Neurosci.* 33(24):10075–10084 (2013).
26. Vassar, R. BACE1 inhibitor drugs in clinical trials for Alzheimer's disease. *Alzheimers. Res. Ther.* 6(9):1–14 (2014).
27. Rakover, I., Arbel, M. & Solomon, B. Immunotherapy against APP beta-secretase cleavage site improves cognitive function and reduces neuroinflammation in Tg2576 mice without a significant effect on brain abeta levels. *Neurodegener. Dis.* 4(5):392–402 (2007).
28. Arbel, M. & Solomon, B. A Novel Immunotherapy for Alzheimers Disease: Antibodies against the Beta-Secretase Cleavage Site of APP. *Curr. Alzheimer Res.* 4(4):437–445 (2007).
29. Chang, W.-P., Downs, D., Huang, X.-P., Da, H., Fung, K.-M. & Tang, J. Amyloid-beta reduction by memapsin 2 (beta-secretase) immunization. *FASEB J.* 21(12):3184–3196 (2007).
30. Muyldermans, S. Nanobodies: natural single-domain antibodies. *Annu. Rev. Biochem.* 82(1):775–797 (2013).
31. Hamers-Casterman, C., Atarhouch, T., Muyldermans, S., Robinson, G., Hamers, C., Songa, E. B., Bendahman, N. & Hamers, R. Naturally occurring antibodies devoid of light chains. *Nature* 363(6428):446–448 (1993).
32. Dumoulin, M., Last, A. M., Desmyter, A., Decanniere, K., Canet, D., Larsson, G., Spencer, A., Archer, D. B., Sasse, J., Muyldermans, S., *et al.* A camelid antibody fragment inhibits the formation of amyloid fibrils by human lysozyme. *Nature* 424(6950):783–788 (2003).
33. Desmyter, A., Spinelli, S., Payan, F., Lauwerys, M., Wyns, L., Muyldermans, S. & Cambillau, C. Three camelid VHH domains in complex with porcine pancreatic alpha-amylase: Inhibition and versatility of binding topology. *J. Biol. Chem.* 277(26):23645–23650 (2002).
34. Muruganandam, A., Tanha, J., Narang, S. & Stanimirovic, D. Selection of phage-displayed llama single-domain antibodies that transmigrate across human blood-brain barrier endothelium. *FASEB J.* 16(2):240–2 (2002).
35. Thinakaran, G., Teplow, D. B., Siman, R., Greenberg, B. & Sisodia, S. S. Metabolism of the 'Swedish' amyloid precursor protein variant in neuro2a (N2a) cells: Evidence that cleavage at the 'beta-secretase' site occurs in the Golgi apparatus. *J. Biol. Chem.* 271(16):9390–9397 (1996).

36. Verheesen, P., Roussis, A., de Haard, H. J., Groot, A. J., Stam, J. C., den Dunnen, J. T., Frants, R. R., Verkleij, A. J., Theo Verrips, C. & van der Maarel, S. M. Reliable and controllable antibody fragment selections from Camelid non-immune libraries for target validation. *Biochim. Biophys. Acta* 1764(8):1307–19 (2006).
37. Hoogenboom, H. R., de Bruijne, A. P., Hufton, S. E., Hoet, R. M., Arends, J. W. & Roovers, R. C. Antibody phage display technology and its applications. *Immunotechnology* 4(1):1–20 (1998).
38. Stockley, J. H. & O'Neill, C. Understanding BACE1: Essential protease for amyloid-beta production in Alzheimer's disease. *Cell. Mol. Life Sci.* 65(20):3265–3289 (2008).
39. Mandell, J. G., Neuberger, T., Drapaca, C. S., Webb, A. G. & Schiff, S. J. The dynamics of brain and cerebrospinal fluid growth in normal versus hydrocephalic mice. *J. Neurosurg. Pediatr.* 6(1):1–10 (2010).
40. Vanderstichele, H., Van Kerschaver, E., Hesse, C., Davidsson, P., Buysse, M. A., Andreasen, N., Minthon, L., Wallin, A., Blennow, K. & Vanmechelen, E. Standardization of measurement of beta-amyloid(1-42) in cerebrospinal fluid and plasma. *Amyloid* 7(4):245–58 (2000).
41. Hansson, O., Zetterberg, H., Vanmechelen, E., Vanderstichele, H., Andreasson, U., Londos, E., Wallin, A., Minthon, L. & Blennow, K. Evaluation of plasma ABeta40 and ABeta42 as predictors of conversion to Alzheimer's disease in patients with mild cognitive impairment. *Neurobiol. Aging* 31(3):357–367 (2010).
42. Selkoe, D. J. Alzheimer's disease: genes, proteins, and therapy. *Physiol. Rev.* 81(2):741–766 (2001).
43. McConlogue, L., Buttini, M., Anderson, J. P., Brigham, E. F., Chen, K. S., Freedman, S. B., Games, D., Johnson-Wood, K., Lee, M., Zeller, M., *et al.* Partial reduction of BACE1 has dramatic effects on Alzheimer plaque and synaptic pathology in APP transgenic mice. *J. Biol. Chem.* 282(36):26326–26334 (2007).
44. Kimura, R., Devi, L. & Ohno, M. Partial reduction of BACE1 improves synaptic plasticity, recent and remote memories in Alzheimer's disease transgenic mice. *J. Neurochem.* 113(1):248–261 (2010).
45. Chabrier, M. A., Blurton-Jones, M., Agazaryan, A. A., Nerhus, J. L., Martinez-Coria, H. & LaFerla, F. M. Soluble a β promotes wild-type tau pathology *in vivo*. *J. Neurosci.* 32(48):17345–50 (2012).
46. Plant, L. D., Boyle, J. P., Smith, I. F., Peers, C. & Pearson, H. a. The production of amyloid beta peptide is a critical requirement for the viability of central neurons. *J. Neurosci.* 23(13):5531–5535 (2003).
47. Chang, W.-P., Huang, X., Downs, D., Cirrito, J. R., Koelsch, G., Holtzman, D. M., Ghosh, A. K. & Tang, J. Beta-secretase inhibitor GRL-8234 rescues age-related cognitive decline in APP transgenic mice. *FASEBJ.* 25(2):775–784 (2011).
48. Devi, L. & Ohno, M. Mechanisms that lessen benefits of β -secretase reduction in a mouse model of Alzheimer's disease. *Transl. Psychiatry* 3(7):e284 (2013).
49. Kijanka, M., Warnders, F. J., El Khattabi, M., Lub-De Hooge, M., Van Dam, G. M., Ntziachristos, V., De Vries, L., Oliveira, S. & Van Bergen En Henegouwen, P. M. P. Rapid optical imaging of human breast tumour xenografts using anti-HER2 VHHs site-directly conjugated to IRDye 800CW for image-guided surgery. *Eur. J. Nucl. Med. Mol. Imaging* 40(11):1718–1729 (2013).
50. Wang, W., Liu, Y. & Lazarus, R. a. Allosteric inhibition of BACE1 by an exosite-binding antibody. *Curr. Opin. Struct. Biol.* 23(6):797–805 (2013).
51. Davies, D. R. The structure and function of the aspartic proteinases. *Annu. Rev. Biophys. Biophys. Chem.* 19:189–215 (1990).
52. Zhou, L., Chávez-Gutiérrez, L., Bockstael, K., Sannerud, R., Annaert, W., May, P. C., Karran, E. & De Strooper, B. Inhibition of β -secretase *in vivo* via antibody binding to unique loops (D and F) of BACE1. *J. Biol. Chem.* 286(10):8677–8687 (2011).
53. Durham, T. B. & Shepherd, T. A. Progress toward the discovery and development of efficacious BACE inhibitors. *Curr. Opin. Drug Discov. Devel.* 9(6):776–91 (2006).
54. Jacobsen, H., Ozmen, L., Caruso, a., Narquizian, R., Hilpert, H., Jacobsen, B., Terwel, D., Tanghe, a. & Bohrmann, B. Combined Treatment with a BACE Inhibitor and Anti-A Antibody Gantenerumab Enhances Amyloid Reduction in APPLondon Mice. *J. Neurosci.* 34(35):11621–11630 (2014).

55. Hayashi, I., Takatori, S., Urano, Y., Iwanari, H., Isoo, N., Osawa, S., Fukuda, M. a., Kodama, T., Hamakubo, T., Li, T., *et al.* Single chain variable fragment against nicastrin inhibits the γ -secretase activity. *J. Biol. Chem.* 284(41):27838–27847 (2009).
56. Fong, J. E., Le Nihouannen, D. & Komarova, S. V. Tumor-supportive and osteoclastogenic changes induced by breast cancer-derived factors are reversed by inhibition of γ -secretase. *J. Biol. Chem.* 285(41):31427–31434 (2010).
57. Huang, H. S., Buck, C. B. & Lambert, P. F. Inhibition of gamma secretase blocks HPV infection. *Virology* 407(2):391–396 (2010).
58. Van Bockstaele, F., Holz, J.-B. & Revets, H. The development of nanobodies for therapeutic applications. *Curr. Opin. Investig. Drugs* 10(11):212–24 (2009).
59. Desmyter, A., Transue, T. R., Ghahroudi, M. A., Thi, M. H., Poortmans, F., Hamers, R., Muyldermans, S. & Wyns, L. Crystal structure of a camel single-domain VH antibody fragment in complex with lysozyme. *Nat. Struct. Biol.* 3(9):803–811 (1996).
60. Vincke, C., Loris, R., Saerens, D., Martinez-Rodriguez, S., Muyldermans, S. & Conrath, K. General strategy to humanize a camelid single-domain antibody and identification of a universal humanized nanobody scaffold. *J. Biol. Chem.* 284(5):3273–84 (2009).
61. Roovers, R. C., Laeremans, T., Huang, L., De Taeye, S., Verkleij, A. J., Revets, H., De Haard, H. J. & Van Bergen En Henegouwen, P. M. P. Efficient inhibition of EGFR signalling and of tumour growth by antagonistic anti-EGFR Nanobodies. *Cancer Immunol. Immunother.* 56(3):303–317 (2007).
62. Harmsen, M. M. & De Haard, H. J. Properties, production, and applications of camelid single-domain antibody fragments. *Appl. Microbiol. Biotechnol.* 77(1):13–22 (2007).
63. Rutgers, K. S., Nabuurs, R. J. A., van den Berg, S. A. A., Schenk, G. J., Rotman, M., Verrips, C. T., van Duinen, S. G., Maat-Schieman, M. L., van Buchem, M. A., de Boer, A. G., *et al.* Transmigration of beta amyloid specific heavy chain antibody fragments across the *in vitro* blood-brain barrier. *Neuroscience* 190:37–42 (2011).
64. Li, T., Bourgeois, J.-P., Celli, S., Glacial, F., Le Sourd, A.-M., Mecheri, S., Weksler, B., Romero, I., Couraud, P.-O., Rougeon, F., *et al.* Cell-penetrating anti-GFAP VHH and corresponding fluorescent fusion protein VHH-GFP spontaneously cross the blood-brain barrier and specifically recognize astrocytes: application to brain imaging. *FASEB J.* 26(10):3969–79 (2012).
65. Yu, Y. J., Atwal, J. K., Zhang, Y., Tong, R. K., Wildsmith, K. R., Tan, C., Bien-Ly, N., Hersom, M., Maloney, J. A., Meilandt, W. J., *et al.* Therapeutic bispecific antibodies cross the blood-brain barrier in nonhuman primates. *Sci. Transl. Med.* 6(261):261ra154 (2014).
66. Rotman, M., Welling, M. M., Bunschoten, A., de Backer, M. E., Rip, J., Nabuurs, R. J. A., Gaillard, P. J., van Buchem, M., van der Maarel, S. M. & van der Weerd, L. Enhanced liposomal brain delivery of an anti-amyloid VHH-2H heavy chain antibody fragment in a mouse model for Alzheimer's disease. *J. Control. Release* 203:40–50 (2015).

* Authors contributed equally to this work.

1. Department of Human Genetics, Leiden University Medical Center, The Netherlands
2. Department of Radiology, Leiden University Medical Center, The Netherlands
3. to-BBB technologies BV, Leiden, The Netherlands

3

CHAPTER

ENHANCED GSH-PEG LIPOSOMAL BRAIN DELIVERY OF VHH-PA2H IN A MOUSE MODEL FOR AD

Adapted from

Enhanced glutathione PEGylated liposomal brain delivery of an anti-amyloid single domain antibody fragment in a mouse model for Alzheimer's disease.

Maarten Rotman ^{1a,*}, Mick M. Welling ^{2,*}, Anton Bunschoten ², Maaike de Backer ³, Jaap Rip ³, Rob J.A. Nabuurs ³, Pieter J. Gaillard ³, Mark A. van Buchem ², Silvère M. van der Maarel ¹ and Louise van der Weerd ^{1a}.

Journal of Controlled Release 203 (2015) 40-50

ABSTRACT

Introduction: Treatment of neurodegenerative disorders such as Alzheimer's disease is hampered by the blood-brain barrier (BBB). This tight cerebral vascular endothelium regulates selective diffusion and active transport of endogenous molecules and xenobiotics into and out of the brain parenchyma. In this study, glutathione targeted PEGylated (GSH-PEG) liposomes were designed to deliver amyloid-targeting antibody fragments across the BBB into the brain. Two different formulations of GSH-PEG liposomes based on 1,2-dimyristoyl-sn-glycero-3-phosphocholine (DMPC) and egg-yolk phosphatidylcholine (EYPC) were produced. Both formulations encapsulate 15 kDa amyloid beta binding llama single domain antibody fragments (VHH-pa2H).

Methods: To follow the biodistribution of VHH-pa2H rather than the liposome, the antibody fragment was labelled with the radioisotope indium-111. To prolong the shelf life of the construct beyond the limit of radioactive decay, an active-loading method was developed to efficiently radiolabel the antibody fragments after encapsulation into the liposomes, with radiolabeling efficiencies of up to 68% after purification. The radiolabeled liposomes were administered via a single intravenous bolus injection to APP_{swe}/PS1dEg double transgenic mice – a mouse model of Alzheimer's disease –, and their wildtype littermates.

Results: Both GSH-PEG DMPC and GSH-PEG EYPC liposomes significantly increased the standard uptake values (SUV) of VHH-pa2H in the blood of the animals compared to free VHH-pa2H. Encapsulation in GSH-PEG EYPC liposomes resulted in the highest increase in SUV in the brains of transgenic animals.

Conclusion: Overall, these data provide evidence that GSH-PEG liposomes may be suitable for specific delivery of single domain antibody fragments over the BBB into the brain.

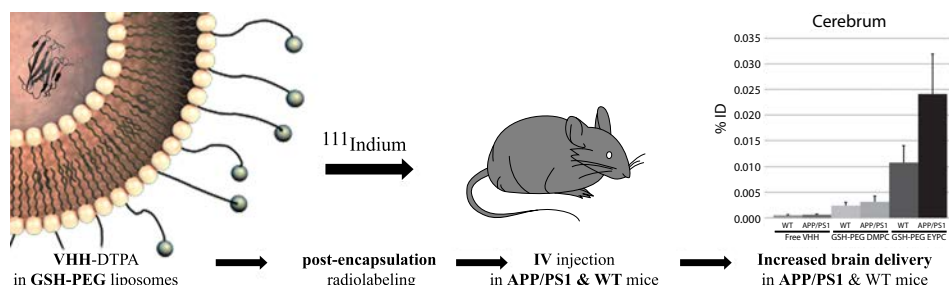


Figure 3.1. Graphical abstract. Encapsulation of VHH-pa2H-DTPA in GSH-PEG liposomes leads to increased uptake in the murine brain.

1. INTRODUCTION

1.1. Alzheimer's disease

Alzheimer's disease (AD) is a progressive neurological disorder, characterized by the cerebral accumulation of amyloid plaque in the brain parenchyma and often along the vascular wall. Not surprisingly, the deposition of oligomerized amyloid beta ($A\beta$) peptides into these amyloid plaques is thought of to be the onset of the pathogenic cascade that eventually leads to cognitive decline, and is postulated as the amyloid cascade hypothesis [1–3]. Despite ongoing research on the processes that trigger amyloid deposition and other mechanisms involved in the process, a cure for AD is not available [4]. Furthermore, making a definitive diagnosis of the disease during life is still not possible [5]. One of the main obstacles is the blood-brain barrier (BBB), which efficiently ensures proper brain functioning and prevents brain penetration of harmful substances. Yet delivery of amyloid binding compounds into the brain is of vital importance in order to detect amyloid accumulation for diagnostic purposes [6–8] and to develop treatments that target cerebral amyloid [9–11].

1.2. Heavy chain antibody fragments

Heavy chain antibody fragments were derived from the camelid heavy chain only antibody repertoire (VHHs). They were selected for their ability to detect $A\beta$ depositions with high affinity [12], to differentiate between vascular and parenchymal $A\beta$ deposits [13], and to cross an *in vitro* BBB model [14]. VHHs are considered non-immunogenic, even after repeated administration [15,16] and have been safely used in human clinical trials [17]. Previously, we investigated the *in vivo* properties of two heavy chain antibody fragments – VHH-ni3A and VHH-pa2H – in double transgenic APP_{swe}/PS1dEg mice, a model characteristic for AD [18]. Intravenously administered VHH showed rapid renal clearance, with blood half-lives of 10–20 min. This observation was similar to other studies with VHH, effectively limiting the BBB passage of the VHH [19–22]. For this reason, extending the blood residential time and exploring alternative cranial delivery methods may be beneficial for enhancing the BBB passage of the VHH and subsequently increasing its accumulation on amyloid plaques in the brain [21]. Since injected VHHs are rapidly cleared from the circulation via the renal pathway, the process of passive filtration of VHH in the nephrons of the kidney should be prevented. This can be achieved by various antibody modification strategies, e.g., increasing their 10–15 kDa size to >65 kDa by PEGylation, polymerization or fusion to other antibody fragments, or by producing bi-specific VHH, where one of the fragments binds a plasma ‘carrier’ such as albumin. However, although effective in prolonging blood residential times, all of these modifications could impair the function and BBB passage of the VHH [19,23–25].

1.3. GSH-PEG liposomes

To elongate blood residential times of the VHH and to deliver them across the BBB, without modifying the VHH itself, we used glutathione targeted PEGylated (GSH-PEG) liposomes, known as G-Technology® [26,27]. Both glutathione and PEGylated liposomes are FDA approved and the G-Technology has recently shown to efficiently deliver an anticancer agent into a mouse brain tumor [28] as well as deliver fluorescent tracers into rat brains [26]. This provides a safe and likely platform for future diagnostic or therapeutic applications of the VHH in AD. Glutathione is an endogenous tripeptide that possesses antioxidant-like properties. It is actively transported across the BBB, although the exact molecular mechanism involved remains to be elucidated [28,29].

We hypothesized that GSH-PEG liposomal VHH-pa2H crosses the BBB, where, after disruption of the liposomes, the VHH-pa2H load will be released and bind to amyloid plaques. In order to follow the *in vivo* biodistribution of the VHH-pa2H itself, rather than the liposome, we radiolabeled DTPA-conjugated VHH-pa2H with radioisotope indium-111 (¹¹¹In). Compared to the random labeling of proteins with technetium-99m [30,31], labeling procedures based on ¹¹¹In incorporation into a DTPA chelator are well defined and widely used in clinical scintigraphy. The DTPA chelator can be conjugated to lysine residues [32] and has been successfully used for the effective and efficient radiolabeling of VHH [18]. Furthermore, incorporation of ¹¹¹In into free DTPA chelators can be achieved after encapsulation in the liposomes [33,34], a technique we here modified to benefit our DTPA-conjugated VHH-pa2H. In this way, a stable stock of liposomes loaded with DTPA-conjugated VHH can be prepared, which can be radiolabeled directly before use, effectively increasing the shelf life of the formulation beyond the limit of radioactive decay.

In this study we evaluated two GSH-PEG liposomal formulations containing DTPA-¹¹¹In labeled VHH-pa2H to determine their delivery of the VHH to the murine brain and analyzed their general biodistribution profiles. We describe the DTPA conjugation to VHH-pa2H, radiochemical analysis, liposomal encapsulation, post encapsulation radiolabeling and testing of immune-reactivity on human AD brain cryosections. Brain uptake and biodistribution of liposomal and free VHH-pa2H-DTPA-¹¹¹In were assessed in transgenic mice versus control littermates.

2. MATERIALS AND METHODS

2.1. Yeast production and purification of VHH-pa2H

Llama heavy chain antibody fragment VHH-pa2H, previously selected against A β [13], was subcloned into a yeast optimized production vector free of any peptide tags (MW 12,799.3 g/mol,

pI 9.86). The VHH was commercially produced by over-expression in *Saccharomyces cerevisiae* (BAC b.v., Leiden, NL) and purified as described previously [35]. The obtained VHH solution was concentrated by absorption of water with polyethylene glycol 6000 (Sigma, NL) through an Uptima CelluSep T1 35000 MWCO dialysis membrane (Interchim, FR), dialyzed against PBS for 3 times > 1 hour and stored at -20°C until use.

2.2. Conjugation of DTPA to VHH-pa2H

To allow radiolabeling with ^{111}In , a DTPA chelator was conjugated to primary amine groups on the five available lysine residues of VHH-pa2H (Figure 3.2 A). The VHH-pa2H solution (pH 8.0) was incubated with 5 × molar excess of the chelator p-SCN-Bn-DTPA ($\text{C}_{22}\text{H}_{28}\text{N}_4\text{O}_{10}\text{S}_3\text{HCl}$, MW 649.92 g/mol, Macrocyclics Inc., USA), i.e. 254.0 µg p-SCN-Bn-DTPA (390.9 nmol) in 50 µl DMSO per 1 mg VHH-pa2H (78.2 nmol) in 100–800 µl PBS. The reaction mixture was incubated at 37°C for 3 h while stirring at 300 rpm. Thereafter, the conjugated VHH-pa2H-DTPA mixture was dialyzed 3 × > 1 h at 4°C against 2.5 l of 25 mM ammonium acetate buffer (pH 5.5), including one overnight dialysis step (Figure 3.2 B). Conjugated and dialyzed preparations were stored in the dark at 4°C.

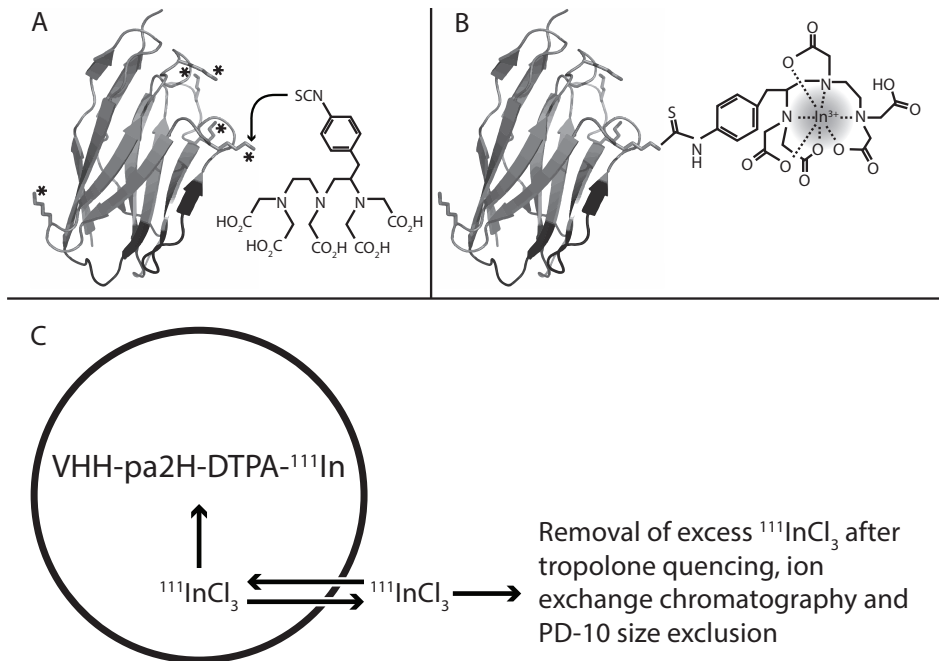


Figure 3.2. Radiolabeling and encapsulation of VHH-pa2H. (A) Figurative representation of the conjugation of the DTPA chelator to llama antibody fragment VHH-pa2H. Asterisks highlight lysine residues with available primary amines which act as potential conjugation sites on the VHH. (B) Schematic representation of VHH-pa2H-DTPA after radiolabeling with ^{111}In , which is bound in the DTPA chelator. (C) Schematic representation of post encapsulation labeling of VHH-pa2H-DTPA, in which $^{111}\text{InCl}_3$ diffuses over the liposomal membrane to bind to DTPA on the VHH molecule. After 3 h non-bound $^{111}\text{InCl}_3$ is removed.

2.3. Analysis of DTPA-conjugated VHH-pa2H

The purity and molecular masses of VHH-pa2H before and after the DTPA conjugation reaction were analyzed and monitored by analytical-scale size exclusion high-performance liquid chromatography (HPLC) using a Reprosil 200 column (Dr. Maisch HPLC GmbH, DE) with a flow-rate of 1 ml PBS/min. Spectra were obtained analyzed at 220 nm. Molecular masses were determined by matrix-assisted laser desorption/ionization time-of-flight mass spectrometry (MALDI-TOF MS) on an Ultraflex II mass spectrometer (Bruker Daltonixs, DE) using sinapic acid (10 mg/ml of 70% ACN/0.5% trifluoroacetic acid in water) as matrix. The mass spectrometer was used in the positive ion reflection mode. Spectra were analyzed in FlexAnalysis 3.0 (Bruker Daltonics) for smoothing, baseline subtraction, and picking. The mass tolerance was set to 50 ppm.

2.4. Radiolabeling and analysis of non-encapsulated VHH-pa2H-DTPA

VHH-pa2H-DTPA was radiolabeled with ^{111}In through incorporation of the isotope into the DTPA chelator. For this purpose $^{111}\text{InCl}_3$ (Covidien, NL) was added to 0.7 mg VHH-pa2H-DTPA in a final volume of 0.8 ml of 0.25 mM ammonium acetate buffer (pH 5.5) and incubated for 2 h at 37°C in the dark while gently stirring at 60 rpm. The amount of $^{111}\text{InCl}_3$ was adjusted depending on radiation strength upon delivery to yield 5 μg of VHH-pa2H at 10–20 MBq per injection at the time of injection. Unbound isotope was removed with a PD-10 desalting column (GE Healthcare, NL) in 20 elution fractions of 0.5 ml PBS. The fractions were counted for radioactivity to determine the yield of labeling and to identify impurities. Fractions containing radio-labeled VHH-pa2H (VHH-pa2H-DTPA- ^{111}In) were pooled and analyzed with instant thin-layer chromatography (ITLC) at various time points to determine the radiochemical stability over time. HPLC analysis was performed to study the radioactive profile of VHH-pa2H-DTPA- ^{111}In on a Jasco HPLC system using a SuperdexTM peptide size exclusion column (GE Healthcare), with a mixture of 0.05 M sodium phosphate and 0.15 M sodium chloride (pH 6.8) as eluent at flow rates of 0.5 ml/min.

2.5. Autoradiography on human brain sections using VHH-pa2H-DTPA- ^{111}In

To confirm conserved immune reactivity for A β of VHH-pa2H after radiolabeling, VHH-pa2H-DTPA- ^{111}In was used to perform autoradiography on human post-mortem AD brain cryosections. All human tissues were obtained from anonymous patients or healthy aged donors as confirmed by neuropathological examination in agreement with the guidelines of the Medical Ethics Committee of the Leiden University Medical Center (Leiden, NL). All tissues were processed in a coded fashion, according to Dutch national ethics guidelines (Code for Proper Secondary Use of Human Tissue, Dutch Federation of Medical Scientific Societies). Immune reac-

tivity was assessed as described before [14,18]. Briefly, acetone fixed serial section (20 µm) were blocked with 4% milk powder (Marvel dried skimmed milk powder, Premier Foods, UK) in PBS (mPBS). Blocked sections were incubated overnight with 600-750 pmol of VHH-pa2H-DTPA-¹¹¹In (0.5-2 MBq) in 0.1 ml mPBS. The sections were exposed for 24 h on autoradiography films, which were then processed and scanned on a Bio-Rad GS800 Densitometer (Bio-Rad Laboratories, USA). Scanned images were evaluated using Quantity One version 4.6.6 (Bio-Rad).

2.6. Liposomal encapsulation of VHH-pa2H-DTPA

Two formulations of glutathione-conjugated polyethylene glycol (PEG) coated liposomes encapsulating VHH-pa2H-DTPA (GSH-PEG liposomal VHH-pa2H-DTPA) were prepared using a post-insertion method. One formulation contained 1,2-dimyristoyl-sn-glycero-3-phosphocholine (DMPC; Lipoid, CH); the other egg-yolk phosphatidylcholine (EYPC; Lipoid). Briefly, 100 mM lipids, either DMPC or EYPC, 75 mM cholesterol (Sigma) and 1.8 mM 1,2-distearoyl-sn-glycero-3-phosphoethanolamine conjugated PEG MW 2000 (mPEG-DSPE, 1 mol%; Lipoid) were dissolved in absolute ethanol and mixed with 6.0 mg/ml VHH-pa2H-DTPA in 25 mM ammonium acetate (pH 5.5). This lipid/protein mixture was extruded through 200 nm and 100 nm Whatman filters (Instruchemie, NL) to reduce particle size and obtain uniform liposomes. Micelles were prepared by mixing glutathione (Sigma) and DSPE-PEG-maleimide (NOF, BE) at a 1.5:1 M ratio for 2 h at room temperature. GSH-PEG-DSPE micelles were incubated with the extruded liposomes for 2 h to obtain GSH-PEG liposomal VHH-pa2H-DTPA. Non-encapsulated VHH-pa2H-DTPA was removed via size exclusion chromatography, using a Sepharose 6 Fast Flow XK16/40 column equilibrated with PBS on an ÄKTA Purifier (GE Healthcare). The size of the liposomes was measured using a Malvern Zetasizer Nano ZS90 (Malvern Instruments, UK). The amount of encapsulated VHH-pa2H-DTPA was quantified using HPLC analysis (Perkin Elmer 200 series with a Waters Xbridge BEH300 C4 3.5 µm, 2.1 × 150 mm). Liposome preparations and free VHH-pa2H-DTPA were stored at 4°C and used within 4 weeks following preparation.

2.7. Radiolabeling of VHH-pa2H-DTPA after liposomal encapsulation

Samples of 1 ml GSH-PEG liposomal VHH-pa2H-DTPA were radiolabeled in 25 mM ammonium acetate buffer (pH 5.5) according to the radiolabeling protocol for free VHH-pa2H-DTPA described above. The radiolabeling was carried out at room temperature, rather than 37°C, because GSH-PEG EYPC liposomes are unstable at 37°C. After 3 h the labeling reaction was quenched by capturing non-bound ¹¹¹In in the reaction mixture with 0.1 ml tropolone (10 mg/ml in 20% v/v ethanol in water) for 1 h at room temperature while stirring at 20 rpm [36,37]. Any VHH-pa2H-DTPA released from the liposomes, as well as ¹¹¹In-tropolone complexes, was removed from the liposomes with 1 ml of ion exchange resin beads (3 × pre-rinsed with 30 ml

PBS) for 1 h at 20°C while stirring at 20 rpm (Figure 3.2 C). Thereafter, the resin beads were settled by gravity and the supernatant was collected and purified on a PD-10 column as described above. Fractions containing GSH-PEG liposomal VHH-pa2H-DTPA-¹¹¹In were pooled and analyzed with ITLC to determine the overall radiochemical yield. The purified tracers were instantly used for further experiments.

2.8. Pharmacokinetic studies in mice

All animal studies have been approved by the institutional Animal Experiments Committee (DEC permits 09132 and 12065) of the Leiden University Medical Center. The *in vivo* studies were performed using 12-16 month old transgenic mice or wildtype littermates from a colony set up using the APP_{swe}/PS1dE9 strain (APP/PS1; JAX[®] Mice and Services, The Jackson Laboratory, USA). The APP/PS1 mice are known to accumulate vascular and parenchymal A β depositions [14,38]. Besides standard genotyping, amyloid pathology was confirmed on brain sections by standard Thioflavin T staining [18].

Animals were injected in the tail vein with 5 μ g VHH-pa2H-DTPA-¹¹¹In (10-20 MBq), either free or encapsulated in liposomes, in 0.2 ml saline. The total injected dose (ID) in each mouse was determined in a dose-calibrator (VDC101, Veenstra Instruments, NL). To determine the clearance of the tracers from the blood, 5 μ l samples were collected from the tail vein at 5, 30, 60, 90, 120, 240 and 1440 min. after injection and counted for radioactivity. After decay correction, radioactivity counts in blood were expressed as the Standard Uptake Value (SUV), defined as (the tissue radioactivity / tissue weight) / (the injected activity / body weight).

The elimination rate constant K_e (h^{-1}) was determined over the time interval 1-24 h from the (%ID/ml) whole blood data for each individual animal as the slope of ¹¹¹In (%ID/ml) over time. The half-life $T_{1/2}$ is equal to $\ln(2) / K_e \cdot AUC_{0-24h}$ and is determined based on %ID/ml whole blood (%ID/ml) * h. The whole blood clearance CL is $1 / (AUC / 100)$, expressed in ml/h. Volume of distribution VD is defined as $(100 / AUC * K_e)$, which should be equal to CL / K_e .

2.9. Micro-SPECT imaging

To study the biodistribution of radiolabeled VHH-pa2H preparations, mice were imaged at 1, 4 and approx. 24 h after administration of free VHH-pa2H-DTPA-¹¹¹In or either GSH-PEG DMPC liposomal VHH-pa2H-DTPA-¹¹¹In or GSH-PEG EYPC liposomal VHH-pa2H-DTPA-¹¹¹In (5-15 MBq/mouse). The animals were scanned in a three-headed U-SPECT-II (MILabs, NL) under continuous 1-2% isoflurane anesthesia. Total body scans were acquired for 30 min. using a 0.6 mm mouse pinhole collimator, and energy setting at 171 keV with a window of 20% [39]. The image was reconstructed using six POSEM iterations with 16 subsets, a 0.2 mm voxel size and

with decay and scatter corrections integrated into the reconstruction. Volume-rendered images were generated and analyzed using Amide 1.0.2. [40].

2.10. Biodistribution

At 24 h after injection of the tracers in APP/PS1 (n=2-8) and wildtype animals (n=2-8) and after collecting the last blood sample, the mice were euthanized by 0.25 ml intraperitoneal injection of 200 mg/ml pentobarbital sodium (Euthasol; AST Pharma, NL). Immediately after, the mice were perfused via cardiac puncture with 15 ml PBS and bladder including urine, the heart, the lungs, the spleen, the liver, both kidneys, part of the left femoral muscle, the cerebrum, and the cerebellum were removed. All tissues and organs were weighed and counted for radioactivity (Wizard2 2470 automatic gamma scintillation counter, Perkin Elmer, USA). Obtained measurements were expressed as SUV.

2.11. Statistical analysis

All data are presented as mean value (\pm SEM) of 2-8 independent measurements. Statistical analysis for differences between groups in the animal studies was performed by Student's paired t-test with one-tailed distribution. Significance was assigned for P-values of <0.05 . All analyses and calculations were performed using Microsoft® Office Excel 2010 and GraphPad Prism version 5.01 for Windows (GraphPad Software, USA).

3. RESULTS

3.1. Production of VHH-pa2H in *S. cerevisiae*

To obtain the high concentrations of VHH which are needed for efficient encapsulation, the yeast-produced VHHs were purified and concentrated. Protein content analysis, i.e. SDS-PAGE, Bradford assay and Nanodrop® spectral absorption at 280 nm, of the concentrated product showed a final yield of 10 mg VHH per 1 l growth medium, at an average concentration of 7 mg/ml VHH in PBS after dialysis.

3.2. Conjugation of p-SCN-Bn-DTPA to VHH-pa2H

Analysis of the conjugation reaction with size exclusion HPLC showed a shift from 8.6 min. of non-conjugated VHH-pa2H (Figure 3.3 A) to 4.5, 5.0, and 6.2 min. for VHH-pa2H-DTPA in the reaction mixtures (Figure 3.3 B); indicating the development of at least three larger species of DTPA-conjugated VHH-pa2H. After 3 h of conjugation no residual non-conjugated VHH could be detected in the reaction mixture. MALDI-TOF MS analysis for VHH-pa2H indicated a MW

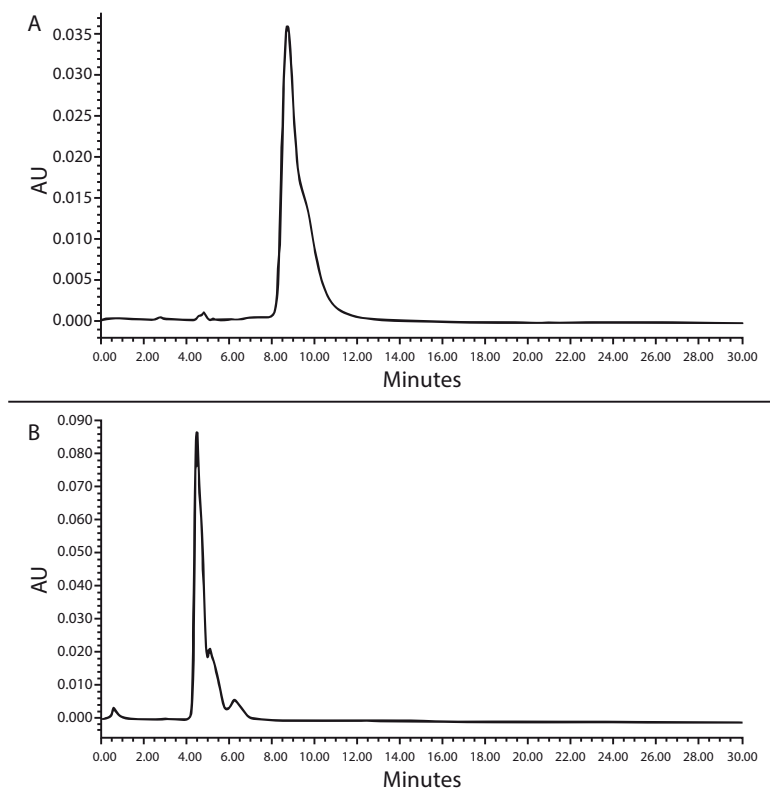


Figure 3.3. HPLC size-exclusion analysis of the conjugation of DTPA to VHH-pa2H at 220 nm shows a clear full shift from 8.6 min. of non-conjugated VHH-pa2H (A) to 4.5, 5.0, and 6.2 min. for VHH-pa2H-DTPA in the reaction mixtures (B); indicating the development of at least three larger species of DTPA-conjugated VHH-pa2H.

of 12,816 g/mol, which is in concordance with the estimated MW of 12,799 g/mol. After conjugation, an increase in MW of approximately 649 g/mol per DTPA moiety should be expected. However, reproducible analysis of DTPA-conjugated VHH-pa2H on MALDI-TOF MS was not possible.

3.3. Analysis of ^{111}In radiolabeled non-liposomal VHH-pa2H-DTPA

Using ITLC analysis, a radiochemical yield of $94.7 \pm 2.1\%$ was determined after 3 h of incubation of VHH-pa2H-DTPA with $^{111}\text{InCl}_3$. HPLC size-exclusion chromatography of VHH-pa2H-DTPA- ^{111}In showed a major peak of $>95\%$ of the injected radioactivity eluting at 12.88 min. (Figure 3.4 A). PD-10 size-exclusion analysis of the same labeling solution confirmed the labeling yield ($n=4$) at $95.3 \pm 3.9\%$ (Figure 3.4 B). Fractions 7-9, containing the majority of the VHH-pa2H-DTPA- ^{111}In , were pooled and used for further studies. Samples were analyzed at room temperature for stability assessment up to 168 h after the onset of radiolabeling. Using

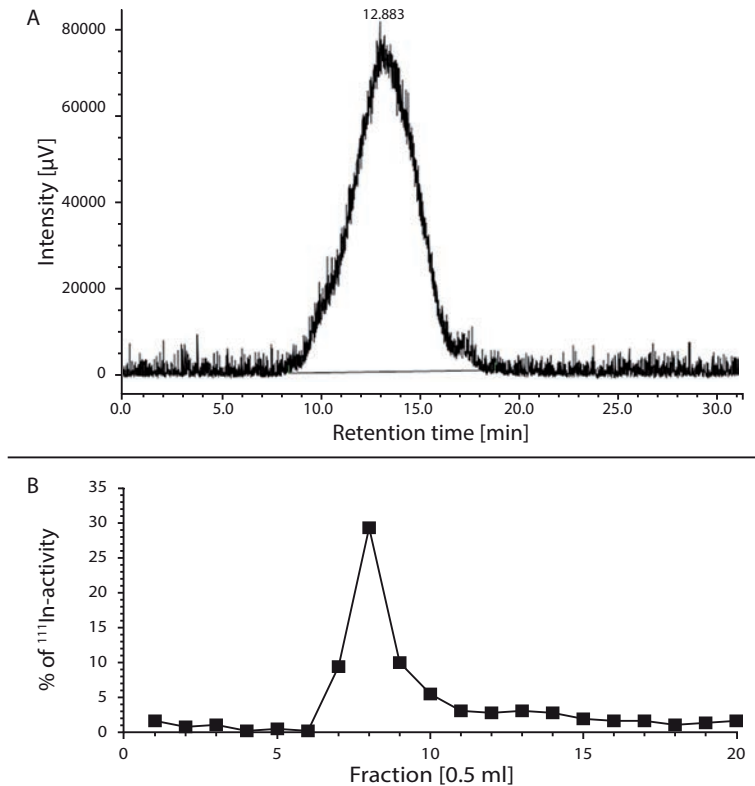


Figure 3.4. Analysis of the ¹¹¹In labeling of VHH-pa2H-DTPA. (A) HPLC size-exclusion analysis of free VHH-pa2H-DTPA-¹¹¹In depicts a radioactivity profile representing >95% of radioactivity eluting at 12.88 min. (B) PD-10 analysis of free VHH-pa2H-DTPA-¹¹¹In shows fraction samples of 0.5 ml in PBS, collected and counted for radioactivity, with a peak in fractions 7 – 9, containing $95.3 \pm 3.9\%$ of the total amount of radioactivity measured.

ITLC analysis within this time span, less than 10% release of the radioactive compound was observed.

3.4. Autoradiography on human patient brain cryosections

Autoradiography performed with VHH-pa2H-DTPA-¹¹¹In showed dense accumulation of the tracer to amyloid depositions in the frontal cortex of an AD patient (Figure 3.5). No accumulation was observed in the cortex or the white matter of an age-matched healthy control which lacks amyloid depositions.

3.5. Liposomal encapsulation of VHH-pa2H-DTPA

The preparation of both GSH-PEG DMPC and GSH-PEG EYPC liposomal VHH-pa2H-DTPA yielded comparable liposomal batches. The average size of GSH-PEG DMPC liposomal VHH-pa2H-DTPA was 110 nm with a polydispersity index (PDI) of 0.105. The GSH-PEG EYPC lipo-

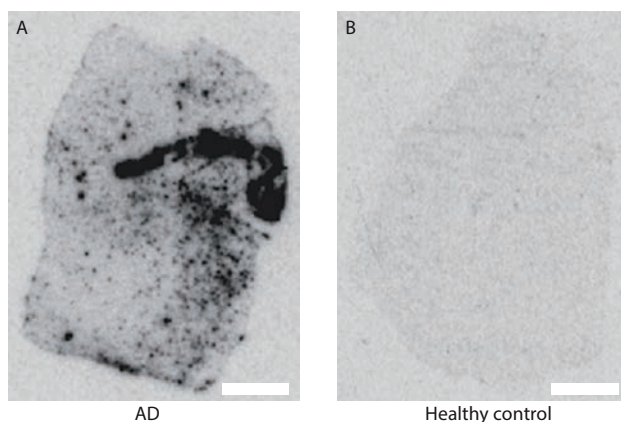


Figure 3.5. Autoradiographs of free VHH-pa2H-DTPA-¹¹¹In on 5 μm thick human cortical AD brain cryosections (A) or age-matched healthy controls (B). The staining on patient material and the absence of it in healthy controls indicate that labeling of the VHH-DTPA with a radioactive ¹¹¹In compound does not interfere with its specific affinity for Aβ.

somal VHH-pa2H-DTPA had an average size of 108 nm with a PDI of 0.061. Encapsulation of the VHH-pa2H-DTPA yielded protein concentrations of 0.25 mg/ml and 0.39 mg/ml in the GSH-PEG DMPC and GSH-PEG EYPC liposomal formulations, respectively.

3.6. Post-encapsulation radiolabeling of liposomal VHH-pa2H-DTPA

After 3 h of incubation with ¹¹¹In, prior to further purification steps, the liposomal associated radioactivity yielded 81.5 ± 9.0% for GSH-PEG DMPC liposomes and 86.4 ± 17.1% for GSH-PEG EYPC liposomes according to ITLC. After purification of non-bound radioactivity from the liposomes by tropolone quenching and ion-exchange purification, over-all labeling yields were calculated to be 68.1 ± 2.6% for the VHH-pa2H-DTPA-¹¹¹In in GSH-PEG DMPC liposomes and 43.1 ± 6.8% for GSH-PEG EYPC liposomes. To determine if the radioactivity was solely bound to VHH-pa2H-DTPA, the liposomes were agitated for 10 s with 1:1 (v/v) acetone to disrupt the liposomes. The amount of ¹¹¹In-activity bound to VHH-pa2H-DTPA was >97% for both liposomal formulations as determined by ITLC analysis. Additional control labeling experiments of free VHH-pa2H showed less than 5% of ¹¹¹In bound to VHH-pa2H as determined by PD-10 analysis. Furthermore, no significant radioactivity was taken up inside empty liposomes as shown by the attempt to radiolabel empty GSH-PEG DMPC liposomes with ¹¹¹In (Figure 3.6).

3.7. Pharmacokinetics

Blood clearance was expressed as percentage of injected dose per ml of blood (%ID/ml), from which the AUC was calculated. Both liposomal preparations clearly showed an increased AUC profile compared to non-encapsulated VHH (Figure 3.7 and Table 3.1). Quantitative analysis of AUC values confirmed that the AUC of non-encapsulated VHH-pa2H-DTPA-¹¹¹In was signifi-

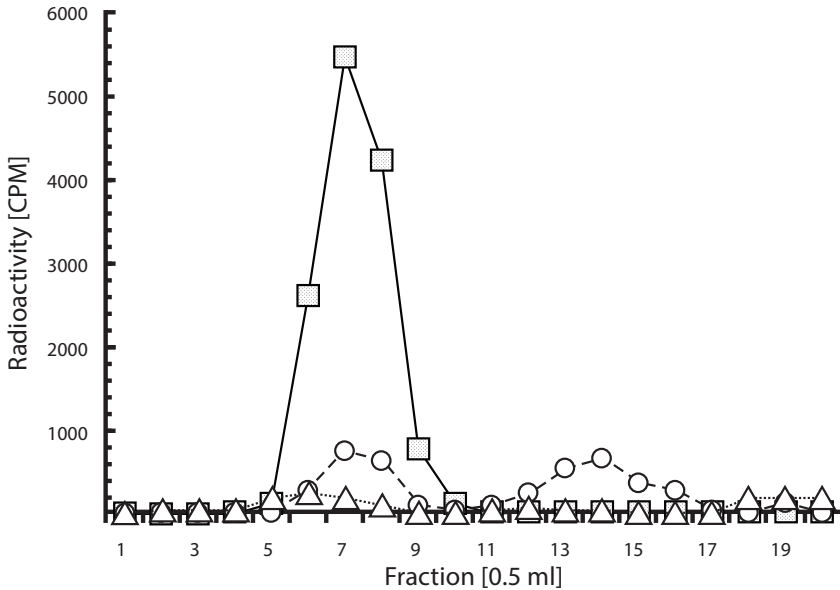


Figure 3.6. PD-10 analysis of ^{111}In -activity in liposomal preparations. Radioactive samples were applied on PD-10 columns and fractions of 0.5 ml PBS were collected and counted for radioactivity. Data are expressed as radioactivity counts in counts per minute (cpm). Closed dotted squares represent GSH-PEG DMPC liposomal VHH-pa2H-DTPA- ^{111}In and show that the majority of radioactivity is associated with encapsulated chelated VHH. Open triangles represent free VHH-pa2H without the DTPA chelator and open circles represent empty GSH-PEG DMPC liposomes and indicate minor binding of the radiotracer to free VHH or empty liposomes.

cantly smaller ($p < 0.05$) than the AUC of VHH-pa2H-DTPA- ^{111}In in GSH-PEG DMPC and GSH-PEG EYPC liposomes. Furthermore, GSH-PEG EYPC liposomal VHH-pa2H-DTPA- ^{111}In showed a significantly increased AUC ($p < 0.05$) compared to the GSH-PEG DMPC formulation (Table 3.1). Clearance rates and volume of distribution are also reported in Table 3.1, and as expected both liposomal formulations are clearly decreased for both CL and VD, with GSH-PEG EYPC liposomes presenting with the slowest clearance and lowest VD.

Table 3.1. Pharmacokinetic parameters of VHH-pa2H-DTPA- ^{111}In in APP^{swE}/PS1Eg transgenic mice (APP/PS1) and wildtype littermates (WT). The mice were injected intravenously with 0.2 ml saline containing 5 μg VHH-pa2H-DTPA- ^{111}In (10–20 MBq) either non-liposomal (Free VHH-pa2H-DTPA- ^{111}In), or encapsulated in either GSH-PEG DMPC or GSH-PEG EYPC liposomes.

	Free VHH-pa2H-DTPA- ^{111}In		GSH-PEG DPMC VHH-pa2H-DTPA- ^{111}In		GSH-PEG EYPC VHH-pa2H-DTPA- ^{111}In	
	WT	APP/PS1	WT	APP/PS1	WT	APP/PS1
K_e [h^{-1}]	0.192	0.193	0.0851	0.0651	0.0518	0.0460
$T_{1/2}$ [h]	3.83	4.36	8.22	11.0	13.8	15.2
AUC _{0–24} [%ID/ml*h]	10.8	12.5	64.1	87.0	465	293
CL [ml/h]	9.24	7.99	1.6	1.15	0.215	0.341
VD [ml]	48.0	41.4	18.3	17.7	4.15	7.41

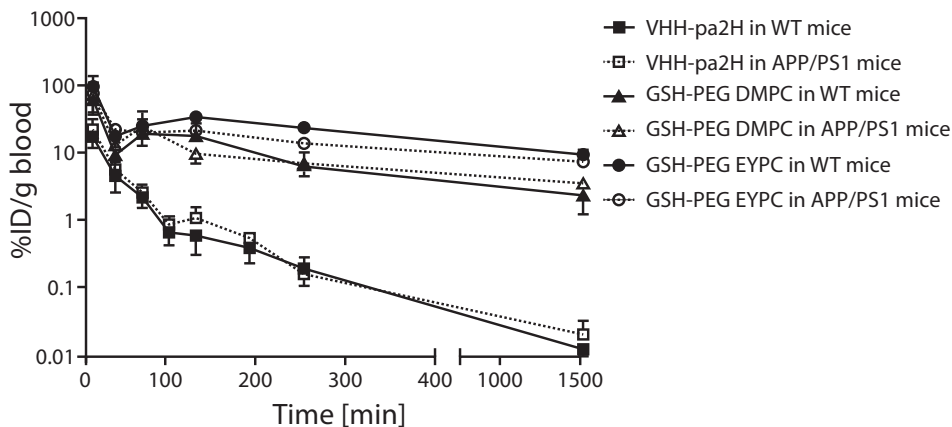


Figure 3.7. Blood clearance of VHH-pa2H-DTPA-¹¹¹In in APP^{swc}/PS1dEg transgenic mice (APP/PS1) and wildtype littermates (WT). Data are the mean \pm SEM of 4-8 observations and are shown as percentage of injected dose per gram of blood (%ID/g) over time.

3.8. Micro-SPECT imaging

Micro-SPECT imaging of the mice visually confirmed the observation that GSH-PEG DMPC liposomal encapsulated VHH-pa2H-DTPA-¹¹¹In had a slower clearance of radioactivity by the kidneys than the non-liposomal VHH-pa2H-DTPA-¹¹¹In. Accumulated radioactivity was mostly located in the renal cortex and was slowly released to the urinary bladder. The slower clearance of GSH-PEG EYPC liposomal encapsulated radiolabeled VHH was even more pronounced. At various time points, reservoirs of radioactivity from the GSH-PEG EYPC tracer were observed in the liver, lungs, spleen, heart, muscle and blood pool (Figure 3.8 A-C). No signal was observed in the regions of the thyroid gland, the gastrointestinal tract or the bone marrow of any of the animals.

3.9. Biodistribution

Radioactivity counts of excised organs and tissues showed that the biodistribution profiles of the different formulations generally follow the blood pharmacokinetics (Table 3.2). As observed in micro-SPECT imaging, the kidneys are the main organ of clearance of the radioactivity of all tracers from the blood pool. In addition, liver clearance is apparent for the liposomal formulations. For free VHH-pa2H-DTPA-¹¹¹In the radioactivity was rapidly excreted via the urinary bladder. At 24 h after injection $90.4 \pm 0.5\%$ of the injected dose had been excreted. Excretion of radioactivity was significantly less ($p < 0.05$) at 24 h after injection with either GSH-PEG DMPC ($72.9 \pm 4.8\%$) or GSH-PEG EYPC ($40.8 \pm 10.9\%$) encapsulated VHH-pa2H-DTPA-¹¹¹In compared to the free VHH. No significant differences were observed in urinary excretion of the three tracers between APP/PS1 mice and wildtype littermates.

When analyzing the total amount of VHH in excised perfused brains, both groups treated with

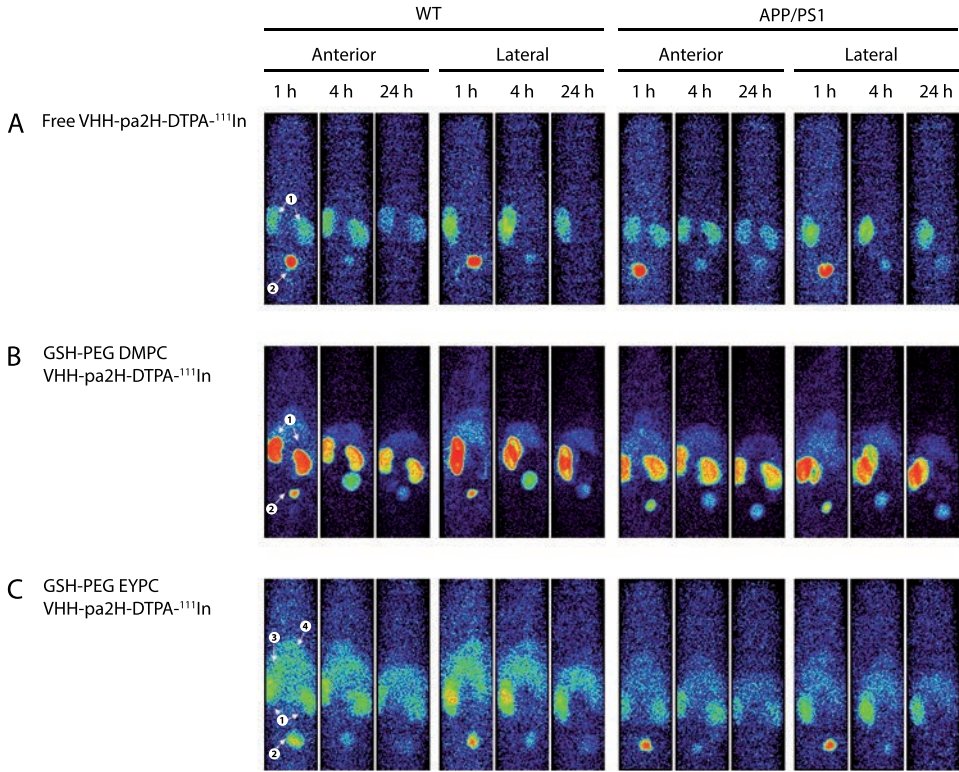


Figure 3.8. Anterior and lateral micro-SPECT scintigraphs show biodistribution and clearance of radiolabeled VHH-pa2H-DTPA-¹¹¹In in APP_{swE}/PS1E9 transgenic mice (APP/PS1) and wildtype littermates (WT) at various time points. The mice were injected intravenously with 0.2 ml saline containing 5 μg VHH-pa2H-DTPA-¹¹¹In (10-20 MBq) either non-liposomal (A), or encapsulated in either GSH-PEG DMPC (B) or GSH-PEG EYPC (C) liposomes. White arrows indicate the kidneys (1), urinary bladder (2), liver (3) and heart (4).

liposomal encapsulated radiolabeled VHH-pa2H showed significantly increased retention of the tracer in the brain compared to free VHH-pa2H ($p < 0.05$; Figure 3.9 A and Table 3.2). To assess whether GSH targeting results in specific uptake in the brain over other organs, the brain/muscle ratio was determined (Figure 3.9 B and Table 3.2). For APP/PS1 transgenic mice, the GSH-PEG EYPC VHH-pa2H-DTPA-¹¹¹In tracer showed about a four-fold increased activity in the brain compared to wildtype littermates, indicating that VHH-pa2H is entering the brain and is being retained in the presence of amyloid plaques. In contrast to AD patients, APP/PS1 mice also have amyloid deposits in the cerebellum; in this experiment indeed both cerebrum and cerebellum showed increased retention of VHH-pa2H in the transgenic mice.

Additional organ/blood and organ/muscle ratios can be found in Supplementary table 3.1 and Supplementary table 3.2.

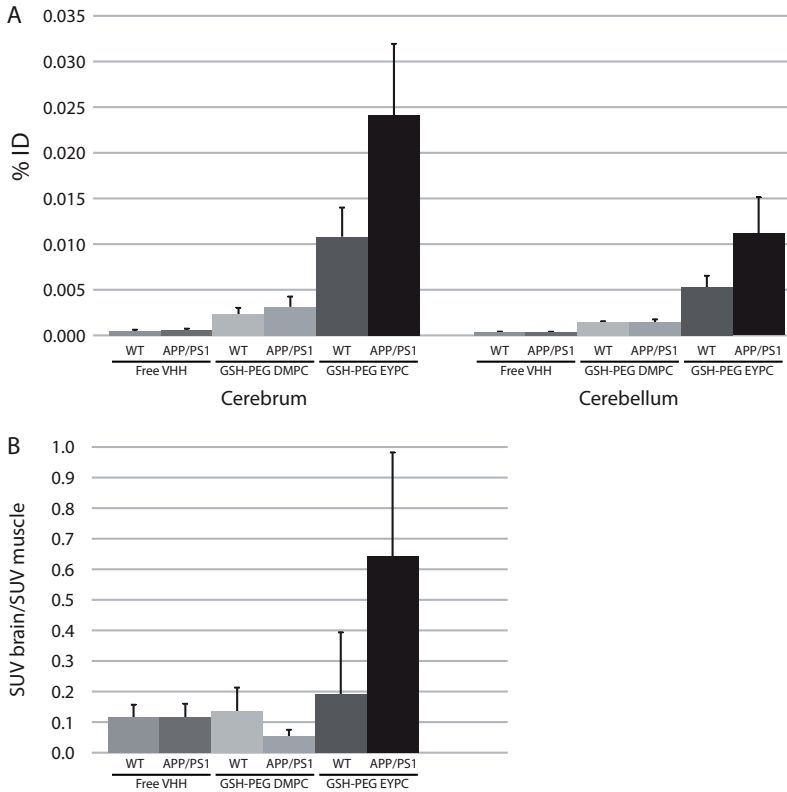


Figure 3.9. Uptake in brain tissues of the radiolabeled VHH-pa2H-DTPA-¹¹¹In in APP^{swE}/PS1dEg transgenic mice (APP/PS1) and wildtype littermates (WT). (A) The mice were injected intravenously with 0.2 ml saline containing 5 µg VHH-pa2H-DTPA-¹¹¹In (10–20 MBq) either non-liposomal (Free VHH), or encapsulated in either GSH-PEG DMPC or GSH-PEG EYPC liposomes. After 24 h the mice were sacrificed and perfused to remove blood from the organs and tissues, after which the cerebrum and cerebellum were removed and counted for radioactivity. Data is shown as the uptake of the tracer in the total brain tissue, expressed as percentage of injected dose (%ID). (B) Relative uptake in the whole brain compared to muscle tissue based on the standard uptake value (SUV) data as presented in Table 3.2.

4. DISCUSSION

In this study we provide evidence that delivery of VHH-pa2H into brains of transgenic APP/PS1 mice can be significantly improved by encapsulation in glutathione targeted PEGylated liposomes.

Previous studies, and confirmed in this study (Figure 3.7), showed that free VHH-pa2H has a fast blood clearance profile and may not cross the BBB in amounts sufficient for diagnostics or therapeutics *in vivo* [18]. Therefore, VHH-pa2H was encapsulated in two different formulations of glutathione targeted liposomes. Liposomes are well-known drug delivery systems which result in longer blood residence of VHHs and potentially increased bioavailability, and glutathione targeting has already been proven to enhance brain uptake of small chemical compounds compared to non-targeted liposomes [26,41].

Table 3.2. Biodistribution of VHH-pazH-DTPA-¹¹¹In in APP^{PSdEg} transgenic mice (APP/PS1) and wildtype littermates (WT) at 24 h after injection. The mice were injected intravenously with 0.2 ml saline containing 5 µg VHH-pazH-DTPA-¹¹¹In (10–20 MBq) either non-liposomal (Free VHH-pazH-DTPA-¹¹¹In), or encapsulated in either GSH-PEG DMPC or GSH-PEG EYPC liposomes. Values are presented as the mean (±SEM) of the radioactivity counted per weighted organ after sacrifice and perfusion, expressed as the standard uptake value (SUV), defined as (tissue radioactivity / tissue weight) / (injected activity / body weight). All values are corrected for radioactive decay over time.

n	Free VHH-pazH-DTPA- ¹¹¹ In		GSH-PEG DMPC VHH-pazH-DTPA- ¹¹¹ In		GSH-PEG EYPC VHH-pazH-DTPA- ¹¹¹ In	
	WT	APP/PS1	WT	APP/PS1	WT	APP/PS1
	8	8	2	2	4	4
	SUV ± SEM (SUV = %ID / g tissue per g mouse)					
Blood 24h	0.005 ± 0.002	0.009 ± 0.005	0.218 ± 0.053	1.071 ± 0.155 #	3.433 ± 0.458 #¶	5.604 ± 1.353 #¶
Urine & bladder	0.246 ± 0.126	0.410 ± 0.180	0.418 ± 0.284	0.192 ± 0.150	2.605 ± 1.145 #	3.970 ± 2.193
Heart	0.009 ± 0.001	0.007 ± 0.001 *	0.189 ± 0.001 #	0.165 ± 0.064	0.560 ± 0.125 #	1.242 ± 0.303 #¶
Lungs	0.008 ± 0.002	0.007 ± 0.001	0.313 ± 0.145	0.081 ± 0.027	0.383 ± 0.042 #	0.714 ± 0.195 #
Spleen	0.034 ± 0.010	0.029 ± 0.006	0.887 ± 0.200	1.173 ± 0.274	7.137 ± 2.278 #	10.138 ± 3.150 #
Liver	0.046 ± 0.011	0.044 ± 0.009	0.947 ± 0.059 #	1.006 ± 0.435	2.460 ± 0.535 #	3.718 ± 0.763 #*
Kidneys	4.236 ± 0.589	4.067 ± 0.667	18.713 ± 0.042 #	16.563 ± 6.459	13.112 ± 0.973 #	19.221 ± 1.990 #*
Muscle	0.021 ± 0.005	0.021 ± 0.007	0.125 ± 0.082	0.158 ± 0.106	0.117 ± 0.025 #	0.233 ± 0.072 #
Cerebrum	0.000 ± 0.000	0.000 ± 0.000	0.003 ± 0.001	0.003 ± 0.002	0.011 ± 0.004 #	0.071 ± 0.025 #*¶
Cerebellum	0.001 ± 0.000	0.001 ± 0.000	0.008 ± 0.002	0.005 ± 0.002	0.015 ± 0.006 #	0.094 ± 0.031 #*¶
Brain	0.001 ± 0.000	0.001 ± 0.000	0.01 ± 0.001 #	0.008 ± 0.004	0.026 ± 0.010 #	0.165 ± 0.056 #*¶
Cerebrum/cerebellum ratio	0.433 ± 0.122	0.550 ± 0.153	0.455 ± 0.234	0.707 ± 0.022 #	0.861 ± 0.182 #	0.734 ± 0.052
Cerebrum/muscle ratio	0.042 ± 0.021	0.041 ± 0.016	0.049 ± 0.038	0.025 ± 0.007	0.089 ± 0.025 #	0.361 ± 0.141
Cerebellum/muscle ratio	0.074 ± 0.020	0.076 ± 0.027	0.086 ± 0.039	0.035 ± 0.008	0.120 ± 0.045	0.461 ± 0.148 #*
Cerebrum/blood ratio	0.095 ± 0.023	0.155 ± 0.053	0.013 ± 0.000	0.003 ± 0.002 #*	0.003 ± 0.001 #¶	0.012 ± 0.003 #*¶
Cerebellum/blood ratio	0.370 ± 0.115	0.422 ± 0.102	0.039 ± 0.019	0.005 ± 0.003	0.004 ± 0.001 #	0.016 ± 0.003 #*
Brain/blood ratio	0.465 ± 0.135	0.577 ± 0.139	0.053 ± 0.019	0.008 ± 0.005	0.007 ± 0.002 #	0.029 ± 0.006 #*
Muscle/blood ratio	7.686 ± 1.891	10.914 ± 3.991	0.706 ± 0.546 #	0.165 ± 0.123	0.035 ± 0.009 #	0.044 ± 0.014 #
Brain/muscle ratio	0.116 ± 0.040	0.117 ± 0.041	0.135 ± 0.078	0.060 ± 0.015	0.209 ± 0.070	0.823 ± 0.289 #

* = p < 0.05 compared to WT mice; # = p < 0.05 compared to non-liposomal VHH-pazH-DTPA-¹¹¹In; ¶ = p < 0.05 compared to GSH-PEG DMPC VHH-pazH-DTPA-¹¹¹In.

As expected, the clearance rate of free VHH-pa2H is higher than for both liposomal formulations (Table 3.2). It should be noted that these calculations are an oversimplification of the PK behavior of the formulations. Firstly, from the time-activity curves in Figure 3.7 it is obvious that the blood elimination is characterized by two-compartmental kinetics. We chose to only fit the slowest rate because the data is not sufficient for stable two-phase fits. One should realize that particularly for the free VHH, most of the activity is cleared much faster than this reported half-life. Secondly, although the bioavailability of the VHH is supposed to be 100%, as the drug is delivered intravenously, we can be certain that the VHH will not be rapidly distributed in the plasma, since it is encapsulated. Thus, these values reflect an average of the intact formulation (VHH-liposome) and released VHH-pa2H in whole blood.

The volume of distribution for the different formulations largely conforms to the well-documented behavior of liposomal carriers [42]. The VD for free VHH-pa2H is high, indicating a wide tissue distribution. The relatively small size (<15 kDa) and high pI (>9) of VHH-pa2H allow a rapid distribution in tissues. For both liposomal formulations, the volume of distribution is significantly reduced, particularly in the GSH-PEG EYPC formulation, where VD approaches the plasma volume (± 3 ml in a mouse). These low values indicate that the large liposomes do not readily cross the blood vessel walls, and are relatively stable. Interestingly, in our study the GSH-PEG EYPC formulation was the more stable variant, contrary to expectation [42].

To assess brain delivery of VHH-pa2H, the ratio between brain and muscle as a non-target region was calculated. An increase in retention in the transgenic mice compared to the wildtype littermates in the GSH-PEG EYPC liposomal formulations was found (Table 3.2 and Figure 3.9). This indicates that the VHH-pa2H indeed crossed the BBB and is retained, but as expected only in the APP/PS1 mice brain and not in the wildtype littermates. This is most likely due to the binding of the VHH to the amyloid depositions present in the brains of only the transgenic animals. When the organ-to-blood ratios are observed (Table 3.2), much lower ratios are found for the liposomal encapsulated VHH compared to the free VHH. We believe that the main contributing factor for this difference is the relatively big difference in blood pool clearance between the free and the encapsulated formulations. The very low blood values for the free VHH at 24 h skew the ratios upwards. However, the most interesting observation is that in the APP/PS1 mice injected with GSH-PEG EYPC VHH-pa2H-DTPA-^{111m}In there is a significant difference with the WT littermates in the brain and not in any other organ, once more confirming the delivery of functional VHH-pa2H across the BBB.

The labeling of the VHH with DTPA and ^{111m}In did not have an effect on the selective binding of the VHH to A β , as is shown in Figure 3.5 A. Previously it has been shown that similar labeling of available primary amines on VHH-pa2H with an Alexa Fluor[®]594 dye or ^{99m}Tc did not influence

the binding efficiency and selectivity either [18]. Furthermore, the complete lack of radioactive signal in the human brain cryosection lacking A β (Figure 3.5 B) indicates that the labeled VHH indeed reacts to A β only, as does its unlabeled counterpart [13]. This observation of selectivity in human *ex vivo* tissue is identical to the observation in the *in vivo* murine brains [18]. The labeling of the VHH with DTPA chelated ¹¹¹In proved to be stable and robust. In the *in vitro* ITLC assay and the PD-10 purification of the post-encapsulation radiolabeled compounds no detectable release of ¹¹¹In was observed (Figure 3.6). It is possible that the ¹¹¹In labeling *in vivo* is less robust. Free ¹¹¹In binds to transferrin in the blood, resulting in high amounts of radioactivity in the bone marrow [43]. In the micro-SPECT imaging of the injected animals in our study, any potential accumulation of radioactivity in the bone marrow was below the detection limit. It might be possible that a small fraction of the observed activity in the isolated blood and liver – which are two additional major sites of free ¹¹¹In accumulation [43]– is due to release of ¹¹¹In from the chelator. Despite this potential caveat, the observed difference in uptake between brains with and without A β deposits corroborates our conclusion that the observed signal in the brain indeed reflects the presence of labeled, functional VHH-pa2H.

Unexpectedly, an increased uptake into the brain was not observed for VHH-pa2H in GSH-PEG DMPC liposomes. Although the blood residential times were significantly increased (Table 3.1 and Figure 3.7), the uptake in the brains of VHH-pa2H in GSH-PEG DMPC liposomes at 24 h after injection was similar to that of free VHH-pa2H. We cannot fully explain this phenomenon although instability of the GSH-PEG DMPC liposomes cannot be excluded. Compared to GSH-PEG EYPC liposomes radioactivity counted in various tissues was lower for GSH-PEG DMPC liposomes but still higher than that for free VHH-pa2H (Table 3.2).

It must be noted that we obtained a significant increase in the uptake in the brain of VHH-pa2H encapsulated in GSH-PEG EYPC liposomes after only a single injection of the tracer. The enhanced tracer level in the brain after GSH-PEG EYPC encapsulation was in the same order of magnitude as previously shown for fluorescent dye with GSH targeting [19]. A similar brain uptake was also shown for other brain-delivery strategies using transferrin-receptor targeted antibodies, which was sufficiently high to exhibit a therapeutic effect [44]. The amount of VHH in the brain can likely be further increased by improving the encapsulation efficiency of VHH-pa2H into the liposomes, by multiple injections of the GSH-PEG liposomes, or by administering higher amounts of liposomal VHH-pa2H using a slow infusion protocol. The analysis of these follow-up experiments may also give more detailed information regarding pharmacokinetic parameters such as the VD specific to GSH-PEG EYPC encapsulated VHH-pa2H. Even though the VHHs are shown to be safe for human clinical trials and both the PEG liposomes and the GSH are FDA approved, long term follow-up studies in which repeated doses of GSH-PEG EYPC VHH-pa2H are administered could include an analysis of potential immune

response activation to confirm that the combination of these products is indeed safe for human application.

Finally, to be able to perform this study, a protocol was developed to load a DTPA modified protein into liposomes and subsequently perform a radioactive labeling of the protein using an active loading method. Most radioactive labeling methods for liposomal proteins or compounds rely on the use of a chelator embedded in the phospholipid membrane, or an active loading of a free radiotracer inside the liposomes [45]. In contrast, our method is actually labeling the protein that needs to be delivered to the brain. The protocol is generally applicable for a broad range of liposomal formulations, and allows pharmacokinetics and biodistribution studies of encapsulated proteins or peptides.

5. CONCLUSION

GSH-PEG liposomal encapsulated VHH showed a significant increase in retention in brains of transgenic mice as compared to wildtype controls, providing evidence that the G-Technology is suitable for specific delivery of targeted drugs, antibody fragments in this case, beyond the blood-brain barrier into the brain.

DISCLOSURE

The indicated authors are employees of to-BBB technologies BV. PJ Gaillard holds founder shares in to-BBB technologies BV. The authors have no other relevant affiliations or financial involvement with any organization or entity with a financial interest in or financial conflict with the subject matter or materials discussed in the manuscript apart from those disclosed.

ACKNOWLEDGMENTS

The authors wish to acknowledge Brigit den Adel, Ingrid Hegeman, Paul Hensbergen, Mark T.M. Rood, Ernst Suidgeest (Leiden University Medical Center, Leiden, The Netherlands), and Maria J.W.D. Vosjan (Department of Otolaryngology Head and Neck Surgery, VU University Medical Center, Amsterdam, The Netherlands) for their technical assistance, and Hendrik Adams, BAC b.v., for supplying the VHH-pa2H. We are very grateful to Thanos Metaxas (Department of Radiology and Nuclear Medicine, VU University Medical Center, Amsterdam, The Netherlands) for his help with the pharmacokinetic analysis. This research was performed within the framework of CTMM, the Center for Translational Molecular Medicine (www.ctmm.nl), project

LeARN (grant 02N-101) and the Center for Medical Systems Biology (grants S-MRI-110010 and S-MRI-110030).

REFERENCES

1. Duyckaerts, C., Delatour, B. & Potier, M.-C. Classification and basic pathology of Alzheimer disease. *Acta Neuropathol.* 118(1):5–36 (2009).
2. Frisoni, G. B., Fox, N. C., Jack, C. R., Scheltens, P. & Thompson, P. M. The clinical use of structural MRI in Alzheimer disease. *Nat. Rev. Neurol.* 6(2):67–77 (2010).
3. Jack, C. R., Knopman, D. S., Jagust, W. J., Shaw, L. M., Aisen, P. S., Weiner, M. W., Petersen, R. C. & Trojanowski, J. Q. Hypothetical model of dynamic biomarkers of the Alzheimer's pathological cascade. *Lancet Neurol.* 9(1):119–128 (2010).
4. Selkoe, D. J. Resolving controversies on the path to Alzheimer's therapeutics. *Nat. Med.* 17(9):1060–1065 (2011).
5. Humpel, C. Identifying and validating biomarkers for Alzheimer's disease. *Trends Biotechnol.* 29(1):26–32 (2011).
6. Drzezga, A. Amyloid-plaque imaging in early and differential diagnosis of dementia. *Ann. Nucl. Med.* 24(2):55–66 (2010).
7. Villemagne, V. L., Klunk, W. E., Mathis, C. a, Rowe, C. C., Brooks, D. J., Hyman, B. T., Ikonomic, M. D., Ishii, K., Jack, C. R., Jagust, W. J., et al. A β Imaging: feasible, pertinent, and vital to progress in Alzheimer's disease. *Eur. J. Nucl. Med. Mol. Imaging* 39(2):209–19 (2012).
8. Wu, C., Pike, V. W. & Wang, Y. Amyloid imaging: from benchtop to bedside. *Curr. Top. Dev. Biol.* 70(05):171–213 (2005).
9. Lang, A. E. Clinical trials of disease-modifying therapies for neurodegenerative diseases: the challenges and the future. *Nat. Med.* 16(11):1223–6 (2010).
10. Panza, F., Frisardi, V., Solfrizzi, V., Imbimbo, B. P., Logroscino, G., Santamato, A., Greco, A., Seripa, D. & Pilotto, A. Immunotherapy for Alzheimer's disease: from anti- β -amyloid to tau-based immunization strategies. *Immunotherapy* 4(2):213–38 (2012).
11. Rozemuller, A. J. M., Gool, W. A. Van & Eikelenboom, P. The Neuroinflammatory Response in Plaques and Amyloid Angiopathy in Alzheimer's Disease: Therapeutic Implications. *Curr. Drug Targets - CNS Neurol. Disord.* 4:223–233 (2005).
12. Klooster, R., Rutgers, K. S. & van der Maarel, S. M. Selection of VHH antibody fragments that recognize different A β depositions using complex immune libraries. *Methods Mol. Biol.* 911:241–53 (2012).
13. Rutgers, K. S., van Remoortere, A., van Buchem, M. A., Verrips, C. T., Greenberg, S. M., Bacskai, B. J., Frosch, M. P., van Duinen, S. G., Maat-Schieman, M. L. & Van der Maarel, S. M. Differential recognition of vascular and parenchymal beta amyloid deposition. *Neurobiol. Aging* 32(10):1774–1783 (2009).
14. Rutgers, K. S., Nabuurs, R. J. A., van den Berg, S. A. A., Schenk, G. J., Rotman, M., Verrips, C. T., van Duinen, S. G., Maat-Schieman, M. L., van Buchem, M. A., de Boer, A. G., et al. Transmigration of beta amyloid specific heavy chain antibody fragments across the in vitro blood-brain barrier. *Neuroscience* 190:37–42 (2011).
15. Harmsen, M. M. & De Haard, H. J. Properties, production, and applications of camelid single-domain antibody fragments. *Appl. Microbiol. Biotechnol.* 77(1):13–22 (2007).
16. De Meyer, T., Muyltermans, S. & Depicker, A. Nanobody-based products as research and diagnostic tools. *Trends in Biotechnology* 32(5):263–70 (2014).
17. Sarker, S. A., Jäkel, M., Sultana, S., Alam, N. H., Bardhan, P. K., Chisti, M. J., Salam, M. A., Theis, W., Hammarström, L. & Frenken, L. G. J. Anti-rotavirus protein reduces stool output in infants with diarrhea: a randomized placebo-controlled trial. *Gastroenterology* 145(4):740–748.e8 (2013).
18. Nabuurs, R. J. A., Rutgers, K. S., Welling, M. M., Metaxas, A., de Backer, M. E., Rotman, M., Bacskai, B. J., van Buchem, M. A., van der Maarel, S. M. & van der Weerd, L. In vivo detection of amyloid- β deposits using heavy chain antibody fragments in a transgenic mouse model for Alzheimer's disease. *PLoS One* 7(6):e38284 (2012).
19. Morais, M., Cantante, C., Gano, L., Santos, I., Lourenço, S., Santos, C., Fontes, C., Aires da Silva, F., Gonçalves, J. & Correia, J. D. G. Biodistribution of a (67)Ga-labeled anti-TNF VHH single-domain antibody containing a bacterial albumin-binding domain (Zag). *Nucl. Med. Biol.* 41 Suppl:e44–8 (2014).

20. De Groeve, K., Deschacht, N., De Koninck, C., Caveliers, V., Lahoutte, T., Devoogdt, N., Muyldermans, S., De Baetselier, P. & Raes, G. Nanobodies as tools for in vivo imaging of specific immune cell types. *J. Nucl. Med.* 51(5):782–9 (2010).
21. Olafsen, T. & Wu, A. M. Antibody vectors for imaging. *Semin. Nucl. Med.* 40(3):167–81 (2010).
22. Rosik, D., Orlova, A., Malmberg, J., Altai, M., Varasteh, Z., Sandström, M., Karlström, A. E. & Tolmachev, V. Direct comparison of ¹¹¹In-labelled two-helix and three-helix Affibody molecules for in vivo molecular imaging. *Eur. J. Nucl. Med. Mol. Imaging* 39(4):693–702 (2012).
23. Altintas, I., Kok, R. J. & Schifferers, R. M. Targeting epidermal growth factor receptor in tumors: from conventional monoclonal antibodies via heavy chain-only antibodies to nanobodies. *Eur. J. Pharm. Sci.* 45(4):399–407 (2012).
24. Iqbal, U., Trojahn, U., Albaghdadi, H., Zhang, J., O'Connor-Mccourt, M., Stanimirovic, D., Tomanek, B., Sutherland, G. & Abulrob, A. Kinetic analysis of novel mono- and multivalent VHH-fragments and their application for molecular imaging of brain tumours. *Br. J. Pharmacol.* 160(4):1016–1028 (2010).
25. Roovers, R. C., van Dongen, G. A. M. S. & van Bergen en Henegouwen, P. M. P. Nanobodies in therapeutic applications. *Curr. Opin. Mol. Ther.* 9(4):327–35 (2007).
26. Gaillard, P. J., Appeldoorn, C. C. M., Rip, J., Dorland, R., van der Pol, S. M. a, Kooij, G., de Vries, H. E. & Reijerkerk, A. Enhanced brain delivery of liposomal methylprednisolone improved therapeutic efficacy in a model of neuroinflammation. *J. Control. Release* 164(3):364–9 (2012).
27. Lindqvist, A., Rip, J., Gaillard, P. J., Björkman, S. & Hammarlund-Udenaes, M. Enhanced brain delivery of the opioid peptide damgo in glutathione pegylated liposomes: A microdialysis study. *Mol. Pharm.* 10(5):1533–1541 (2013).
28. Gaillard, P. J., Appeldoorn, C. C. M., Dorland, R., van Kregten, J., Manca, F., Vugts, D. J., Windhorst, B., van Dongen, G. A. M. S., de Vries, H. E., Maussang, D., et al. Pharmacokinetics, brain delivery, and efficacy in brain tumor-bearing mice of glutathione pegylated liposomal doxorubicin (2B3-101). *PLoS One* 9(1):e82331 (2014).
29. Kannan, R., Chakrabarti, R., Tang, D., Kim, K. J. & Kaplowitz, N. GSH transport in human cerebrovascular endothelial cells and human astrocytes: Evidence for luminal localization of Na⁺-dependent GSH transport in HCEC. *Brain Res.* 852(2):374–382 (2000).
30. Welling, M. M., Paulusma-Annema, A., Balter, H. S., Pauwels, E. K. & Nibbering, P. H. Technetium-99m labeled antimicrobial peptides discriminate between bacterial infections and sterile inflammations. *Eur. J. Nucl. Med.* 27(3):292–301 (2000).
31. Welling, M. M., Mongera, S., Lupetti, A., Balter, H. S., Bonetto, V., Mazzi, U., Pauwels, E. K. J. & Nibbering, P. H. Radiochemical and biological characteristics of ^{99m}Tc-UBI 29-41 for imaging of bacterial infections. *Nucl. Med. Biol.* 29(4):413–22 (2002).
32. Vera, D. R., Hall, D. J., Hoh, C. K., Gallant, P., McIntosh, L. M. & Mattrey, R. F. Cy5.5-DTPA-galactosyl-dextran: a fluorescent probe for in vivo measurement of receptor biochemistry. *Nucl. Med. Biol.* 32(7):687–93 (2005).
33. Beaumier, P. L. & Hwang, K. J. An efficient method for loading indium-111 into liposomes using acetylacetone. *J. Nucl. Med.* 23(9):810–5 (1982).
34. Hwang, K. J., Merriam, J. E., Beaumier, P. L. & Luk, K.-F. Encapsulation, with high efficiency, of radioactive metal ions in liposomes. *Biochim. Biophys. Acta* 716(1):101–109 (1982).
35. Gorlani, A., Brouwers, J., McConville, C., van der Bijl, P., Malcolm, K., Augustijns, P., Quigley, A. F., Weiss, R., De Haard, H. & Verrips, T. Llama Antibody Fragments Have Good Potential for Application as HIV Type 1 Topical Microbicides. *AIDS Res. Hum. Retroviruses* 27(00) (2011).
36. Choi, H. O. & Hwang, K. J. Application of anion-exchange resin to remove lipophilic chelates from liposomes. *Anal. Biochem.* 156(1):176–81 (1986).

37. Choi, H. O. & Hwang, K. J. Mechanism of ionophoric transport of indium-111 cations through a lipid bilayer membrane. *J. Nucl. Med.* 28(1):91-6 (1987).
38. Jankowsky, J. L., Slunt, H. H., Ratovitski, T., Jenkins, N. a, Copeland, N. G. & Borchelt, D. R. Co-expression of multiple transgenes in mouse CNS: a comparison of strategies. *Biomol. Eng.* 17(6):157-65 (2001).
39. Branderhorst, W., Vastenhouw, B., van der Have, F., Blezer, E. L. a, Bleeker, W. K. & Beekman, F. J. Targeted multi-pinhole SPECT. *Eur. J. Nucl. Med. Mol. Imaging* 38(3):552-61 (2011).
40. Loening, A. M. & Gambhir, S. S. AMIDE: a free software tool for multimodality medical image analysis. *Mol. Imaging* 2(3):131-7 (2003).
41. Rip, J., Chen, L., Hartman, R., van den Heuvel, A., Reijkerk, A., van Kregten, J., van der Boom, B., Appeldoorn, C., de Boer, M., Maussang, D., et al. Glutathione PEGylated liposomes: pharmacokinetics and delivery of cargo across the blood-brain barrier in rats. *J. Drug Target.* 22(5):460-7 (2014).
42. Drummond, D. C., Meyer, O., Hong, K., Kirpotin, D. B. & Papahadjopoulos, D. Optimizing liposomes for delivery of chemotherapeutic agents to solid tumors. *Pharmacol. Rev.* 51(4):691-743 (1999).
43. McAfee, J. G., Subramanian, G., Aburano, T., Thomas, F. D., Fernandes, P., Gagne, G., Lyons, B. & Zapf-Longo, C. A new formulation of Tc-99m minimicroaggregated albumin for marrow imaging: comparison with other colloids, In-111 and Fe-59. *J. Nucl. Med.* 23(1):21-28 (1982).
44. Yu, Y. J., Atwal, J. K., Zhang, Y., Tong, R. K., Wildsmith, K. R., Tan, C., Bien-Ly, N., Hersom, M., Maloney, J. A., Meilandt, W. J., et al. Therapeutic bispecific antibodies cross the blood-brain barrier in nonhuman primates. *Sci. Transl. Med.* 6(261):261ra154 (2014).
45. Ogawa, M., Umeda, I. O., Kosugi, M., Kawai, A., Hamaya, Y., Takashima, M., Yin, H., Kudoh, T., Seno, M. & Magata, Y. Development of 111In-labeled liposomes for vulnerable atherosclerotic plaque imaging. *J. Nucl. Med.* 55(1):115-20 (2014).

3

CHAPTER

❖ SUPPLEMENTARY DATA

Adapted from

Enhanced glutathione PEGylated liposomal brain delivery of an anti-amyloid single domain antibody fragment in a mouse model for Alzheimer's disease

Supplementary table 3.1. Ratios organ to blood standard uptake value (SUV) of VHH-pazH-DTPA-¹¹¹In in APP^{swE/PS1E9} transgenic mice (APP/PS1) and wildtype littermates (WT) at 24 h after injection. The mice were injected intravenously with 0.2 ml saline containing 5 µg VHH-pazH-DTPA-¹¹¹In (10-20 MBq) either non-liposomal (Free VHH-pazH-DTPA-¹¹¹In), or encapsulated in either GSH-PEG DMPC or GSH-PEG EYPC liposomes. Values are presented as the mean (±SEM) of the radioactivity counted per weighted organ after sacrifice and perfusion divided by the same value counted per blood volume, expressed as the ratio of the SUV, defined as (tissue radioactivity / tissue weight) / (injected activity / body weight). All values are corrected for radioactive decay over time.

n	Free VHH-pazH-DTPA- ¹¹¹ In		GSH-PEG DMPC VHH-pazH-DTPA- ¹¹¹ In		GSH-PEG EYPC VHH-pazH-DTPA- ¹¹¹ In	
	WT	APP/PS1	WT	APP/PS1	WT	APP/PS1
	8	8	2	2	4	4
	SUV ± SEM (SUV = %ID / g tissue per g mouse)					
Urine/blood ratio	37.455 ± 17.608	98.148 ± 49.372	2.373 ± 1.878	0.162 ± 0.117	0.701 ± 0.268	0.603 ± 0.255
Heart/blood ratio	2.448 ± 0.438	2.699 ± 0.587	0.919 ± 0.217	0.166 ± 0.084 #	0.160 ± 0.029 #	0.226 ± 0.034 #
Lungs/blood ratio	2.155 ± 0.572	2.645 ± 0.719	1.694 ± 1.074	0.081 ± 0.037	0.113 ± 0.007 #	0.128 ± 0.019 #
Spleen/blood ratio	7.648 ± 1.556	10.108 ± 2.255	4.556 ± 2.021	1.156 ± 0.423 #	2.002 ± 0.496 #	1.770 ± 0.311 #¶
Liver/blood ratio	10.43 ± 1.784	16.070 ± 4.548 *	4.683 ± 1.405	1.019 ± 0.554	0.719 ± 0.133 #	0.762 ± 0.217 #
Kidneys/blood ratio	1209.019 ± 241.261	1594.124 ± 389.412	91.214 ± 22.255 #	16.682 ± 8.442 #	3.926 ± 0.343 #	3.954 ± 0.825 #
Muscle/blood ratio	7.686 ± 1.891	10.914 ± 3.991	0.706 ± 0.546 #	0.165 ± 0.123	0.035 ± 0.009 #	0.044 ± 0.014 #
Cerebrum/blood ratio	0.095 ± 0.023	0.155 ± 0.053	0.013 ± 0.000	0.003 ± 0.002 *#	0.003 ± 0.001 #¶	0.012 ± 0.003 *#¶
Cerebellum/blood ratio	0.370 ± 0.115	0.422 ± 0.102	0.039 ± 0.019	0.005 ± 0.003	0.004 ± 0.001 #	0.016 ± 0.003 *#
Brain/blood ratio	0.465 ± 0.135	0.577 ± 0.139	0.053 ± 0.019	0.008 ± 0.005	0.007 ± 0.002 #	0.029 ± 0.006 *#

* = p < 0.05 compared to WT mice; # = p < 0.05 compared to non-liposomal VHH-pazH-DTPA-¹¹¹In; ¶ = p < 0.05 compared to GSH-PEG DMPC VHH-pazH-DTPA-¹¹¹In.

Supplementary table 3.2. Ratios organ to muscle standard uptake value (SUV) of VHH-paz2H-DTPE-¹¹¹In in APP^{swe}/PS1dE9 transgenic mice (APP/PS1) and wildtype littermates (WT) at 24 h after injection. The mice were injected intravenously with 0.2 ml saline containing 5 µg VHH-paz2H-DTPE-¹¹¹In (10-20 MBq) either non-liposomal (Free VHH-paz2H-DTPE-¹¹¹In), or encapsulated in either GSH-PEG DMPC or GSH-PEG EYPC liposomes. Values are presented as the mean (\pm SEM) of the radioactivity counted per weighted organ after sacrifice and perfusion divided by the same value counted per muscle sample, expressed as the ratio of the SUV, defined as (tissue radioactivity / tissue weight) / (injected activity / body weight). All values are corrected for radioactive decay over time.

n	Free VHH-paz2H-DTPE- ¹¹¹ In		GSH-PEG DMPC VHH-paz2H-DTPE- ¹¹¹ In		GSH-PEG EYPC VHH-paz2H-DTPE- ¹¹¹ In	
	WT	APP/PS1	WT	APP/PS1	WT	APP/PS1
	8	8	2	2	4	4
	SUV \pm SEM (SUV = %ID / g tissue per g mouse)					
Blood/muscle ratio	0.932 \pm 0.638	1.017 \pm 0.610	3.523 \pm 2.725	13.536 \pm 10.062	33.714 \pm 7.375 #	29.904 \pm 7.635 #
Urine/muscle ratio	48.566 \pm 32.701	37.758 \pm 17.286	3.245 \pm 0.149	3.371 \pm 3.213	19.579 \pm 8.499	16.812 \pm 8.407
Heart/muscle ratio	0.938 \pm 0.422	0.761 \pm 0.261	2.645 \pm 1.738	1.407 \pm 0.538	4.773 \pm 0.602 #	6.391 \pm 1.781 #
Lungs/muscle ratio	0.850 \pm 0.374	0.964 \pm 0.451	3.042 \pm 0.832	0.729 \pm 0.321	3.793 \pm 0.891 #	3.393 \pm 0.595 #
Spleen/muscle ratio	4.832 \pm 2.689	2.977 \pm 1.126	10.545 \pm 5.294	11.392 \pm 5.908	60.368 \pm 14.291 #	55.233 \pm 21.903 #
Liver/muscle ratio	6.274 \pm 3.560	4.988 \pm 1.939	12.670 \pm 7.810	8.222 \pm 2.759	22.501 \pm 4.163 #	25.100 \pm 13.061
Kidneys/muscle ratio	383.620 \pm 158.656	424.990 \pm 174.318	260.716 \pm 170.126	140.866 \pm 53.588	127.871 \pm 26.024	125.826 \pm 53.019
Muscle/muscle ratio	1.000 \pm 0.000	1.000 \pm 0.000	1.000 \pm 0.000	1.000 \pm 0.000	1.000 \pm 0.000	1.000 \pm 0.000
Cerebrum/muscle ratio	0.042 \pm 0.021	0.041 \pm 0.016	0.049 \pm 0.038	0.025 \pm 0.007	0.089 \pm 0.025 #	0.361 \pm 0.141
Cerebellum/muscle ratio	0.074 \pm 0.020	0.076 \pm 0.027	0.086 \pm 0.039	0.035 \pm 0.003	0.120 \pm 0.045	0.461 \pm 0.018 #
Brain/muscle ratio	0.116 \pm 0.040	0.117 \pm 0.041	0.135 \pm 0.078	0.060 \pm 0.015	0.209 \pm 0.070	0.823 \pm 0.289 #

* = p < 0.05 compared to WT mice; # = p < 0.05 compared to non-liposomal VHH-paz2H-DTPE-¹¹¹In; ¶ = p < 0.05 compared to GSH-PEG DMPC VHH-paz2H-DTPE-¹¹¹In.

1. Department of Human Genetics, Leiden University Medical Center, The Netherlands
2. Department of Radiology, Leiden University Medical Center, The Netherlands

4

CHAPTER

FUSION OF HUMAN FC TO VHH-PA2H INCREASES BLOOD RESIDENTIAL TIME, BUT NOT BRAIN UPTAKE

Adapted from

Fusion of hIgG1-Fc to ¹¹¹In-anti-amyloid single domain antibody fragment VHH-pa2H prolongs blood residential time in APP/PS1 mice but does not increase brain uptake.

Maarten Rotman ^{1,2}, Mick M. Welling ², Marlinde L. van den Boogaard ¹, Laure Grand Moursel ^{1,2}, Linda M. van der Graaf ^{1,2}, Mark A. van Buchem ², Silvère M. van der Maarel ² and Louise van der Weerd ^{2,3}.

Nuclear Medicine and Biology 42 (2015) 695-702

ABSTRACT

Introduction: Llama single domain antibody fragments (VHH), which can pass endothelial barriers, are being investigated for targeting amyloid plaque load in Alzheimer's disease (AD). Contrary to conventional human or murine antibodies consisting of IgG or F(ab')₂ antibody fragments, VHH are able to effectively pass the blood-brain barrier (BBB) *in vitro*. However, in earlier *in vivo* studies, anti-amyloid VHH showed poor BBB passage due to their short serum half-lives. It would be of interest to develop a VHH based protein with elongated serum half-life to enhance BBB passage, allowing the VHH to more easily reach the cerebral amyloid deposits.

Methods: To increase serum persistence, the Fc portion of the human IgG₁ antibody (hinge plus CH₂ and CH₃ domains) was fused to the C-terminus of the VHH (VHH-pa2H-Fc). To determine the pharmacokinetics and biodistribution profile of the fusion protein, the chelator p-SCN-Bz-DTPA was linked to the protein and thereafter labelled with radioactive indium-111 (¹¹¹In). Double transgenic APP_{swe}/PS1dE9 and wildtype littermates were injected with 20 µg VHH-pa2H-Fc-DTPA-¹¹¹In (10-20 MBq). Pharmacokinetics of the tracer was determined in blood samples at 10 intervals after injection and imaging using microSPECT was performed. The biodistribution of the radioactivity in various excised tissues was measured at 48 h after injection.

Results: We succeeded in the expression of the fusion protein VHH-pa2H-Fc in HEK293T cells with a yield of 50 mg/ml growth medium. The fusion protein showed homodimerization – necessary for successful Fc neonatal receptor recycling. Compared to VHH-pa2H, the Fc tailed protein retained high affinity for amyloid beta on human AD patient brain tissue sections, and significantly improved serum retention of the VHH. However, at 48 h after systemic injection of the non-fused VHH-pa2H-DTPA-¹¹¹In and the VHH-pa2H-Fc-DTPA-¹¹¹In fusion protein in transgenic mice, the specific brain uptake of VHH-pa2H-Fc-DTPA-¹¹¹In was not improved compared to non-fused VHH-pa2H-DTPA-¹¹¹In.

Conclusion: Using VHH-Fc conjugates increases the blood half-life of the protein. However, purely extending the time window for brain uptake does not increase BBB passage. Nevertheless, VHH-Fc holds promise for therapeutic applications where a sustained systemic circulation of VHH is advantageous.

1. INTRODUCTION

Due to their long, protruding and highly variable CDR₃ section, llama derived single domain antibody fragments (VHH) have the ability to access epitopes normally hidden for conventional antibodies. As such they are a very successful class of therapeutics, with applications ranging from interference with enzymatic active sites leading to neutralization of toxins [1–3] and viruses [4], blocking of apoptotic pathways in autoimmune diseases [5] and preventing aberrant protein aggregations [6], to binding spatially different amyloid beta (A β) depositions [7].

On the other hand, their small size (12–15 kDa) and inherent short blood half-life can be a hindrance to target their epitopes. Monovalent VHH may not have enough time to interact with hard-to-reach epitopes or to cross regulated endothelial barriers – such as the blood-brain barrier (BBB) – in sufficient amounts [8]. They may be rapidly filtered out of the system, unless they are either injected at very high doses, or continuously via infusion or unless the BBB is locally impaired [9,10]. Even though for imaging applications short half-lives are interesting [11], for systemic immunotherapeutic applications, elongated serum half-lives of VHH are preferred. For our application of VHH as amyloid targeting therapeutics, both increased BBB passage and extension of serum half-life would be desired and the second may prove to be a means to achieve the first.

Elongation of serum half-life time of unmodified VHH can be achieved by repeated injections or slow infusion administration [12,13], but a less invasive, and thus preferable way to increase serum retention is by fusing the antibody fragment to an IgG fragment crystallizable region (Fc, i.e. CH₂ and CH₃) and the hinge region. Due to the inherent dimeric nature of the Fc fragment, VHH-Fc fusions are produced as homodimeric proteins with interchain disulfide bridges between the cysteine amino acids in the hinge region [14]. The total protein complex size of the dimeric VHH-Fc increases to 80 kDa, i.e. above the molecular weight cut-off limit of globular filtration by the kidneys, which is approximately 60 kDa. Additionally, the CH₂ and CH₃ domains will interact with the neonatal Fc receptor (FcRn) in early endosomes, favoring recycling and transcytosis over catabolism, which in turn increases the retention of the protein in the body [15–17].

The Fc-fusion approach has been performed earlier with single chain antibody fragments (scFv) [12,13], which too are recombinant antibody fragments. These scFv-Fc fusion proteins have been produced and applied both *in vitro* and *in vivo* [18–20], and studies indeed show increased blood residential times of the constructs [21]. VHH-Fc fusion constructs have been developed and produced in plant cells [22–24] as well as in cultured murine cell lines [2] as in cultured human cell lines [5,25]. However, until very recently the *in vivo* biodistribution profiles of VHH-Fc fusion proteins have not been extensively reported, with a single reference reporting a

generally increased blood half-life in BALB/c mice [26] and one more extensive report showing improved pharmacokinetic potency and increased BBB passage in Wistar rats [27].

This study reports on the production and validation of an Fc-fusion VHH directed against human A β and the pharmacokinetics and biodistribution profiles of this Fc-fusion VHH in transgenic APP^{swe}/PS1^{dEg} mice compared to the unmodified VHH antibody fragment. Here we describe the production in human embryonic kidney cells (HEK293T) and purification of anti-A β VHH-pa2H fused to the Fc domain and hinge region of a human IgG1. Furthermore, we determined whether specific affinity for A β in pathological brain materials was retained for the secreted fusion protein. Finally, we measured and describe the biodistribution profile and performed SPECT imaging in mice using the radiolabeled VHH-Fc to show the effect of increased retention in the blood on BBB passage.

2. MATERIALS AND METHODS

2.1. Construction of VHH-pa2H-Fc in pINFUSE-hIgG1-Fc1 vector

VHH-pa2H was cloned from the pUR5071 vector [7] into an intermediate subcloning vector to introduce the chicken lysozyme secretion signal (ss) [5'-ATGAGGTCCTTGCTAATCTTG-GTGCTTTGCTTCCTGCCCTGGCTGCTCTGGGG-3'] [28] directly upstream of the VHH (SS-VHH-pa2H). A BglII and an EcoRI restriction enzyme consensus sequence were introduced respectively upstream and downstream of the ss-VHH-pa2H sequence via PCR [fwd primer BglII: 5'-agaagatctcgcagcagctgaggat-3'; rev primer EcoRI: 5'-gcagaattcatgaggtcttgctaattctt-3']. The construct was then cloned into a pINFUSE-hIgG1-Fc1 vector (InvivoGEN, USA) using the introduced restriction sites, to create the ss-VHH-pa2H-hIgG1-Fc (VHH-pa2H-Fc) fusion protein construct under the control of a hEF1-HTLV composite promotor (Figure 4.1).

2.2. Production of VHH-pa2H-Fc in HEK293T and quality control

The VHH-pa2H-Fc fusion protein was produced in HEK293T cells under serum-free conditions as described before [29]. The fusion protein contained in the cell-free medium fraction was affinity purified using Protein A resin (nProteinA sepharose 4 Fast Flow, GE Healthcare, NL). After washing with PBS, the VHH-pa2H-Fc was eluted from the Protein A resin with 0.1 M sodium citrate at pH 2.0. Fractions containing the purified VHH-pa2H-Fc were pooled and neutralized to pH 7.5 by adding 1M NaOH buffer solution and dialyzed three times against PBS including one step overnight. The amount of purified protein was assessed using the Bradford assay and Nanodrop® spectral absorption at 280 nm. The purity of VHH-pa2H-Fc was determined with size exclusion chromatography on an ÄKTA FLPC system (GE Healthcare) using a size

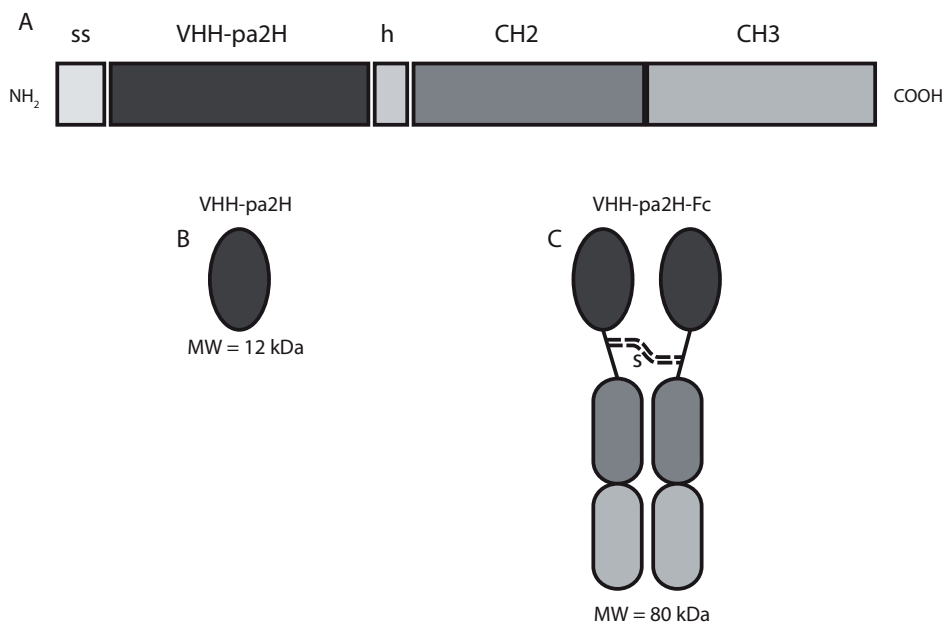


Figure 4.1. Schematic representation of ss-VHH-pa2H-Fc. (A) The llama antibody fragment pa2H is fused to the hinge (h) region and the CH₂ and CH₃ domains of the crystallizable fragment (Fc) of the human IgG₁. The N-terminal lyszyme secretion signal (ss; amino acid sequence MRSLILVLCFPLAAGAQPA) forces the protein to be secreted into the extracellular space. (B + C) Due to the fusion of the Fc domain, the VHH-pa2H, which is normally 12 kDa in size, will form two disulfide bridges in the attached hinge region and reach a total size of approximately 80 kDa as a homodimeric protein complex.

exclusion column (SuperdexTM 75 10/300 GL). To confirm the formation of the homodimeric VHH-pa2H-Fc products, purified samples were on SDS-PAGE under reducing and non-reducing conditions. Reduced VHH-pa2H-Fc samples were prepared with dithiothreitol (DTT; Sigma, NL), whereas in the non-reducing conditions DTT was omitted. Purified VHH-pa2H-Fc was stored at 4°C until use. For comparison studies non-fused VHH-pa2H was produced as described before [8].

2.3. Immunofluorescence analysis

To confirm the retained affinity of VHH-pa2H-Fc and VHH-pa2H-Fc-DTPA (see section 2.4.) for A β depositions, immunofluorescence staining was performed on human post-mortem AD brain and aged matched healthy control cryosections. All human tissues were obtained from anonymous patients or healthy aged donors as confirmed by neuropathological examination in agreement with the guidelines of the Medical Ethics Committee of the Leiden University Medical Center, The Netherlands. All tissues were processed in a coded fashion, according to Dutch national ethical guidelines (Code for Proper Secondary Use of Human Tissue, Dutch Federation of Medical Scientific Societies). Briefly, acetone fixed serial cryosections (5 μ m) were blocked for 1-2 h with 4% milk powder (Marvel dried skimmed milk powder, Premier

Foods, UK) in PBS (mPBS). Blocked sections were incubated overnight with 20 ng/μl purified VHH-pa2H-Fc or VHH-pa2H-Fc-DTPA. After 3 × 5 min. washing steps with PBS, the sections were exposed to mouse anti human IgG1 (1:500, m1325 Sanquin Pelicclass, NL) for 1-2 h, washed and then incubated with Alexa Fluor 488 – goat anti mouse (1:500, A-11001, Life Technologies, USA) for 1 h. To confirm Aβ presence, adjacent mPBS blocked sections were incubated with mouse anti Aβ (4G8, Covance, NL) for 1 h, washed and then incubated with Alexa Fluor 594 – goat anti mouse (1:500, A-11032, Life Technologies) for 1 h. All antibody dilutions were performed in mPBS. Fluorescence signal was detected on a Leica DM5500B microscope with a Leica DFC360FX camera and analyzed with Leica LAS-AF v.2.3.6 software (Leica Microsystems, NL). Whole slide overview images were acquired with a BZ-9000 BIOREVO HS All-in-One Fluorescence microscope (Keyence, BE).

2.4. DTPA conjugation to VHH-pa2H-Fc and radiolabeling with indium-111

To enable the radiolabeling of the VHH with indium-111 (¹¹¹In), the chelator p-SCN-Bn-DTPA (C₂₂H₂₈N₄O₁₀S·3HCl, MW 649.92 g/mol, Macrocyclics Inc., USA) was conjugated to primary amine groups on the VHH-pa2H-Fc fusion protein as described previously [8]. In short, a 5 × molar excess of the chelator was incubated with VHH-pa2H-Fc at 37°C for 3 h in PBS at pH 8.2 and dialyzed against the labeling buffer 250 mM ammonium acetate at pH 5.5 for at three times at 4°C including one overnight step. Conjugated and dialyzed preparations were stored in the dark at 4°C.

Before *in vivo* use, the VHH-pa2H-Fc-DTPA construct was radiolabeled with ¹¹¹In though incorporation of the isotope into the DTPA chelator as described before [8]. In short ¹¹¹InCl₃ (Covidien, NL) was added to the DTPA conjugated VHH-Fc, incubated at 37°C in 250 mM ammonium acetate buffer at pH 5.5 for 3 h under gentle shaking, and then purified with a PD-10 desalting column (GE Healthcare) in 20 elution fractions of 0.5 ml PBS. Fractions containing radioactive ¹¹¹In-labeled VHH-pa2H-Fc-DTPA (VHH-pa2H-Fc-DTPA-¹¹¹In) were pooled and used for animal studies. The amount of ¹¹¹InCl₃ added to the labeling solution was adjusted depending on radiation strength upon delivery to yield 20 μg of VHH-pa2H-Fc-DTPA-¹¹¹In at 10-20 MBq per injection.

2.5. Pharmacokinetics

All *in vivo* studies were performed using 12-16 month old double transgenic mice (n = 4-8) from a colony set up using the APP^{swe}/PS1^{dE9} strain (APP/PS1; JAX® Mice and Services, The Jackson Laboratory, USA) on a C57BL/6 background and their wildtype littermates (WT). The strain is known to rapidly develop a vascular (CAA) and parenchymal Aβ associated phenotype [30–32]. Animals were kept on a strict 12 h day/night light cycle with unlimited access to nor-

mal chow and water. All animal studies have been approved by the Leiden University Medical Center institutional Animal Experiments Committee (DEC permits 10097 and 12065). Besides standard genotyping, A β pathology was confirmed on brain sections by standard Thioflavin T staining [10].

Animals were injected intravenously with 20 μ g VHH-pa2H-Fc-DTPA-¹¹¹In (10-20 MBq). At 0.5, 2, 3, 4, 6, 22, 24, 26, 28 and approximately 48 h after injection 5 μ l blood samples were taken from the tail vein and counted for radioactivity. After correction for radioactive decay, the total injected dose (ID), blood clearance rates, area under the curve values (AUC) and standard uptake values (SUV, i.e. the percentage of the ID per gram blood – or gram tissue – per gram mouse) in blood were calculated as described before [8].

2.6. *MicroSPECT imaging*

To visually analyze the biodistribution profiles, transgenic and WT animals, injected with the radiolabeled VHH-pa2H-Fc-DTPA-¹¹¹In, were imaged for 40 minutes under continuous 1-2% isoflurane inhalation anesthesia on a three-headed U-SPECT-II microSPECT (MILabs, NL). Images were obtained at 48 h after administration of the radiolabeled VHH using a 0.6 mm mouse pinhole collimator, and energy setting at 171 keV with a window of 20% [8]. Total body images were reconstructed using six POSEM iterations with 16 subsets, a 0.2 mm voxel size and with decay and scatter corrections integrated into the reconstruction using dedicated MILabs reconstruction software. Volume-rendered images were generated and analyzed using a freeware tool from Amide.exe 1.0.2 Medical Image Data Examiner (<http://amide.sourceforge.net>) [8,33].

2.7. *Biodistribution*

Directly after imaging and collecting the last blood sample, the mice were euthanized and perfused with 15 ml PBS [8]. Thereafter, the bladder including urine, heart, lungs, spleen, liver, both kidneys, part of the left femoral muscle, cerebrum, and cerebellum were removed. All tissues and organs were weighed and counted for radioactivity using a Wizard2 2470 automatic gamma scintillation counter (Perkin Elmer, USA) and obtained measurements of radioactivity uptake in tissues and organs were calculated and reported as SUV.

2.8. *Statistical analysis*

All data are presented as mean value (\pm SEM) of 4-8 independent measurements. Statistical analysis for differences between groups in the animal studies were performed by Student's paired t-test with one-tailed distribution. Significance was assigned for p-values of <0.05. All analyses and calculations were performed using Microsoft® Office Excel 2010 and GraphPad Prism version 5.01 for Windows (GraphPad Software, USA).

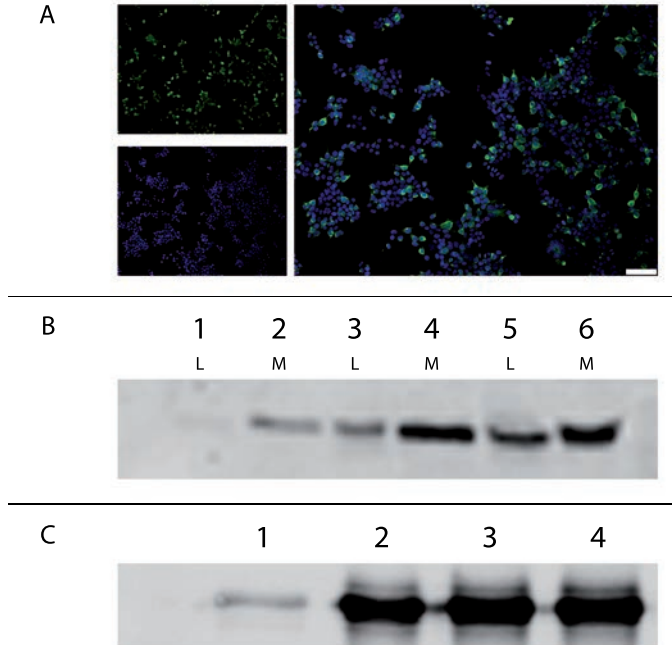


Figure 4.2. HEK293T production of VHH-pa2H-Fc. (A) Transfection of HEK293T cells with the pINFUSE-ss-VHH-pa2H-Fc vector and PEI transfection reagent consistently yields high transfection efficiencies. Blue channel shows DAPI stained nuclei, green channel shows VHH-pa2H-Fc stained with mouse-anti-hIgG₁ and Alexa Fluor – 488 goat-anti-mouse. White bar indicates 75 μ m. (B) Western blot analysis of the effect of Fetal Calf Serum (FCS) in the medium indicates the need for FCS during the first 24 h after transfection. Lanes 1 and 2 = 0% FCS, lanes 3 and 4 = 10% FCS during the first 24 h, 0% FCS during the second 24 h, lanes 5 and 6 = 10% FCS. Samples were taken 48 h after transfection. L = cell lysate sample, M = cell-free medium sample. Bands run at approximately 42 kDa. Primary antibody: mouse-anti-hIgG₁, secondary antibody: IRD-CW800-goat-anti-mouse. (C) VHH-pa2H-Fc secreted into the cell medium at 0, 24, 48 and 72 h after switching to FCS free medium at 24 h after transfection (lanes 1 to 4, respectively) indicate immediate and effective secretion of the produced VHH-pa2H-Fc fusion protein. Bands run at approximately 42 kDa. Primary antibody: mouse-anti-hIgG₁, secondary antibody: IRD-CW800-goat-anti-mouse.

3. RESULTS

3.1. VHH-pa2H-Fc production and quality control

Transfection of pINFUSE-ss-pa2H-Fc into HEK293T cells yielded high transfection efficiencies (Figure 4.2 A) and nearly immediate production and secretion of the fusion protein (Figure 4.2 B and C). The best production and purification of VHH-pa2H-Fc was obtained with transfection in medium supplemented with fetal calf serum (FCS) and maintained in FCS-free condition from 24 h after transfection. This set-up yielded 50 mg secreted VHH-pa2H-Fc per litre growth medium, at an average final concentration after purification and dialysis of 1.0 mg/ml VHH-pa2H-Fc in PBS.

The produced and secreted VHH-pa2H-Fc and the VHH-pa2H-Fc-DTPA both retained functional specificity for A β depositions in plaques and around vessel walls in brain tissue sections from

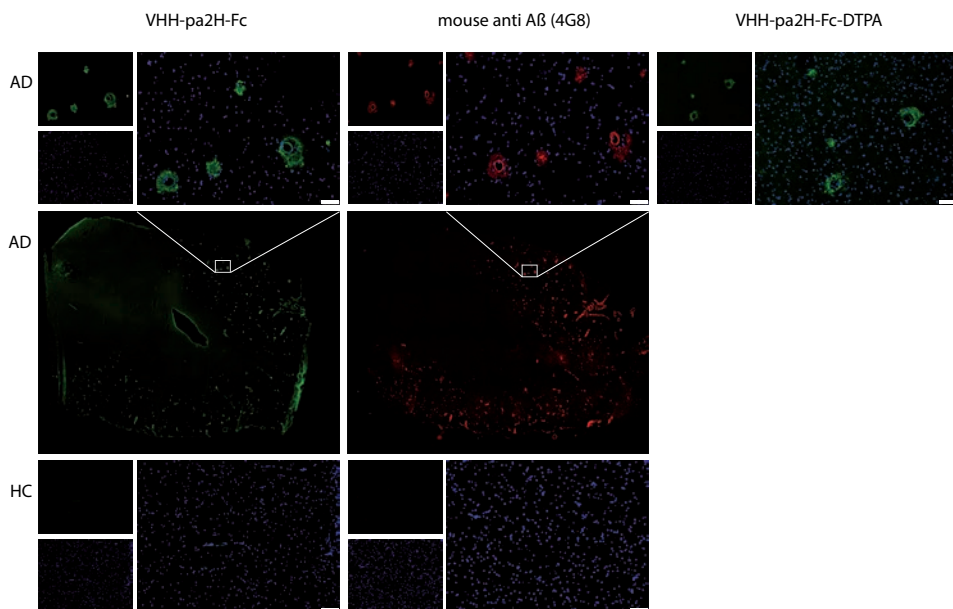


Figure 4.3. IHC on serial sections of *post mortem* patient brain material (AD) and aged matched healthy control (HC) stained for amyloid deposits with either VHH-pa2H-Fc (left: green) or VHH-pa2H-Fc-DTPA (right: green) or 4G8 (middle: red) show outstanding and highly specific recognition of VHH-pa2H-Fc for both vascular and parenchymal A β , regardless of DTPA conjugation. Secondary antibody: mouse-anti-human IgG for the VHH; Alexa Fluor 594 – goat-anti-mouse for the 4G8 staining. Tertiary antibody for the VHH-pa2H-Fc and VHH-pa2H-Fc-DTPA only: Alexa Fluor 488 – goat-anti-mouse. Nuclei stained in blue with DAPI. Top row images represent vascular and parenchymal amyloid deposits, middle row shows the remainder of the section and bottom row images are representative of parenchymal and vascular areas in aged matched healthy controls devoid of A β deposits. White bars indicate 75 μ m.

human patient material and does not show a specific binding in control tissue (Figure 4.3). The immunoreactivity is highly similar to conventional monoclonal anti-A β antibodies (e.g. clone 4G8) and to the specificity previously shown by unmodified VHH-pa2H [7,8,10,30]. Addition of the chelator DTPA to VHH-pa2H-Fc did not impair the ability to recognize and bind A β .

3.2. VHH-pa2H-Fc dimerization

For interaction of the VHH-Fc with FcRn, which is necessary to prolong the blood half-life, the fusion protein must form disulphide bridge based dimers as shown in Figure 4.1. The formation of the homodimers was confirmed on SDS-PAGE under reducing and non-reducing conditions. Under reducing conditions the VHH-Fc fusion protein ran at the expected monomer height of approximately 40 kDa (Figure 4.4 A). The samples under non-reducing conditions showed a higher band on gel, indicating the presence of a homodimeric protein complex. The exact size of the higher bands cannot be determined in this experiment, as bands resulting from non-reduced proteins cannot be compared with the used marker. However, with size exclusion chromatography (SEC), a mass of approximately 83,900 Da was determined, which is in concordance with the theoretical size of a VHH-pa2H-Fc homodimer (Figure 4.4 B).

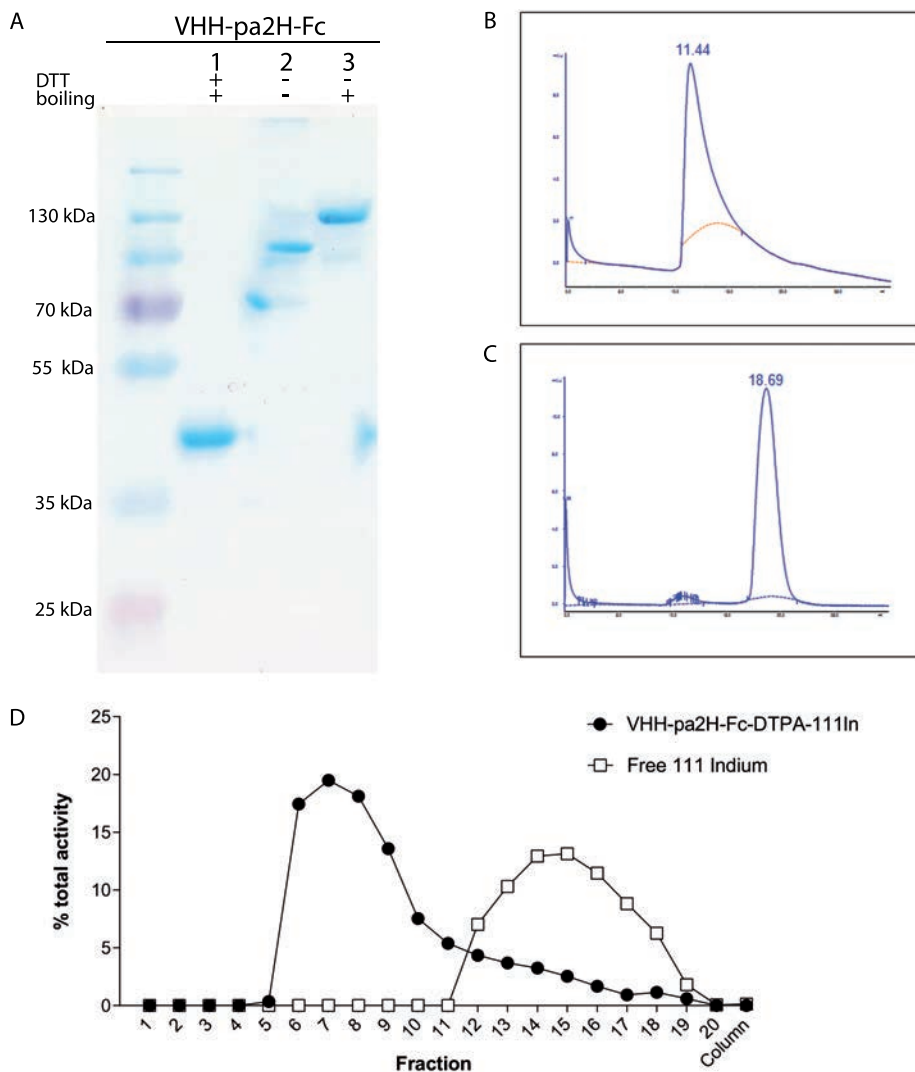


Figure 4.4. Quality control of VHH-pa2H-Fc, VHH-pa2H-Fc-DTPA and VHH-pa2H-Fc-DTPA-¹¹¹In. (A) SDS-PAGE analysis of VHH-pa2H-Fc under denaturing (+DTT) and non-denaturing (-DTT) conditions shows a denatured protein at approximately 42 kDa and much higher bands under non-denaturing conditions, indicating the formation of a complex protein. (B + C) Size exclusion chromatography confirms the addition of at least one DTPA molecule to VHH-pa2H-Fc as indicated by the near-complete shift of the peak from 11.44 to 18.69 ml. (D) PD-10 column purification indicated highly successful radiolabeling of ¹¹¹In to the DTPA labeled VHH-pa2H-Fc, as no significant peaks were detected in fractions 12-18, in which free radiotracer elutes from the column.

3.3. DTPA conjugation to VHH-pa2H-Fc and radiolabeling with ¹¹¹In

Successful DTPA conjugation to the fusion protein was confirmed with SEC, in which the retention time of the peak for the non-radiolabeled VHH-pa2H-Fc almost completely shifted from 11.44 to 18.69 ml after the conjugation (Figure 4.4 B and C). After radiolabeling, VHH-pa2H-Fc-DTPA-¹¹¹In was purified on a PD-10 column to remove labelling reactants. The highest radioac-

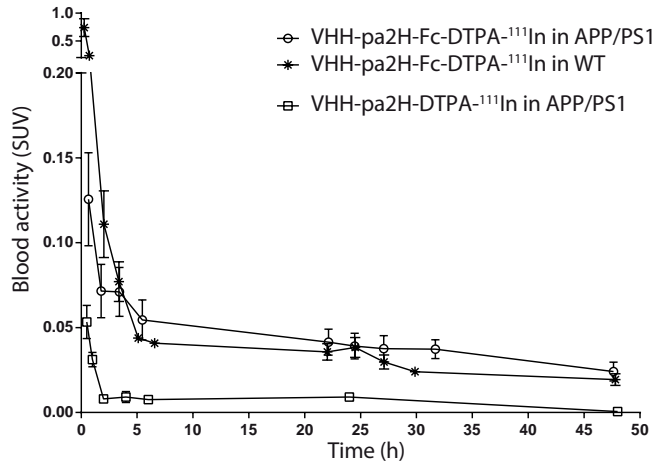


Figure 4.5. Pharmacokinetics. Blood clearance of VHH-pa2H-DTPA-¹¹¹In and VHH-pa2H-Fc-DTPA-¹¹¹In in double transgenic APP^{swc}/PS1dE9 (APP/PS1) and wildtype littermates (WT). Data are mean ± SEM of 4-8 observations at time points up to 48 h after injection and are shown as standard uptake values (SUV).

Table 4.1. Area Under the Curve (AUC) values calculated based on the data depicted in Figure 4.5, show significant increases for the Fc fused VHH compared to the non-fused VHH-pa2H in APP^{swc}/PS1dE9 transgenic mice (APP/PS1) and wildtype littermates (WT). All mice were injected with 20 µg VHH labeled with ¹¹¹In at 10-20 MBq at the time of injection.

n	VHH-pa2H-DTPA- ¹¹¹ In		VHH-pa2H-Fc-DTPA- ¹¹¹ In	
	WT	APP/PS1	WT	APP/PS1
	-	4	8	8
AUC	nd	17.1 ± 2.7	116.3 ± 12.3 *	124.7 ± 21.3 *

*=p<0.05 compared to VHH-pa2H-DTPA-¹¹¹In, nd = not determined.

tivity was found in fractions 6-9 (Figure 4.4 D), which were pooled for *in vivo* administration. No significant peaks were detected in the shoulder in fractions 12-18, indicating the absence of free ¹¹¹In. The amount of radioactivity in the pooled fractions amounted to 89% of the total radioactivity.

3.4. Pharmacokinetics

The blood clearance of the VHH fusion protein VHH-pa2H-Fc-DTPA-¹¹¹In and the control tracer VHH-pa2H-DTPA-¹¹¹In were calculated and expressed as SUV, from which the AUC was calculated (Figure 4.5 and Table 4.1). Based on the AUC values and clearance graphs it is clear that the fusion of the human IgG Fc domain leads to a significant increase in retention in the blood of the fused VHH compared to the unmodified VHH-pa2H. Even though slightly higher in the transgenic group, between the APP/PS1 group and the WT littermates the AUC of the blood clearance of VHH-pa2H-Fc-DTPA-¹¹¹In was not significantly different.

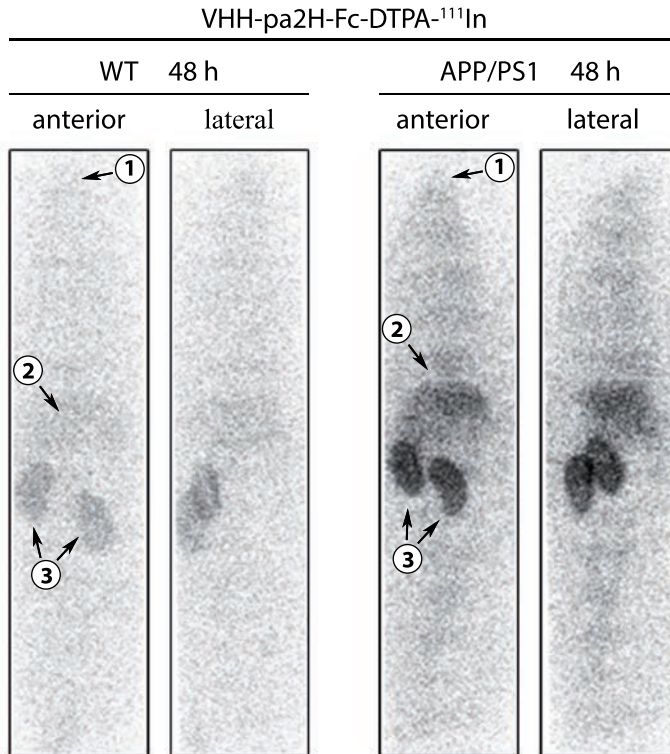


Figure 4.6. Anterior and lateral microSPECT scintigraphs show the difference in biodistribution and pharmacokinetic profile of VHH-pa2H-Fc-DTPA-¹¹¹In between double transgenic APP^{swE}/PS1dE9 (APP/PS1) and wildtype littermates (WT) at 48 h after injection. In both strains, the majority of the signal originates from the kidneys (3) and the liver (2), while the brain (1) does not contain more signal compared to the rest of the body. Overall, there seems to be less signal originating from the WT animals compared to the APP/PS1, which is in concordance with the data obtained from the pharmacokinetics. All mice were injected with 20 µg VHH labeled with ¹¹¹In at 10–20 MBq at the time of injection and imaged at 48 h for 30 minutes.

3.5. MicroSPECT imaging

MicroSPECT imaging of the mice injected with VHH-pa2H-Fc-DTPA-¹¹¹In confirmed that the Fc-fused VHH was still present in the mice at 48 h, mainly in the renal cortex and in the liver (Figure 4.6). However, the images depicted clearly that the protein was not found to be accumulating in the transgenic brains, i.e. at the amyloid deposits, as there was no significant difference in signal in that area between APP/PS1 and WT animals.

3.6. Biodistribution

Radioactivity counts of excised organs and tissues at 48 h after injection showed that the profiles of the Fc tagged VHH generally follow the plasma pharmacokinetics, i.e. higher counts are found in the organs for the VHH-pa2H-Fc-DTPA-¹¹¹In injected group compared the group injected with the non-Fc VHH (Table 4.2). The kidneys are the main organ of clearance of the radioactivity of VHH-pa2H-Fc-DTPA-¹¹¹In, corroborating the microSPECT data. For the non-fused

Table 4.2. Biodistribution of VHH-pa2H-DTPA-¹¹¹In and VHH-pa2H-Fc-DTPA-¹¹¹In in 12-14 month old double transgenic APP_{PS1dE9}/PS1dE9 (APP/PS1) and wildtype littermates (WT) at 48 h after injection. Values are presented as the mean ± SEM of the radioactivity counted per weighed tissue after sacrificing and corrected for total body weight expressed as the standard uptake value (SUV) of 4-8 observations. All values are corrected for radioactive decay over time, nd = not determined. All mice were injected with 20 µg VHH labeled with ¹¹¹In at 10-20 MBq at the time of injection and blood and all tissues were obtained at approximately 48 h after injection.

	n	VHH-pa2H-DTPA- ¹¹¹ In		VHH-pa2H-Fc-DTPA- ¹¹¹ In	
		WT	APP/PS1	WT	APP/PS1
		4		8	
		SUV ± SEM (SUV = %ID / g tissue per g mouse)			
Blood	nd	0.007 ± 0.0001	0.0194 ± 0.0034 *	0.0242 ± 0.0149 *¶	
Urine & bladder	nd	0.0291 ± 0.0079	0.0237 ± 0.0036	0.0140 ± 0.0025	
Heart	nd	0.0015 ± 0.0003	0.0099 ± 0.0011 *	0.0121 ± 0.0022 *¶	
Lungs	nd	0.0016 ± 0.0002	0.0188 ± 0.0018 *	0.0188 ± 0.0035 *¶	
Spleen	nd	0.2939 ± 0.1362	0.0412 ± 0.0072 *	0.0207 ± 0.0037 *¶	
Liver	nd	0.0007 ± 0.0001	0.0658 ± 0.0168 *	0.0135 ± 0.0091	
Kidneys	nd	0.1493 ± 0.0095	0.2194 ± 0.0119 *	0.0874 ± 0.0455	
Muscle	nd	0.0008 ± 0.0001	0.0054 ± 0.0012	0.0048 ± 0.0009 *¶	
Cerebrum	nd	0.0001 ± 0.0000	0.0011 ± 0.0004	0.0008 ± 0.0003	
Cerebellum	nd	0.0003 ± 0.0003	0.007 ± 0.0001 *	0.0008 ± 0.0002 *	
Brain	nd	0.0004 ± 0.0002	0.0017 ± 0.0005	0.0016 ± 0.0005	
Brain/blood ratio	nd	0.5796 ± 0.1546	0.0829 ± 0.0059 *	0.0640 ± 0.0066 *¶	
Muscle/blood ratio	nd	1.3040 ± 0.4035	0.3192 ± 0.0761 *	0.2225 ± 0.0219 *¶	
Ratio brain/blood to muscle/blood	nd	0.4376 ± 0.1083	0.3719 ± 0.1041	0.3157 ± 0.0629	

* = p < 0.05 compared to VHH-pa2H-DTPA-¹¹¹In; ¶ = p < 0.05 compared to WT mice.

VHH, 98.10 ± 0.04 %ID is secreted after 48 h, with the remainder residing mainly in the spleen. This secretion is significantly higher ($p < 0.006$) compared to the fusion protein VHH-pa2H-Fc-DTPA-¹¹¹In in both the transgenic mice (92.47 ± 0.59 %ID) and the WT littermates (94.77 ± 0.19 %ID) at 48 h after injection. For VHH-pa2H-Fc-DTPA-¹¹¹In the excretion was significantly lower ($p < 0.01$) in APP/PS1 mice compared to WT animals.

When analyzing the amount of radioactivity found in the brain, it is interesting to note that the brain to blood ratio seems to be significantly higher for the non-fused VHH than for the Fc fused moieties. However, by comparing this ratio to the muscle to blood ratio, a calculation which indicates the specificity of the brain to blood ratio, it is clear that the exceedingly low blood values in the non Fc fused VHH group are confounding the obtained ratios. The ratio “brain/ blood to muscle/blood” is not significantly different between any of the analyzed groups.

4. DISCUSSION

In this study we provide evidence that the blood clearance of VHH-pa2H-DTPA-¹¹¹In in WT and APP/PS1 transgenic mice can be significantly slowed down by fusion to the Fc region of the human IgG protein. Earlier we have shown that free, unmodified VHH have a fast blood clearance profile and may not effectively cross the *in vivo* BBB; a limitation which must be overcome for the development of brain amyloid targeted diagnostics or therapeutics in AD [8,10]. The rapid renal clearance of non-Fc tagged VHH-pa2H-DTPA-¹¹¹In is once more confirmed in this study (Figure 4.5 and Table 4.2).

As the transport of these A β -targeting VHH over the BBB is an active process [30,34,35], we hypothesized that prolonging the blood residential time of the VHH could increase its delivery into the brain. To achieve this, a human IgG1 Fc domain (hinge, CH₂ and CH₃ region) was fused to the C-terminus of VHH-pa2H (Figure 4.1). As a result, the homodimer forming fusion protein reached a total molecular weight of 80 kDa, above the renal filtration cut-off of approximately 60 kDa. Furthermore, interaction of the fusion protein with the FcRn provides additional systemic retention of the construct. As the increased AUC values show, the fusion of the Fc domain did indeed significantly prolong the blood residential time of the VHH-pa2H-Fc-DTPA-¹¹¹In (Figure 4.5).

Between the two groups of mice – the APP/PS1 double transgenic and the WT littermates – there is no significant difference in retention of VHH-pa2H-Fc-DTPA-¹¹¹In. This indicates that indeed the presence of the Fc tail, rather than the presence of an A β phenotype, is the cause of the increased retention in the circulation, even if the trend in the AUC graph and values indicates a slightly higher retention in the APP/PS1 animals (Figure 4.5). This trend is also observed

in the microSPECT images obtained at 48 h after injection, in which certain organs, most notably the kidneys and the liver, seem to have a slightly stronger signal (Figure 4.6). In accordance, less radioactivity was excreted from transgenic mice compared to WT at 48 h.

The pharmacokinetics data (Figure 4.5) furthermore suggest a dramatic reduction in volume of distribution (VD) as a result of the fusion of the Fc tail. This is especially pronounced in the WT group injected with VHH-pa2H-Fc-DTPA-¹¹¹In. This would indicate that the unmodified VHH-pa2H-DTPA-¹¹¹In is more rapidly distributed over the organs and tissues in the animal body, while the Fc-fused protein remains in the bloodstream. However, keeping in mind that unmodified VHH have significantly shorter blood half-lives and are quickly cleared by the renal system, it must be noted that the organ biodistribution profile should be analyzed shortly after injection to confidently calculate actual VD values.

The biodistribution data (Table 4.2) show that most organs in the groups injected with VHH-pa2H-Fc-DTPA-¹¹¹In have significantly higher SUVs compared to the non-fused VHH. However, when the ratios between the brain-to-blood and muscle-to-blood are compared, it is clear that there is no relative increase in uptake in the brain compared to uptake in the muscle. Interestingly, there is no specific increase in the brain of the transgenic animals compared to the WT littermates either. In previous studies, it has been shown that once the VHH reaches the amyloid deposits in the brain, the antibody fragments remains associated with the amyloid and will thus be retained in the brain [8,10]. It can therefore be assumed that VHH-pa2H-Fc-DTPA-¹¹¹In does not reach the BBB protected brain more efficiently than the non-fused VHH-pa2H-DTPA-¹¹¹In, despite the increased blood circulation time.

The 80 kDa size of the VHH-Fc, a significant increase over the 12 kDa of the unmodified VHH, may hypothetically obstruct the blood-brain barrier passage. However, an increase in size of the VHH does not necessarily exclude BBB passage [9]. Even full length IgGs can be transported over the BBB when an active transport is involved [36,37], as is the case with the VHHs. Indeed, Farrington *et al.* recently described the enhanced *in vivo* passage of an Fc tagged VHH compared to the free VHH over the rat BBB [27]. It must be noted however, that in the latter example a 5-15 times higher concentration of VHH-fc derivative had been injected compared to the current study and species differences might play a role in the amount of BBB penetration [38].

The VHH-pa2H-Fc construct does, however, recognize A β (Figure 4.3). Fusion of the Fc region to the antibody fragment is therefore not detrimental to its function, and may in fact improve its binding capacity [27]. As a result, VHH-pa2H-Fc could still be used for peripheral applications in general and more specifically investigated for use in the peripheral sink theory [39–41]. Furthermore, it also means that the concept of VHH-Fc fusion proteins can be extrapolated to other VHHs. In this study we did not examine whether the VHH-pa2H-Fc-DTPA-¹¹¹In in the

blood is free in the plasma or bound to circulating host cells. It may be plausible that the interaction of the fusion protein with Fc receptors or other compounds increases the blood residential time, but also actively prevents the fusion protein to reach and cross the BBB [42].

The use of the chelator p-SCN-Bz-DTPA to label VHH-pa2H and VHH-pa2H-Fc with ¹¹¹In could cause the VHH to act differently in an *in vivo* setting. However, based on the experiments in this study (Figure 4.3) and on previous experience, we know that the DTPA labeling has no effect on the amyloid beta binding characteristics of the VHH [8,10], and that the labeling itself is very stable over time [8]. Also, it has been shown that conjugation with Alexa dyes, which occurs via a similar NHS-ester conjugation, shows no difference in characteristic binding or biodistribution profiles for single VHHs [10], or for Fc conjugated VHHs [27] and that the similar binding of a NOTA chelator can be used to follow the biodistribution of VHHs *in vivo* [43].

5. CONCLUSION

VHH-pa2H-Fc can be effectively produced in HEK293T cells and retains its biological activity. It shows significantly increased systemic retention due to the fusion of the llama antibody fragment to the hinge, CH₂ and CH₃ domains of a human IgG1. However, increasing the blood circulation time alone does not result in increased BBB penetration.

DISCLOSURE

No potential conflicts of interest are to be disclosed.

ACKNOWLEDGMENTS

The authors wish to acknowledge Ernst Suidgeest and Tessa Buckle (Leiden University Medical Center, NL) for their technical assistance and Hendrik Adams (BAC b.v., NL) for supplying the VHH-pa2H. This research was performed within the framework project LeARN (grant 02N-101) and the Center for Medical Systems Biology (grants S-MRI-110010 and S-MRI-110030).

REFERENCES

1. Yardehnavi, N., Behdani, M., Pooshang Bagheri, K., Mahmoodzadeh, A., Khanahmad, H., Shahbazzadeh, D., Habibi-Anbouhi, M., Ghassabeh, G. H. & Muyldermans, S. A camelid antibody candidate for development of a therapeutic agent against *Hemiscorpius lepturus* envenomation. *FASEB J.* 28(9):4004–14 (2014).
2. Hmila, I., Abdallah R, B. A. Ben, Saerens, D., Benlasfar, Z., Conrath, K., Ayeb, M. El, Muyldermans, S. & Bouhaouala-Zahar, B. VHH, bivalent domains and chimeric Heavy chain-only antibodies with high neutralizing efficacy for scorpion toxin AahI. *Mol. Immunol.* 45(14):3847–3856 (2008).
3. Gad, W., Ben-Abderrazek, R., Wahni, K., Vertommen, D., Muyldermans, S., Bouhaouala-Zahar, B. & Messens, J. Wheat germ in vitro translation to produce one of the most toxic sodium channel specific toxins. *Biosci. Rep.* 34(4) (2014).
4. Cardoso, F. M., Ibañez, L. I., Van den Hoecke, S., De Baets, S., Smet, A., Roose, K., Schepens, B., Descamps, F. J., Fiers, W., Muyldermans, S., *et al.* Single-domain antibodies targeting neuraminidase protect against an H5N1 influenza virus challenge. *J. Virol.* 88(15):8278–96 (2014).
5. Scheuplein, F., Rissiek, B., Driver, J. P., Chen, Y.-G., Koch-Nolte, F. & Serreze, D. V. A recombinant heavy chain antibody approach blocks ART2 mediated deletion of an iNKT cell population that upon activation inhibits autoimmune diabetes. *J. Autoimmun.* 34(2):145–54 (2010).
6. Impagliazzo, A., Tepper, A. W., Verrips, T. C., Ubbink, M. & van der Maarel, S. M. Structural basis for a PABPN1 aggregation-preventing antibody fragment in OPMD. *FEBS Lett.* 584(8):1558–64 (2010).
7. Rutgers, K. S., van Remoortere, A., van Buchem, M. A., Verrips, C. T., Greenberg, S. M., Bacsikai, B. J., Frosch, M. P., van Duinen, S. G., Maat-Schieman, M. L. & Van der Maarel, S. M. Differential recognition of vascular and parenchymal beta amyloid deposition. *Neurobiol. Aging* 32(10):1774–1783 (2009).
8. Rotman, M., Welling, M. M., Bunschoten, A., de Backer, M. E., Rip, J., Nabuurs, R. J. A., Gaillard, P. J., van Buchem, M., van der Maarel, S. M. & van der Weerd, L. Enhanced liposomal brain delivery of an anti-amyloid VHH-2H heavy chain antibody fragment in a mouse model for Alzheimer's disease. *J. Control. Release* 203:40–50 (2015).
9. Li, T., Bourgeois, J.-P., Celli, S., Glacial, F., Le Sourd, A.-M., Mecheri, S., Weksler, B., Romero, I., Couraud, P.-O., Rougeon, F., *et al.* Cell-penetrating anti-GFAP VHH and corresponding fluorescent fusion protein VHH-GFP spontaneously cross the blood-brain barrier and specifically recognize astrocytes: application to brain imaging. *FASEB J.* 26(10):3969–79 (2012).
10. Nabuurs, R. J. A., Rutgers, K. S., Welling, M. M., Metaxas, A., de Backer, M. E., Rotman, M., Bacsikai, B. J., van Buchem, M. A., van der Maarel, S. M. & van der Weerd, L. *In vivo* detection of amyloid- β deposits using heavy chain antibody fragments in a transgenic mouse model for Alzheimer's disease. *PLoS One* 7(6):e38284 (2012).
11. Rotman, M., Snoeks, T. J. A. & van der Weerd, L. Pre-clinical optical imaging and MRI for drug development in Alzheimer's disease. *Drug Discovery Today: Technologies* 8(2-4):e117–e125 (2011).
12. Kontermann, R. E. Strategies to extend plasma half-lives of recombinant antibodies. *BioDrugs* 23(2):93–109 (2009).
13. Kontermann, R. E. Strategies for extended serum half-life of protein therapeutics. *Curr. Opin. Biotechnol.* 22(6):868–76 (2011).
14. Gunasekaran, K., Pentony, M., Shen, M., Garrett, L., Forte, C., Woodward, A., Ng, S. Bin, Born, T., Retter, M., Manchulenko, K., *et al.* Enhancing antibody Fc heterodimer formation through electrostatic steering effects: applications to bispecific molecules and monovalent IgG. *J. Biol. Chem.* 285(25):19637–46 (2010).
15. Martin, W. L., West, A. P., Gan, L. & Bjorkman, P. J. Crystal structure at 2.8 Å of an FcRn/heterodimeric Fc complex: mechanism of pH-dependent binding. *Mol. Cell* 7(4):867–77 (2001).

16. Olafsen, T., Kenanova, V. E. & Wu, A. M. Tunable pharmacokinetics: modifying the *in vivo* half-life of antibodies by directed mutagenesis of the Fc fragment. *Nat. Protoc.* 1(4):2048–60 (2006).
17. Ying, T., Ju, T. W., Wang, Y., Prabakaran, P. & Dimitrov, D. S. Interactions of IgG1 CH2 and CH3 Domains with FcRn. *Front. Immunol.* 5:146 (2014).
18. Gould, L. H., Sui, J., Foellmer, H., Oliphant, T., Wang, T., Ledizet, M., Murakami, A., Noonan, K., Lambeth, C., Kar, K., *et al.* Protective and therapeutic capacity of human single-chain Fv-Fc fusion proteins against West Nile virus. *J. Virol.* 79(23):14606–13 (2005).
19. Ono, K.-I., Kamihira, M., Kuga, Y., Matsumoto, H., Hotta, A., Itoh, T., Nishijima, K.-I., Nakamura, N., Matsuda, H. & Iijima, S. Production of anti-prion scFv-Fc fusion proteins by recombinant animal cells. *J. Biosci. Bioeng.* 95(3):231–8 (2003).
20. Kamihira, M., Ono, K., Esaka, K., Nishijima, K., Kigaku, R., Komatsu, H., Yamashita, T., Kyogoku, K. & Iijima, S. High-level expression of single-chain Fv-Fc fusion protein in serum and egg white of genetically manipulated chickens by using a retroviral vector. *J. Virol.* 79(17):10864–74 (2005).
21. Powers, D. B., Amersdorfer, P., Poul, M., Nielsen, U. B., Shalaby, M. R., Adams, G. P., Weiner, L. M. & Marks, J. D. Expression of single-chain Fv-Fc fusions in *Pichia pastoris*. *J. Immunol. Methods* 251(1-2):123–35 (2001).
22. Richard, G., Meyers, A. J., McLean, M. D., Arbabi-Ghahroudi, M., MacKenzie, R. & Hall, J. C. *In vivo* neutralization of α -cobratoxin with high-affinity llama single-domain antibodies (VHHs) and a VHH-Fc antibody. *PLoS One* 8(7):e69495 (2013).
23. De Buck, S., Virdi, V., De Meyer, T., De Wilde, K., Piron, R., Nolf, J., Van Lerberge, E., De Paepe, A. & Depicker, A. Production of camel-like antibodies in plants. *Methods Mol. Biol.* 911:305–24 (2012).
24. De Buck, S., Nolf, J., De Meyer, T., Virdi, V., De Wilde, K., Van Lerberge, E., Van Droogenbroeck, B. & Depicker, A. Fusion of an Fc chain to a VHH boosts the accumulation levels in Arabidopsis seeds. *Plant Biotechnol. J.* 11(8):1006–16 (2013).
25. Veggiani, G., Ossolengo, G., Aliprandi, M., Cavallaro, U. & de Marco, A. Single-domain antibodies that compete with the natural ligand fibroblast growth factor block the internalization of the fibroblast growth factor receptor 1. *Biochem. Biophys. Res. Commun.* 408(4):692–6 (2011).
26. Bell, A., Wang, Z. J., Arbabi-Ghahroudi, M., Chang, T. a., Durocher, Y., Trojahn, U., Baardsnes, J., Jaramillo, M. L., Li, S., Baral, T. N., *et al.* Differential tumor-targeting abilities of three single-domain antibody formats. *Cancer Lett.* 289(1):81–90 (2010).
27. Farrington, G. K., Caram-Salas, N., Haqqani, A. S., Brunette, E., Eldredge, J., Pepinsky, B., Antognetti, G., Baumann, E., Ding, W., Garber, E., *et al.* A novel platform for engineering blood-brain barrier-crossing bispecific biologics. *FASEB J.* 28(11):4764–4778 (2014).
28. Bazl, M. R., Rasaei, M. J., Foruzandeh, M., Rahimpour, A., Kiani, J., Rahbarizadeh, F., Alirezapour, B. & Mohammadi, M. Production of chimeric recombinant single domain antibody-green fluorescent fusion protein in Chinese hamster ovary cells. *Hybridoma (Larchmt).* 26(1):1–9 (2007).
29. Aliprandi, M., Sparacio, E., Pivetta, F., Ossolengo, G., Maestro, R. & de Marco, A. The availability of a recombinant anti-SNAP antibody in VHH format amplifies the application flexibility of SNAP-tagged proteins. *J. Biomed. Biotechnol.* 2010:658954 (2010).
30. Rutgers, K. S., Nabuurs, R. J. A., van den Berg, S. A. A., Schenk, G. J., Rotman, M., Verrips, C. T., van Duinen, S. G., Maat-Schieman, M. L., van Buchem, M. A., de Boer, A. G., *et al.* Transmigration of beta amyloid specific heavy chain antibody fragments across the *in vitro* blood-brain barrier. *Neuroscience* 190:37–42 (2011).
31. Reiserer, R. S., Harrison, F. E., Syverud, D. C. & McDonald, M. P. Impaired spatial learning in the APPSwe + PSEN1DeltaEg bigenic mouse model of Alzheimer's disease. *Genes. Brain. Behav.* 6(1):54–65 (2007).

32. Jankowsky, J. L., Fadale, D. J., Anderson, J., Xu, G. M., Gonzales, V., Jenkins, N. A., Copeland, N. G., Lee, M. K., Younkin, L. H., Wagner, S. L., *et al.* Mutant presenilins specifically elevate the levels of the 42 residue beta-amyloid peptide *in vivo*: evidence for augmentation of a 42-specific gamma secretase. *Hum. Mol. Genet.* 13(2):159–70 (2004).
33. Loening, A. M. & Gambhir, S. S. AMIDE: a free software tool for multimodality medical image analysis. *Mol. Imaging* 2(3):131–7 (2003).
34. Abulrob, A., Sprong, H., Van Bergen en Henegouwen, P. & Stanimirovic, D. The blood-brain barrier transmigration single domain antibody: mechanisms of transport and antigenic epitopes in human brain endothelial cells. *J. Neurochem.* 95(4):1201–14 (2005).
35. Muruganandam, A., Tanha, J., Narang, S. & Stanimirovic, D. Selection of phage-displayed llama single-domain antibodies that transmigrate across human blood-brain barrier endothelium. *FASEB J.* 16(2):240–2 (2002).
36. Pardridge, W. M. & Boado, R. J. Reengineering biopharmaceuticals for targeted delivery across the blood-brain barrier. *Methods Enzymol.* 503:269–92 (2012).
37. Niewoehner, J., Bohrmann, B., Collin, L., Urich, E., Sade, H., Maier, P., Rueger, P., Stracke, J. O., Lau, W., Tissot, A. C., *et al.* Increased brain penetration and potency of a therapeutic antibody using a monovalent molecular shuttle. *Neuron* 81(1):49–60 (2014).
38. Warren, M. S., Zerangue, N., Woodford, K., Roberts, L. M., Tate, E. H., Feng, B., Li, C., Feuerstein, T. J., Gibbs, J., Smith, B., *et al.* Comparative gene expression profiles of ABC transporters in brain microvessel endothelial cells and brain in five species including human. *Pharmacol. Res.* 59(6):404–13 (2009).
39. Wang, Y.-J., Gao, C.-Y., Yang, M., Liu, X.-H., Sun, Y., Pollard, A., Dong, X.-Y., Wu, X.-B., Zhong, J.-H., Zhou, H.-D., *et al.* Intramuscular delivery of a single chain antibody gene prevents brain A β deposition and cognitive impairment in a mouse model of Alzheimer's disease. *Brain Behav. Immun.* 24(8):1281–93 (2010).
40. Sagare, A., Deane, R., Bell, R. D., Johnson, B., Hamm, K., Pendu, R., Marky, A., Lenting, P. J., Wu, Z., Zarcone, T., *et al.* Clearance of amyloid-beta by circulating lipoprotein receptors. *Nat. Med.* 13(9):1029–31 (2007).
41. Weiner, H. L. & Frenkel, D. Immunology and immunotherapy of Alzheimer's disease. *Nat. Rev. Immunol.* 6(5):404–16 (2006).
42. Tarzi, R. M., Davies, K. A., Robson, M. G., Fossati-Jimack, L., Saito, T., Walport, M. J. & Cook, H. T. Nephrotoxic nephritis is mediated by Fc γ receptors on circulating leukocytes and not intrinsic renal cells. *Kidney Int.* 62(6):2087–2096 (2002).
43. Morais, M., Cantante, C., Gano, L., Santos, I., Lourenço, S., Santos, C., Fontes, C., Aires da Silva, F., Gonçalves, J. & Correia, J. D. G. Biodistribution of a (67)Ga-labeled anti-TNF VHH single-domain antibody containing a bacterial albumin-binding domain (Zag). *Nucl. Med. Biol.* 41 Suppl:e44–8 (2014).

1. Department of Human Genetics, Leiden University Medical Center, The Netherlands
2. Department of Radiology, Leiden University Medical Center, The Netherlands
3. Department of Neuroscience, Mayo Clinic, Jacksonville, FL, USA

5

CHAPTER

FUNCTIONALLY SECRETED VHH-EMGFP BINDS AMYLOID PLAQUES AND CAN BE VISUALIZED *IN* *VIVO*

Adapted from

Functionally secreted single domain antibody fragment VHH-EmGFP binds amyloid plaques and can be visualized in vivo.

Maarten Rotman^{1,2,3}, Laure Grand Moursel^{1,2}, Anna Carrano³, Linda M. van der Graaf^{1,2}, Marlinde L. van den Boogaard¹, Ernst Suidgeest², Mark van Buchem², Silvère M. van der Maarel¹, Pritam Das³ and Louise van der Weerd^{1,2}.

Submitted 2017

ABSTRACT

Introduction: Llama antibody fragments (VHH) are able to bind and interfere with aggregated protein depositions, such as amyloid beta ($A\beta$). In this study, we examined one such VHH, VHH-pa2H-EmGFP, for its propensity to target and reduce $A\beta$ *in vivo*.

Methods: VHH-EmGFP were fused to an N-terminal lysozyme secretion signal and a C-terminal Emerald GFP (EmGFP). The constructs were packaged in Adeno Associated Virus serotype 2/1 (AAV2/1), tested *in vitro* for expression, secretion and functionality and injected intracranially in P0 and adult APP^{swe}/PS1^{dE9} transgenic mice (APP/PS1), a mouse model for Alzheimer's disease. A subset of mice received a cranial window through which amyloid depositions were followed longitudinally for up to 4 months using multiphoton microscopy.

Results: VHH-EmGFP are secreted as fully functional VHH fusion proteins, retaining affinity for $A\beta$ depositions *in vitro* and *in vivo*. Early, long-term exposure to VHH-pa2H-EmGFP may reduce or prevent amyloid burden in APP/PS1 mice. AAV-mediated VHH transduction after onset of plaque formation did not significantly reduce amyloid burden. The expression and colocalization of VHH-pa2H-EmGFP with $A\beta$ in the brain parenchyma and vasculature could be followed *in vivo* for at least 4 months after installment of the cranial window. *Ex vivo* analysis showed that transduction and expression was limited to the hippocampus, and in particular to the stratum pyramidale of CA1 and CA2 in most cases, but that the secreted VHH-pa2H-EmGFP was able to travel well beyond this region, colocalizing with $A\beta$ depositions in the cortex and other areas of the brain.

Conclusion: Functional VHH-pa2H-EmGFP, delivered to the brain via intracranial injection of AAV2/1, may be of use in treatment of pre-onset AD. Furthermore, the *in vivo* delivery method described in this manuscript can be employed in a variety of neurodegenerative disorders and can be used to screen the therapeutic potential of VHH in real-time *in vivo*.

1. INTRODUCTION

VHH, camelid single domain heavy chain only antibody fragments, have a very wide range of applications, among which the detection and the prevention of aggregation of proteins [1–5]. In that light, various VHH have been studied as potential diagnostic, therapeutic and even theragnostic tools for Alzheimer's disease (AD) [6–9], in which aggregation of the amyloid beta peptide ($A\beta$) plays a major role [10]. A number of VHH have shown outstanding $A\beta$ recognition, both in specificity and selectivity, and one of these, VHH-pa2H [11], is investigated further in this study.

Interestingly, a small amount of VHH-pa2H applied directly to the exposed brain of an adult APP^{swe}/PS1^{dE9} (APP/PS1) mouse model for AD leads to an acute reduction of parenchymal $A\beta$ plaques (Supplemental Data I). However, it is not known whether this effect is sustained over time and if it can be used to reduce and prevent $A\beta$ aggregation in AD. Here we test the hypothesis that prolonged treatment with VHH-pa2H can significantly reduce the $A\beta$ burden in a mouse model for AD. VHH-pa2H has a short blood half life (i.e. 15–20 minutes) and shows only limited unassisted blood-brain barrier (BBB) passage [12,13]; repeated peripheral injection is unlikely to suffice. Virally-mediated gene delivery allows for continuous expression of therapeutic proteins at the site of action. By injecting the viral particles intracranially, i.e. beyond the BBB, passage limitations can be circumvented. Small proteins, such as VHH, are very well suited for this approach. We have therefore injected Adeno Associated Virus serotype 2/1 (AAV2/1) vectors [14] encoding a fusion construct ss-VHH-EmGFP into the hippocampal area of neonatal and adult APP/PS1 mice and examined the effect on plaque deposition in the murine brain. For secretion into the extracellular space of the parenchyma of the mice, the lysozyme secretion signal was fused N-terminal of the VHH [15]. For *in vivo* real-time observation of the expression and effect of the VHH in the brain, an Emerald GFP (EmGFP) fragment was fused C-terminal of the VHH [16].

The aims of this study were twofold. Firstly, we aimed to assess the feasibility of AAV-mediated production and excretion of functionally intact VHH-EmGFP *in vitro* and *in vivo*. Secondly, we tested the central hypothesis that AAV-mediated VHH-pa2H attenuates amyloid burden in a mouse model of AD.

2. MATERIALS AND METHODS

2.1. Animals

All *in vivo* studies were performed in neonatal, young adult (7–9 months old), and adult (12–14

months old) double transgenic APP^{swe}/PS1^{dE9} mice (APP/PS1; JAX[®] Mice and Services, The Jackson Laboratory, USA) on a mixed C57BL/6 x C3H background and bred in-house at the Leiden University Medical Center in Leiden, the Netherlands or at the Mayo Clinic in Jacksonville, Florida, USA. The strain rapidly develops a vascular (CAA; cerebral amyloid angiopathy) and parenchymal A β associated phenotype [8,13,17]. Genotyping of the mice was performed by PCR following the supplier's instructions. All animals were kept on a strict 12 hour day/night light cycle with unlimited access to normal chow and water. The mice were distributed randomly over the experimental groups. All surgeries and imaging sessions were done under 1-2% isoflurane gas inhalation anesthetics, which is safer for the animals in the described complex and time-consuming operations compared to injection anesthetics [18]. All surgeries and imaging sessions were initiated and performed during the light cycle. A maximum of 8 mice were planned per operation or imaging day, 2 of each of the 4 groups to evenly distribute the groups throughout the experiment. To reduce stress associated with a novel environment, while allowing the anesthetized animals to recover in a relatively clean cage, the animals were placed in a new, clean cage 12-24 h before the operation or imaging session, or were returned to a clean cage to which a handful of old bedding material was added. All animal studies have been approved by the Leiden University Medical Center institutional Animal Experiments Committee (DEC permits 10097 and 12080; adult injections and *in vivo* multiphoton imaging) and the Mayo Clinic Institutional Animal Care and Use Committee (IACUC number A71713; neonatal and adult injections) in accordance with all national, European and NIH guidelines. All animal studies are reported in accordance with ARRIVE guidelines [19].

2.2. Cloning of pDG2-ss-VHH-EmGFP plasmids

To create the VHH-EmGFP fusion constructs, an intermediate pUC57-based shuttle vector was made. The shuttle vector contains, in order from 5' to 3': a 5' lysozyme secretion signal (ss) [13,16], a multiple cloning site (MCS) designed to allow entry of any VHH digested from the pUR5071 phagemid vector [11] while conserving the open reading frame (ORF) both with and without an VHH insert, a triple alanine linker and a 3' Emerald Green Fluorescent Protein (EmGFP) [20–22]. The EmGFP sequence is codon-optimized for production in murine cells (Baseclear, the Netherlands). The fragments are flanked by a 5' HindIII and a 3' SalI site. See Supplementary Data II for exact sequences.

A total of six ss-VHH-EmGFP fusion constructs were created: ss-VHH-pa2H-EmGFP, ss-VHH-va2E-EmGFP, ss-VHH-vaE2-EmGFP, ss-VHH-pa1E-EmGFP, ss-VHH-G7-EmGFP and ss-VHH-HttF4-EmGFP. The llama antibody fragments VHH-pa2H, -va2E, -vaE2, -pa1E, and -G7 were previously selected for efficient *in vivo* and/or *in vitro* binding to A β [8,11–13,23,24]. The llama antibody fragment VHH-Htt7F4 was selected as a negative control VHH from a library

directed against Huntingtin as described previously [25,26] and found not to associate with A β (Supplementary Data I). VHH sequences were lifted from the pUR5071 phagemid vector using the SfiI and BstEII restriction sites and introduced into the specialized MCS of the pUC57-based shuttle vector. As a second control next to VHH-Htt7F4, the MCS was left empty, which leads to the expression of an ss-MCS-EmGFP fusion protein. The complete constructs were introduced from the shuttle vector into the pDG2 AAV production vector, flanked by Inverted Terminal Repeats-2 (ITR2) and under the control of a mouse CMV promoter. The pDG2 vector was a kind gift from dr. M.A.F.V. Gonçalves and dr. R.C. Hoeben, LUMC, The Netherlands [27,28]. See Figure 5.1 for a complete overview of the cloning process.

2.3. *In vitro* analysis of the ss-VHH-EmGFP fusion construct

Correct and functional expression and secretion of the fusion protein was analyzed by transfection of the pDG2 vector into HEK293T cells using polyethyleneimine (PEI, 25000 MW; Thermo-Fisher Scientific) under standard reaction conditions. In short, in a 6-wells plate, 4.5×10^5 HEK293T cells, cultured in Dulbecco's modified Eagle's medium (DMEM) with 10% fetal bovine serum, 4.5 g/l glucose, 2 mM GlutaMAX, 100 U/ml penicillin and 100 μ g/ml streptomycin (DMEM; Thermo-Fisher Scientific), were transfected with 2 μ g pDG2-ss-VHH-EmGFP in 6 μ g PEI.

Cell-free supernatant was collected at two and three days after transfection, centrifuged and analyzed for EmGFP emission in Costar black bottom half-area 96-wells plates using a BioTek Synergy HT microplate reader (ex: 485 nm, em: 528 nm). Cells grown on coverslips were fixed with 3.7% formaldehyde, mounted using Vectashield with DAPI (Vector Laboratories Inc.) and analyzed with a Leica DM 5500B fluorescent microscope.

To confirm retained affinity of secreted ss-VHH-pa2H-EmGFP for A β depositions, immunohistochemistry was performed on human post-mortem AD brain and age-matched healthy control cryosections, as described before [13], however without the need for secondary antibodies. Briefly, acetone fixed, blocked, serial cryosections (5 μ m) were incubated overnight with 150 μ l undiluted HEK293T cell supernatant. After washing, the sections were mounted using Vectashield with DAPI (Vector Laboratories Inc.) and analyzed with a Leica DM 5500B fluorescence microscope. Adjacent sections were stained using mouse anti A β (4G8, Covance) as described before [13]. All human tissues were obtained from anonymous patients or healthy age-matched donors as confirmed by neuropathological examination in agreement with the guidelines of the Medical Ethics Committee of the Leiden University Medical Center (Leiden, The Netherlands). All tissues were processed in a coded fashion, according to Dutch national ethical guidelines (Code for Proper Secondary Use of Human Tissue, Dutch Federation of Medical Scientific Societies).

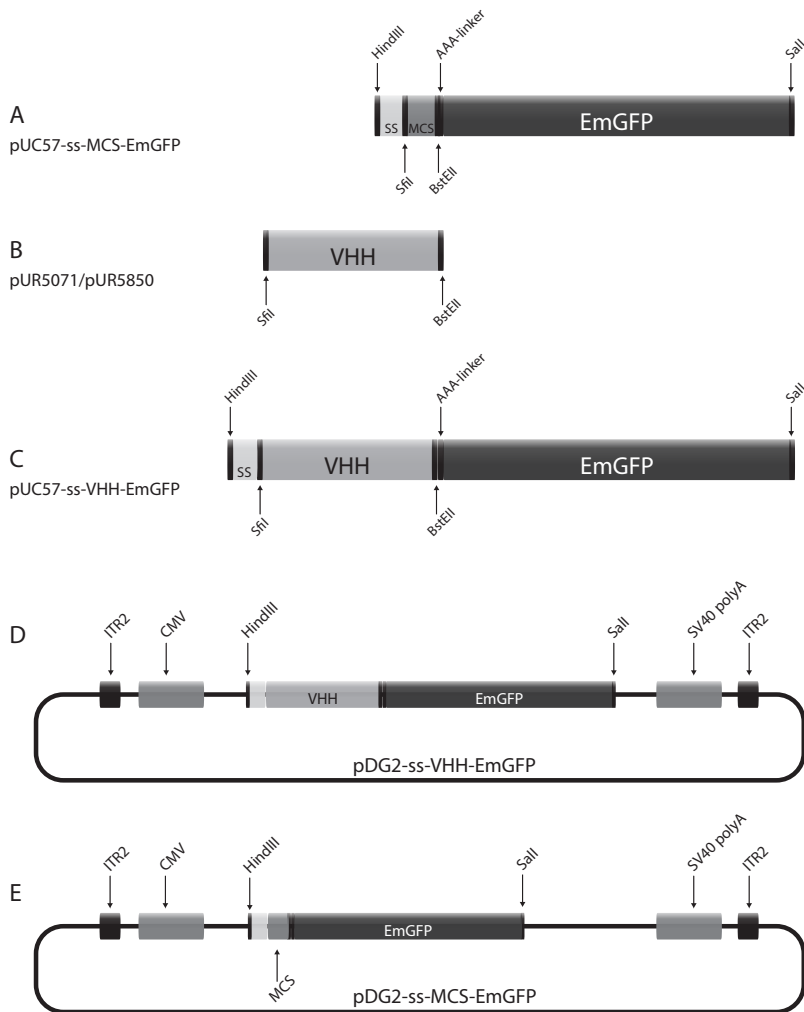


Figure 5.1. Schematic representation of the AAV cloning process. (A) The shuttle vector pUC₅₇ containing a lysozyme secretion signal (ss), a specialized multiple cloning site (MCS), triple alanine (AAA) linker and the murine codon optimized Emerald GFP (EmGFP). (B + C) Using the SfiI and BstEII restriction sites, the VHH is lifted from the pUR₅₀₇₁ vector and inserted into the pUC₅₇ shuttle vector. (D) Using the HindIII and the Sall restriction sites, the entire construct is lifted out of the shuttle vector and introduced between the ITR₂ regions in the pDG₂ vector. (E) If no VHH is inserted before inserting the construct into the pDG₂ vector, the translated product will contain a secretion signal, the multiple cloning site and the EmGFP as a functional fusion protein. The depicted sizes of the ss, MCS, VHH, and EmGFP are in relative relation to each other, based on the number of basepairs for each part.

2.4. Production of AAV_{2/1} ss-VHH-EmGFP particles

Three of the constructs were selected for the production of high titer AAV particles, i.e. ss-VHH-pa2H-EmGFP, ss-VHH-Htt7F4-EmGFP and ss-MCS-EmGFP. The pDG₂ (rAAV₂) plasmids were packaged in the AAV serotype 1 capsid and produced in HEK293T cells (human embryonic kidney; ATCC CRL-3216) as described previously [29]. In short, the pDG₂ vector containing the ss-VHH-EmGFP constructs were mixed with helper vectors encoding for

the serotype 1 AAV capsid proteins VP 1, 2 and 3. The mixture was transfected into HEK293T cells using PEI. After three days viral particles were harvested over an iodixinol gradient (Thermo-Fisher Scientific). The rAAV2/1-ss-VHH/MCS-EmGFP preparations were quantified by qPCR, adjusted to $1\text{-}3 \times 10^{12}$ genomic particles/ml (gp/ml) in PBS and stored at -80°C until use.

To confirm transduction capacity of the viral particles, HEK293T cells, NiE155 cells (mouse neuroblastoma cell line; ATCC CRL-2263) and HELA cells (human epithelial adenocarcinoma cell line; ATCC CCL-2) were seeded at very low confluency (approx. 1000 cells per well in a 6-well plate), exposed to $2 \mu\text{l}$ rAAV2/1-ss-VHH-EmGFP and cultured for up to 2 weeks at standard conditions without refreshing of the medium or splitting of the cells and imaged with an inverted a Leica DM 5500B fluorescence microscope. The conditioned cell medium was harvested and analyzed for EmGFP emission as described above.

2.5. Intracranial injections

Neonatal injections (P₀; <24 hours after birth) were performed as described previously [29]. Briefly, P₀ mice were cryo-anesthetized on ice for 5 minutes and injected bilaterally with $2 \mu\text{l}$ rAAV2/1-ss-VHH-pa2H-EmGFP or PBS, using a $10 \mu\text{l}$ Hamilton syringe with a 30G needle. The P₀ injections were performed manually at the approximate middle of each of the parietal bone structures of the skull. As the breeder lines are heterozygotes for the APP/PS1 genotype, genotyping was performed to confirm the transgenic status of the P₀ injection animals. Double transgenic APP/PS1 mice injected with rAAV2/1-ss-VHH-pa2H-EmGFP (n=3) or sham-injected with PBS (n=2) were sacrificed at 12 months. Wildtype mice injected with the viral particles (n=2) were sacrificed at 3 weeks.

Adult injections were performed using a stereotactic frame as described previously [30]. Briefly, isoflurane anesthetized mice were fixated in a Stoelting stereotaxic frame (Stoelting Europe, Ireland) and injected with $2 \mu\text{l}$ rAAV2/1-ss-VHH-pa2H-EmGFP, rAAV2/1-ss-VHH-Htt7F4-EmGFP, rAAV2/1-ss-MCS-EmGFP or PBS (n=6 per group), using a $10 \mu\text{l}$ World Precision Instruments (WPI) NanoFill syringe with a 36G beveled needle. Injection coordinates were -1.70 caudal, ± 1.50 lateral and -1.00 ventral from bregma, which corresponds to the hippocampal region of the average adult murine brain. A UMP3 Microsyringe Injector and Micro4 Controller (WPI) were used to inject at a constant rate of $0.25 \mu\text{l}$ per minute over period of 8 minutes. After an additional 2 minutes the needle was slowly raised and the scalp was closed aseptically using standard tissue glue. The mice were allowed to recover for 1 week before placement of the cranial window.

2.6. Intravital multiphoton microscopy

Adult and young adult mice received cranial windows following craniectomy as described before [12]. Briefly, a circular plate of approx. 5 mm in diameter was removed from the exposed skull between lambda and bregma, leaving the dura intact. An 8 mm round glass coverslip was carefully placed on top and secured to the skull using a mixture of dental cement and acrylate glue. The mice were allowed to recover for at least 1 week before intravital imaging.

A small group of mice received a window that was placed on the right lateral side of the midline. In this group the circular plate that was removed from the skull was approximately 3 mm in diameter and the round coverslip 5 mm.

Intravital multiphoton microscopy was performed at week 2, 5, 9, 13 and 17 after injection of the viral particles. The method of imaging was as described before [12]. Briefly, mice received intraperitoneal (i.p.) injections of 10 mg/kg Methoxy-X04 in the tail vein one day before the first and the last imaging session, but not in between [31]. Vessels were visualized via intravascular (i.v.) injection of 0.5 mg Dextran-Texas Red (70,000 MW, Life Technologies) directly before each imaging session. Images were acquired with a Zeiss LSM 710 microscope equipped with a Ti:Sapphire laser (Mai tai, Spectra Physics) set at 800 nm excitation pulse wavelength. The mice were sacrificed after the last imaging session.

2.7. Tissue sampling and histology

The mice were sacrificed and the brains were perfused via cardiac perfusion and fixed in paraformaldehyde, snap-frozen in isobutanol cooled on dry ice and stored at -80°C until use. Coronal sections (20 µm) were cut from a region including the hippocampus and stored at -20°C until use. Selected sections were analyzed for presence of Aβ via immunofluorescence staining with mouse-anti-Aβ antibody 4G8 (1:500, Covance) followed by donkey-anti-mouse-AlexaFluor-594 (1:500, Invitrogen) as described before [13]. Presence of EmGFP was determined via its native 509 nm emission signal after excitation. Entire brain sections were imaged with a Leica DM 5500B fluorescence microscope and stitched together with proprietary software of Leica.

2.8. Quantification of amyloid plaque burden

The stitched images were analyzed in WCIF ImageJ v. 1.73c. All images underwent processed using the following pipeline to obtain an unbiased analysis of plaque load: The background was subtracted using a rolling ball setting (radius 50, no white background), the color was set to 8-bit grayscale, threshold was set to 30 minimum and 255 maximum. The build-in package “analyze particles” was used, set at “size 0.01-100, circularity 0.00-1.00”. Using these settings, plaques can be detected even in areas of higher background, such as in damaged tissues un-

derneath the location of the cranial window. Areas that maintain high background even after the application of the settings, for example areas where the tissue is folded back onto itself, are automatically ignored. Obtained values were analyzed in Microsoft Excel 2010.

3. RESULTS

3.1. In vitro analysis of pDG2-ss-VHH-EmGFP expression shows efficient secretion of functional VHH-EmGFP

To be of use, the VHH-EmGFP construct delivered by the AAV needs to be expressed inside the cells and subsequently secreted into the brain parenchyma while remaining fully functional both as antibody fragment and as fluorescent protein. All six VHH-EmGFP constructs, plus the MCS-EmGFP control construct, were able to transfect 50-70% of HEK293T cells, and produce a functional EmGFP product, as evident by the EmGFP signal in the cells at 72 h after transfection (Figure 5.2 A and B). No increased cell death was observed among the EmGFP construct transfected cells, compared to mock transfected cells.

The fluorescent signal of the secreted EmGFP was detected in the conditioned cell-free medium at 24 h after transfection (Figure 5.2 C). The EmGFP signal in the medium increased over time to 500% of the initial measurement at 72 hours after transfection. The control VHH, VHH-Htt7F4-EmGFP, showed the highest increase in signal over time. Non-transfected cells did not show any increase of background signal. This indicates that the observed increase in signal is not an artifact of changing physiological conditions, such as the changing of color of the standard medium additive phenol red, which as pH indicator changes color from red to yellow as the medium turns more acidic over time.

Finally, the functionality of VHH-pa2H-EmGFP was confirmed by efficient, single step staining of A β depositions in human brain cryosections obtained from AD/CAA patients (Figure 5.2 D). No non-specific or background staining was detected in brain material obtained from healthy age-matched controls devoid of A β depositions (Figure 5.2 F). Remarkably, neither purification nor concentration of the conditioned cell medium, nor signal amplification via secondary antibodies, was necessary to acquire the outstandingly bright staining of the parenchymal and vascular amyloid depositions. The control VHH, VHH-Htt7F4-EmGFP did not associate with any amyloid depositions, nor other vascular or parenchymal structures in the patient or the control material (Figure 5.2 E and G).

After production of the viral particles, their ability to transduce cells was confirmed in multiple cultured cell lines. Expression of the EmGFP constructs was detected by fluorescence micros-

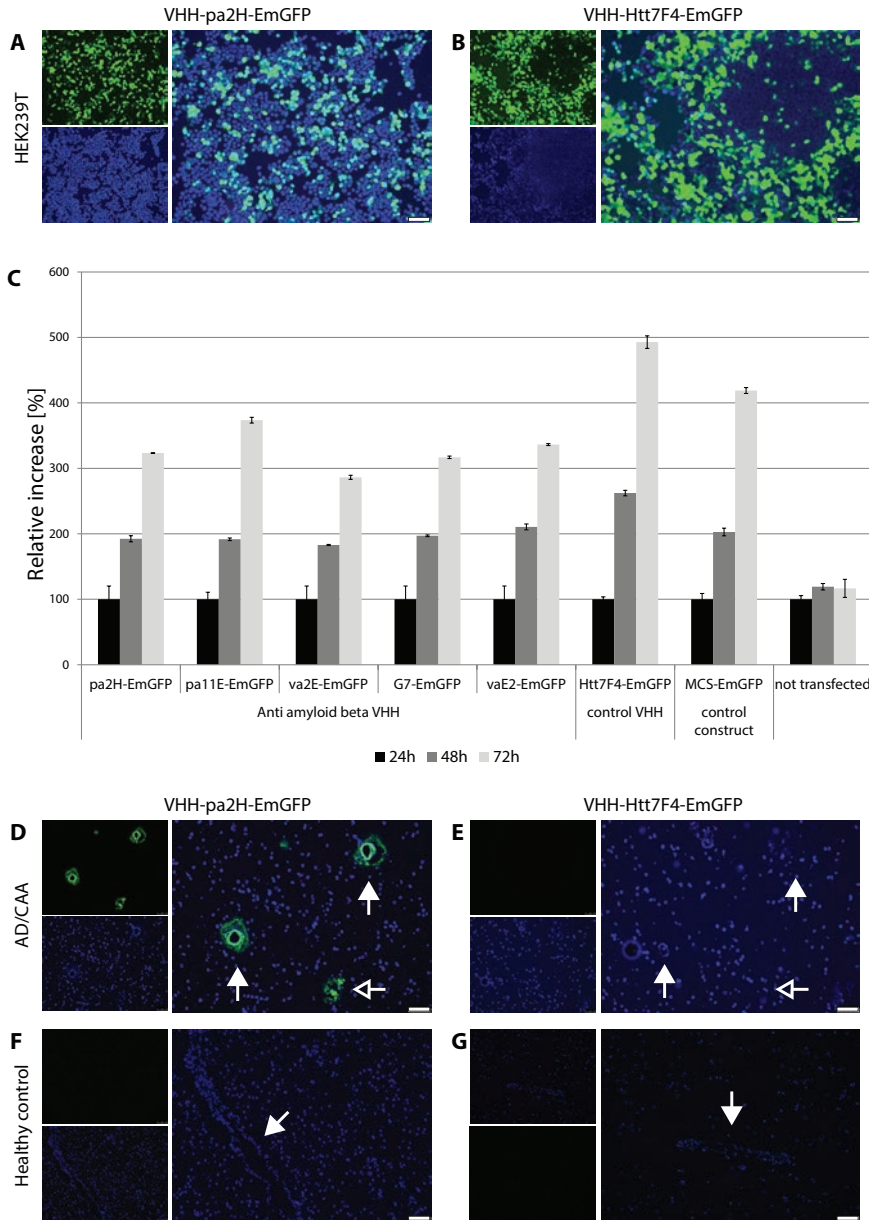


Figure 5.2. *In vitro* analysis of pDG2-ss-VHH-EmGFP. Transfection of the pDG2-ss-pa2H-EmGFP (A) and the pDG2-ss-Htt7F4-EmGFP (B) plasmids into HEK293T cells led to widespread expression of the EmGFP fusion constructs after 72 h. Other VHH-EmGFP constructs showed similar highly efficient EmGFP expression (Data not shown). Cell-free samples of the conditioned medium taken at 24, 48 and 72 h after transfection showed a steady increase of EmGFP signal for all constructs over time (C). Samples taken from HEK293T cells that were not transfected did not show any increase in background signal. Non-purified cell-free conditioned medium containing secreted VHH-pa2H-EmGFP was able to stain parenchymal and vascular amyloid depositions in fresh frozen brain cryosections from AD/CAA patients (D). No background staining was detected in cryosections from healthy, age-matched controls (F). Secreted VHH-Htt7F4-EmGFP did not stain amyloid plaques or any other non-specific structures in AD/CAA nor control cryosections (E + G). Closed arrows indicate cerebral vessels, open arrows indicate the location of parenchymal plaques. White bars represent 75 μ m.

copy approximately two weeks after application of the viral particles (Supplementary figure 5.6).

3.2. Long-term, pre-onset expression of VHH-pa2H-EmGFP may reduce plaque build-up

The AAV expressing ss-VHH-EmGFP was injected intracranially in one group of APP/PS1 mice directly after birth (P₀) and in another at 5 months of age (adult). Both groups were sacrificed at 12 months of age. The EmGFP signal was detected in both groups upon *ex vivo* examination, though more prominently in the adult injection group (Figure 5.3 A - D). In the adult injected group, the EmGFP signal colocalized with the A β depositions in serial coronal cranial sections (Figure 5.3 C - F). Both A β and EmGFP were detected at both parenchymal and vascular depositions. Interestingly, the amount of A β depositions detected was less in the P₀ injected group compared to the adult injected group, though the with-in group variance is high (Figure 5.3 G). No EmGFP signal was detected in the wildtype littermates that were sacrificed at 3 weeks of age, indicating an *in vivo* interval of at least 3 weeks between transduction of the virus and expression of the EmGFP tagged VHH (data not shown).

3.3. Adult AAV injections lead to *in vivo* expression of functionally secreted VHH-GFP fusion proteins that can be followed by intravital multiphoton microscopy

The mice that received the cranial window after injection of AAVs showed bright expression of the EmGFP signal, traceable over time, through the window in the living mice (Figure 5.4 and Figure 5.5). This was most notably the case for the mice expressing the VHH-pa2H-EmGFP construct, where the signal colocalized with the vascular and parenchymal amyloid depositions (Figure 5.4 A and B). This colocalization did not occur in the mice injected with the AAV expressing the VHH-Htt7F4 control construct (Figure 5.4 C and D). Interestingly, in a limited number of animals of the ss-MCS-EmGFP group, the EmGFP signal was detected in cells that may resemble astrocytes or microglia in shape (Figure 5.4 F). The association with these cell structures did not seem to be dependent on the local presence or absence of A β at the particular area. Also, this observation was not seen in all animals in the group, nor in any animal in any of the other groups.

A separate group of animals was intracranially injected with the viral constructs, or the control constructs, without the i.p. coinjection of Methoxy-X₀₄ (Figure 5.4 B, D, F and H). Methoxy-X₀₄ crosses the BBB and binds to A β depositions, and has a rather wide emission spectrum, potentially bleeding into the green channel, which may cause doubt whether the observed signal originates from the Methoxy-X₀₄ dye or from the VHH-EmGFP fusion protein. By omitting the Methoxy-X₀₄ it is clear that virally expressed VHH-pa2H-EmGFP binds the parenchymal and vascular A β depositions (Figure 5.4 B), while the other constructs are expressed, but do not

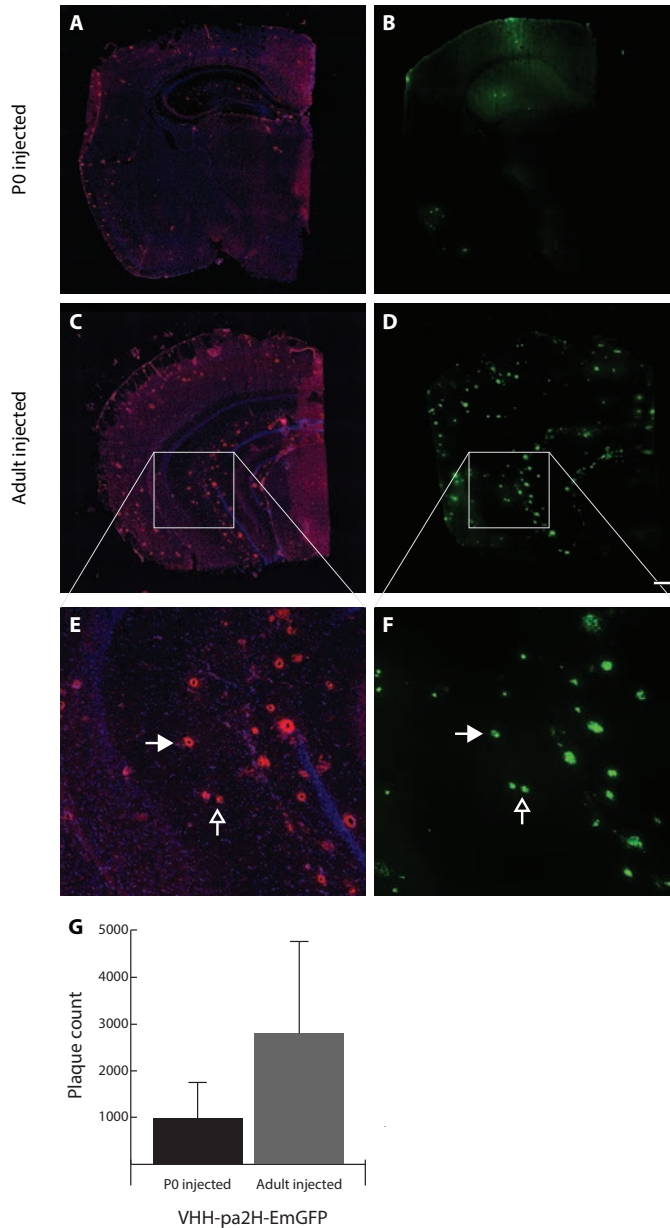


Figure 5.3. Mice injected directly after birth with the AAV expressing VHH-pa2H-EmGFP showed reduced A β load compared to the mice that were injected at an age of 5 months. Shown are serial coronal sections of a region including the hippocampus of a total of two 12 month old APP/PS1 mice injected either at P0 (A + B) or at 5 months (C + D). E and F show the details in the indicated areas of C and D. In A, C and E A β is shown in red, stained using the conventional antibody 4G8, as well as a nuclear staining using DAPI in blue. In B, D and F the native fluorescent signal of the VHH-pa2H-EmGFP is shown in green. In the details depicted in E and F the colocalization between the A β aggregates in red and the VHH-pa2H-EmGFP in green in the sequential section is clearly evident. Quantification of the amyloid burden measured in the entire slices (G) confirms the reduced A β load in the P0 group, however shows a great individual variance in signal within the groups. Plaque count indicates the total number of individual circular staining in the red channel, after subtraction of the background as described in the Materials and Methods section. Closed arrows indicate cerebral vessels, open arrows indicate the location of parenchymal plaques.

bind A β (Figure 5.4 D and F). No signal was detected in the green channel in mice injected with PBS as control (Figure 5.4 G and H).

By imaging the exact same location in the same mouse multiple times over a period of 4 months, it is possible to follow the effect of the VHH-EmGFP constructs on individual plaques (Figure 5.5). Omission of Methoxy-X04 (Figure 5.5 B, D, F and H) makes it more difficult to identify the same location upon subsequent imaging sessions, but it is still feasible to identify the same area based on the vascular structures. Unfortunately, unlike the remarkable result upon topical application of VHH-pa2H (Supplementary figure 5.3), during the longitudinal imaging sessions no significant differences were detected in the A β burden in the area under the cranial window within the individual mice injected with the AAV2/1 expressing VHH-pa2H-EmGFP. The shown images are multiple intensity projections. As a result, the seemingly slightly different position of the plaques green, in relation to the blood vessels in red, is an effect of the way the images for the multiple intensity projections are composed.

Of the 24 mice that received a cranial window, 4 died after placement of the window, before multiphoton microscopy could be performed. The remaining animals all survived until the planned endpoint at 17 weeks after placement of the window. Of the mice that died prematurely, two had received an injection with AAV2/1 VHH-Htt7F4-EmGFP, while the other two were injected with PBS.

3.4. Long-term, post-onset expression of VHH-pa2H-EmGFP throughout the hippocampus does not change amyloid burden

The brains of the mice which received a cranial window after injection with the various AAV constructs were perfused with PBS, removed and cryo-preserved. Subsequently, coronal sections were cut including the location of the cranial window and the hippocampus. A schematic anatomical map of a coronal section indicating the hippocampal and cortical subregions that are mentioned below, is supplied in Figure 5.6. The sections were analyzed for presence of A β using the conventional anti-A β antibody 4G8 and as well as for presence of EmGFP signal (Figure 5.7 and Figure 5.8). EmGFP signal was detected in all brains of mice that were injected with AAV expressing EmGFP constructs, but, as expected, not in the brains of mice that were injected with PBS. VHH-associated EmGFP expression was confined to the Cornu Ammonis regions 1 and 2 (CA1 and CA2) of the murine hippocampus, and was not found in the CA3 region, CA4 region, or the dentate gyrus. Expression of VHH-pa2H-EmGFP and especially VHH-Htt7F4-EmGFP was found predominantly in the stratum pyramidale of the CA2 (i.e. the dense band containing the cell bodies of the pyramidal neurons of the hippocampus, Figure 5.7 A and B; Figure 5.6 for anatomical reference). In contrast, expression of MCS-EmGFP, the EmGFP construct without a VHH, was found throughout the strata oriens, pyramidale,

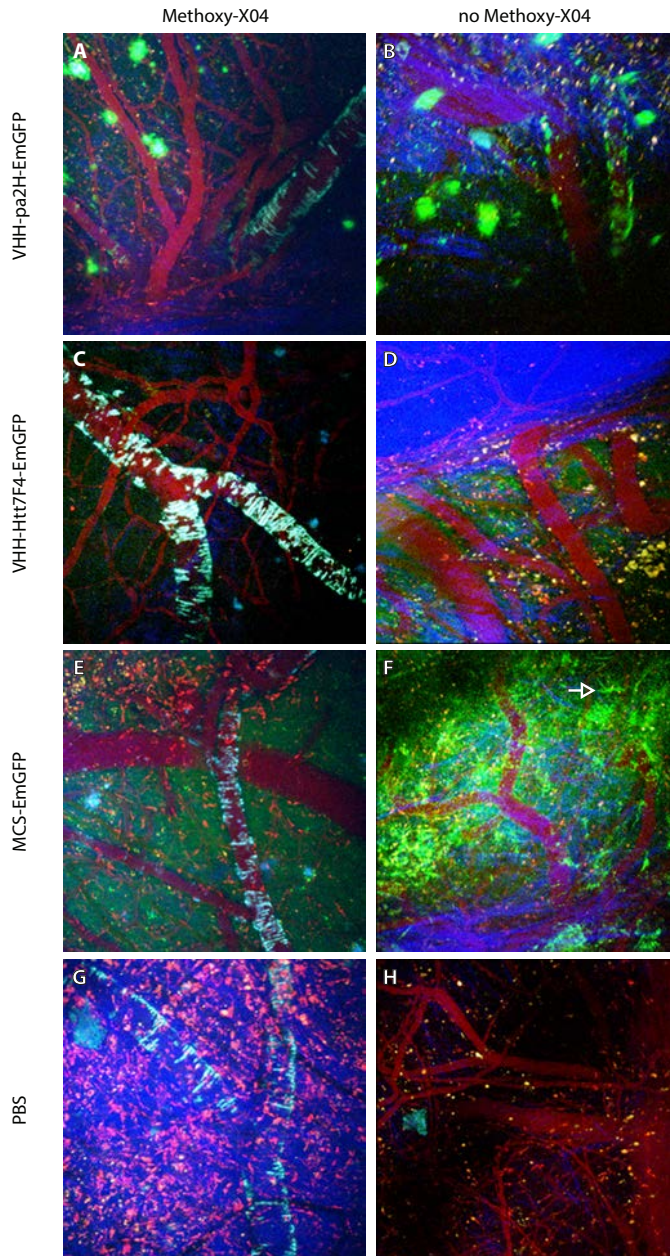


Figure 5.4. Shown are multiple intensity projection images of z-stacks spanning up to 200 μm into the cortex of a total of eight APP/PS1 mice through cranial windows. The images were taken 3-4 months after cranial injection with the indicated AAVs expressing (VHH)-EmGFP fusion proteins (A – F) or with PBS as sham injected control (G and H). Furthermore, the mice were either intraperitoneally injected with the dye Methoxy-X04 (left column) or not injected with the dye at all (right column). Methoxy-X04 readily crosses the blood brain barrier and binds A β depositions, and emits a wide spectrum, but predominantly blue, fluorescent signal. Only in the mice injected with the AAV expressing VHH-pa2H-EmGFP a green signal is found around the vascular walls and in the parenchymal plaques (A and B). Images from the mice from the other groups show the Methoxy-X04 signal, but no EmGFP signal is found on the characteristic A β depositions (C – H). The vasculature is visualized in red by intravenous injection of Dextran-Texas red shortly before imaging. Open arrow in F indicates an example of EmGFP signal that resembles a glial-like structure.

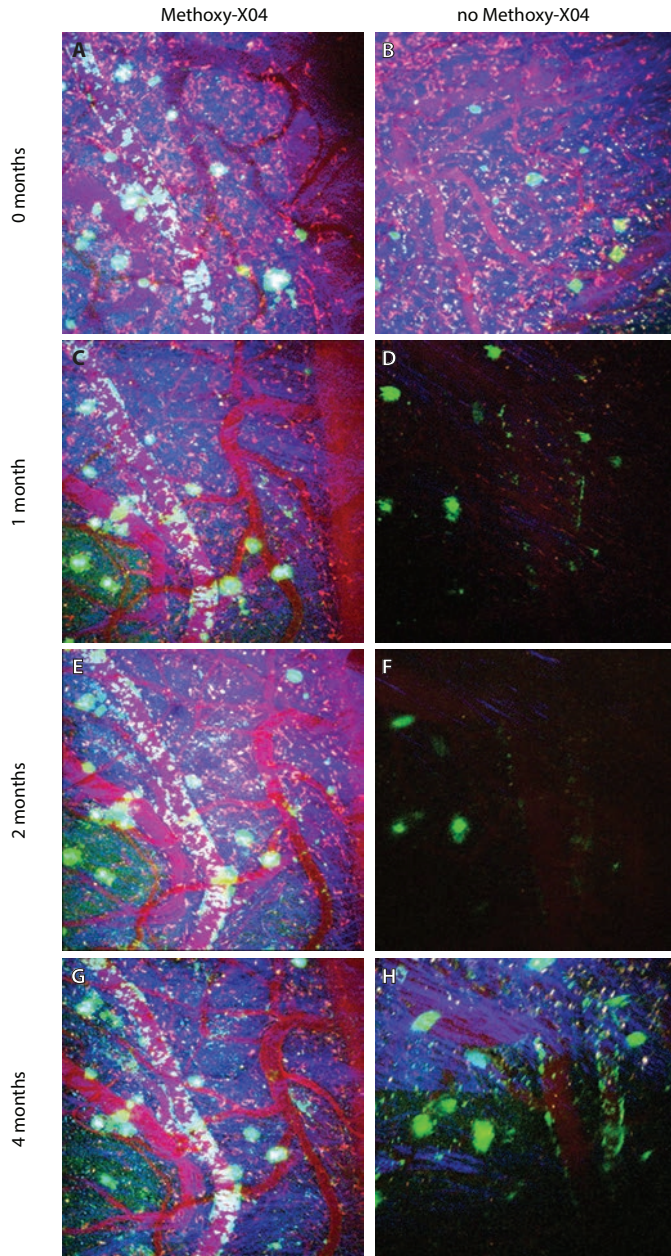


Figure 5.5. Shown are multiple intensity projection images of z-stacks spanning up to 200 μm into the cortex of a total of two APP/PS1 mice through cranial windows. The images were taken at regular intervals spanning up to four months after cranial injection of the AAV expressing VHH-pa2H-EmGFP. The mice were either intraperitoneally injected with the dye Methoxy-X04 (left column) or not injected with the dye at all (right column). Methoxy-X04 readily crosses the blood brain barrier and binds A β depositions, and emits a wide spectrum, but predominantly blue, fluorescent signal. The vasculature is visualized in red by intravenous injection of Dextran-Texas red shortly before imaging. Using the vasculature and visible A β depositions, longitudinal images were taken at exactly the same location, allowing for close examination of the effect of the VHH. Unfortunately, no abrupt disappearance of the parenchymal plaques was observed.

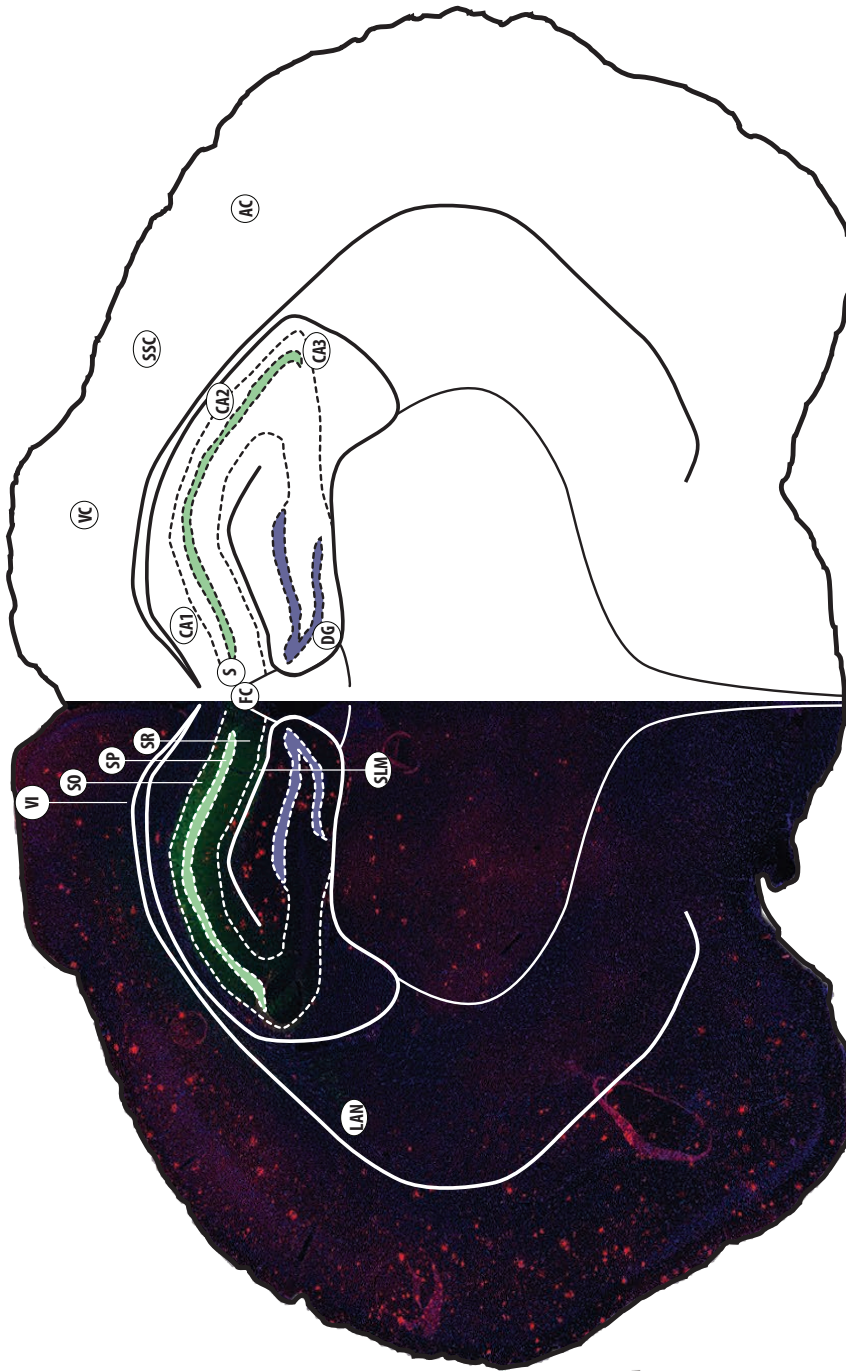


Figure 5.6. Schematic representation of the murine brain overlaid on a coronal section of an APP^{swE}/PS1^{dE9} double transgenic mouse injected with AAV-MCS-EmGFP (visible in green), stained for Aβ (red) and nuclei (blue). Common brain regions are indicated with abbreviations in circles. On the brain image (left) hemisphere: LAN: lateral amygdaloid nucleus; VI: VI layer of cortex; SO: stratum oriens; SP: stratum pyramidale; SR: stratum radiale; SLM: stratum lacunosum moleculare. On the schematic (right) hemisphere: FC: fascia cinereturum; S: subiculum; CA1-3: cornu ammonis 1-3; DG: dentate gyrus; VC: visual cortex; SSC: somatosensory cortex; AC: auditory cortex.

radiale, and lacunosum moleculare of CA1 and CA2, as well as the subiculum and the fasciola cinereum (Figure 5.7 C). Weak EmGFP signal was detected in the CA3 region of the hippocampus, the VI region of the visual, somatosensory, and auditory cortexes, and lateral amygdaloid nucleus. In sections without the conventional anti-A β staining, plaque associated EmGFP signal is still visible in the brains of the mice injected with the AAV2/1 expressing VHH-pa2H-EmGFP, but not in the other experimental groups (Figure 5.8).

Unfortunately, analysis of the amyloid burden in the entire coronal sections did not show the expected reduction of A β plaques in the mice injected with AAV2/1 expressing VHH-pa2H-EmGFP compared to the mice injected with other constructs (Figure 5.9).

4. DISCUSSION

In this study we tested the hypothesis that prolonged treatment with the antibody fragment VHH-pa2H can significantly reduce the A β burden in the APP/PS1 mouse model for AD. In order to do so, we fused Emerald GFP to the VHH and showed that it can be produced in mammalian HEK293 cells and subsequently secreted from these cells. Furthermore, we showed that both the VHH and the EmGFP are functional after secretion from the cells. Finally we prove that it is possible to use AAV2/1 to transduce the construct into the brain of APP/PS1 mice, both new-born and adult, and follow the secreted fusion protein *in vivo* through a cranial window over a period of at least 4 months.

Various VHH-EmGFP constructs were expressed in HEK293 cells, which indeed showed a very strong EmGFP signal upon excitation (Figure 5.2 A-B). The EmGFP was chosen over different versions of GFP (e.g. eGFP) for its reported superior folding and brightness [22,32,33]. HEK293T transfection rates were 50-70% in all conditions and no increased cell death was observed, indicating efficient, yet non-cytotoxic, expression of the protein. The EmGFP signal seemed to be present throughout the entire cell, suggesting that the fusion protein was not entrapped in any lysosomal degradation pathway. Furthermore, the EmGFP signal was remarkably strong in most, but not all cells, leading to a very narrow dynamic range for imaging; i.e. the signal was easily overexposed in many cells, even at very short exposure times and minimal gain. The use of a confocal microscopy system might have been advisable in this case, should one want to determine the exact pattern of expression of EmGFP fusion proteins within individual cells.

The *in vitro* observations justify the use of EmGFP for *in vivo* applications, which requires a high fluorescence yield. EmGFP has, despite its benefits of superior folding and brightness compared to other GFP variants, the disadvantage of more rapid photo bleaching [20]. However, rapid photo bleaching was considered to be of minor importance in view of the eventual

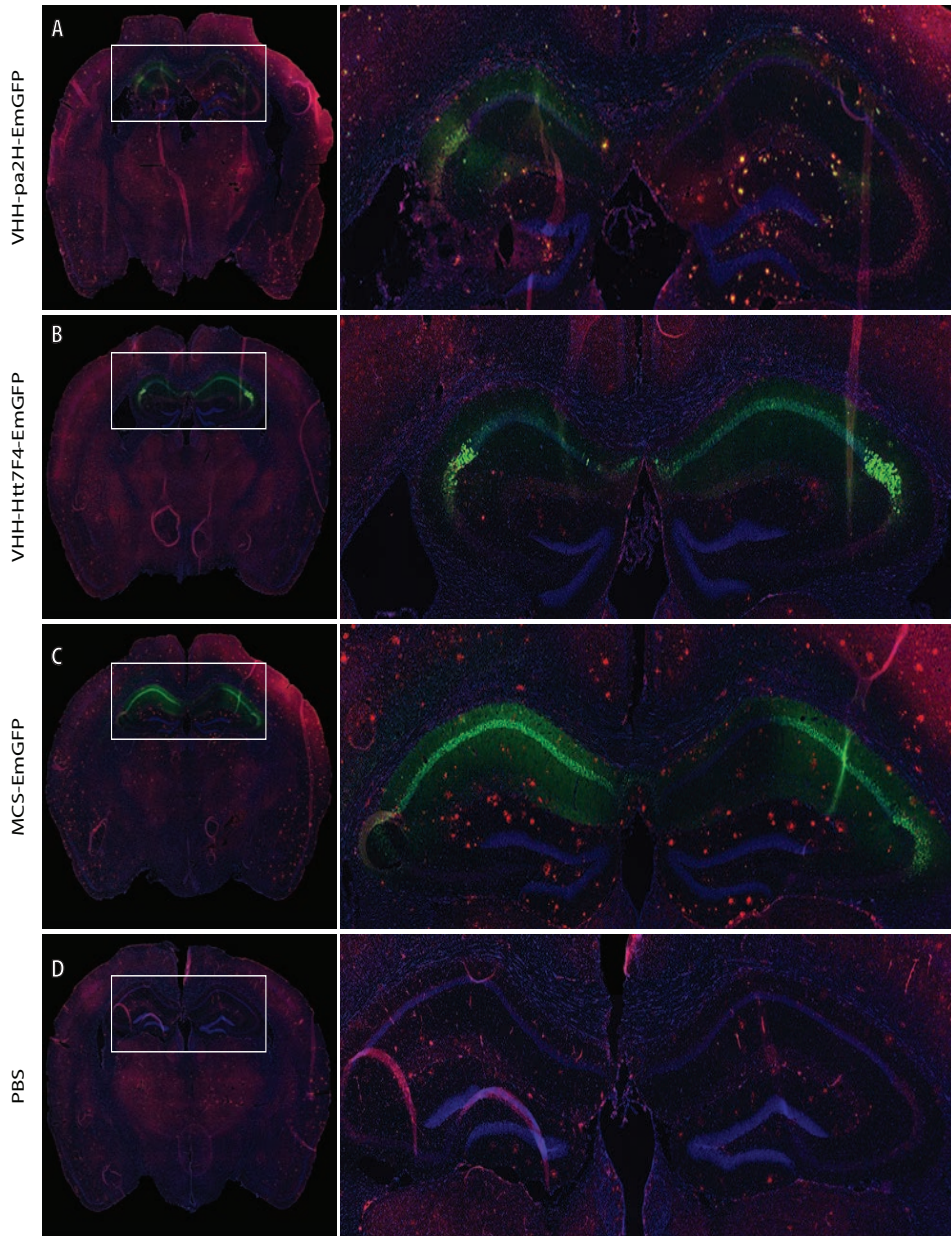


Figure 5.7. Shown are coronal sections of a region including the hippocampus, close to the injection site, under the location of the cranial window, in APP/PS1 mice. Wide-spread expression of the EmGFP constructs is found in all mice injected with the AAV constructs (A-C). The mice that were injected with AAV2/1 expressing VHH-pa2H-EmGFP show colocalization of EmGFP signal (green) with amyloid plaques stained using conventional 4G8 anti-A β antibodies (red) (A). Furthermore, the colocalization is found well beyond the sites of apparent VHH-EmGFP expression. The colocalization with A β is not seen in the mice injected with constructs expressing VHH-Htt7F4-EmGFP (B), nor non-VHH controls (C and D). Nuclei are stained with DAPI (blue).

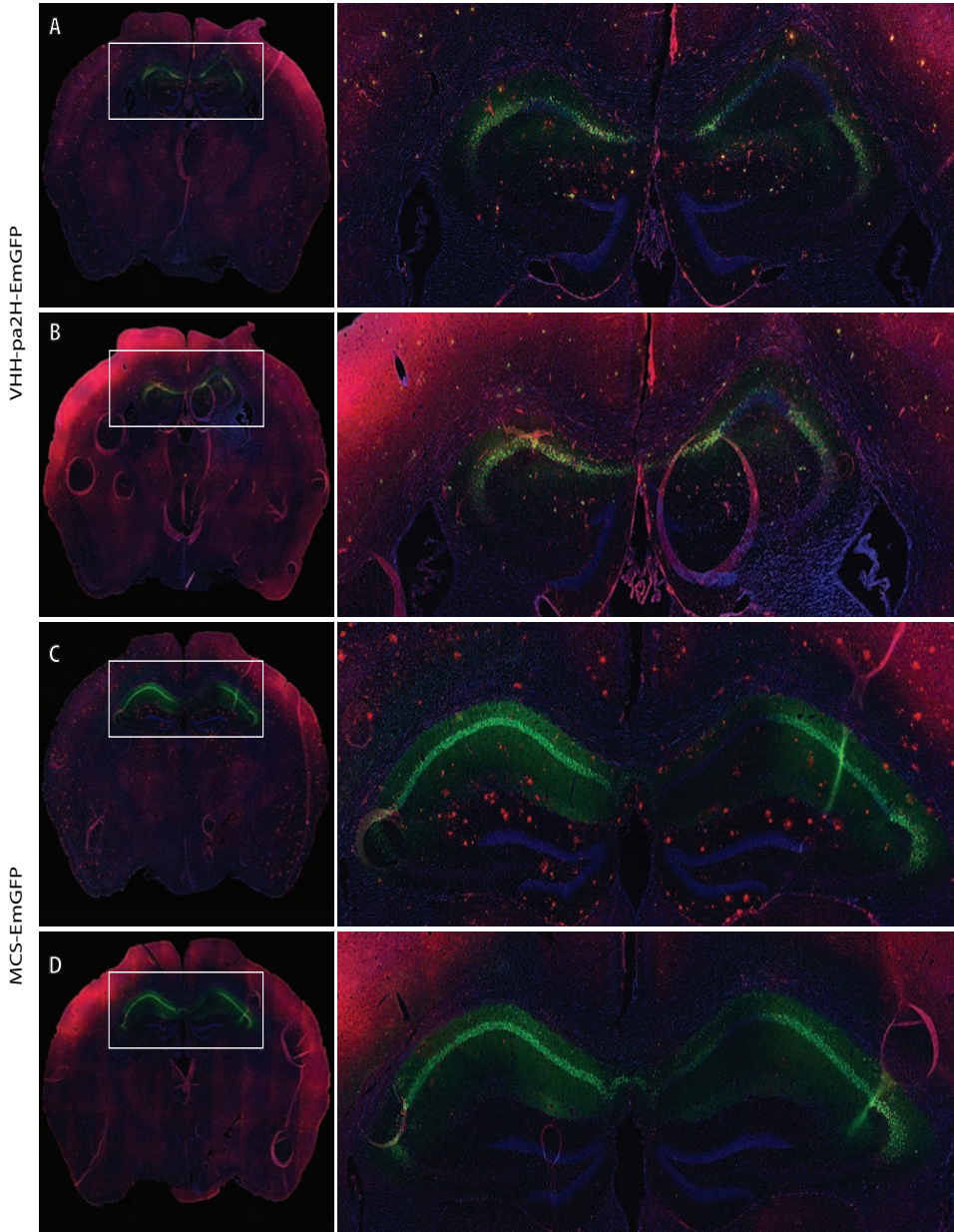


Figure 5.8. Shown are coronal sections of a region including the hippocampus, close to the injection site, under the location of the cranial window, in APP/PS1 mice. (A) APP/PS1 mice injected with AAV2/1 expressing VHH-pa2H-EmGFP show colocalization of EmGFP signal (green) with amyloid plaques stained using conventional 4G8 anti-A β antibodies (red). (B) A serial coronal section of the same mouse brain, not stained with 4G8, still shows the A β depositions in green as a result from the association of VHH-pa2H-EmGFP with A β . No association with A β plaques was detected in mice injected with AAV2/1 expressing the control construct MCS-EmGFP, both with and without the conventional 4G8 staining (C and D). Nuclei are stained with DAPI (blue).

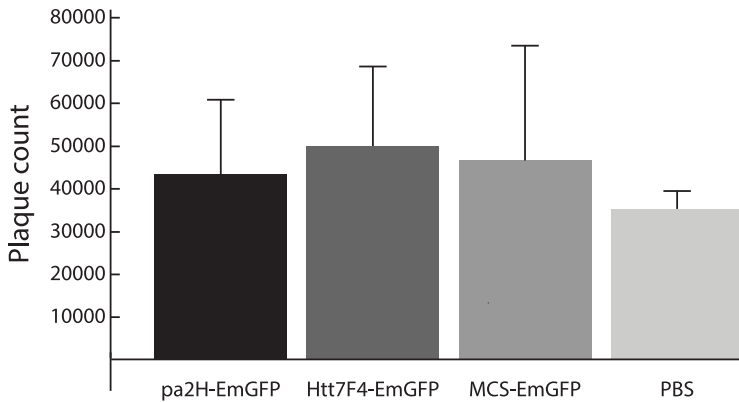


Figure 5.9. Quantification of the amyloid plaque load in the brains of the mice injected with the various VHH showed no significant difference between the groups.

application of the VHH-EmGFP construct. The fusion protein would, after all, be continuously produced in the brain and exposed to relatively short excitation times through intravital multiphoton microscopy. Furthermore, the use of multiphoton microscopy, by design, eliminates off-target photo-bleaching and photo-damage outside the region of excitation [34,35].

Cellular secretion of the VHH-EmGFP constructs was detected via a straightforward fluorescence detection assay, for which unprocessed, cell-free conditioned medium was sampled at various time-points after transfection (Figure 5.2 C). The impressive increase in fluorescence signal over 3 days, up to 500% from the first measurement, was obtained despite the presence of Fetal Bovine Serum, Phenol Red and other medium additives. The complete lack of change in fluorescence signal in the control sample, i.e. cell-free conditioned medium from non-transfected HEK293 cells, indicates that the incremental fluorescent signal originates only from the secreted fusion protein.

The most definitive proof that the fusion protein is expressed and secreted as a completely functional VHH-EmGFP construct, comes from the highly efficient, highly specific, single step staining of A β depositions in human AD cryosections by VHH-pa2H-EmGFP from untreated, cell-free conditioned medium (Figure 5.2 D). The control construct, VHH-Htt7F4-EmGFP, does not associate with any A β depositions, which indicates that the A β association is solely the result of a fully functional VHH-pa2H and not of non-specific aggregation of any VHH or EmGFP to putatively sticky A β (Figure 5.2 E). Furthermore, the absence of EmGFP signal in all controls, indicates that neither the VHH nor the EmGFP itself associate with any other vascular or parenchymal structure and that the amyloid depositions themselves do not pose an issue of auto fluorescence in these sections.

The observation that the completely untreated cell-free medium of HEK293 cells expressing

VHH-pa2H-EmGFP can be used for highly efficient and single step staining of A β depositions in human cryosections opens up innovative pathways for A β detection. The concept can be routinely exploited to circumvent costly and time-consuming protocols of A β detection using conventional antibodies in combination with secondary compounds, such as Covance's 4G8 in combination with Life Technology's anti-mouse Alexa-488/594. Expression and secretion from transiently transfected HEK293 cells seem to suffice for efficient staining protocols. Such constructs can also be stably expressed in CHO cells [16,36], which can be maintained in an FBS-free environment under suspension culture conditions, allowing significant upscaling of the production and purification of functional VHH-EmGFP, or similar constructs [36,37].

Given the fact that the VHH-EmGFP constructs can be functionally expressed in, and be secreted from, mammalian cells, longitudinal experiments were planned, directed at the question whether VHH-pa2H could have a therapeutic effect *in vivo*. Expression of VHH-pa2H-EmGFP in APP/PS1 mice starting at age P₀, showed reduced plaque load compared to the APP/PS1 mice injected at adulthood (Figure 5.3). The reduction in plaque load detected in the P₀ mice vs the adult mice, may be due to the earlier exposure to the VHH (P₀ vs 5 months of age), or due to the longer exposure to the VHH (theoretically 12 vs 7 months) or (unrelated to the VHH exposure) due to individual variation within the mice. Start of expression of the VHH construct after delivery by the AAV takes at least 3 weeks, as is evident by the lack of EmGFP signal in the brains of the P₀ injected wildtype mice that were sacrificed at 3 weeks of age. Once expressed, the EmGFP constructs are present in the neuronal cells up until at least 4 months after transduction (Figure 5.4-Figure 5.8), however, it has not been tested whether the AAV delivered VHH-pa2H-EmGFP was expressed continuously throughout the 12 and 7 months in the P₀ and adult injected mice, respectively. Therefore, it cannot be stated unambiguously that the prolonged exposure to the VHH is the cause of the reduced A β load in the P₀ injected mice compared to the adult injected mice, but the obtained results are encouraging.

Given the difference in plaque load between the P₀ and adult injected mice, it is interesting to speculate that VHH-pa2H-EmGFP can prevent, but not revert, amyloid aggregation. It must be noted however that it is generally accepted that the APP/PS1 mouse strain develops amyloid plaques at around 6 months of age, i.e. shortly after, rather than before, the adult injections [38,39]. It is, nonetheless, possible, and likely, that at the adult injection time, an age of 5 months, the first seeds for the aggregates have already been planted. After all, A β levels in plasma in the double transgenic mice start to rise as early as at 3 months of age [40], and by 6 months of age the first signs of aberrant behavior are visible in certain, but not all, memory tests, e.g. contextual memory [41,42]. This may suggest that the VHH is able to prevent aggregation only if A β is exposed to the VHH well before the first aggregation events occur. This, in turn, would mean that as a possible therapeutic the VHH needs to be administered well before

onset of even the pre-clinical hallmarks of AD development. The timely decision to supply the VHH as a therapeutic to one who is by all means of standard diagnosis not even a patient, may prove difficult, if not impossible, in all but the select group of carriers of dominantly inherited genetic APP mutations [43].

The benefit of the combination of secreted VHH and attached EmGFP stably expressed from neuronal cells, is most evident in the studies involving the placement of a cranial window. Individual plaques can be detected and monitored in living mice, provided that the exact location can be traced each time the animal is placed under the multiphoton microscope. We were able to see expression of the constructs and could identify individual plaques due to direct colocalization of VHH-pa2H-EmGFP with A β (Figure 5.4). Omitting the amyloid dye Methoxy-Xo4 proved that the observed signal is indeed originating from the EmGFP, rather than from the broad emission profile of the dye. However, individual parenchymal plaques did not disappear or become smaller over time as a result of VHH-pa2H-EmGFP presence (Figure 5.5), contrary to what was seen in previous preliminary experiments (Supplementary figure 5.3). Also *ex vivo* quantification of the amyloid burden in the brains of the treated animals showed no differences among the various treatments (Figure 5.9), although all constructs were expressed in the brain (Figure 5.7). VHH-pa2H-EmGFP was found on parenchymal plaques well beyond the hippocampus, which is the location where the AAV constructs were injected and where expression was predominantly found (Figure 5.7 and Figure 5.8). AAV2/1 was chosen for its expected decent wide-spread transduction efficiency, especially if injected at Po [44,45], as well as ability to transduce many different cell-types, including neurons and microglia [46]. However, in this study, AAV2/1 transduced the neuronal cells at and around the injection site (the hippocampus), but did not seem to spread much further beyond that area. Variations in AAV capsid and ITR serotypes may lead to different results in expression, both in terms of spread over the brain and transduction across multiple neuronal cell types [47,48].

The expressed and secreted VHH-EmGFP travel well beyond the area of transduction and spread readily over the cortex and other areas. This is important, and perhaps even more important than the efficiency of transduction for VHH that need to act outside the host cells, as in this case where VHH-pa2H-EmGFP targets extracellular A β . Efficient distribution of the secreted VHH allows for injection of the viral particles at locations that may be spatially removed from the expected site of action, yet in a region of the brain that is perhaps more accessible or less vulnerable to physical injection damage [49,50]. The mode of transport, e.g. diffusion, flow of interstitial fluids, has not been investigated in this study.

It is interesting to note that the AAV expressing the non-VHH construct MCS-EmGFP has a much broader expression profile within the hippocampus. MCS-EmGFP is significantly smaller than

the VHH-fused counterparts (Figure 5.1). While VHH-pa2H-EmGFP and VHH-Htt7F4-EmGFP are predominantly found in the stratum pyramidale of the hippocampus, MCS-EmGFP is found throughout strata of the CA1 and CA2 regions, and even, faintly, in the VI layer of the cortex and the lateral amygdaloid nucleus. Whether the increased area of expression is a result of better transduction efficiency of the AAV due to a smaller package load in general, or due to the lack of the VHH specifically is unknown. It is possible that the constructs expressing the VHHs are more easily targeted by the immune system of the host, even though VHH are generally accepted to be non-immunogenic [51,52].

Whether or not the secretion signal was, as expected, removed from the VHH-EmGFP during the secretion process, at which efficiency this was done and to what extent the remaining presence of the secretion signal may have had an influence on the binding of VHH-pa2H to amyloid plaques has not been determined. The fact that the virally produced VHH did not show any obvious difference in recognition of amyloid beta on cryoimmunostainings compared to the bacterially produced VHH, suggests that binding had not been affected and no further investigation in this matter has been deemed necessary for the purpose of this study. The small size of the secretion signal (18 amino acids, less than 2 kDa) and the location (N-terminal to the VHH, away from the CDR3 loop) provides no platform to suspect otherwise. However, the same cannot be said for the EmGFP, which at 239 amino acids and with a molecular weight of 26.9 kDa is in fact twice bigger than the VHH itself. Association to amyloid depositions in itself is no longer sufficient to assume insignificant-to-none influence on the physiological effects of VHH binding. Now that it has been established that the combination of the AAV2/1 and the lysozyme secretion signal is a successful method to deliver functional VHH to the brain parenchyma, it is of interest to perform longitudinal VHH delivery experiments with constructs devoid of the EmGFP fragment. This allows to control for the possible effects of the EmGFP construct, albeit at the expense of the possibility to monitor the delivery of the VHH *in vivo* in real time.

The observed lack of VHH-pa2H-EmGFP to prevent or reduce amyloid plaque formation over a longitudinal study period is rather disappointing. It would be of great interest however, to analyze the long term *in vivo* effect of other amyloid-targeting VHH. The modular build-up of the described procedure in this paper, allows one to create an AAV-expressing VHH with or without the secretion signal and with or without the EmGFP visual tracer. The concept of EmGFP-tagged VHH delivered as AAV constructs to the brain can be widely adapted to a variety of neurological disorders and can easily be used as a screening tool to analyze, in real-time, the *in vivo* efficacy of disease modifying antibody fragments or similar treatments. Furthermore, the concept of efficient, long term expression of VHH in the brain, delivered by a single viral injection, can easily be adapted to similar VHH targeted against other cerebral targets, either intra- or extra-cellular.

5. CONCLUSION

The efficient *in vivo* transduction, expression, and secretion of functional VHH-pa2H-EmGFP proofs that VHH can readily be employed in future gene therapy applications. While VHH-pa2H-EmGFP did not proof to completely reduce pre-existing amyloid burden in this study, it did show potential in long-term preventive application in the AD model of APP/PS1 double transgenic mice.

DISCLOSURE

No potential conflicts of interest are to be disclosed.

ACKNOWLEDGMENTS

The authors would like to thank dr. M.A.F.V. Gonçalves and dr. R.C. Hoeben (MCB, LUMC) for the donation of the pDG2 vector, E.C. Whitelaw and K. Jansen-West (Neuroscience, Mayo Clinic) for their support in the production of the rAAV particles, A. Van der Laan and J. Wiegant (MCB, LUMC) for their support in the use of the intravital multiphoton microscope, and dr. R.J.A. Nabuurs (RADI, LUMC) and dr. W.E. Klunk (Uni. of Pittsburgh) for the donation of the Methoxy-X04.

REFERENCES

1. Verheesen, P., de Kluijver, A., van Koningsbruggen, S., de Brij, M., de Haard, H. J., van Ommen, G. J. B., van der Maarel, S. M. & Verrips, C. T. Prevention of oculopharyngeal muscular dystrophy-associated aggregation of nuclear poly(A)-binding protein with a single-domain intracellular antibody. *Hum. Mol. Genet.* 15(11):1105–111 (2006).
2. Chartier, A., Raz, V., Sterrenburg, E., Verrips, C. T., van der Maarel, S. M. & Simonelig, M. Prevention of oculopharyngeal muscular dystrophy by muscular expression of Llama single-chain intrabodies *in vivo*. *Hum. Mol. Genet.* 18(10):1849–59 (2009).
3. Dumoulin, M., Last, A. M., Desmyter, A., Decanniere, K., Canet, D., Larsson, G., Spencer, A., Archer, D. B., Sasse, J., Muyldermans, S., et al. A camelid antibody fragment inhibits the formation of amyloid fibrils by human lysozyme. *Nature* 424(6950):783–788 (2003).
4. Jones, D. R., Taylor, W. A., Bate, C., David, M. & Tayebi, M. A camelid anti-PrP antibody abrogates PrP replication in prion-permissive neuroblastoma cell lines. *PLoS One* 5(3):e9804 (2010).
5. Tayebi, M., Jones, D. R., Taylor, W. A., Stileman, B. F., Chapman, C., Zhao, D. & David, M. PrP(Sc)-specific antibodies with the ability to immunodetect prion oligomers. *PLoS One* 6(5):e19998 (2011).
6. Dorresteyn, B., Rotman, M., Faber, D., Schraivesande, R., Suidgeest, E., van der Weerd, L., van der Maarel, S. M., Verrips, C. T. & El Khattabi, M. Camelid heavy chain only antibody fragment domain against β -site of amyloid precursor protein cleaving enzyme 1 inhibits β -secretase activity *in vitro* and *in vivo*. *FEBS J.* 282(18):3618–3631 (2015).
7. Li, T., Bourgeois, J.-P., Celli, S., Glacial, F., Le Sourd, A.-M., Mecheri, S., Weksler, B., Romero, I., Couraud, P.-O., Rougeon, F., et al. Cell-penetrating anti-GFAP VHH and corresponding fluorescent fusion protein VHH-GFP spontaneously cross the blood-brain barrier and specifically recognize astrocytes: application to brain imaging. *FASEB J.* 26(10):3969–79 (2012).
8. Rotman, M., Welling, M. M., Bunschoten, A., de Backer, M. E., Rip, J., Nabuurs, R. J. A., Gaillard, P. J., van Buchem, M., van der Maarel, S. M. & van der Weerd, L. Enhanced liposomal brain delivery of an anti-amyloid VHH-2H heavy chain antibody fragment in a mouse model for Alzheimer's disease. *J. Control. Release* 203:40–50 (2015).
9. Lafaye, P., Achour, I., England, P., Duyckaerts, C. & Rougeon, F. Single-domain antibodies recognize selectively small oligomeric forms of amyloid beta, prevent Abeta-induced neurotoxicity and inhibit fibril formation. *Mol. Immunol.* 46(4):695–704 (2009).
10. Duyckaerts, C., Delatour, B. & Potier, M.-C. Classification and basic pathology of Alzheimer disease. *Acta Neuropathol.* 118(1):5–36 (2009).
11. Rutgers, K. S., van Remoortere, A., van Buchem, M. A., Verrips, C. T., Greenberg, S. M., Bacskai, B. J., Frosch, M. P., van Duinen, S. G., Maat-Schieman, M. L. & Van der Maarel, S. M. Differential recognition of vascular and parenchymal beta amyloid deposition. *Neurobiol. Aging* 32(10):1774–1783 (2009).
12. Nabuurs, R. J. A., Rutgers, K. S., Welling, M. M., Metaxas, A., de Backer, M. E., Rotman, M., Bacskai, B. J., van Buchem, M. A., van der Maarel, S. M. & van der Weerd, L. *In vivo* detection of amyloid- β deposits using heavy chain antibody fragments in a transgenic mouse model for Alzheimer's disease. *PLoS One* 7(6):e38284 (2012).
13. Rotman, M., Welling, M. M., van den Boogaard, M. L., Moursel, L. G., van der Graaf, L. M., van Buchem, M. A., van der Maarel, S. M. & van der Weerd, L. Fusion of hIgG1-Fc to mIn-anti-amyloid single domain antibody fragment VHH-p2H prolongs blood residential time in APP/PS1 mice but does not increase brain uptake. *Nucl. Med. Biol.* 42(8):695–702 (2015).
14. Levites, Y., Jansen, K., Smithson, L. a., Dakin, R., Holloway, V. M., Das, P. & Golde, T. E. Intracranial adeno-associated virus-mediated delivery of anti-pan amyloid beta, amyloid beta40, and amyloid beta42 single-chain variable fragments attenuates plaque pathology in amyloid precursor protein mice. *J. Neurosci.* 26(46):11923–8 (2006).

15. Bazl, M. R., Rasaei, M. J., Foruzandeh, M., Rahimpour, A., Kiani, J., Rahbarizadeh, F., Alirezapour, B. & Mohammadi, M. Production of chimeric recombinant single domain antibody-green fluorescent fusion protein in Chinese hamster ovary cells. *Hybridoma (Larchmt)*. 26(1):1–9 (2007).
16. Robbins, E. M., Betensky, R. A., Domnitz, S. B., Purcell, S. M., Garcia-Alloza, M., Greenberg, C., Rebeck, G. W., Hyman, B. T., Greenberg, S. M., Frosch, M. P., et al. Kinetics of cerebral amyloid angiopathy progression in a transgenic mouse model of Alzheimer disease. *J. Neurosci*. 26(2):365–71 (2006).
17. Reiserer, R. S., Harrison, F. E., Syverud, D. C. & McDonald, M. P. Impaired spatial learning in the APPSwe + PSEN1DeltaE9 bigenic mouse model of Alzheimer's disease. *Genes. Brain. Behav.* 6(1):54–65 (2007).
18. Domnitz, S. B., Robbins, E. M., Hoang, A. W., Garcia-Alloza, M., Hyman, B. T., Rebeck, G. W., Greenberg, S. M., Bacskai, B. J. & Frosch, M. P. Progression of cerebral amyloid angiopathy in transgenic mouse models of Alzheimer disease. *J. Neuropathol. Exp. Neurol.* 64(7):588–94 (2005).
19. Kilkenny, C., Browne, W. J., Cuthill, I. C., Emerson, M. & Altman, D. G. Improving Bioscience Research Reporting: The ARRIVE Guidelines for Reporting Animal Research. *PLoS Biol.* 8(6):e1000412 (2010).
20. Shaner, N. C., Patterson, G. H. & Davidson, M. W. Advances in fluorescent protein technology. *J. Cell Sci.* 120(Pt 24):4247–60 (2007).
21. Shaner, N. C., Campbell, R. E., Steinbach, P. A., Giepmans, B. N. G., Palmer, A. E. & Tsien, R. Y. Improved monomeric red, orange and yellow fluorescent proteins derived from *Discosoma* sp. red fluorescent protein. *Nat. Biotechnol.* 22(12):1567–72 (2004).
22. Shaner, N. C., Steinbach, P. A. & Tsien, R. Y. A guide to choosing fluorescent proteins. *Nat. Methods* 2(12):905–9 (2005).
23. Rutgers, K. S., Nabuurs, R. J. A., van den Berg, S. A. A., Schenk, G. J., Rotman, M., Verrips, C. T., van Duinen, S. G., Maat-Schieman, M. L., van Buchem, M. A., de Boer, A. G., et al. Transmigration of beta amyloid specific heavy chain antibody fragments across the *in vitro* blood-brain barrier. *Neuroscience* 190:37–42 (2011).
24. Dorresteyn, B. Llama VHH as immunotherapeutics in Alzheimer's disease. Thesis (Utrecht University, 2013). at <<http://dspace.library.uu.nl/handle/1874/261032>>
25. Schut, M. H., Pepers, B. A., Klooster, R., van der Maarel, S. M., El Khatabi, M., Verrips, T., den Dunnen, J. T., van Ommen, G.-J. B. & van Roon-Mom, W. M. C. Selection and characterization of llama single domain antibodies against N-terminal huntingtin. *Neurol. Sci.* 36(3):429–34 (2015).
26. Pepers, B. A., Schut, M. H., Vossen, R. H., van Ommen, G.-J. B., den Dunnen, J. T. & van Roon-Mom, W. M. Cost-effective HRMA pre-sequence typing of clone libraries; application to phage display selection. *BMC Biotechnol.* 9(1):50 (2009).
27. Grimm, D., Kern, A., Rittner, K. & Kleinschmidt, J. A. Novel tools for production and purification of recombinant adenoassociated virus vectors. *Hum. Gene Ther.* 9(18):2745–60 (1998).
28. Gonçalves, M. A. F. V. Adeno-associated virus: from defective virus to effective vector. *Viol. J.* 2:43 (2005).
29. Kim, J., Miller, V. M., Levites, Y., West, K. J., Zwizinski, C. W., Moore, B. D., Troendle, F. J., Bann, M., Verbeeck, C., Price, R. W., et al. BRI2 (ITM2b) inhibits Abeta deposition *in vivo*. *J. Neurosci.* 28(23):6030–6 (2008).
30. Chakrabarty, P., Jansen-West, K., Beccard, A., Ceballos-Diaz, C., Levites, Y., Verbeeck, C., Zubair, A. C., Dickson, D., Golde, T. E. & Das, P. Massive gliosis induced by interleukin-6 suppresses Abeta deposition *in vivo*: evidence against inflammation as a driving force for amyloid deposition. *FASEB J.* 24(2):548–59 (2010).
31. Klunk, W. E., Bacskai, B. J., Mathis, C. A., Kajdasz, S. T., McLellan, M. E., Frosch, M. P., Debnath, M. L., Holt, D. P., Wang, Y. & Hyman, B. T. Imaging Abeta plaques in living transgenic mice with multiphoton microscopy and methoxy-Xo4, a systemically administered Congo red derivative. *J. Neuropathol. Exp. Neurol.* 61(9):797–805 (2002).
32. Tsien, R. Y. The green fluorescent protein. *Annu. Rev. Biochem.* 67:509–44 (1998).
33. Patterson, G. H., Knobel, S. M., Sharif, W. D., Kain, S. R. & Piston, D. W. Use of the green fluorescent protein and its mutants in quantitative fluorescence microscopy. *Biophys. J.* 73(5):2782–90 (1997).

34. Patterson, G. H. & Piston, D. W. Photobleaching in two-photon excitation microscopy. *Biophys. J.* 78(4):2159–62 (2000).
35. Denk, W., Strickler, J. H. & Webb, W. W. Two-photon laser scanning fluorescence microscopy. *Science* 248(4951):73–6 (1990).
36. Agrawal, V., Slivac, I., Perret, S., Bisson, L., St-Laurent, G., Murad, Y., Zhang, J. & Durocher, Y. in *Methods in molecular biology* (Clifton, N.J.) (eds. Saerens, D. & Muyldermans, S.) 911:485–490 (Humana Press, 2012).
37. Oberbek, A., Matasci, M., Hacker, D. L. & Wurm, F. M. Generation of stable, high-producing CHO cell lines by lentiviral vector-mediated gene transfer in serum-free suspension culture. *Biotechnol. Bioeng.* 108(3):600–10 (2011).
38. Jankowsky, J. L., Fadale, D. J., Anderson, J., Xu, G. M., Gonzales, V., Jenkins, N. A., Copeland, N. G., Lee, M. K., Younkin, L. H., Wagner, S. L., et al. Mutant presenilins specifically elevate the levels of the 42 residue beta-amyloid peptide *in vivo*: evidence for augmentation of a 42-specific gamma secretase. *Hum. Mol. Genet.* 13(2):159–70 (2004).
39. Garcia-Alloza, M., Robbins, E. M., Zhang-Nunes, S. X., Purcell, S. M., Betensky, R. A., Raju, S., Prada, C., Greenberg, S. M., Bacskai, B. J. & Frosch, M. P. Characterization of amyloid deposition in the APP^{Swe}/PS1^{E9} mouse model of Alzheimer disease. *Neurobiol. Dis.* 24(3):516–524 (2006).
40. Ordóñez-Gutiérrez, L., Antón, M. & Wandosell, F. Peripheral amyloid levels present gender differences associated with aging in A β PP/PS1 mice. *J. Alzheimers. Dis.* 44(4):1063–8 (2015).
41. Janus, C., Flores, A. Y., Xu, G. & Borchelt, D. R. Behavioral abnormalities in APP^{Swe}/PS1^{E9} mouse model of AD-like pathology: comparative analysis across multiple behavioral domains. *Neurobiol. Aging* 36(9):2519–32 (2015).
42. Kilgore, M., Miller, C. A., Fass, D. M., Hennig, K. M., Haggarty, S. J., Sweatt, J. D. & Rumbaugh, G. Inhibitors of class 1 histone deacetylases reverse contextual memory deficits in a mouse model of Alzheimer's disease. *Neuropsychopharmacology* 35(4):870–80 (2010).
43. Bateman, R. J., Xiong, C., Benzinger, T. L. S., Fagan, A. M., Goate, A., Fox, N. C., Marcus, D. S., Cairns, N. J., Xie, X., Blazey, T. M., et al. Clinical and biomarker changes in dominantly inherited Alzheimer's disease. *N. Engl. J. Med.* 367(9):795–804 (2012).
44. Chakrabarty, P., Rosario, A., Cruz, P., Sieminski, Z., Ceballos-Diaz, C., Crosby, K., Jansen, K., Borchelt, D. R., Kim, J.-Y., Jankowsky, J. L., et al. Capsid serotype and timing of injection determines AAV transduction in the neonatal mice brain. *PLoS One* 8(6):e67680 (2013).
45. McFarland, N. R., Lee, J.-S., Hyman, B. T. & McLean, P. J. Comparison of transduction efficiency of recombinant AAV serotypes 1, 2, 5, and 8 in the rat nigrostriatal system. *J. Neurochem.* 109(3):838–45 (2009).
46. Ayers, J. I., Fromholt, S., Sinyavskaya, O., Sieminski, Z., Rosario, A. M., Li, A., Crosby, K. W., Cruz, P. E., DiNunno, N. M., Janus, C., et al. Widespread and efficient transduction of spinal cord and brain following neonatal AAV injection and potential disease modifying effect in ALS mice. *Mol. Ther.* 23(1):53–62 (2015).
47. Kim, J.-Y., Grunke, S. D., Levites, Y., Golde, T. E. & Jankowsky, J. L. Intracerebroventricular viral injection of the neonatal mouse brain for persistent and widespread neuronal transduction. *J. Vis. Exp.* (91):51863 (2014). doi:10.3791/51863
48. Cearley, C. N. & Wolfe, J. H. A single injection of an adeno-associated virus vector into nuclei with divergent connections results in widespread vector distribution in the brain and global correction of a neurogenetic disease. *J. Neurosci.* 27(37):9928–40 (2007).
49. Cetin, A., Komai, S., Eliava, M., Seeburg, P. H. & Osten, P. Stereotaxic gene delivery in the rodent brain. *Nat. Protoc.* 1(6):3166–73 (2006).
50. Lowery, R. L. & Majewska, A. K. Intracranial injection of adeno-associated viral vectors. *J. Vis. Exp.* (45) (2010). doi:10.3791/2140
51. Hamsen, M. M. & De Haard, H. J. Properties, production, and applications of camelid single-domain antibody fragments. *Appl. Microbiol. Biotechnol.* 77(1):13–22 (2007).
52. Muyldermans, S. Nanobodies: natural single-domain antibodies. *Annu. Rev. Biochem.* 82(1):775–797 (2013).

5

CHAPTER

❖ SUPPLEMENTARY DATA

Adapted from

Functionally secreted single domain antibody fragment VHH-EmGFP binds amyloid plaques and can be visualized in vivo.

SUPPLEMENTARY DATA I

A short pilot study was performed to test the acute effect of various VHH on the A β burden in the APP/PS1 mice. For this pilot study the anti-A β VHH-pa2H and the control VHH-Htt7F4 were produced in *E. coli* and purified using TALON metal affinity purification. Production yield was approximately 4.5 mg VHH per 1 L of growth medium. Both VHH were obtained at a maximum concentration of approximately 4.8 mg/ml and diluted down to 0.5 mg/ml before *in vivo* use (Supplementary figure 5.1). The correct functionality of VHH-pa2H and absence of amyloid recognition by VHH-Htt7F4 were confirmed by standard immunocytochemistry staining on brain cryosections (Supplementary figure 5.2).

Both VHH-pa2H and VHH-Htt7F4 were applied to the exposed brain parenchyma of two different 10 month old APP/PS1 mice. The mice were subsequently imaged through a cranial window using a multiphoton microscope. Imaging took place immediately after the application of the VHH as well as three days later. Amyloid depositions were visualized using Methoxy-X04. A striking difference was observed between the effect of application of the anti-A β VHH-pa2H and the control VHH-Htt7F4. In the case of VHH-pa2H, the amyloid plaques present in the parenchyma at day 1, directly after application of the VHH, were mostly undetectable at day 3, i.e. 72 hours after the application. This effect was not similarly evident in mice treated with the control VHH, VHH-Htt7F4 (Supplementary figure 5.3). Vascular deposition did not change in either case.

Subsequent *ex vivo* analysis of the amyloid burden in the brains showed that there were, on average, less plaques in the cortical sections obtained from the mice treated with VHH-pa2H compared to those obtained from the mice treated with VHH-Htt7F4 (Supplementary figure 5.4 and Supplementary table 5.1). Furthermore, the total area of the brain occupied by amyloid plaques was less in the VHH-pa2H treated mice. However, the average size per plaque did not change between the two groups. Control images, where the primary antibody was omitted, show that the amyloid plaques themselves did not pose an auto fluorescence issue, but that the damaged area under the former cranial window did indeed cause auto fluorescence in the red channel (Supplementary figure 5.5).

Experimental procedures with regards to Supplementary Data I are described in Supplementary Materials and Methods.

SUPPLEMENTARY DATA II

The following sequence was designed to create the intermediate pUC57-based shuttle vector.

All sequences are given from 5' to 3'. Amino acid translation are indicated below the second base of the corresponding codon.

5' HindIII flanked by the lysozyme secretion signal (ss):

```
aagc ttatg aggt cttt gcta atct ttgg tgc tttg cttc ctgc ccct ggct gctc tgggg      60
  K  L  M  R  S  L  L  I  L  V  L  C  F  L  P  L  A  A  L  G
```

Followed by the VHH – specialized multiple cloning site (MCS), containing SfiI, PstI and BstEII sites, flanked by a triple alanine linker (AAA):

```
gccc agcc ggc catgg ccc aggt acag ctgc aggt gctgc ggtc cacc gtct cctc agct      60
  A  Q  P  A  M  A  Q  V  Q  L  Q  A  A  A  V  T  V  S  S  A

gctg cg                                           66
  A  A
```

Followed by the codon optimized Emerald GFP (EmGFP):

```
atgg tgag caag ggc gagg agct gttc accg gggg tgg tgc ccat cctg gtgc gagct ggac      60
  M  V  S  K  G  E  E  L  F  T  G  V  V  P  I  L  V  E  L  D

ggc gacg taaac ggc caca agtt cagc gtgt ccgg cgag ggc gagg gcgat gccac ctac      120
  G  D  V  N  G  H  K  F  S  V  S  G  E  G  E  G  D  A  T  Y

ggca agct gacc ctga agtt catct gcacc accg gca agct gccg tgcct ggccc acc      180
  G  K  L  T  L  K  F  I  C  T  T  G  K  L  P  V  P  W  P  T

ctcg tgacc acctt gacct agcgt gcag tgc ttc gcccg ctac ccc gacc cacat gaag      240
  L  V  T  T  L  T  Y  G  V  Q  C  F  A  R  Y  P  D  H  M  K

cagc acg actt cttc aaagt ccg ccat gccc gaagg ctac gtcc agg agcgc cacc atcttc      300
  Q  H  D  F  F  K  S  A  M  P  E  G  Y  V  Q  E  R  T  I  F

ttca aggac gacg gca actaca agacc ccg cgg aggt gaagt tcg aggg cgac accctg      360
  F  K  D  D  G  N  Y  K  T  R  A  E  V  K  F  E  G  D  T  L

gtga accg catc gagct gaag ggc atc gact tca agg agg acg gca acat cctg ggg cac      420
  V  N  R  I  E  L  K  G  I  D  F  K  E  D  G  N  I  L  G  H

aagct gtag taca actaca acag ccaca aggt ctata tcacc gccg gaca agc aga aga ac      480
  K  L  E  Y  N  Y  N  S  H  K  V  Y  I  T  A  D  K  Q  K  N

ggcat caag gtga actt caag accc gcc caca acat cgagg acggc agcgt gcag ctcg cc      540
  G  I  K  V  N  F  K  T  R  H  N  I  E  D  G  S  V  Q  L  A

gacc actacc agc aga acac ccccat cggc gacgg ccccg tgc tgc tgc cccg gaca accac      600
  D  H  Y  Q  Q  N  T  P  I  G  D  G  P  V  L  L  P  D  N  H

tacct gagc accc agtcc gccc tgc agc aaag acccca acg aga agc gcgat cacat ggctc      660
  Y  L  S  T  Q  S  A  L  S  K  D  P  N  E  K  R  D  H  M  V
```

ctgctggagttcgtgaccgccgcccgggatcactctcggcatggacgagctgtacaag 717
L L E F V T A A G I T L G M D E L Y K

And finally a double stop signal followed by a 3' Sall site:

tgataagtcgacgcccggcga 21
- - V D A A A

SUPPLEMENTARY MATERIALS AND METHODS

Production and application of non-EmGFP fused VHH

VHH without the EmGFP tag were produced in *E. coli* (BL21⁺ strain) as described before [1–4]. In short, the VHH, on a pUC5071 or pUC5850 vector backbone, were produced in log-phase BL21⁺ *E. coli* by induction with 1 mM IPTG for 5–6 h at 37°C. The VHH were subsequently harvested from the periplasmic fraction of the bacteria, affinity-purified via their hexa-histidine tag on Clontech Talon beads and dialyzed against PBS.

The VHH were tested for correct A β recognition via standard immunohistochemistry staining as described before [1]. In short, analysis was performed on 5 μ m thick human post-mortem brain cryosections of AD/CAA patients and age-matched healthy controls, using the VHH as primary and mouse-anti-c-myc (clone 9E10, Santa Cruz Biotechnology, 1:6000) as secondary antibody and EnVision+ system labelled Polymer-HRP anti-Mouse (Dako Cytomation) as tertiary entity. All human tissues were obtained from anonymous patients or healthy age-matched donors as confirmed by neuropathological examination in agreement with the guidelines of the Medical Ethics Committee of the Leiden University Medical Center (Leiden, The Netherlands). All tissues were processed in a coded fashion, according to Dutch national ethical guidelines (Code for Proper Secondary Use of Human Tissue, Dutch Federation of Medical Scientific Societies).

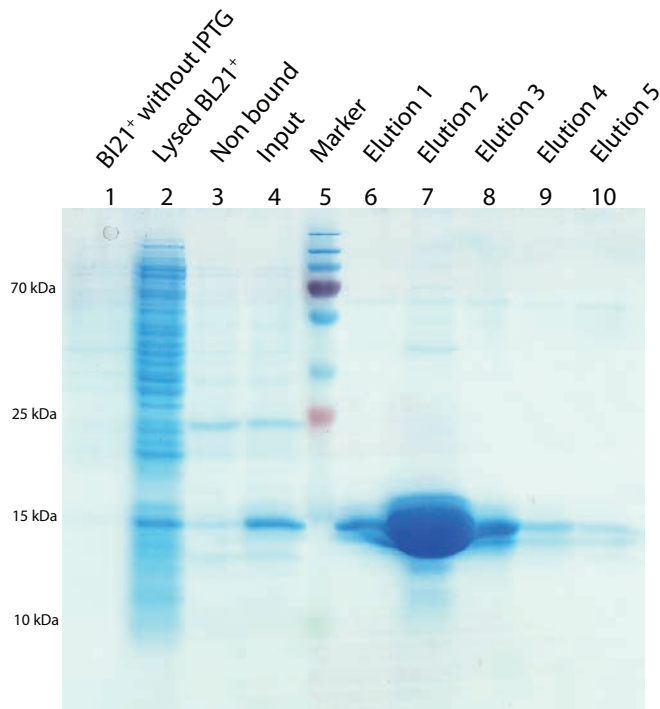
Four APP^{swe}/PS1dEg mice (two mice per treatment) received a cranial window as described in the Materials and Methods section Intravital multiphoton microscopy. Purified VHH (0.2–0.5 mg/ml) were applied in a drop-wise manner (50 μ l) to the exposed brain parenchyma during the application of the cranial window, just prior to fixation of the glass coverslip as described before [3]. Intravital multiphoton microscopy was performed directly after placement of the window and three days after the placement. All animal studies have been approved by the Leiden University Medical Center institutional Animal Experiments Committee (DEC permits 10097 and 12080) in accordance with all national and European guidelines.

Quantification of amyloid plaque burden

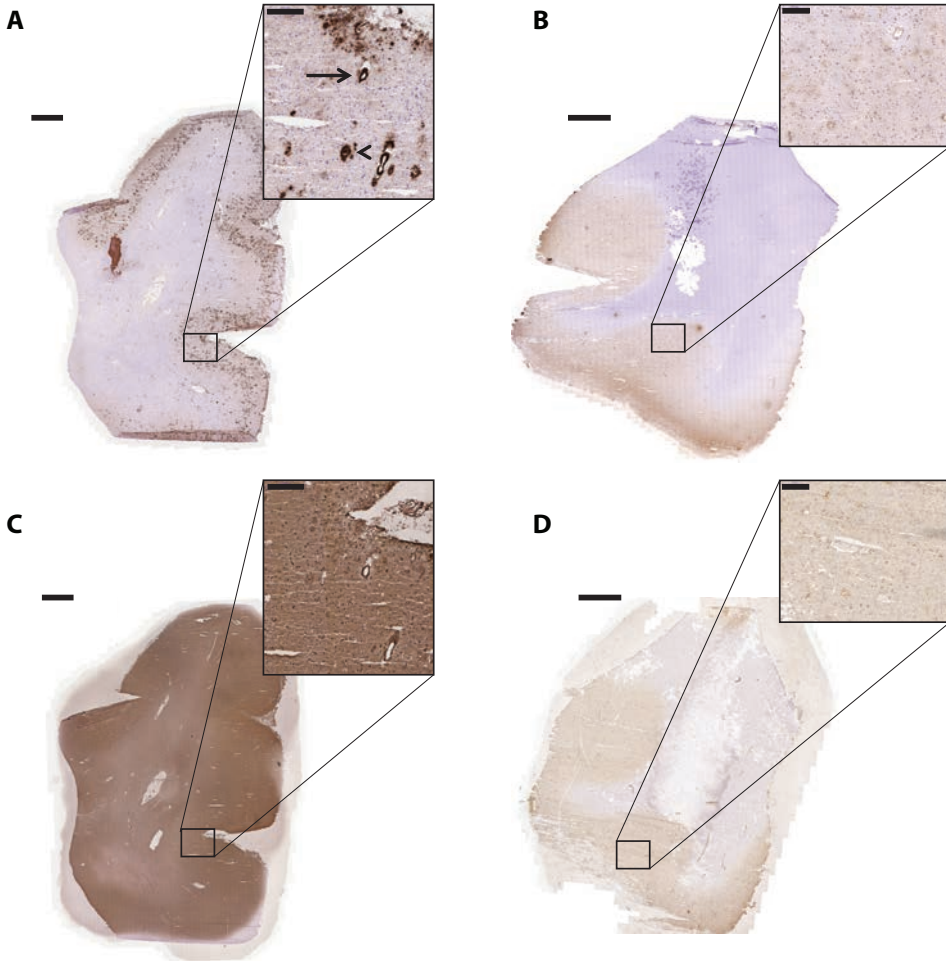
After the second imaging session, the mice were sacrificed and the brains were perfused via cardiac perfusion and fixed in PFA, snap-frozen in isobutanol cooled on dry ice and stored at -80°C until use. Coronal sections ($20\ \mu\text{m}$) were cut from a region including the hippocampus and stained for presence of amyloid beta using mouse-a-A β antibody 4G8 (1:500, Covance) and donkey-a-mouse-Alexa594 (1:500, Invitrogen). The brains were imaged with a Leica DM 5500B fluorescence microscope. Images of the cortical region were stitched together using Adobe Photoshop CS5. The stitched images were analyzed in WCIF ImageJ v. 1.73c. All images underwent the following modifications to obtain an unbiased analysis of plaque load. The background was subtracted using a rolling ball setting (radius 50, no white background), the color was set to 8-bit grayscale, threshold was set to 30 minimum and 255 maximum. The build-in package “analyze particles” was used, set at “size 0.01-100, circularity 0.00-1.00”. Obtained values were analyzed in Microsoft Excel 2010.

SUPPLEMENTARY REFERENCES

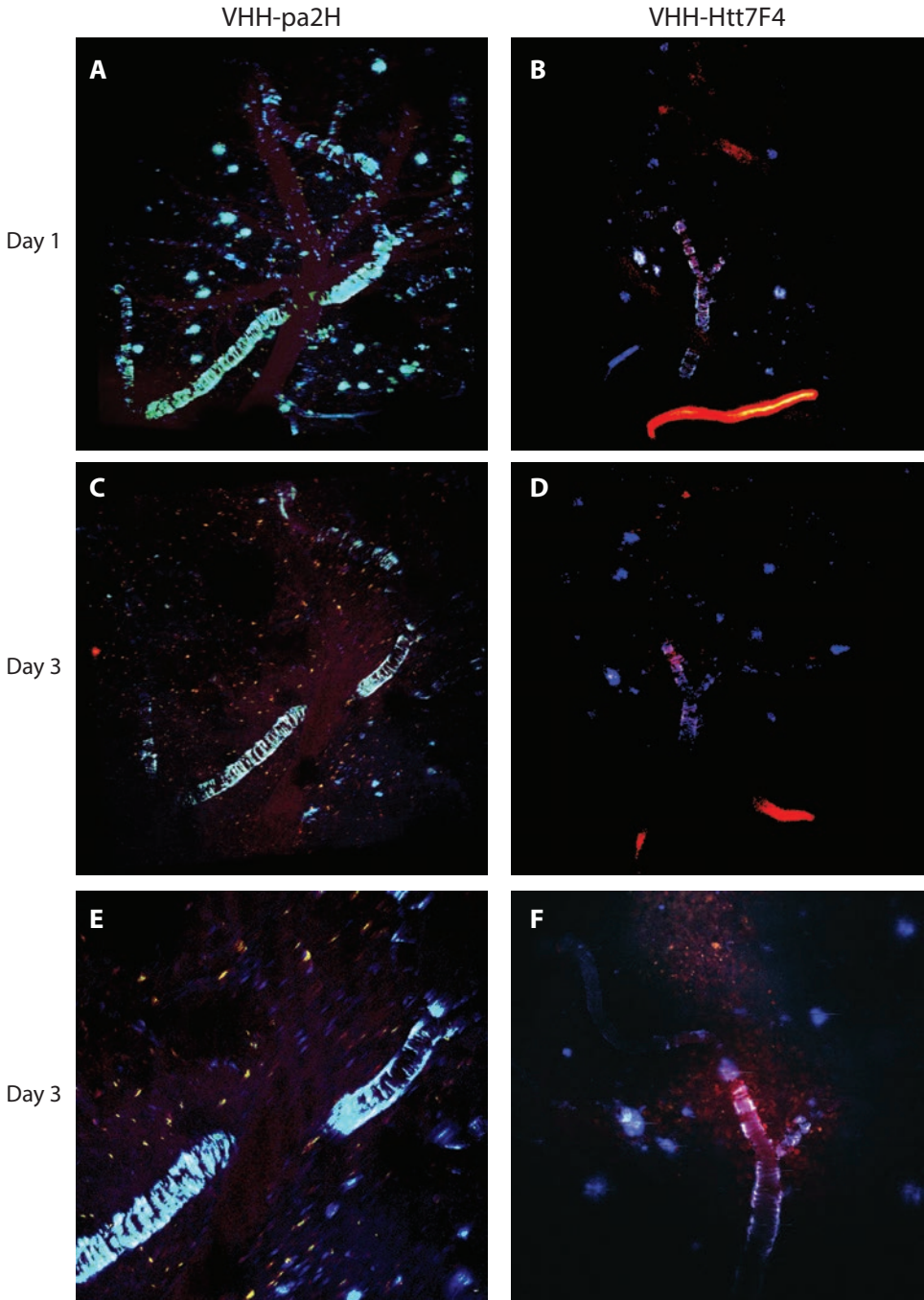
1. Rutgers, K. S., van Remoortere, A., van Buchem, M. A., Verrips, C. T., Greenberg, S. M., Bacskai, B. J., Frosch, M. P., van Duinen, S. G., Maat-Schieman, M. L. & Van der Maarel, S. M. Differential recognition of vascular and parenchymal beta amyloid deposition. *Neurobiol. Aging* 32(10):1774–1783 (2009).
2. Rutgers, K. S., Nabuurs, R. J. A., van den Berg, S. A. A., Schenk, G. J., Rotman, M., Verrips, C. T., van Duinen, S. G., Maat-Schieman, M. L., van Buchem, M. A., de Boer, A. G., et al. Transmigration of beta amyloid specific heavy chain antibody fragments across the *in vitro* blood-brain barrier. *Neuroscience* 190:37–42 (2011).
3. Nabuurs, R. J. A., Rutgers, K. S., Welling, M. M., Metaxas, A., de Backer, M. E., Rotman, M., Bacskai, B. J., van Buchem, M. A., van der Maarel, S. M. & van der Weerd, L. *In vivo* detection of amyloid- β deposits using heavy chain antibody fragments in a transgenic mouse model for Alzheimer's disease. *PLoS One* 7(6):e38284 (2012).
4. Dorresteyn, B., Rotman, M., Faber, D., Schraevesand, R., Suidgeest, E., van der Weerd, L., van der Maarel, S. M., Verrips, C. T. & El Khattabi, M. Camelid heavy chain only antibody fragment domain against β -site of amyloid precursor protein cleaving enzyme 1 inhibits β -secretase activity *in vitro* and *in vivo*. *FEBS J.* 282(18):3618–3631 (2015).



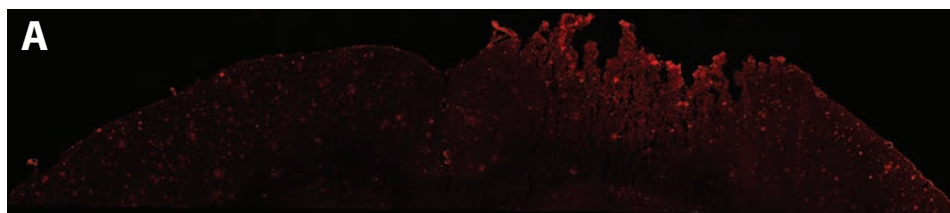
Supplementary figure 5.1. Production of non-EmGFP fused VHH analyzed on SDS-PAGE, visualized by Coomassie Blue staining. VHH-pa2H and VHH-Htt7F4 were produced in BL21+ strain *E. coli*. Production of the VHH was induced by addition of 1 mM IPTG into the growth medium. On the displayed 12% SDS-PAGE gel, VHH-pa2H is the protein band just below 15 kDa. A sample of the medium just before addition of the IPTG (lane 1) as well as a whole sample of the harvested *E. coli* pellet (lane 2) were taken, clearly showing presence of the expected product in the induced cells. A sample of the periplasmic space lysate was taken before and after addition of the TALON Metal Affinity beads (lanes 4 and 3, respectively), showing binding of the VHH to the beads. The VHH was eluted in 5 fractions (lanes 6-10) using 300 mM imidazole and subsequently dialyzed against PBS. Peak protein concentration was determined by photo absorption to be 4.8 mg/ml (elution sample 2, lane 7). A total of approximately 14 mg VHH-pa2H was purified from 3000 ml BL21+ *E. coli* culture. Production, purification and analysis of VHH-Htt7F4 followed the same procedure and yielded the same numbers (data not shown).



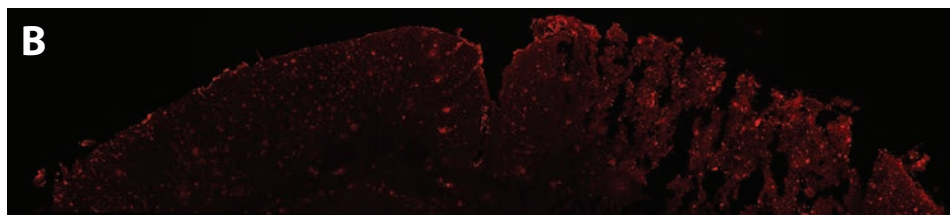
Supplementary figure 5.2. VHH-pa2H and VHH-Htt7F4 staining of human post-mortem brain cryosections of AD/CAA patients and healthy controls. VHH-pa2H stains A β in both parenchymal and vascular depositions in AD/CAA brain material (A). VHH-pa2H does not give specific staining on cryosections derived from healthy controls (B). Inserts show magnifications of the entire sections, with arrows indicating vascular depositions and arrow heads indicating parenchymal plaques. The staining of amyloid depositions by VHH-pa2H is in accordance with previously published results and match previously published A β stainings using conventional antibodies such as mouse-anti-A β clone 4G8 (Covance). In contrast, the control VHH-Htt7F4 does not recognize vascular nor parenchymal amyloid depositions, even when the chemical development reaction is allowed to proceed until beyond reasonable limits, in order to detect the faintest presence of the VHH (C). Similar to VHH-pa2H, VHH-Htt7F4 does not stain the brain material of healthy controls either (D). Black bars represent either 2000 μ m (whole slides) or 200 μ m (inserts).



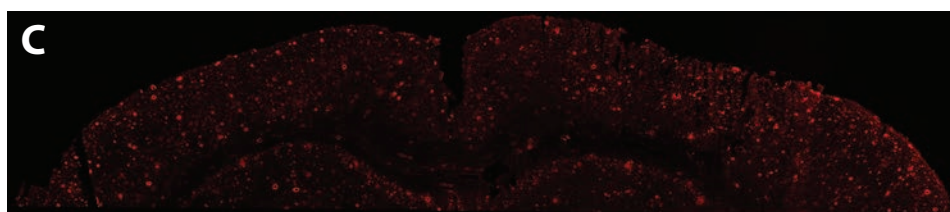
Supplementary figure 5.3. Topical application of VHH-pa2H and VHH-Htt7F4 on exposed brains of APP/PS1 mice, visualized by multiphoton microscopy. Application of the anti-A β VHH VHH-pa2H resulted in the markedly reduced presence of A β deposits in the parenchyma three days after the application (A and C). The application of the control VHH VHH-Htt7F4 did not have the same effect (B and D). Panels E and F show magnifications of the situation at day 3. Parenchymal amyloid plaques and vascular amyloid depositions are visualized by in blue-to-white by Methoxy-Xo4, vascular structure is faintly visualized in red by dextran-Texas Red.



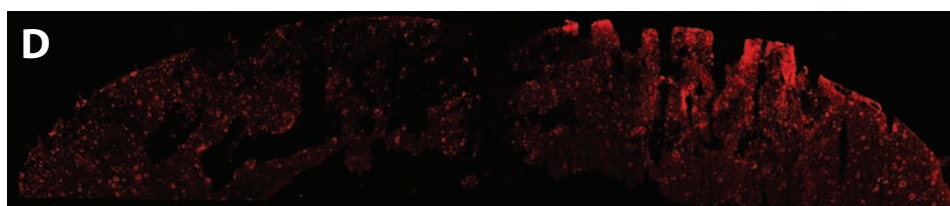
VHH-pa2H mouse 7226123 section 22



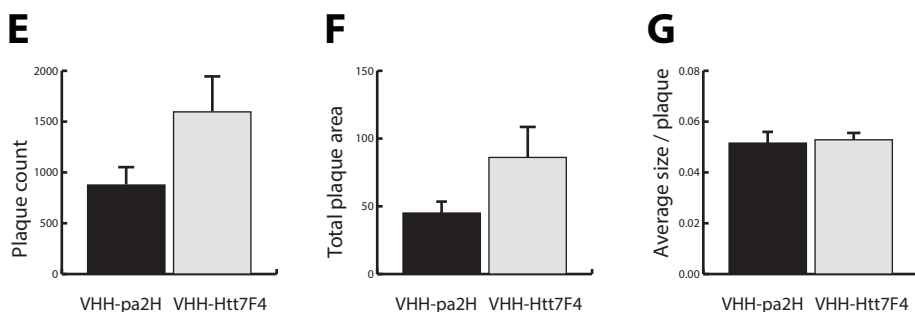
VHH-pa2H mouse 7226125 section 22



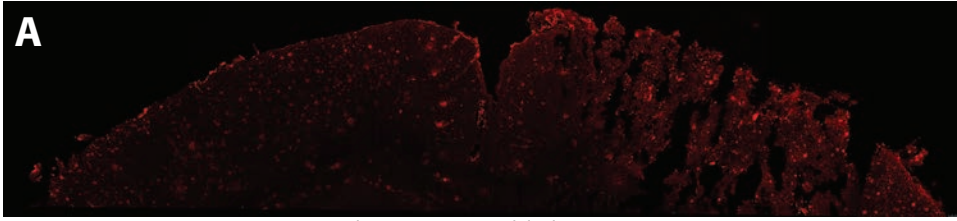
VHH-Htt7F4 mouse 7226164 section 22



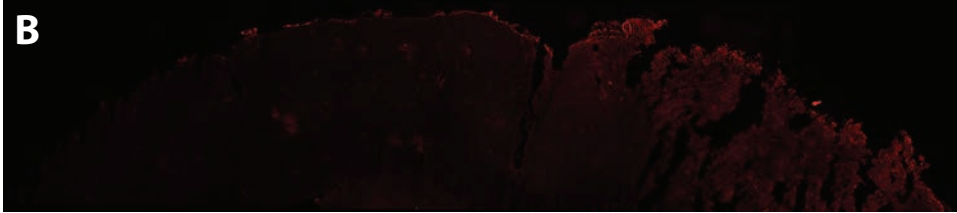
VHH-Htt7F4 mouse 7226177 section 22



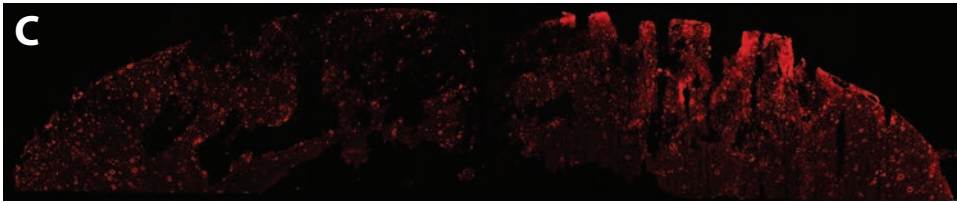
Supplementary figure 5.4. Quantification of plaque burden in VHH-pa2H and VHH-Htt7F4 treated mice. Mice were topically treated with either VHH-pa2H or VHH-Htt7F4, and sacrificed after 3 days. $n=2$ per treatment. Cortical sections of 20 μm thick were cut from snap-frozen brains. Sections were stained with mouse-a-A β (4G8; 1:500; Covance) and donkey-a-mouse-Alexa594 (1:500). One section from each mouse is displayed, showing reduction of signal in the VHH-pa2H treated mice (A and B) compared to the VHH-Htt7F4 treated mice (C and D). This *ex vivo* observation corroborates the apparent reduction of amyloid beta deposition in the brains of the VHH-pa2H treated mice. Quantification of the signal shows that both the amount of plaques and the total area of brain occupied by plaques are reduced in the mice treated with VHH-pa2H compared to those treated with VHH-Htt7F4 (E and F), while the average size per plaque remains the same (G).



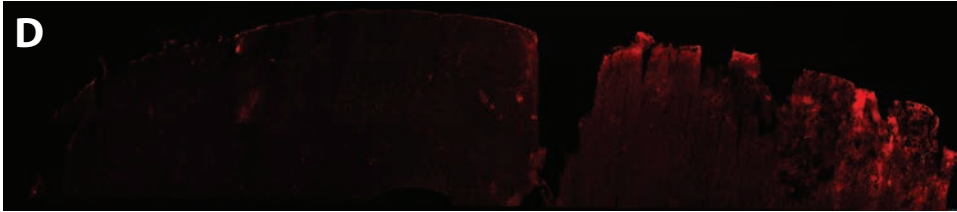
VHH-pa2H mouse 7226125 section 22; m-a-Aβ 4G8 (1:500) and donkey-a-mouse-A594 (1:500)



VHH-pa2H mouse 7226125 section 23; PBS and donkey-a-mouse-A594 (1:500)

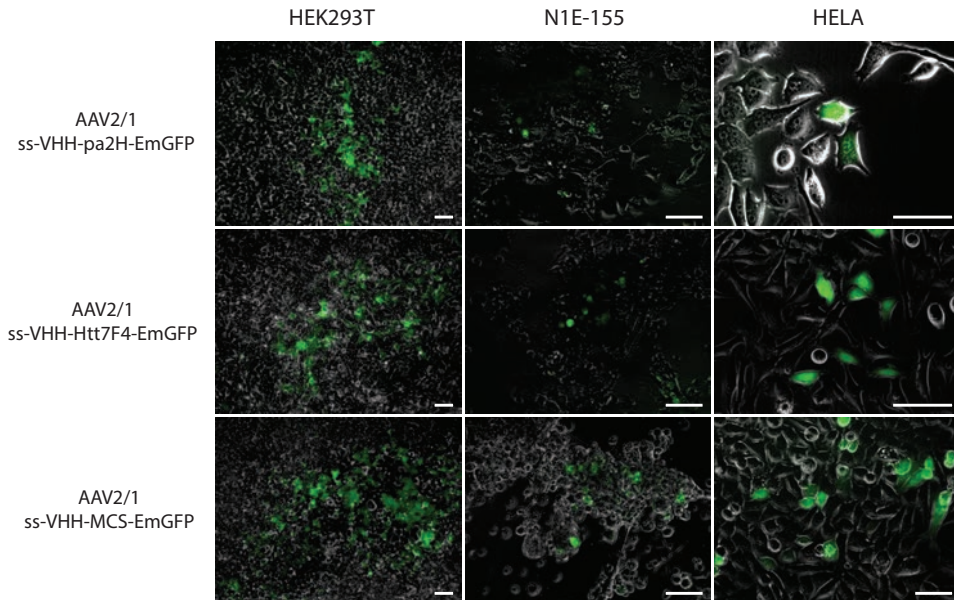


VHH-Htt7F4 mouse 7226177 section 22; m-a-Aβ 4G8 (1:500) and donkey-a-mouse-A594 (1:500)



VHH-Htt7F4 mouse 7226177 section 23; PBS and donkey-a-mouse-A594 (1:500)

Supplementary figure 5.5. Quantification of plaque burden in VHH-pa2H and VHH-Htt7F4 treated mice. Mice were topically treated with either VHH-pa2H or VHH-Htt7F4, and sacrificed after 3 days. $n=2$ per treatment. Cortical sections of $20\ \mu\text{m}$ thick were cut from snap-frozen brains. Sections were stained with mouse-a-A β (4G8; 1:500; Covance) and donkey-a-mouse-Alexa594 (1:500). Two sections from each treatment is displayed, showing either staining with (A and C) or without (B and D) the primary antibody against A β . The results indicate the general lack of both auto fluorescence of the amyloid plaques in the red channel and affinity for amyloid beta by the secondary antibody. The damaged area, on the right hemisphere, below the former cranial window does show general auto fluorescence.



Supplementary figure 5.6. *In vitro* transduction of cell lines. Cells were cultured under normal cell culture conditions for up to two weeks without splitting or changing medium, in order to detect signal of secreted EmGFP in the cells and conditioned medium. The image from in the green channel (EmGFP) was merged with the phase contrast image of the live cells. Displayed images were taken at 2 weeks after addition of the viral particles ($2 \mu\text{l}$ at 1×10^{12} genomic particles). N1E-155 cells were imaged at 10x, HEK293T cells at 20x, and HELA cells at 20x and 40x magnification. White scale bars indicate $200 \mu\text{m}$.

Supplementary table 5.1. Quantification of plaque burden in VHH-pa2H and VHH-Htt7F4 treated mice. Mice were topically treated with either VHH, and sacrificed after 3 days. $n=2$ per treatment. Mice treated with VHH-pa2H show, on average, less plaques and less total plaque area than mice treated with VHH-Htt7F4. Average size per plaque is relatively identical for all mice.

VHH treatment	Mouse number	Section number	Plaque count	Total plaque area	Average plaque size	Area fraction
VHH-pa2H	7226123	2	645	25.409	0.0394	0.57 %
		12	749	40.635	0.0543	0.83 %
		22	683	40.099	0.0587	0.86 %
		32	878	53.750	0.0612	1.11 %
	7226125	12	1194	58.632	0.0491	1.32 %
		22	1109	51.680	0.0466	1.19 %
VHH-Htt7F4	7226164	12	1172	56.766	0.0484	1.22 %
		22	1326	63.876	0.0482	1.37 %
	7226177	12	1886	98.599	0.0523	2.12 %
		22	2000	125.090	0.0625	2.52 %

6

CHAPTER

GENERAL DISCUSSION

In December 11, 2013, health ministers of the G8 stated the ambition to have a cure or a disease-modifying therapy for Alzheimer's disease (AD) available by 2025. An ambitious goal, which requires a tremendous world-wide, combined, effort, as currently not even a suggestion of either definitive cure or modifying therapy has yet been announced. In fact, the correct diagnosis of early stages of AD, accurate individualized prediction of disease progression, and even the exact etiology of the affliction are all very much elusive, yet essential for the fulfilment of the G8's ambition. Without it, AD remains the main cause of dementia and one of the great health-care challenges of the 21st century [1]. This thesis describes the potential use of llama antibody fragments (VHH) in an effort to detect, remove and prevent aggregates of the peptide amyloid beta ($A\beta$) in the brain in a pre-clinical research setting. Aggregation of $A\beta$ is one of the hallmarks of AD and the focus of the majority of AD research, and it is mimicked in APP^{swe}/PS1^{dE9} mice (APP/PS1), the model used throughout the thesis. We aim to answer two main questions: first, can we use VHH to alter $A\beta$ aggregation and second, and equally important, how can we get the VHH into the brain. This thesis focusses on two VHH in particular: VHH-B3a, selected against the beta-secretase enzyme BACE1, and VHH-pazH, selected against $A\beta$.

Anti-BACE1 VHH-B3a

In **chapter two**, a number of VHH are selected from an immune phage library derived from llama immunized with recombinant BACE1. The beta-secretase enzyme BACE1 is one of the enzymes that sequentially cleave the precursor protein APP into the peptide A β . Three VHH, VHH-B3a, -B1a, and -B5a, were analyzed and found to alter the activity of the secretase BACE1. VHH-B3a inhibits BACE1 activity, while VHH-B1a and -B5a both stimulate the enzyme's activity, each to a different extent. Inhibition of BACE1 has shown to be an efficient method to reduce not only brain A β levels, plaque burden and associated pathology in AD mouse models [2]. Furthermore, BACE1 inhibition has been able to reduce cognitive deficit such as in contextual fear conditioning, without leading to problems such as microhemorrhages, demyelination, neuromuscular dysfunction or other unexpected side-effects, even upon chronic treatment [3]. Naturally, these dramatic effects were observed in pre-clinical models in which the driver of the disease is over-expression of the human APP, often with mutations to further enhance preferential cleavage by BACE1 over the α -secretase complex. Nonetheless, a number of BACE1 modulating drugs are currently being investigated for clinical efficacy [4]. Although some of the studies were halted due to unexpected side-effects (e.g. BACE1 inhibitor LY2886721, NCT01561430, terminated by Eli Lilly and Company in 2014 due to abnormal liver enzyme elevations in 4 out of 70 patients [5]), other studies have progressed to phase 3 clinical trials (e.g. Verubecestat/MK-8931, NCT01953601 [6]). The results from these trials provide a promising outlook for BACE1 inhibiting VHH such as VHH-B3a [6-8].

Anti-A β VHH-pa2H

VHH-pa2H was selected from an immune phage library derived from llama immunized with brain parenchyma homogenates from a Down syndrome (DS) patient [9]. Due to the trisomy of chromosome 21, which carries the APP gene, DS patients tend to develop A β aggregates relatively early on in life [10]. VHH-pa2H has been selected for outstanding recognition against aggregates of A β , both post mortem in brain cryosections of humans and mice and *in vivo* in murine APP/PS1 brains [9,11]. Originally, over eight potential anti-A β VHH were characterized, including in addition to VHH-pa2H, the VHH-ni3A, -va2E, -vaE2, and pa1E. Throughout the thesis, we have used primarily VHH-pa2H as model VHH to develop and test new methods to get VHH into the brain. These new methods include liposomal delivery, elongation of blood half life via a human IgG1-Fc tail, and viral delivery. The main driving force behind the decision to select VHH-pa2H as model VHH over the other candidates was an early preliminary result showing acute disappearance of parenchymal plaques in APP/PS1 topically treated with the VHH; a study described in **chapter five**. Furthermore, VHH-pa2H was immediately available for efficient tag- and endotoxin-free production in yeast, which due to its scalability would

make this VHH a more favorable candidate for longitudinal *in vivo* studies compared to the other VHH.

VHH-B3a and -pa2H as AD therapeutics

One of the two main questions in this thesis is whether or not VHH can be employed as therapeutics for AD and related neurological disorders. As mentioned in the introduction of this thesis, VHH have been demonstrated to be highly applicable as therapeutics in general: inhibiting enzymatic active sites, preventing viral propagation, reducing aggregated proteins [12–19]. VHH-B3a described in **chapter two** does indeed inhibit the enzymatic activity of BACE1 *in vitro*, in a cellular based assay and *in vivo* in APP/PS1 mice, resulting in reduced A β concentrations in both plasma and brain. Longitudinal assays with VHH-pa2H, as described in **chapter five**, also seems to reduce the amyloid burden in mice, likely by interfering with the aggregation of A β , provided the VHH is present at a very early stage. However, despite the positive results, there are major caveats. Unlike the potent inhibition *in vitro* and in the cellular assay, the effect of VHH-B3a *in vivo* is rather low, and less consistent. This difference cannot be attributed to the addition of the dye IRD800CW, with which the VHH was tagged to facilitate monitoring of its *in vivo* presence. Also for VHH-pa2H, the *in vivo* effect was positive, yet largely inconsistent. Furthermore, VHH-pa2H seemed to have the most potential when delivered to the mice at the earliest possibility, directly after birth at Po. It must however be noted that in the *in vivo* longitudinal study with VHH-pa2H, the number of mice that could be included in the final analysis of amyloid burden is very low, and bears repetition to further increase significance and reduce the influence of individual variation. It is nonetheless clear that although VHH-pa2H is likely able to influence aggregation to some degree, it is not able to completely prevent or revert A β aggregation in the AD mouse model. Like the anti-BACE1 VHH-B3a, the anti-A β VHH-pa2H seems to have a restricted or limited influence on the hallmarks of AD. A minimal amount of A β might be crucial for neuronal cell survival and control of synaptic activity [20,21], so complete inhibition of A β production may not necessarily be desirable, yet it is unlikely that the currently observed effects prove to be sufficient for efficient treatment or prevention of AD. That being said, it does not take away the fact that the two VHH did have an effect. One of the VHH acted on the pathways before A β production and one after the A β peptide was already made. The finding provides evidence that it is possible to interfere with the pathway that leads up to A β production by selecting and utilizing the right VHH, and thus that the right VHH may indeed be able to alter the disease. Given the characteristics of VHH in general, and the positive effects of these VHH in particular, it is highly unlikely that no VHH can be selected, or created, that is able to influence the course of the disease more efficiently. To develop the VHH that is suitable for successful use as an AD therapeutic, one might however need to reconsider the entire chain of VHH selection.

VHH selection

VHH selection starts with the creation of a VHH cDNA library. VHH libraries are often created by immunizing llama or other members of the camelidae family with the antigen against which a VHH is desired. After development of an immune response, mRNA is isolated from lymphocytes, from which in turn a cDNA library of variable heavy chain domains, the VHH, is created [22–24]. The cDNA is then used to express the VHH as fusion protein with M13 bacteriophage coat proteins, allowing VHH to be presented by the phages, i.e. phage display. The phages can be selected by allowing the VHH to bind an immobilized antigen, wash away non-bound phages and then elute the bound phages from the antigen. These selected phages are then used to infect *Escherichia coli*, which are subsequently used to create a new, enriched, phage library. Multiple panning rounds of this selection procedure allows to enrich for a small number of highly favorable VHH, which then need to be identified as unique, e.g. via sanger sequencing, high resolution melting curve analysis, a combination of these methods, and characterized for their actual binding affinity [25]. Selected VHH can subsequently be cloned into vectors suitable for downstream applications, such as described in **chapters three, four and five** in this thesis. The whole process of immunization, library creation, VHH selection and characterization takes at least 3 to 4 months, and success is highly dependent on careful selection of the immunization antigen [26,27].

Although it is not strictly required to immunize the host camelid in order to obtain a diverse VHH library, it has been demonstrated that careful immunization with correctly folded antigen will determine the quality of the obtained VHH library and in turn the likelihood of selecting potent, usable VHH [26]. This effect is evident in the immune library that yielded VHH-pa2H, compared to the naive library from which VHH-ni3A was selected [9]. While the naive library-derived VHH-ni3A seems to have a preference for vascular A β depositions, it has become clear that VHH-pa2H has a much higher affinity for the aggregated peptide [9,11,27,28]. Specialized immunization programs may be able to create libraries naturally enriched for VHH that recognize epitopes limited to very specific variants of A β related dementias. This is especially relevant for variants of dementia caused by dominantly inherited mutations in APP. One example of such variant is Hereditary Cerebral Hemorrhages with Amyloidosis-Dutch type (HCHWA-D). HCHWA-D is a variant in which A β has a characteristic E22Q mutation (also known as E693Q in A β 's precursor APP). As a result of the mutation, A β deposits heavily in the cerebral vasculature. It stands to reason that by immunizing a camelid with carefully isolated A β depositions that are found in afflicted cerebral vessels from a HCHWA-D patient, rather than recombinant A β -E22Q peptides, there will be a higher chance to discover a VHH that binds HCHWA-D pathology with exceedingly high specificity and efficiency.

Further optimization can be achieved in the stringent selection of candidate VHH. As is seen

in **chapter two** of this thesis, the competitive elution of VHHs from inside or around enzymatic active sites by supplying increasing amounts of conventional enzyme specific ligands, can yield VHHs that are not only highly specific, but also able to modulate enzymatic activity, either in the inhibitory or excitatory direction [29].

Selection via phage display under application conditions is another way to improve the changes of enriching primarily for a blockbuster VHH [30]. In the case of HCHWA-D this may be selection on post mortem brain cryosections obtained from HCHWA-D patient material, or possibly in animal models that exhibit an HCHWA-D-like phenotype [31]. However, in view of screening throughput, both selection methods may only be feasible after initial panning rounds on classical phage-ELISA set-ups, where the antigen, here most likely recombinant A β -E22Q, is immobilized in a 96-wells plate.

However, these classical methods of VHH selection do not fully benefit from the advantages that the VHH can theoretically provide. While slightly outside the scope of this thesis, it is strongly advisable to modernize the process of VHH selection for scientific and therapeutic applications. The VHH has the advantage that it is a fully functional single domain antibody, made from one genetic fragment of around 600 basepairs, with three variable complementary determining regions (CDR) bordered by four highly conserved frameworks. Since there is no interplay between a heavy and a light chain as there is with conventional antibodies, mutations in the CDR, and especially the longer CDR3 loop, will primarily affect antigen recognition. As long as the mutations do not intervene with the folding or maturation of the VHH, randomization of these regions allows for the creation of a wide variety of VHH, able to bind a potentially unlimited array of antigens. Libraries containing these VHH with artificially randomized CDR loops are called synthetic phage display libraries. Synthetic phage display libraries are already routinely used to isolate VHH when their intended antigens cannot be used to induce an immune response in llamas or camels, e.g. when the antigen is highly toxic, pathogenic or non-immunogenic [32,33]. However, the libraries themselves are still very much random, selection of the one desired VHH out of these libraries is still done the conventional way, the eventually selected VHH may not be the most ideal VHH in the library, and on top of that, the theoretically most ideal VHH may not even be present in the randomly generated library. However, keeping the relatively simple lay-out of the genetic structure of VHH in mind, with the ever progressing technological advances in terms of sequencing of DNA, computing power, and massive database storage, it is technically possible to create a database in which the CDR diversity of known VHH is linked to their respective antigens, and subsequently used to predict, *de novo* and *in silico*, novel VHH sequences targeted towards very specific characteristics in terms of antigen recognition, enzyme interference, active transport mechanisms [22,34]. Selection of the VHH is the single most important step in developing the camelid antibody based therapeutic, diag-

nostic or theragnostic tool that will one day diagnose and prevent AD and related afflictions. To find the right VHH, if not by sheer serendipitous luck and a high number of iterations, the entire R&D chain surrounding VHH, from immunization, to selection, to identification, must be improved. The possibilities are endless and the rewards by far outweigh the investment, yet a major caveat needs to be overcome: it is currently not even fully understood how the natural antibodies are able to create their impressive array of epitope recognition, let alone predict that of the relatively new VHHs. The fact that the interaction is now focused on only one domain with three or four CDRs to be elucidated, does make it promising, but the *in silico* prediction of epitope and paratope interaction is still in its infancy [35]

Blood brain barrier delivery

Once a VHH is selected and identified, the second main question in this thesis needs to be addressed: how can we get enough VHH effectively into the brain? This is not as straightforward as it may sound. The brain is the control center of the body. Together with the spinal cord it forms the central nervous system (CNS), and is arguably the single most important human organ. In order for the brain to work efficiently, even during severe bodily stress, it is crucial that the CNS maintains a strictly stable internal microenvironment; significantly more controlled than any other organ in the body. The CNS contains specific cell types not found in any other organ in the human body. In general it comes down to two categories of cells: neurons and glial cells [36]. While neurons are the cell-type that defines the brain, the neural specific supporting glial cells (astrocytes, oligodendrocytes, and microglia) as well as pericytes contribute to the local homeostasis and outnumber the neurons in certain areas of the brain, such as the cerebral cortex where the glia/neuron ratio equals approx. 3.72 [37–40]. To regulate and control the homeostasis in the CNS, specialized barriers strictly regulate both molecular influx and efflux at the interface between the CNS and the circulating blood. These barriers are either at the level of the cerebrospinal fluid (CSF) in the ventricles and the subdural space, forming the blood-CSF barrier (BCSFB), or at the level of the capillaries in the brain parenchyma, forming the blood-brain barrier (BBB) [41,42].

At the BBB tight junctions between adjacent endothelial cells close what normally would be the fenestræ; openings in the blood vessels that allow fast and efficient exchange of nutrients, macromolecules and circulating immune cells between the capillary bed and the organ. Together with pericytes, astrocytes and microglia, the capillary endothelium forms a modular neurovascular unit (NVU), each modular segment strictly regulating the microenvironment of a limited number of neurons (typically < 8) [43]. Passive exchange between the luminal and abluminal sides of the NVU is limited to diffusion of small non-polar solutes (< 600 Da in size),

Box 6.1. VHH Genetics

The family of Camelidae have three major subclasses of circulating γ immunoglobulins: IgG1, IgG2 and IgG3. IgG1 is a hetero tetrameric antibody (i.e. two heavy chains and two light chains) while IgG2 and IgG3 are homodimers of only heavy chains (i.e. two heavy chains, and no light chains) (Figure 6.1). The subtype IgG1 is composed by a variable domain that interacts with the antigen (VH) and three constant domains, named CH1, CH2 and CH3, with a hinge region between CH1 and CH2. Directly after translation of the mRNA of the IgG1 heavy chain, the Endoplasmic Reticulum (ER) associated chaperon protein Heavy chain Binding Protein, BiP, binds the CH1 domain. This CH1-BiP interaction prevents folding of the domain, until BiP is replaced by a light chain. Should no light chain be present to replace BiP, the CH1/BiP complex stays in the ER until it gets ubiquitinated via ubiquitin ligase U3, exported to the cytoplasm and degraded by the proteasome [65]. If BiP is removed prematurely, the heavy chain domain folds into an unstable protein fragment, with hydrophobic amino acid side chains exposed to the intracellular environment, a situation that in humans leads to a variety of rare heavy chain diseases [66].

In the camelid subtypes IgG2 and IgG3, however, the CH1 domain is not present [67]. This is the direct result of a G>A+1 point mutation in the 3' splice site recognition sequence between the CH1 exon and the downstream intron [68]. The consensus, conserved among nearly all mammals, at the splice site between the 3' CH1 exon and the 5' intron boundary (I) is TG|GT, but in the camel it is GG|AT [68]. Modification of the first invariant position (G+1) usually causes the skipping of the preceding exon [69,70]. Therefore, while it is highly homologous to other mammalian CH1 domains, and would be perfectly in frame with the rest of the mRNA, the exon containing the camelid CH1 domain for IgG2 and IgG3 gets spliced out and the resulting IgG heavy chain is devoid of the CH1 domain. The skipped CH1 exon does contain a Cys208Ser mutation that renders a crucial internal disulphide bridge impossible. It is thus possible that if the CH1 exon would be translated, it may eventually still not be able to form a stable domain, which suggests that the exon skip was the only evolutionary option. Nonetheless, the Cys208Ser may also have been introduced after the silencing of the CH1 exon occurred [68]. As a result of the absence of the CH1 domain, the chaperone protein BiP cannot bind the heavy chain IgG and no light chain will be recruited before the heavy chain folds into its final, lowest free energy conformation and is released through the ER secretory pathways [71]. A 700-Å² hydrophobic area on the camelid VH domain, which is normally covered by the variable domain of the light chain (VL), contains several crucial mutations and non-destructive side-chain rotations to greatly reduce the hydrophobicity [67,72], which allows the folded heavy chain only antibody to remain functional and not succumb to the fate of heavy chain disease mentioned above. Once again, it is uncertain whether these mutations are an evolutionary driver or rather an evolutionary result of the CH1 exon skip. Beside the evolutionary drive behind the genetic method, i.e. which genetic fact occurred first, the evolutionary reason for the general occurrence of heavy chain antibodies is an unsolved mystery, especially considering the co-occurrence of this type of antibody in various completely different animals (e.g. in camelidae [73] but also in cartilaginous fish [74–76]). In a review by Flajnik *et al.* three possible explanations have been offered: First it could have been used by a virus as a co-receptor for infection of B lymphocytes, causing light chain deletion. Second, light chains could be causative of amyloidosis, and thus its disappearance could be beneficial. And third, it could have arisen as a means to reach less accessible epitopes [75,77]. Regardless of the genetic evolutionary background, if one is to create a method for *in silico*, *de novo* VHH design, these crucial mutations, especially the ones in the formerly hydrophobic VH-VL interface area, are not to be meddled with.

all other compounds must follow either carrier-mediated influx (e.g. for glucose and amino acids), or receptor- or adsorptive mediated transcytosis (e.g. for transferrin and insulin) [42,44].

Since the VHH is, at on average 12-15 kDa, far larger than 600 Da, transport across the BBB must happen via active transport, i.e. specific receptor- or nonspecific absorptive-mediated trans-

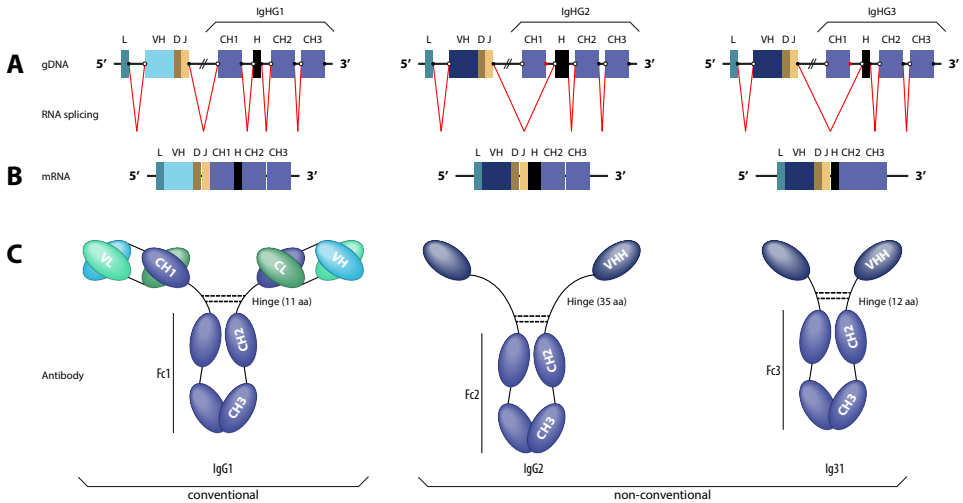


Figure 6.1. Members of the camelid family have three circulating IgG isoforms (A). Two of these – IgG2 and IgG3 – lack the CH1 domain in the messenger RNA (mRNA), due to an exon skip during splicing caused by a point mutation in the 3' splice site recognition sequence of that exon (B). Due to the lack of the CH1 domain, the light chain is not recruited to complement the IgG, and as a result, the final IgG2 and IgG3 antibodies are heavy chain only antibodies (C). Specific mutations in the variable domain of these IgGs prevent exposure of hydrophobic residues to the environment and allow IgG2 and IgG3 to function as complete, though non-conventional antibodies. L: leader sequence for sorting the protein into the correct secretory pathway; D and J: part of the Variable, Diversity and Joint region which allows for somatic recombination leading to the diversity of antibody repertoires; H: hinge region. The figure has been modelled after data and figures from IMGT[®], the international ImMunoGeneTics information system[®] <http://www.imgt.org> (founder and director: Marie-Paule Lefranc, Montpellier, France) under permission of a general academic licence.

cytosis. This hypothesis is corroborated by the finding that VHH-ni3A when tested for *in vitro* BBB passage, could cross the *in vitro* BBB model only at 37°C and not at 4°C [28]. Furthermore, the finding that VHH with a high isoelectric point (pI) of around 9.4 were able to cross the BBB *in vivo*, while those that have a lower pI of around 7.7 do not, suggests that the presence of positive charges on the surface of the VHH, at physiological pH, are required for transcytosis [45]. This could be indicative that the transport of VHH is dependent on the negatively charged clathrin-coated pits, which are particularly enriched in the brain endothelium compared to peripheral endothelia and are the location to which cell surface receptors are generally recruited [46]. This is furthermore confirmed for a VHH specifically selected for *in vitro* and *in vivo* BBB passage, VHH-Fc5, which colocalizes with clathrin-coated pits and vesicles in human cerebral endothelial cells in culture [47]. It is not completely certain what receptor is responsible for the transcytosis of FC5, although over the years the $\alpha(2,3)$ -sialoglycoprotein receptor and the TME-M30A receptor have been put forward as the putative candidate by the same research group [47–49]. Evidence has solely been provided from *in vitro* research, and while VHH-FC5 has been used to shuttle other compounds effectively into the brain, currently no data is publically available showing the $\alpha(2,3)$ -sialoglycoprotein receptor, nor TMEM30A, as the BBB transporter of VHH *in vivo* [50]. It would be of monumental importance to determine, or confirm, which

receptor is required for the active transport of VHH across the BBB *in vivo*, with these receptors as primary candidates.

Although peripheral injection has reportedly led to cerebral uptake for some VHH, previous results for VHH-pa2H showed insufficient uptake *in vivo*, combined with a blood half-life of less than 20 minutes. The VHH gets rapidly cleared via the renal pathway [11]. There is no reason to assume the anti BACE1 VHH B3a will behave differently, especially given its low pI, see Table 6.1. To overcome this barrier, and to answer the second main question of this thesis, the studies described in this work explored various alternative delivery methods, i.e. intracerebral injection, liposomal delivery, elongation of the blood half-life and viral delivery.

Intracerebral injection

The BACE1 inhibitory VHH-B3a has a theoretical pI of 7.63, significantly lower than the recommended pI of 9.4 (Table 6.1), so it is not expected to cross the BBB via nonspecific adsorptive mediated transcytosis in the clathrin-coated pits and vesicles. Instead, to get VHH-B3a into the brain, an invasive injection straight into one of the cerebral ventricles was chosen. Although the method is technically challenging, correct injection leads to successful and widespread delivery, as was evident by both the *in vivo* and *ex vivo* imaging of the IRD800 labeled VHH (Figure 2.6 in chapter two) and the measured effect of the VHH on A β production (Figure 2.7). Efflux of the VHH was limited in so far that at least 24 hours after injection, the VHH was still measurable throughout the brain. However, for various reasons, intracerebral injections are not necessarily a sustainable method for long-term treatment of AD. For example, murine intracerebral injections are limited to 2-10 μ l volumes. As a result, to achieve a relevant concentration of VHH throughout the brain – which for VHH-B3a is approximately 1 μ M – the concentration of VHH to be injected is necessarily very high, i.e. 500 μ M, or approximately 6-7 mg/ml. Depending on the VHH in question, at such high concentrations the VHH may start to form aggregates and may lose its desired characteristics and may no longer be suitable for intracerebral injection. For regular applications, a therapeutic cerebral concentration of 1 μ M may be difficult, if not impossible, to achieve. It is theoretically possible to lower the VHH concentration in the solution and repeat the injections multiple times to eventually achieve therapeutically relevant concentrations. However, the increased invasiveness of the treatment may be difficult to justify. Furthermore, depending on the actual efflux rate of the VHH from the brain into the periphery, it may not even be possible to sufficiently reduce the concentration of the injectable VHH, while staying within reasonable injection intervals. Delivering the VHH directly into the cerebral spinal fluid (CSF) via an outlet catheter from an implantable reservoir or pump may be preferred over repeated injections. However, CSF delivery is not necessarily the most ideal route. Although VHH-B3a was present throughout the brain, it may

Table 6.1. List of characteristics of studied VHHs. In general, most VHH have a theoretical pI around 8 to 10, an amino acid count between 120 and 130 and a molecular weight around 13 to 15 kDa. The addition of a hexahistidine (6his) and myc tag increases the size with a little over 2.5 kDa or 15-20 amino acids and lowers the pI slightly. The addition of a VSV and 6his tag has the same general effect, albeit a little less pronounced. The addition of the Fc tag and especially the addition of the EmGFP tag reduces the pI significantly, while the size of the VHH construct more than doubles. The theoretical pI was calculated using the ExPASy bioinformatics resource Portal program ProtParam, based on the guidelines described by Bjellqvist *et al.* [51].

VHH	Theoretical pI	AA	MW (kDa)
pa2H	9.86	120	13.000
pa2H-6his-myc	9.26	146	15.735
pa2H-Fc	8.96	351	38.856
pa2H-EmGFP	7.15	362	40.094
Htt7F4	5.29	130	14.058
Htt7F4-vsv-6his	6.57	147	16.202
Htt7F4-EmGFP	5.64	372	41.151
B1a	9.47	19	14.156
B3a	7.63	125	13.437
B5a	8.97	124	13.313
FC5	9.23	124	13.447
MCS-EmGFP	5.71	257	28.596
panE	9.56	120	12.884
panE-vsv-6his	9.47	137	15.029
panE-6his-myc	8.64	140	15.206
ni3A	9.56	126	13.834
ni3A-vsv-6his	9.46	143	15.978
va1G	7.80	148	15.621
pa4D	9.46	139	15.586
va2E	8.97	119	13.052
vaE2	8.62	126	13.895
ni8B	9.93	126	13.687

not necessarily have penetrated efficiently enough into the cortex [52]. CSF is found in the subarachnoid space, the ventricles and within the brain parenchyma in an area known as the Virchow Robin space, the area surrounding blood vessels that penetrate into the parenchyma. The Virchow Robin space gets obliterated, however, at the level of the capillary bed, restricting the CSF from reaching the deepest levels of the NVU [53]. As the cerebral vasculature has the largest, and most complete, interface with the rest of the brain (12-20 m² in the average adult human brain), and the one allowing for the shortest diffusion distance to neurons, a peripheral approach would still be preferred over CSF delivery [42]. Therefore, **chapters three and four** aim at methods to deliver VHH-pa2H from the blood circulation into the brain.

Liposomal delivery

In **chapter three**, VHH-pa2H is encapsulated in GSH-PEG liposomes. GSH-PEG liposomes are glutathione-targeted and have previously been able to transfer small molecules across the BBB [54–56]. However, the use of GSH-PEG liposomes as encapsulating BBB-crossing carriers for bigger, functional proteins had not yet been demonstrated. In **chapter three** we show that it is possible to target VHH towards the murine brain using these liposomes. Once VHH-pa2H enters the parenchyma, it remains significantly longer in the brain of APP/PS1 mice compared to wildtype mice. The main difference between the APP/PS1 mice and the wildtype littermates is the presence of A β depositions in the former. It strongly suggests that VHH-pa2H is able to enter the brain and anchors onto the deposits if present, while it is rapidly removed again should the A β deposits not be there.

The rapid removal of VHH-pa2H from the wildtype brain is an interesting contrast with the observation found for the anti-BACE1 VHH-B3a, which stays around in the wildtype brain for at least 24 h, even though it does get slowly removed over time. A straightforward explanation could be that VHH-B3a binds ubiquitously expressed BACE1 on the cell surface of neurons, regardless of the presence of amyloid plaques. However, it is possible that the low pI of VHH-B3a hampers its interaction with the BBB transport receptor in the clathrin-coated pits on the abluminal side of the BBB, while VHH-pa2H is able to interact with the receptor and does experience efflux if not bound to plaques in the parenchyma. As VHH-pa2H, without any tags such as myc, vsv or hexahistidine, has a theoretical pI of around 9.86, while VHH-B3a has a theoretical pI of around 7.63, this explanation would match with the theory that the VHH must have a pI of above 9.4 to transfer across the BBB, albeit in efflux direction in this case. One way to address the question whether the lack of efflux is due to binding to ubiquitous BACE1 or due to another reason, is to inject VHH-B3a directly into the brains of BACE1 knockout animals as a control next to wildtype littermates. It is important to understand the mechanism behind the difference in observed efflux, as the rapid removal of nonbound VHH can be either beneficial or a hindrance depending on the intended use of the VHH. The rapid efflux of nonbound VHH-pa2H can be considered beneficial, especially if the VHH is to be employed as a marker for brain imaging, in which this effect will increase the signal-to-noise ratio of the VHH that is bound to the plaques [57]. However, when a prospective VHH must rather stay around in the brain, in order to continuously interfere with enzymatic activity, as is the case for VHH-B3a, then retention during reduced enzyme presence can be required.

Interestingly, only one of the two GSH-PEG liposomal formulations was able to shuttle VHH-pa2H into the brain, i.e. GSH-PEG EYPC and not GSH-PEG DMPC. This was observed despite the fact that the blood half-life for the GSH-PEG DMPC encapsulated VHH-pa2H was increased compared to the non-encapsulated VHH, albeit less than for the GSH-PEG EYPC li-

posomal formulation. The exact reason behind this difference was not clear. The two liposomal formulations differ slightly in chemical composition, but the size of the particles was highly similar. It is possible that the GSH-PEG DMPC liposomes are less stable than the GSH-PEG EYPC when loaded with protein fragments in an *in vivo* setting. It justifies optimizing the formulation of the liposomes for the *in vivo* use of encapsulated proteins such as VHH-pa2H, increasing *in vivo* stability and thereby possibly increasing the delivery of the antibody fragment into the brain even further. Another way to increase delivery might be to increase the concentration of the VHH inside the liposomes. In the experiments described in **chapter three**, VHH-pa2H had a maximum concentration of less than 0.4 mg per ml. While keeping in mind the objections against too heavily concentrated VHH solutions addressed before, 0.4 mg per ml is well below the critical concentration for VHH-pa2H, and increasing the pay-load of the liposomes will likely increase the yield of VHH crossing the BBB.

The use of the liposomes increases the retention of the VHH in the blood, but not necessarily the exposure time of the VHH to the BBB. It stands to reason that the increased signal in the blood over time comes solely from encapsulated VHH, and that as soon as the VHH is released from the liposome, the normal kinetics for non-tagged VHH come into play, yielding rapid renal clearance. The increased BBB transport is either the result of complete carriage of the liposome containing the VHH over the BBB, or the creation of a very local increased concentration of VHH at the BBB as the liposomes accumulate at the luminal side due to their glutathion targeting. For increased exposure of the VHH to the BBB, the VHH needs to be altered. For example, as described in **chapter four**, by the fusion of the VHH to the crystalizable fraction of the IgG tail, the Fc.

Fc-fusion

In **chapter four**, VHH-pa2H is fused to a human IgG₁ Fc tail. Doing so increases the size of the VHH above the renal cut-off of 65 kDa, and additionally allows for recirculation by the neonatal Fc receptor (FcRn), both characteristics aimed to increase the blood half life of the VHH. By increasing the blood half life, the VHH has, theoretically, more time to interact at the BBB, and thus more time to engage in active transport into the brain. Indeed, 48 hours after intravenous injection, the amount of VHH-pa2H-Fc fusion protein in the blood was significantly higher in both APP/PS₁ and wildtype mice compared to non Fc-fused VHH-pa2H. However, brain uptake of the fusion VHH was not higher in the transgenic mice compared to the wildtypes. In **chapter three** it was already determined that once the VHH gets into the brain, it will bind amyloid depositions if present. The fusion of the Fc tail to VHH-pa2H did not hamper its ability to bind amyloid depositions in cryosections, and therefore there is no reason to assume that the fusion VHH would not bind the amyloid plaques in the brains of the APP/PS₁ mice if it would

have gotten past the BBB. It is therefore clear that VHH-pa2H-Fc, despite the increased time that it has spend in the circulation, did not fully cross the BBB into the murine brain. There are multiple possible explanations for this observation. First and foremost, the addition of the Fc tail may have reduced the propensity of the VHH to cross the BBB in itself. The theoretical pI of VHH-pa2H, already not ideal, becomes even lower due to the addition of the tail (see Table 6.1). Furthermore, the increased molecular weight of the construct, on one hand the necessary trick to keep the VHH longer in the bloodstream, may on the other hand be a cause for steric hindrance, preventing adequate interaction with whichever transporter is normally recruited to shuttle the VHH into the brain. And finally, the interaction of the VHH-Fc fusion protein with the FcRn not only recycles the construct in the periphery, it may also be responsible for the directed efflux of IgG from the brain parenchyma into the blood, which may mean that transported VHH immediately gets removed, even before it reaches the extracellular A β depositions [58–60]. Secondly, despite the increased presence of the VHH in the blood and thus its increased presentation to the BBB, VHH-pa2H itself may not be the ideal candidate to cross the barrier from the blood into the brain, regardless of its tail. A study by Farrington *et al.* showed how the fusion of an Fc tail to their VHH-FC₅ yielded similarly increased blood retention and reported that the fusion construct was able to drag more of an analgesic opioid peptide into the brain compared to controls, as was evident in an attenuated pain response in male Wistar rats. However, it must be noted that the concentration of VHH-FC₅ used in that study was significantly higher than what was used for VHH-pa2H-Fc. Increasing the amount of VHH-pa2H-Fc to 25 mg/kg per injection may help to increase BBB passage. But, to increase the presence of VHH-pa2H in the parenchyma beyond any doubt a third option was explored, which takes full advantage of the small size and incredible stability and foldability of the single domain antibody fragment, delivery via adeno associated virus (AAV) directly inside the brain.

Viral delivery

In **chapter five**, the genetic code of VHH-pa2H is delivered to the neuronal cells via means of adeno associated virus (AAV). The transduced cells in the brain subsequently produce the VHH themselves, continuously replenishing any effluxed VHH. A C-terminally fused Emerald Green Fluorescent Protein (EmGFP) allowed for real-time *in vivo* monitoring of the longitudinal effect of the VHH-EmGFP construct through a permanent cranial window. The results from the longitudinal study suggests that the tested VHH-pa2H may have preventive characteristics against A β accumulation. However, acute effects on pre-existing A β burden was not observed.

AAV is ideally suited for the *in vivo* delivery of VHH constructs. The small size of the VHH, at less than 600 bp, stays well within the packaging limits of AAV, i.e. 4.7 kb between the Inverted Terminal Repeat elements.

There were some interesting observations in this study. First of all, VHH-pa2H-EmGFP was actively expressed in and secreted from standard HEK293T cells in cell culture. The secreted fusion protein retained both its high specificity for A β depositions provided by VHH-pa2H and the bright fluorescence of the EmGFP. As a result, brief exposure to cultured medium from the cells was sufficient to label amyloid plaques and CAA in both human and murine brain cryosections with the fluorescent EmGFP visible under both a standard fluorescent microscope as well as under the multiphoton microscope. Not only did this reduce the duration of the protocol for staining AD/CAA positive material from multiple days down to a few hours, it also provides any research lab that has access to a standard cell culture set-up, with an affordable in-house and on demand, inexhaustible production line for anti-A β immunofluorescence. Furthermore, there is no reason to expect that this procedure of functionally secreted VHH-EmGFP cannot be translated to other VHH and other fluorescent biomolecules.

Secondly, the VHH-EmGFP delivered as AAV constructs directly after birth, were not expressed within the first three weeks after injection. This observation of delayed onset of ubiquitous expression within transduced cells was also observed in the cell culture. This delay hampered viability of *in vitro* cellular studies, as cells reach full confluency before a signal is detected. However, for the purpose of continuous and sustained delivery of VHH to the parenchyma in the *in vivo* settings, the delay is not an issue. In fact, in the case of the mice which received a cranial window to observe the VHH expression and its effect on amyloid depositions in real time, the delay allowed for ample time to install the window and allow the animals some time to recover before the first imaging session was to take place.

Expression of the VHH-pa2H-EmGFP construct within neuronal cells in the mice that were injected at five months of age and sacrificed up to seven months later was no longer detected. This was in stark contrast with the mice that were injected as adults and sacrificed up to three months later. Nonetheless, while VHH-pa2H-EmGFP was no longer visibly produced, it was very visibly present on the A β depositions in the parenchyma and around the vasculature in the “five months old mice”. This observation once more reiterates the potency of VHH-pa2H to bind amyloid plaques. Unfortunately, it also shows that VHH-pa2H may not be able to remove amyloid plaques once they are formed.

In recent years pre-clinical and clinical research into gene-therapy as treatment of genetically inherited diseases, certain types of cancer, Parkinson's disease and even HIV has grown exponentially [61–64]. VHH can play a major role in this development, as demonstrated in **chapter five** of this thesis.

Side effects of VHH alterations

Whether the addition of fusion proteins or chelators affects the affinity or the function of the VHH is something that needs to be examined in much greater detail. As seen in this thesis, creating a VHH-EmGFP allows for single step immunofluorescence on cryosections and allows for efficient *in vivo* monitoring. The addition of the Fc tail to the VHH immediately led to a significant increased retention of the VHH in the periphery of the mice. However, it is crucial to determine the effect of the fused protein on the physiological functions of the VHH. For example, it is interesting to note that the recognition pattern for VHH-pa2H-Fc and VHH-pa2H-EmGFP are very similar but not exactly the same. It may have to do with the brightness of EmGFP, or the need for secondary antibodies when using VHH-pa2H-Fc, but even when these factors are taken into account the Fc fused VHH seems to recognize a broader pattern around the parenchymal plaques compared to the more dense pattern obtained by the EmGFP fusion construct. The fact that the control VHH, VHH-Htt7F4, in both cases does not associate with the amyloid depositions, suggests that the binding of VHH-pa2H is specific; it is not a random sticky association of the fusion proteins to the amyloidosis as a result of any addition to any VHH. Neither do the additions create nonspecific association to other structures in the brain, such as the non-amyloidogenic vasculature, as none of the anti-A β VHH fused to either Fc or EmGFP show any binding on control cryosections derived from healthy age-matched donors. Therefore, the different patterns between VHH-pa2H-Fc and ss-VHH-pa2H-EmGFP must be driven by the effect that the fusion moiety has on the binding specificity of the VHH itself. Whether it is caused by the steric difference between the VHH and its fusion protein, e.g. EmGFP is twice as big as the VHH itself, or the difference in pI or other molecular effects, is a topic that has not been explored in this thesis, but warrants further investigation, especially to solidify the use of VHH as mainstream alternatives for current conventional antibody applications.

However, from a practical point of view, to determine to what extent this effect alters the function of the VHH is ultimately relevant in particular to the already selected and accepted VHH. Merely to understand and accept that the addition of, for example, EmGFP may alter the function of VHH, is sufficient if one changes the way the VHH are selected. The current generation of VHH has been selected by looking for a VHH that binds immobilized A β and once that had been done, we started to look what else we could do with them. Yet, if one is to ultimately apply the VHH in combination with a fusion protein, such as EmGFP, it would make more sense to display not a VHH, but a VHH-EmGFP to the antigen of interest. Now that it is known that the VHH can easily maintain such an addition, there is no reason not to create a library in which the pUC5071 phagemid vector is updated to pUC5072: where EmGFP is automatically inserted C-terminally to the VHH, or pUC5073: VHH-Fc. Once more, all these factors can still be taken into account in the envisioned *in silico* design of VHH.

Outlook for VHH

VHH are the antibodies of the future and the future is now. The antibody market, especially for therapeutical purposes, is rapidly expanding. Monoclonal antibodies dominate the top-10 billion dollar generating blockbuster drug list, expecting to grow in market value from 150 billion USD in 2011 to over 250 billion USD in 2017 [78]. Meanwhile, VHH have all the benefits of conventional antibodies, complemented with the intrinsic characteristics of the protruding CDR3 loop. At a practical, academic level, they are easily produced in standard laboratory settings, providing an unlimited supply of fresh, ready-to-use antibody compound for standard characterization of proteins for which otherwise expensive full size antibodies need to be obtained. Sharing VHH among academics can be as convenient as maintaining a public database. Researchers can then simply synthesize a 600 bp dna fragment, a commercial outsourceable venture that can cost less than 150 USD in 2016, which is less than most off-the-shelf conventional antibodies. It even allows researchers to create their own VHH, add their own tags, be it tags to purify like 6-HIS or Flag or tags to detect, like myc, V5, or fluorophores like EmGFP or mCherry. Furthermore, it is then possible to easily combine the VHH into biheads or pentamers with VHH that have different, complementary characteristics. The commercialization of VHH selection and production is expected to rapidly increase in the coming years, as many of the patents associated with heavy-chain only antibodies, mostly in the hands of the biopharmaceutical company Ablynx, will expire in Europe and the USA between 2013 and 2017 [79].

The versatility of the antibody fragments, as demonstrated in this thesis, is unmatched by conventional IgGs. The only downside of many selected VHH is their difficulty to recognize linearized epitopes in applications such as Western blot. However, some VHH are able to recognize antigens presented on Western blot membranes (M. Schut, unpublished data) and the generally observed reluctance to bind linearized epitopes is possibly a result of the method of selection, which usually involves immobilized, correctly folded antigens, in phage display. When one would like to enrich for VHH that are able to recognize linearized epitopes, selection procedures can be adjusted accordingly and there is no reason to expect that no suitable VHH can be found. As stated repeatedly before, improved use of *in silico* and *de novo* VHH selection can be of use in this regard.

Within the field of dementia research, even specifically within AD research, a wealth of opportunities await the further development of the llama antibody fragments. The VHH discussed throughout the majority of this thesis, VHH-pa2H, has been focused on the removal of existing amyloid beta peptides, either while forming or after forming amyloid plaques. However, AD may be fought in a plethora of different ways. As discussed and touched upon in **chapter two**, a therapy may aim to interfere in the production of the A β peptide itself by addressing the

cleavage of the precursor protein by BACE1 secretase, forcing the processing of APP into the non-amyloidogenic pathway.

Alternatively, one could address the initial presentation of APP to the secretases, rather than interfering with their overall function. Secretase activity is not evenly distributed throughout neurons, as each of the involved enzymes is a target of highly specific polarized sorting events. Furthermore, APP trafficking throughout the neuronal cells is mediated by sorting receptors such as Sortilin and SorLA [80]. SorLA-APP interaction prevents APP from routing into late endosomes where proteolytic cleaves occurs [81–83]. As a result, less APP will be cleaved into A β , leading to a reduced amyloid phenotype in mice [84–86]. Developing a VHH that is able to stimulate this process, similarly to the stimulatory effect observed for VHH-B1a and VHH-B5a, may help to reduce the presence of A β by reducing the processing of APP altogether. As less APP will be cleaved, it automatically means less sAPP α will be created as well. What the effect of this reduction will be on the brain and the rest of the body, will need to be elucidated [87]. However, it is a distinct possibility that the overly abundant presence of A β is rather a symptom than a cause of AD, especially for the sporadic variant, and a VHH can possibly be developed that addresses the root cause of the problem, once elucidated.

Finally, as discussed before, VHH can be employed not only as therapeutic entities, but also as diagnostic tools. The development of the fluorescently tagged VHH-EmGFP may help in this regard, but for this aspect both BBB passage and *in vivo* fluorescent detection in humans needs to be improved. Radioactively labeled VHH, such as used in **chapter three**, can be a better alternative, but even then one must keep in mind that detecting absolute A β burden may not be the ultimate way to diagnose AD and especially AD progression, but merely establish whether an individual is A β positive [88,89]. However, the application of VHH is not limited to the murine AD brain; the theoretical possibilities are endless. In fluorescence guided surgery, one can employ a VHH-EmGFP tagged with DTPA-In^m to be used in the same way as various similar hybrid tracers are currently used for sentinel node detection [90]. However, like conventional antibodies, the VHH can be selected for any targetable epitope, while, unlike conventional antibodies, remain within reasonable production costs even at the high doses necessary to allow for intraoperative imaging of the fluorescent moiety. In any diagnostics one can create a chip where you spot your target, such as a drop of patient blood or CSF, a skin or muscle biopsy, and subsequently flow an array of differently fluorescent VHH fusions, e.g. VHH-EmGFP, VHH-YFP, VHH-mCherry, and read-out the final fluorescent spectrum to obtain immediate, single-step, quantitative diagnostic read-outs, akin to a modified ELISA [91–93]. The stability of VHH may make them suitable for harsh conditions such as in (tropical) field hospitals, which can be crucial for applications such as the detection of mosquito-borne diseases like malaria, Zika, and dengue, other viruses and parasites.

Overall conclusion.

The two main questions in this thesis are whether the VHH can be used as an anti-AD therapeutic and how do we get the VHH into the brain most efficiently. VHH-pa2H and VHH-B3a do have the potential to be used as therapeutic, perhaps in combination therapy, but are not sufficiently potent by themselves to revert or inhibit AD progression once the disease has a foothold in the brain. However, VHH in general should be able to be developed into an efficient therapeutic, but the ideal VHH still needs to be found, or designed. For this, in silico VHH design should receive more attention in future years. To get the VHH into the brain, gene-therapy seems to be the easiest and most efficient route, fully utilizing the advantage that VHH have over other antibody approaches, namely the short, single domain, antigen interacting fragment, translated from a single gene fragment, which, even with the fusion to a large fluorescent protein or other tag, can still be delivered via the small, easy to create and deploy, adeno associated virus.

REFERENCES

1. Scheltens, P., Blennow, K., Breteler, M. M. B., de Strooper, B., Frisoni, G. B., Salloway, S. & Van der Flier, W. M. Alzheimer's disease. *Lancet* (London, England) 388(10043):505–17 (2016).
2. Ghosh, A. K., Brindisi, M. & Tang, J. Developing β -secretase inhibitors for treatment of Alzheimer's disease. *J. Neurochem.* 120 Suppl(SUPPL. 1):71–83 (2012).
3. Thakker, D. R., Sankaranarayanan, S., Weatherspoon, M. R., Harrison, J., Pierdomenico, M., Heisel, J. M., Thompson, L. a., Haskell, R., Grace, J. E., Taylor, S. J., et al. Centrally Delivered BACE1 Inhibitor Activates Microglia, and Reverses Amyloid Pathology and Cognitive Deficit in Aged Tg2576 Mice. *J. Neurosci.* 35(17):6931–6936 (2015).
4. Vassar, R. BACE1 inhibitor drugs in clinical trials for Alzheimer's disease. *Alzheimers. Res. Ther.* 6(9):1–14 (2014).
5. May, P. C., Willis, B. A., Lowe, S. L., Dean, R. A., Monk, S. A., Cocke, P. J., Audia, J. E., Boggs, L. N., Borders, A. R., Brier, R. A., et al. The potent BACE1 inhibitor LY2886721 elicits robust central A β pharmacodynamic responses in mice, dogs, and humans. *J. Neurosci.* 35(3):1199–210 (2015).
6. Yan, R. Stepping closer to treating Alzheimer's disease patients with BACE1 inhibitor drugs. *Transl. Neurodegener.* 5:13 (2016).
7. Evin, G. Future Therapeutics in Alzheimer's Disease: Development Status of BACE Inhibitors. *BioDrugs* 30(3):173–94 (2016).
8. Panza, F., Seripa, D., Solfrizzi, V., Imbimbo, B. P., Lozupone, M., Leo, A., Sardone, R., Gagliardi, G., Lofano, L., Creanza, B. C., et al. Emerging drugs to reduce abnormal β -amyloid protein in Alzheimer's disease patients. *Expert Opin. Emerg. Drugs* 11–15 (2016). doi:10.1080/14728214.2016.1241232
9. Rutgers, K. S., van Remoortere, A., van Buchem, M. A., Verrips, C. T., Greenberg, S. M., Bacskai, B. J., Frosch, M. P., van Duinen, S. G., Maat-Schieman, M. L. & Van der Maarel, S. M. Differential recognition of vascular and parenchymal beta amyloid deposition. *Neurobiol. Aging* 32(10):1774–1783 (2009).
10. Head, E., Lott, I. T., Wilcock, D. M. & Lemere, C. A. Aging in Down Syndrome and the Development of Alzheimer's Disease Neuropathology. *Curr. Alzheimer Res.* 13(1):18–29 (2016).
11. Nabuurs, R. J. A., Rutgers, K. S., Welling, M. M., Metaxas, A., de Backer, M. E., Rotman, M., Bacskai, B. J., van Buchem, M. A., van der Maarel, S. M. & van der Weerd, L. In vivo detection of amyloid- β deposits using heavy chain antibody fragments in a transgenic mouse model for Alzheimer's disease. *PLoS One* 7(6):e38284 (2012).
12. Yardehnavi, N., Behdani, M., Pooshang Bagheri, K., Mahmoodzadeh, A., Khanahmad, H., Shahbazzadeh, D., Habibi-Anbouhi, M., Ghassabeh, G. H. & Muyldermans, S. A camelid antibody candidate for development of a therapeutic agent against Hemiscorpius lepturus envenomation. *FASEB J.* 28(9):4004–14 (2014).
13. Hmila, I., Abdallah R, B. A. Ben, Saerens, D., Benlasfar, Z., Conrath, K., Ayeb, M. El, Muyldermans, S. & Bouhaouala-Zahar, B. VHH, bivalent domains and chimeric Heavy chain-only antibodies with high neutralizing efficacy for scorpion toxin AahI. *Mol. Immunol.* 45(14):3847–3856 (2008).
14. Gad, W., Ben-Abderrazek, R., Wahni, K., Vertommen, D., Muyldermans, S., Bouhaouala-Zahar, B. & Messens, J. Wheat germ in vitro translation to produce one of the most toxic sodium channel specific toxins. *Biosci. Rep.* 34(4) (2014).
15. Cardoso, F. M., Ibañez, L. I., Van den Hoecke, S., De Baets, S., Smet, A., Roose, K., Schepens, B., Descamps, F. J., Fiers, W., Muyldermans, S., et al. Single-domain antibodies targeting neuraminidase protect against an H5N1 influenza virus challenge. *J. Virol.* 88(15):8278–96 (2014).
16. Garaicoechea, L., Aguilar, A., Parra, G. I., Bok, M., Sosnovtsev, S. V., Canziani, G., Green, K. Y., Bok, K. & Parreño, V. Llama nanoantibodies with therapeutic potential against human norovirus diarrhea. *PLoS One* 10(8):e0133665 (2015).

17. Dolk, E., van der Vaart, M., Lutje Hulsik, D., Vriend, G., de Haard, H., Spinelli, S., Cambillau, C., Frenken, L. & Verrips, T. Isolation of llama antibody fragments for prevention of dandruff by phage display in shampoo. *Appl. Environ. Microbiol.* 71(1):442–50 (2005).
18. Scheuplein, F., Rissiek, B., Driver, J. P., Chen, Y.-G., Koch-Nolte, F. & Serreze, D. V. A recombinant heavy chain antibody approach blocks ART2 mediated deletion of an iNKT cell population that upon activation inhibits autoimmune diabetes. *J. Autoimmun.* 34(2):145–54 (2010).
19. Impagliazzo, A., Tepper, A. W., Verrips, T. C., Ubbink, M. & van der Maarel, S. M. Structural basis for a PABPN1 aggregation-preventing antibody fragment in OPMD. *FEBS Lett.* 584(8):1558–64 (2010).
20. Plant, L. D., Boyle, J. P., Smith, I. F., Peers, C. & Pearson, H. a. The production of amyloid beta peptide is a critical requirement for the viability of central neurons. *J. Neurosci.* 23(13):5531–5535 (2003).
21. Pearson, H. A. & Peers, C. Physiological roles for amyloid beta peptides. *J. Physiol.* 575(Pt 1):5–10 (2006).
22. Dmitriev, O. Y., Lutsenko, S. & Muyldermans, S. Nanobodies as Probes for Protein Dynamics in Vitro and in Cells. *J. Biol. Chem.* 291(8):3767–75 (2016).
23. Ignatovich, O., Jaspers, L., Tomlinson, I. M. & de Wildt, R. M. T. Creation of the large and highly functional synthetic repertoire of human VH and V λ domain antibodies. *Methods Mol. Biol.* 911:39–63 (2012).
24. Olichon, A. & de Marco, A. Preparation of a naïve library of camelid single domain antibodies. *Methods Mol. Biol.* 911:65–78 (2012).
25. Pepers, B. A., Schut, M. H., Vossen, R. H., van Ommen, G.-J. B., den Dunnen, J. T. & van Roon-Mom, W. M. Cost-effective HRMA pre-sequence typing of clone libraries; application to phage display selection. *BMC Biotechnol.* 9(1):50 (2009).
26. Pardon, E., Laeremans, T., Triest, S., Rasmussen, S. G. F., Wohlkönig, A., Ruf, A., Muyldermans, S., Hol, W. G. J., Kobilka, B. K. & Steyaert, J. A general protocol for the generation of Nanobodies for structural biology. *Nat. Protoc.* 9(3):674–93 (2014).
27. Klooster, R., Rutgers, K. S. & van der Maarel, S. M. Selection of VHH antibody fragments that recognize different A β depositions using complex immune libraries. *Methods Mol. Biol.* 911:241–53 (2012).
28. Rutgers, K. S., Nabuurs, R. J. A., van den Berg, S. A. A., Schenk, G. J., Rotman, M., Verrips, C. T., van Duinen, S. G., Maat-Schieman, M. L., van Buchem, M. A., de Boer, A. G., et al. Transmigration of beta amyloid specific heavy chain antibody fragments across the in vitro blood-brain barrier. *Neuroscience* 190:37–42 (2011).
29. Dorresteyn, B., Rotman, M., Faber, D., Schraivesande, R., Suidgeest, E., van der Weerd, L., van der Maarel, S. M., Verrips, C. T. & El Khattabi, M. Camelid heavy chain only antibody fragment domain against β -site of amyloid precursor protein cleaving enzyme 1 inhibits β -secretase activity in vitro and in vivo. *FEBS J.* 282(18):3618–3631 (2015).
30. Dolk, E., Verrips, T. & de Haard, H. Selection of VHHs under application conditions. *Methods Mol. Biol.* 911:199–209 (2012).
31. Herzig, M. C., Eisele, Y. S., Staufenberg, M. & Jucker, M. E22Q-mutant Abeta peptide (AbetaDutch) increases vascular but reduces parenchymal Abeta deposition. *Am. J. Pathol.* 174(3):722–6 (2009).
32. Yan, J., Li, G., Hu, Y., Ou, W. & Wan, Y. Construction of a synthetic phage-displayed Nanobody library with CDR3 regions randomized by trinucleotide cassettes for diagnostic applications. *J. Transl. Med.* 12(1):343 (2014).
33. Sabir, J. S. M., Atef, A., El-Domyati, F. M., Edris, S., Hajrah, N., Alzohairy, A. M. & Bahieldin, A. Construction of naïve camelids VHH repertoire in phage display-based library. *C. R. Biol.* 337(4):244–9 (2014).
34. Rutten, L., de Haard, H. & Verrips, T. Improvement of proteolytic stability through in silico engineering. *Methods Mol. Biol.* 911:373–81 (2012).
35. Peng, H.-P., Lee, K. H., Jian, J.-W. & Yang, A.-S. Origins of specificity and affinity in antibody-protein interactions. *Proc. Natl. Acad. Sci. U. S. A.* 111(26):E2656–65 (2014).
36. Bergmann, C. C., Lane, T. E. & Stohlman, S. A. Coronavirus infection of the central nervous system: host-virus stand-off. *Nat. Rev. Microbiol.* 4(2):121–32 (2006).

37. Azevedo, F. A. C., Carvalho, L. R. B., Grinberg, L. T., Farfel, J. M., Ferretti, R. E. L., Leite, R. E. P., Jacob Filho, W., Lent, R. & Herculano-Houzel, S. Equal numbers of neuronal and nonneuronal cells make the human brain an isometrically scaled-up primate brain. *J. Comp. Neurol.* 513(5):532–41 (2009).
38. Herculano-Houzel, S. The glia/neuron ratio: How it varies uniformly across brain structures and species and what that means for brain physiology and evolution. *Glia* 62(9):1377–1391 (2014).
39. Han, X., Chen, M., Wang, F., Windrem, M., Wang, S., Shanz, S., Xu, Q., Oberheim, N. A., Bekar, L., Betstadt, S., et al. Forebrain engraftment by human glial progenitor cells enhances synaptic plasticity and learning in adult mice. *Cell Stem Cell* 12(3):342–53 (2013).
40. Prinz, M. & Priller, J. Microglia and brain macrophages in the molecular age: from origin to neuropsychiatric disease. *Nat. Rev. Neurosci.* 15(5):300–12 (2014).
41. Johanson, C. E., Stopa, E. G. & McMillan, P. N. The blood-cerebrospinal fluid barrier: structure and functional significance. *Methods Mol. Biol.* 686:101–31 (2011).
42. Abbott, N. J. Blood-brain barrier structure and function and the challenges for CNS drug delivery. *J. Inherit. Metab. Dis.* 36(3):437–49 (2013).
43. Iadecola, C. & Nedergaard, M. Glial regulation of the cerebral microvasculature. *Nat. Neurosci.* 10(11):1369–76 (2007).
44. Abbott, N. J., Patabendige, A. a K., Dolman, D. E. M., Yusof, S. R. & Begley, D. J. Structure and function of the blood-brain barrier. *Neurobiol. Dis.* 37(1):13–25 (2010).
45. Li, T., Bourgeois, J.-P., Celli, S., Glacial, F., Le Sourd, A.-M., Mecheri, S., Weksler, B., Romero, I., Couraud, P.-O., Rougeon, F., et al. Cell-penetrating anti-GFAP VHH and corresponding fluorescent fusion protein VHH-GFP spontaneously cross the blood-brain barrier and specifically recognize astrocytes: application to brain imaging. *FASEB J.* 26(10):3969–79 (2012).
46. Hervé, F., Ghinea, N. & Schermann, J.-M. CNS delivery via adsorptive transcytosis. *AAPS J.* 10(3):455–72 (2008).
47. Abulrob, A., Sprong, H., Van Bergen en Henegouwen, P. & Stanimirovic, D. The blood-brain barrier transmigration single domain antibody: mechanisms of transport and antigenic epitopes in human brain endothelial cells. *J. Neurochem.* 95(4):1201–14 (2005).
48. Muruganandam, A., Tanha, J., Narang, S. & Stanimirovic, D. Selection of phage-displayed llama single-domain antibodies that transmute across human blood-brain barrier endothelium. *FASEB J.* 16(2):240–2 (2002).
49. Haqqani, A. S., Delaney, C. E., Tremblay, T.-L., Sodja, C., Sandhu, J. K. & Stanimirovic, D. B. Method for isolation and molecular characterization of extracellular microvesicles released from brain endothelial cells. *Fluids Barriers CNS* 10(1):4 (2013).
50. Farrington, G. K., Caram-Salas, N., Haqqani, A. S., Brunette, E., Eldredge, J., Pepinsky, B., Antognetti, G., Baumann, E., Ding, W., Garber, E., et al. A novel platform for engineering blood-brain barrier-crossing bispecific biologics. *FASEB J.* 28(11):4764–4778 (2014).
51. Bjellqvist, B., Hughes, G. J., Pasquali, C., Paquet, N., Ravier, F., Sanchez, J. C., Frutiger, S. & Hochstrasser, D. The focusing positions of polypeptides in immobilized pH gradients can be predicted from their amino acid sequences. *Electrophoresis* 14(10):1023–31 (1993).
52. Bennewitz, M. F. & Saltzman, W. M. Nanotechnology for delivery of drugs to the brain for epilepsy. *Neurotherapeutics* 6(2):323–36 (2009).
53. Brinker, T., Stopa, E., Morrison, J. & Klinge, P. A new look at cerebrospinal fluid circulation. *Fluids Barriers CNS* 11:10 (2014).
54. Rip, J., Chen, L., Hartman, R., van den Heuvel, A., Reijkerker, A., van Kregten, J., van der Boom, B., Appeldoorn, C., de Boer, M., Maussang, D., et al. Glutathione PEGylated liposomes: pharmacokinetics and delivery of cargo across the blood-brain barrier in rats. *J. Drug Target.* 22(5):460–7 (2014).
55. Lindqvist, A., Rip, J., Gaillard, P. J., Björkman, S. & Hammarlund-Udenaes, M. Enhanced brain delivery of the opioid peptide damgo in glutathione pegylated liposomes: A microdialysis study. *Mol. Pharm.* 10(5):1533–1541 (2013).

56. Salem, H. F., Ahmed, S. M., Hassaballah, A. E. & Omar, M. M. Targeting brain cells with glutathione-modulated nanoliposomes: in vitro and in vivo study. *Drug Des. Devel. Ther.* 9:3705–27 (2015).
57. Rotman, M., Snoeks, T. J. A. & van der Weerd, L. Pre-clinical optical imaging and MRI for drug development in Alzheimer's disease. *Drug Discovery Today: Technologies* 8(2–4):e117–e125 (2011).
58. Sand, K. M. K., Bern, M., Nilsen, J., Noordzij, H. T., Sandlie, I. & Andersen, J. T. Unraveling the Interaction between FcRn and Albumin: Opportunities for Design of Albumin-Based Therapeutics. *Front. Immunol.* 5:682 (2014).
59. Schlachetzki, F., Zhu, C. & Pardridge, W. M. Expression of the neonatal Fc receptor (FcRn) at the blood-brain barrier. *J. Neurochem.* 81(1):203–6 (2002).
60. Cooper, P. R., Ciambone, G. J., Kliwinski, C. M., Maze, E., Johnson, L., Li, Q., Feng, Y. & Hornby, P. J. Efflux of monoclonal antibodies from rat brain by neonatal Fc receptor, FcRn. *Brain Res.* 1534:13–21 (2013).
61. Bainbridge, J. W. B., Smith, A. J., Barker, S. S., Robbie, S., Henderson, R., Balaggan, K., Viswanathan, A., Holder, G. E., Stockman, A., Tyler, N., et al. Effect of gene therapy on visual function in Leber's congenital amaurosis. *N. Engl. J. Med.* 358(21):2231–9 (2008).
62. Levine, B. L., Humeau, L. M., Boyer, J., MacGregor, R.-R., Rebello, T., Lu, X., Binder, G. K., Slepishkin, V., Lemiale, F., Mascola, J. R., et al. Gene transfer in humans using a conditionally replicating lentiviral vector. *Proc. Natl. Acad. Sci. U. S. A.* 103(46):17372–7 (2006).
63. LeWitt, P. A., Rezai, A. R., Leehey, M. A., Ojemann, S. G., Flaherty, A. W., Eskandar, E. N., Kostyk, S. K., Thomas, K., Sarkar, A., Siddiqui, M. S., et al. AAV2-GAD gene therapy for advanced Parkinson's disease: a double-blind, sham-surgery controlled, randomised trial. *Lancet. Neurol.* 10(4):309–19 (2011).
64. Allen, P. J. & Feigin, A. Gene-based therapies in Parkinson's disease. *Neurotherapeutics* 11(1):60–7 (2014).
65. Lee, Y. K., Brewer, J. W., Hellman, R. & Hendershot, L. M. BiP and immunoglobulin light chain cooperate to control the folding of heavy chain and ensure the fidelity of immunoglobulin assembly. *Mol. Biol. Cell* 10(7):2209–19 (1999).
66. Wahner-Roedler, D. L. & Kyle, R. A. Heavy chain diseases. *Best Pract. Res. Clin. Haematol.* 18(4):729–746 (2005).
67. Muyldermans, S., Atarhouch, T., Saldanha, J., Barbosa, J. A. & Hamers, R. Sequence and structure of VH domain from naturally occurring camel heavy chain immunoglobulins lacking light chains. *Protein Eng.* 7(9):1129–35 (1994).
68. Nguyen, V. K., Hamers, R., Wyns, L. & Muyldermans, S. Loss of splice consensus signal is responsible for the removal of the entire CH1 domain of the functional camel IGG2A heavy-chain antibodies. *Mol. Immunol.* 36(8):515–524 (1999).
69. Robberson, B. L., Cote, G. J. & Berget, S. M. Exon definition may facilitate splice site selection in RNAs with multiple exons. *Mol. Cell. Biol.* 10(1):84–94 (1990).
70. Comi, G. P., Cialfoni, E., de Silva, H. A., Prella, A., Bardoni, A., Rigoletto, C., Robotti, M., Bresolin, N., Moggio, M. & Fortunato, F. A G+10A transversion at the 5' splice site of intron 69 of the dystrophin gene causing the absence of peripheral nerve Dp116 and severe clinical involvement in a DMD patient. *Hum. Mol. Genet.* 4(11):2171–4 (1995).
71. Nguyen, V. K., Zou, X., Lauwereys, M., Brys, L., Brüggemann, M. & Muyldermans, S. Heavy-chain only antibodies derived from dromedary are secreted and displayed by mouse B cells. *Immunology* 109(1):93–101 (2003).
72. Muyldermans, S., Cambillau, C. & Wyns, L. Recognition of antigens by single-domain antibody fragments: the superfluous luxury of paired domains. *Trends Biochem. Sci.* 26(4):230–235 (2001).
73. Hamers-Casterman, C., Atarhouch, T., Muyldermans, S., Robinson, G., Hamers, C., Songa, E. B., Bendahman, N. & Hamers, R. Naturally occurring antibodies devoid of light chains. *Nature* 363(6428):446–448 (1993).
74. Feige, M. J., Gräwert, M. A., Marcinowski, M., Hennig, J., Behnke, J., Ausländer, D., Herold, E. M., Peschek, J., Castro, C. D., Flajnik, M., et al. The structural analysis of shark IgNAR antibodies reveals evolutionary principles of immunoglobulins. *Proc. Natl. Acad. Sci. U. S. A.* 11(22):8155–60 (2014).

75. Flajnik, M. F. & Dooley, H. The generation and selection of single-domain, v region libraries from nurse sharks. *Methods Mol. Biol.* 562:71–82 (2009).
76. Flajnik, M. F., Deschacht, N. & Muyldermans, S. A case of convergence: why did a simple alternative to canonical antibodies arise in sharks and camels? *PLoS Biol.* 9(8):e1001120 (2011).
77. Smolarek, D., Bertrand, O. & Czerwinski, M. Variable fragments of heavy chain antibodies (VHHs): A new magic bullet molecule of medicine? *Postepy Higieny i Medycyny Doswiadczalnej* 66:348–358 (2012).
78. Kovaleva, M., Ferguson, L., Steven, J., Porter, A. & Barelle, C. Shark variable new antigen receptor biologics - a novel technology platform for therapeutic drug development. *Expert Opin. Biol. Ther.* 14(10):1527–39 (2014).
79. de Marco, A. Biotechnological applications of recombinant single-domain antibody fragments. *Microb. Cell Fact.* 10:44 (2011).
80. Gustafsen, C., Glerup, S., Pallesen, L. T., Olsen, D., Andersen, O. M., Nykjær, A., Madsen, P. & Petersen, C. M. Sortilin and SorLA display distinct roles in processing and trafficking of amyloid precursor protein. *J. Neurosci.* 33(1):64–71 (2013).
81. Andersen, O. M., Reiche, J., Schmidt, V., Gotthardt, M., Spoelgen, R., Behlke, J., von Arnim, C. a F., Breiderhoff, T., Jansen, P., Wu, X., et al. Neuronal sorting protein-related receptor sorLA/LR11 regulates processing of the amyloid precursor protein. *Proc. Natl. Acad. Sci. U. S. A.* 102(38):13461–13466 (2005).
82. Schmidt, V., Sporberr, A., Rohe, M., Reimer, T., Rehm, A., Andersen, O. M. & Willnow, T. E. SorLA/LR11 Regulates Processing of Amyloid Precursor Protein via Interaction with Adaptors GGA and PACS-1. *J. Biol. Chem.* 282(45):32956–32964 (2007).
83. Rohe, M., Hartl, D., Fjorback, A. N., Klose, J. & Willnow, T. E. SORLA-mediated trafficking of TrkB enhances the response of neurons to BDNF. *PLoS One* 8(8):e72164 (2013).
84. Rohe, M., Carlo, A.-S., Breyhan, H., Sporberr, A., Miltz, D., Schmidt, V., Wozny, C., Harmeyer, A., Erdmann, B., Bales, K. R., et al. Sortilin-related receptor with A-type repeats (SORLA) affects the amyloid precursor protein-dependent stimulation of ERK signaling and adult neurogenesis. *J. Biol. Chem.* 283(21):14826–34 (2008).
85. Dodson, S. E., Andersen, O. M., Karmali, V., Fritz, J. J., Cheng, D., Peng, J., Levey, A. L., Willnow, T. E. & Lah, J. J. Loss of LR11/SORLA enhances early pathology in a mouse model of amyloidosis: evidence for a proximal role in Alzheimer's disease. *J. Neurosci.* 28(48):12877–86 (2008).
86. Mehmedbasic, A., Christensen, S. K., Nilsson, J., Rüetschi, U., Gustafsen, C., Poulsen, A. S. A., Rasmussen, R. W., Fjorback, A. N., Larson, G. & Andersen, O. M. SorLA Complement-type Repeat Domains Protect the Amyloid Precursor Protein against Processing. *J. Biol. Chem.* 290(6):3359–3376 (2015).
87. Chasseigneaux, S. & Allinquant, B. Functions of A β , sAPP α and sAPP β : similarities and differences. *J. Neurochem.* 120 Suppl:99–108 (2012).
88. Villemagne, V. L., Klunk, W. E., Mathis, C. a, Rowe, C. C., Brooks, D. J., Hyman, B. T., Ikonomic, M. D., Ishii, K., Jack, C. R., Jagust, W. J., et al. A β Imaging: feasible, pertinent, and vital to progress in Alzheimer's disease. *Eur. J. Nucl. Med. Mol. Imaging* 39(2):209–19 (2012).
89. Klunk, W. E., Engler, H., Nordberg, A., Wang, Y., Blomqvist, G., Holt, D. P., Bergström, M., Savitcheva, I., Huang, G. F., Estrada, S., et al. Imaging Brain Amyloid in Alzheimer's Disease with Pittsburgh Compound-B. *Ann. Neurol.* 55(3):306–319 (2004).
90. KleinJan, G. H., Bunschoten, A., van den Berg, N. S., Olmos, R. A. V., Klop, W. M. C., Horenblas, S., van der Poel, H. G., Wester, H.-J. & van Leeuwen, F. W. B. Fluorescence guided surgery and tracer-dose, fact or fiction? *Eur. J. Nucl. Med. Mol. Imaging* 43(10):1857–1867 (2016).
91. Jiang, W., Cossey, S., Rosenberg, J. N., Oyler, G. A., Olson, B. J. S. C. & Weeks, D. P. A rapid live-cell ELISA for characterizing antibodies against cell surface antigens of *Chlamydomonas reinhardtii* and its use in isolating algae from natural environments with related cell wall components. *BMC Plant Biol.* 14:244 (2014).

92. Fatima, A., Wang, H., Kang, K., Xia, L., Wang, Y., Ye, W., Wang, J. & Wang, X. Development of VHH antibodies against dengue virus type 2 NS1 and comparison with monoclonal antibodies for use in immunological diagnosis. *PLoS One* 9(4):e95263 (2014).
93. Kol, S., Kallehauge, T. B., Adema, S. & Hermans, P. Development of a VHH-Based Erythropoietin Quantification Assay. *Mol. Biotechnol.* 57(8):692–700 (2015).

7

CHAPTER

APPENDICES

SUMMARY

Alzheimer's disease (AD) is the main contributor to the syndrome dementia, one of the major health care concerns in the developed, as well as the aging developing, world. AD is characterized by progressive cognitive impairment and characteristic pathological hallmarks. These hallmarks include aggregates of the protein tau in neurons and of the peptide amyloid beta ($A\beta$) in plaques outside the neurons as well as around the blood vessels in the brain. Currently there is no drug available that can prevent or cure AD. One of the reasons of the difficulty in developing a drug based cure, is the presence of a very strictly regulated barrier between the brain and the circulation; the blood-brain barrier. Potential therapeutics need not only be effective; they also need to be delivered into the brain, crossing this barrier. Recent clinical trials mainly focus on the use of antibodies that bind the $A\beta$ peptide, aiming to reduce the amount of aggregates either through prevention of build-up or reduction of existing plaque burden. In this thesis we have been focussing on the development of a special type of antibody, the llama heavy chain only antibody fragment VHH. As described in detail in chapters 1 and 6, llamas and other members of the camelid family have an additional group of antibodies that differ from the universal antibody; these camelid antibodies lack the light chain. The VHH is the part of this special antibody that binds the antigen. VHH have a number of benefits: for example, they are 10 times smaller than conventional full length antibodies, they are easier to produce, more stable in terms of temperature and pH and can be modified to fit a wide range of applications. One such application is the detection and prevention of protein aggregation by certain selected VHH. This makes VHH interesting candidates for various therapeutic angles in AD research. The first aim of this thesis is to determine the potential of our previously selected VHH in the fight against AD. The second aim is to find ways in getting VHH into the brain, across the blood-brain barrier.

Chapter 1 contains a general introduction to AD as well as a basic explanation of the selection, generation and application of VHH. Next, chapter 2 focusses on the use of VHH to intervene in the production of the $A\beta$ peptide. The proof of principle was demonstrated using VHH selected against the function of the beta-secretase BACE1. One VHH, VHH-B3a, was shown to inhibit the activity of the secretase by 50%, which in turn results in a reduction in production of $A\beta$. This inhibition was shown in an *in vitro* assay, and then confirmed in a cellular assay. The effect of the inhibition, i.e. reduction of $A\beta$ production, was finally demonstrated in a living mouse model for AD. The results of VHH-B3a are promising, and the therapeutic value of this reduction should be confirmed in behavioural studies. However, to get VHH-B3a into the brain, a crude method of direct injection into the cerebral ventricles was chosen. This method is effective, as shown in chapter 2, but is not ideal as a long term therapeutic application. Although

VHH-B3a has great potential as a BACE1 inhibitor, no VHH is of use without minimally invasive, yet efficient delivery across the blood-brain barrier. For this reason, chapters 3, 4, and 5 all focus on various methods of delivery. The VHH selected to test the delivery methods is VHH-pa2H, a VHH selected previously against A β aggregations. VHH-pa2H has a very high affinity for A β aggregates.

In chapter 3 we tested the ability to deliver the VHH as a cargo in liposomes that are targeted to a protein present on the blood-brain barrier. We tested two different types of liposomes; EYPC and DMPC. The use of DMPC did not increase the delivery of the VHH to the brain. However, encapsulation in EYPC did increase the delivery of VHH-pa2H into the brain, and the VHH accumulated in the brains of the mouse models that present A β plaques onto which VHH-pa2H can bind. To follow the presence of the VHH in the brain, we used a radioactive particle that we bound to the VHH after it was encapsulated in the liposome. This allowed us not only to follow only the VHH, rather than the liposomes which happens more commonly; it also allowed to us to make the liposomal encapsulated VHH in advance and attach the radioactive label just before use. This increases the shelf-life of the VHH-liposome construct which can be crucial in case of therapeutic use of a radioactively labelled VHH. Brain delivery of VHH in EYPC liposomes seems to be a possibility that can be employed for VHH-pa2H and undoubtedly other VHH.

We then went on to determine if it is possible to let the VHH cross the blood-brain barrier without the help of liposomes. One of the down sides of being small is that the VHH are rapidly cleared from the blood after injection. We therefore reasoned that if the VHH is able to interact with the barrier for a longer period, it might be able to cross the barrier via an active process. To allow more time for interaction, we attached the tail of a conventional antibody to the VHH, as described in chapter 4. Adding the tail indeed increased the time that the VHH spend in the blood significantly. However, not more of the VHH with the tail was delivered into brain compared to the VHH without the tail. We therefore concluded that although the addition was successful, more time in the blood alone did not help to let VHH-pa2H cross the barrier.

Finally, in chapter 5 we made use of the fact that the genetic information of the VHH is contained in such a small piece of DNA, that we can easily package this in a small viral particle, called Adeno Associated Virus, or AAV. We injected the AAV into the brain of the mouse models, allowing them to continuously produce the VHH themselves right in the brain, exploring a form of gene therapy. Using a special signal sequence, the VHH is secreted from the neuronal cells that are producing them, allowing it to bind the A β plaques that are in the brain but outside the cells. Additionally, we attached a special fluorescent protein to the VHH, allowing us to track the secreted VHH in real time using an *in vivo* microscopy technique. By giving the

viral treatment right after birth, it seems that VHH-pa2H may reduce the total plaque burden over time; however, this effect is not seen when given to older animals. However, the number of very young animals treated with the VHH is very limited and should be increased to make a definitive conclusion. In the older animals, expression of the VHH in the brain of the living mice is easily seen using the *in vivo* microscope. Only VHH-pa2H and not the control VHH, are able to bind the amyloid plaques. All in all, viral delivery of VHH, using the AAV particles, is an excellent and efficient way to deliver the antibody fragments into the brain. Future research should focus on the optimization of delivery of VHH via AAV, using for example slightly different versions of AAV, or finding the optimal age for injection. It should also focus on the long term benefits of delivering VHH, such as the anti-amyloid VHH-pa2H or BACE1 inhibiting VHH-B3a, to the brain of the mouse models for AD. VHH such as these hold great promise in the fight against neurodegenerative diseases like AD and viral delivery of VHH seems to be an outstanding method to ensure the crucial presence of VHH on the brain side of the blood brain barrier in this fight.

NEDERLANDSTALIGE SAMENVATTING

De ziekte van Alzheimer (AD) is een belangrijke oorzaak van het syndroom dementie, één van de meest ernstige bedreigingen voor de volksgezondheid in zowel de ontwikkelde wereld als in ontwikkelingslanden ten gevolge van de toenemende vergrijzing. AD wordt gekenmerkt door progressieve cognitieve achteruitgang en karakteristieke pathologische afwijkingen. Deze afwijkingen zijn onder andere ophopingen van het eiwit tau en van het peptide amyloïd beta ($A\beta$). Tau hoopt zich op in de neuronen, de zenuwcellen in de hersenen. Het peptide $A\beta$ hoopt zich op in de hersenen buiten de cellen en hoopt zich ook op rondom de bloedvaten van de hersenen. Door deze ophopingen kunnen de cellen en de bloedvaten hun werk niet goed meer doen.

Er is op dit moment geen medicijn beschikbaar welke AD kan voorkomen. Eén van de problemen van het ontwikkelen van een medicijn is de bloed-hersenbarrière, een zeer strict gereguleerde barrière tussen het bloed en de hersenen. Potentiële medicijnen moeten niet alleen effectief zijn tegen de ziekte; ze moeten ook deze barrière passeren. Recente klinische proeven richten zich voornamelijk op het gebruik van antistoffen welke het $A\beta$ peptide kunnen binden. Het doel is dan de ophopingen te verminderen, door ofwel de ophoping te voorkomen, ofwel de bestaande ophopingen te verwijderen. In dit proefschrift hebben we ons gericht op het gebruik van een deel van een speciaal type antistof welke voorkomt in lama's en andere kameelachtigen. Dit speciale lama antistof is kleiner dan de normale antistoffen, en het fragment dat wij gebruiken heet VHH.

Het VHH is het deel van dit kleinere antistof dat het antigeen bindt, in ons geval bijvoorbeeld het peptide $A\beta$. VHHs hebben een aantal voordelen: ze zijn 10 keer kleiner dan conventionele antistoffen, ze zijn gemakkelijker te produceren, ze zijn stabiel qua temperatuur en qua pH gevoeligheid, en ze kunnen aangepast worden voor een breed aantal toepassingen. Een voorbeeld van zo'n toepassing is de detectie en preventie van $A\beta$ ophopingen door speciaal geselecteerde VHHs. Dit alles maakt VHHs interessante kandidaten voor verschillende therapeutische strategieën in het AD onderzoek. Het eerste doel van dit proefschrift is het bepalen van het potentieel van onze geselecteerde VHHs in de strijd tegen AD. Het tweede doel is verschillende manieren te onderzoeken om de VHHs de bloed-hersenbarrière te laten passeren, om ze zo de plaats van bestemming (oftewel de hersenen) te laten bereiken.

Hoofdstuk 1 bevat een algemene inleiding tot AD en een uitleg over de selectie, productie en toepassing van VHHs. In hoofdstuk 2 worden VHHs gebruikt om invloed uit te oefenen op de productie van het $A\beta$ peptide. Hierbij is gebruik gemaakt van VHHs welke zijn geselecteerd tegen de functie van het beta-secretase eiwit BACE1. Eén VHH, VHH-B3a, verminderde de

activiteit van BACE1 met 50%. Hierdoor wordt er uiteindelijk minder A β geproduceerd. Deze rem op de activiteit van BACE1 is aangetoond in zowel een *in vitro* test als in een test op basis van gekweekte cellen. Het effect, de verminderde productie van A β , is vervolgens aangetoond in levende AD muismodellen. De resultaten van VHH-B3a zijn veelbelovend, en het therapeutisch nut van de verminderde A β productie als gevolg van VHH-B3a moet nu worden aangetoond in gedragsstudies in de muismodellen. Echter, om VHH-B3a in de hersenen te krijgen, is een ruwe methode toegepast, waarbij het VHH direct in de hersenventricels is geïnjecteerd. Hoewel hoofdstuk 2 aantoont dat deze methode effectief is, is deze methode niet ideaal voor een langdurige therapeutische toepassing. En ondanks dat VHH-B3a zeer interessant is als BACE1 remmer, is geen enkel VHH bruikbaar als het niet in staat is de bloed-hersenbarrière efficiënt te passeren op een niet-invasieve manier. Daarom richten de hoofdstukken 3, 4, en 5 zich allen op verschillende methodes om VHHs over deze barrière te transporteren. VHH-pa2H is gekozen om de transportmethodes te testen. Dit voornamelijk omdat VHH-pa2H A β ophopingen zeer efficiënt kan binden.

In hoofdstuk 3 hebben we getest of het mogelijk is VHH-pa2H als cargo in liposomen over de bloed-hersen barrière te transporteren. We hebben twee verschillende type liposomen getest; EYPC en DMPC. Het gebruik van DPMC zorgde niet voor een hoger transport van VHH-pa2H de hersenen in. Maar het gebruik van EYPC liposomen daarentegen zorgde wel voor een hoger transport, en het VHH hoopte zich op in de hersenen van de muismodellen welke de karakteristieke A β deposities hebben waaraan VHH-pa2H kan binden. Om de opname van het VHH in de hersenen te kunnen volgen, hebben we een radioactief molecuul aan het VHH gekoppeld, maar pas nadat het in het liposoom was opgenomen. Dit stelde ons niet alleen in staat om alleen het VHH te volgen, en niet, zoals doorgaans gebruikelijk is, het liposoom; maar ook om het VHH-liposoom complex ruim van te voren klaar te maken, en slechts vlak voor gebruik te labelen met het radioactieve molecuul. Hierdoor wordt het VHH-liposoom complex interessanter voor therapeutisch gebruik in combinatie met toepassingen met radioactief VHH. Het transporteren van VHHs over de bloed-hersen barrière met behulp van liposomen lijkt een goede mogelijkheid te zijn voor VHH-pa2H en kan zonder twijfel worden toegepast voor andere VHHs.

Vervolgens hebben we onderzocht of het mogelijk is VHHs de bloed-hersen barrière te laten passeren zonder de hulp van liposomen. Een van de nadelen van het feit dat VHHs zo klein zijn, is dat ze zeer snel uit het bloed worden verwijderd na injectie. Daarom beredeneerden we dat als het VHH meer tijd heeft om in contact te blijven met de barrière, het beter in staat zou zijn de barrière door middel van een actief proces te passeren. Om het VHH meer tijd te gunnen, hebben we de staart van een normaal antistof aan het VHH gekoppeld, zoals beschreven is in hoofdstuk 4. Door de staart bleef VHH-pa2H inderdaad veel langer in het bloed. Echter, er werd

niet meer VHH met staart in de hersenen aangetroffen dan in de situatie waarbij het VHH geen staart heeft. Daarom concludeerden we dat hoewel het aanbrengen van een staart succesvol is met betrekking tot het verlengen van de mogelijkheid tot interactie, het verlengen van de tijd in het bloed alleen niet voldoende is om VHH-pa2H over de barrière te helpen.

Tot slot wordt in hoofdstuk 5 beschreven hoe we de genetische informatie van VHH-pa2H in een klein virusdeeltje hebben geplaatst. Het specifieke virus dat hiervoor gebruikt is, wordt AAV genoemd. We hebben dit virus in de hersenen van de muismodellen geïnjecteerd. Hierdoor zijn de muizen in staat zelf continu het VHH aan te maken, direct in de hersenen. Dit is een vorm van gentherapie. Door een speciale signaalsequentie wordt VHH-pa2H nadat het aangemaakt is in de hersencellen, uit de cellen getransporteerd. Hierdoor kan het VHH de A β ophopingen binden, welke zich in de hersenen, maar buiten de cellen, bevinden. Daarnaast hebben we een bijzonder fluorescerend eiwit aan het VHH vastgemaakt, waardoor we het VHH continu kunnen volgen via een speciale microscoop techniek waarbij we in de hersenen van de levende muizen kunnen kijken. Bij muizen waarbij het virus direct na geboorte wordt toegediend, voordat er ophopingen zijn, lijken er door de aanwezigheid van VHH-pa2H uiteindelijk minder ophopingen te zijn dan in de muizen die geen virusdeeltjes hebben gekregen. Echter deze vermindering van hoeveelheid ophopingen wordt niet gezien als het virus aan oudere dieren wordt gegeven. Helaas is de hoeveelheid jonge muizen waarin dit effect is gezien aan de lage kant. Uitgebreidere studies zijn nodig om een definitieve conclusie te kunnen trekken. In oudere dieren kan het VHH duidelijk gevolgd worden via de speciale microscoop. Alleen VHH-pa2H, en niet de controle VHHs, kan de amyloïde ophopingen binden. Uiteindelijk kan worden geconcludeerd dat de virale toediening van VHHs, met behulp van de AAV virussen, een excellente en efficiënte methode is om de antilichaam fragmenten in de hersenen te krijgen. In de toekomst moet worden gewerkt aan het optimaliseren van de efficiëntie van de virale hersentoediening, door bijvoorbeeld net andere types AAV te gebruiken, of na te gaan op welke leeftijd van de dieren de efficiëntie het hoogst is. Ook zou het onderzoek zich moeten richten op de positieve gevolgen op de lange termijn van deze vorm van gentherapie, met gebruik van VHHs zoals de anti-A β VHH-pa2H of de anti-BACE1 VHH-B3a, in de hersenen van muismodellen van AD. Dit soort VHHs zijn zeer veelbelovend in de strijd tegen neurodegeneratieve ziektes, waaronder AD, en de AAV gentherapie lijkt een uitgelezen mogelijkheid te bieden om de in deze strijd cruciale aanwezigheid te verzekeren van de VHHs aan de hersenkant van de bloed-hersen barrière.

LIST OF PUBLICATIONS

Rotman M, Grand Moursel L, Carrano A, van der Graaf LM, van den Boogaard MM, Suidgeest E, van Buchem MA, van der Maarel SM, Das P, van der Weerd L. Functionally secreted single domain antibody fragment VHH-EmGFP binds amyloid plaques and can be visualized *in vivo*. *Submitted to Molecular Therapy* 2017.

Dorresteyn B, **Rotman M**, Faber D, Schravensande R, Suidgeest E, van der Weerd L, van der Maarel SM, Verrips CT, El Kattabi M. Camelid heavy chain only antibody fragment domain against β -site of amyloid precursor protein cleaving enzyme 1 inhibits β -secretase activity *in vitro* and *in vivo*. *The FEBS Journal* 2015; 282:3618-3631

Rotman M, Welling MM, van den Boogaard ML, Grand Moursel L, van der Graaf LM, van Buchem MA, van der Maarel SM, van der Weerd L. Fusion of hIgG1-Fc to ¹¹¹In-anti-amyloid single domain antibody fragment VHH-pa2H prolongs blood residential time in APP/PS1 mice but does not increase brain uptake. *Nuclear Medicine and Biology* 2015; 42:695-702

Rotman M*, Welling MM*, Bunschoten A, de Backer ME, Rip J, Nabuurs RJA, Gaillard PJ, van Buchem MA, van der Maarel SM, van der Weerd L. Enhanced glutathione PEGylated liposomal brain delivery of an anti-amyloid single domain antibody fragment in a mouse model for Alzheimer's disease. *Journal of Controlled Release* 2015; 203:40-50

Nabuurs RJ, Rutgers KS, Welling MM, Metaxas A, de Backer ME, **Rotman M**, Bacskai BJ, van Buchem MA, van der Maarel SM, van der Weerd L. *In vivo* detection of amyloid-beta deposits using heavy chain antibody fragments in a transgenic mouse model for Alzheimer's disease. *PLoS. One* 2012; 7:e38284

Rutgers KS, Nabuurs RJ, van den Berg SA, Schenk GJ, **Rotman M**, Verrips CT, van Duinen SG, Maat-Schieman ML, van Buchem MA, de Boer AG, van der Maarel SM. Transmigration of beta amyloid specific heavy chain antibody fragments across the *in vitro* blood-brain barrier. *Neuroscience* 2011; 190:37-42

Rotman M, Snoeks TJA, van der Weerd L. Pre-clinical optical imaging and MRI for drug development in Alzheimer's disease. *Drug Discovery Today: Technologies* 2011; 8:e117-e125

Dorresteyn B*, **Rotman M***, de Kimpe L, Schasfoort RBM, Scheper W, van der Maarel SM, van der Weerd L, Verrips CT, El Khattabi M. Characterization of llama single domain antibodies reveals an amyloid-beta aggregation and toxicity inhibiting antibody. *Manuscript in preparation*.

Zimmerman RME, Sun J, Tian J, de Smit M, Danen-van Oorschot AA, **Rotman M**, Snel P, Voskamp P, Noteborn MHM, Backendorf C. Cellular partners of the apoptin-interacting protein 3. *Manuscript in preparation*.

* Authors contributed equally to this work.

CURRICULUM VITAE

Maarten Rotman was born on the 23rd of January, 1984, in De Wijk, the Netherlands. He completed the Dutch pre-university secondary education (VWO) at the former Peter Stuyvesant College on the Caribbean island Curaçao, former Netherlands Antilles. Subsequently, he attended both Leiden University, in Leiden, the Netherlands and Delft University of Technology, in Delft, the Netherlands, where he obtained the Bachelor of Science (2007) and the Master of Science (2010) degrees in Life Science and Technology. In 2010 he started his PhD in Neuroscience with a focus on Alzheimer's disease and Hereditary Cerebral Haemorrhage with Amyloidosis-Dutch type (HCHWA-D) at Leiden University Medical Center under the combined mentorship of prof. dr. ir. Silvère van der Maarel (Chair of the Department of Human Genetics) and prof. dr. Mark van Buchem, M.D. (Chair of the Department of Radiology), and the daily supervision and guidance of associate professor dr. Louise van der Weerd. During his PhD training, Maarten was awarded a personal fellowship grant from Alzheimer Nederland, an independent foundation aimed at research and care towards dementia patients, to study at the Department of Neuroscience at the nonprofit medical practice and research hospital Mayo Clinic in Jacksonville, Florida, USA. On January 1st, 2015, he continued his academic career at Mayo Clinic Florida, as a researcher in the lab of prof. dr. Anders Nykjær, focusing on the role of VPS10P-domain containing sorting proteins (Sortilin, SorLA, SorCS1-3) in the development of the neurological afflictions in general and Alzheimer's disease in particular. As of January 2017, he started to explore new scientific horizons by focussing his research on glioblastoma multiforme, or brain tumors, in the lab of prof. dr. Alfredo Quiñones-Hinojosa at Mayo Clinic Florida.

ACKNOWLEDGEMENTS / DANKWOORD

Allereerst wil ik mijn promotoren Silvère en Mark danken voor hun steun, advies en sturing tijdens mijn promotie traject. Het is niet eenvoudig om tijd te maken als je een volledig departement (of zelfs twee) leiding moet geven, en het feit dat jullie beiden dat toch altijd deden is schitterend en zeer bewonderenswaardig.

Voor mijn uitstekende dagelijkse begeleiding kijk ik heel specifiek naar twee personen: Rinse en Louise. Rinse, in het eerste jaar heb ik alles wat ik moest leren over VHHs, phagen en de wetenschap in zijn geheel van jouw geleerd. Daarnaast was je gewoon de super post-doc die elke PhD student naast zich moet hebben staan! Louise, ik hoop dat ik over de jaren ook maar een klein beetje heb kunnen opsteken van jouw inzicht in alles wat proefdieren en academisch schrijven en denken aangaat. Elke tekst en presentatie waarvan ik dacht dat het wel lekker inelkaar stak, kwam rood van de track-changes terug; elke keer tig keer beter dan voorheen. Elke alinea die redelijk soepel loopt in dit proefschrift is rechtstreeks te wijden aan jou invloed! Niets in dit proefschrift zou overigens mogelijk zijn geweest zonder het eerdere uitgebreide werk van mijn voorgangers Kim en Rob, die de VHHs hebben geselecteerd en de technieken voor de cranial window experimenten naar Leiden hebben gebracht.

Zonder het keiharde werk van Ernst, Linda, Laure en Mick zou dit proefschrift heel wat minder pagina's tellen. De samenwerking met jullie was niet alleen efficient, maar vooral ook heel plezierig. Plezier had ik sowieso heel veel in het LUMC. En dat is te danken aan de uitzonderlijk goede sfeer: ik kan iedereen van de http://www.humgen.nl/HKG_all.php lijst wel gaan opnoemen hier. Maar vooral Lab F en mijn kamergenoten: Maartje, Ilona, Fatiha, Amanda, Andrea, Kelly, Marlinde, en nogmaals Laure en Linda. Verder natuurlijk ook nog Leon, Marjolein, Brigit, Dana, en Maaïke. De sfeer en samenwerking binnen HumGen en binnen Louise's groep in Radiologie is in mijn ogen een voorbeeld voor elke werkvloer.

To the students that have helped me out with this work: Audald (gràcies), Hannah (tack), Tamara and Marlinde, you helped me with this work more than you can imagine, and my gratitude is enormous.

Ik heb dit werk niet alleen binnen HG en Radi gedaan: mijn dank gaat dan ook uit naar Bram (UU), Pieter en Jaap (ToBBB), Manuel en Rob (MCB, AAV), Annelies (MCB/Multiphoton) en Ingrid (Pathologie).

While working on the AAV study I was fortunate enough to be able to visit Mayo Clinic, in Jacksonville, Florida. Pritam, thank you for accepting me into your lab and allowing me to work here. My thanks also extends to Anna, Christoff, and Sarah for their help while I was here, as

well as to the members of dr. Petrucelli's lab: especially Karen and Ena for their expert help in creating those great AAVs. Now working at Mayo I have found out that there are so many great scientists here; your enthusiasm motivated me to finish writing this thesis, even if the amazing extra-curricular activities organized by you may have helped delay it the tiniest of bits further. I thank you all, and especially my direct colleagues Daar and Arul.

Ik wil ook mijn oma, ouders en zus bedanken voor hun nimmer aflatende steun (en verzoeken, vooral van de ouders, om op te schieten met die therapie. Motivatie is heel belangrijk!). The same goes out to my Italian mom, dad, and sister, my Haitian sister and godchild, and my Dutch, Dutch/Swiss and Dutch/France family members. Tineke belongs here too. Family is all, no matter who and where you are.

Most importantly, Anna, I know distance means nothing: in the words of the Venetian poet Mario Stefani "*Solitudine non è essere soli, è amare gli altri inutilmente*". My bright and beautiful: supervision, student, colleague, friend, family; I am happy and fortunate to be able to put you in literally every paragraph of these acknowledgements.

One of the effects of taking this long to hand in the final version of the thesis, is that the amount of people that I met during these years, and who in some way have contributed to the development of the thesis, has become staggering. I thank you all for your help, influence and patience, and I sincerely apologize to all whom I could not mention here by name.

